GENERATION AND PROPAGATION OF ULTRASHORT LASER PULSES USING NONLINEAR WAVEGUIDES

Zengli Su

A Thesis Submitted for the Degree of PhD
at the
University of St Andrews

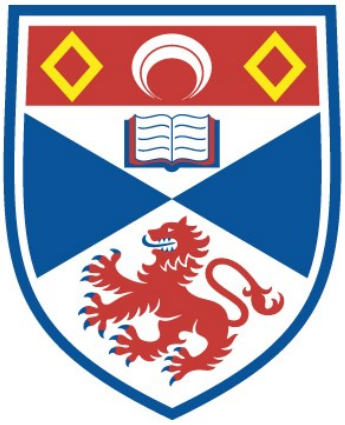

1995

Generation and Propagation of Ultrashort Laser Pulses Using Nonlinear Waveguides

Thesis submitted for the degree of Doctor of Philosophy
to the University of St. Andrews
by
Zengli Su, B.Sc.
(November 1994)

J. F. Allen Physics Research Laboratories
Department of Physics and Astronomy
University of St. Andrews
North Haugh
St. Andrews
Scotland KY16 9SS
U.K.

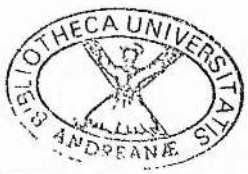

Declaration

I, Zengli Su, hereby certify that this thesis has been composed by myself, that is a record of my own work, and that it has not been accepted in partial or complete fulfilment of any other degree or professional qualification.

I was admitted to the Faculty of Science of the University of St. Andrews as a candidate for the degree of Ph.D under ordinance general No. 12 on 1st October 1990.

Signed Date 30/11/94

Certificate

I hereby certify that the candidate has fulfilled the conditions of the Resolution and the Regulations appropriate to the degree of Ph.D.

Signature of Supervisor Date 30/11/94

Copyright

In submitting this thesis to the University of St. Andrews I understand that I am giving permission for it to be made available for use in accordance with the regulations of the University Library for the time being in force, subject to any copyright vested in the work not being affected thereby. I also understand that the title and abstract will be published, and that a copy of the work may be made and supplied to any bona fide library or research worker.

To my parents

&

my wife Huali, my son Leler

Abstract

The main objectives in this research project related to the generation of ultrashort laser pulses using a KCl:Tl colour-centre laser and the study of their propagation in optical waveguides. Coupled-cavity mode-locking of the KCl:Tl colour-centre laser using either monomode optical fibre or passive AlGaAs waveguides as the nonlinear element in the control-cavity have been investigated. With the optical fibre as the nonlinear element, pulses as short as 63 fs have been generated.

The large nonlinearity of the AlGaAs waveguides illuminated near the half-bandgap energy has been confirmed through the propagation of ultrashort laser pulses, and nonlinear phase shift in excess of 2π has been observed. By undertaking the studies described here, the measurements have indicated that the waveguides used have a linear loss of 0.74 cm^{-1}, a two-photon-absorption coefficient of about 0.1 cm/GW, and a nonlinear refractive index of 0.8×10^{-13} cm^2/W.

Coupled-cavity mode-locking with passive AlGaAs waveguides as the control-cavity nonlinear element has been achieved, and two different guiding geometries of the AlGaAs waveguides have been used. With a straight waveguide geometry, pulses having duration of ~ 230 fs have been generated. When a curved waveguide geometry was utilised and appropriate dispersion compensation applied then pulses as short as 160 fs have been produced. By employing waveguides having reduced lengths (down to 1.2 mm), some further shortening of the output pulses was achieved and pulses as short as 150 fs have been recorded. By using a gold coating on rear facet of the waveguide, successful coupled-cavity mode-locking has been achieved at an output power level as low as 4 mW.

Some applications using the coupled-cavity mode-locked KCl:Tl colour-centre laser have been performed. Femtosecond pulses at 1.3- μm spectral region have been produced through the process of self-phase-modulation mediated four-wave-mixing in an erbium-doped fibre. Measurement on the group-velocity-dispersion of the AlGaAs waveguide has also been made, and a value of D = -1100 ps/nm/km has been deduced.

Contents

Chapter 1

General Introduction

1.1 Background introduction

The last few years have seen a dramatic progress in the physics and technology associated with the generation of ultrashort laser pulses [1-16]. Novel mode locking techniques have been developed and used on a number of laser systems [4, 5]. Most notably, the exploitation of optical nonlinearities in the generation of ultrashort light pulses has received considerable attention. Coupled-cavity mode locking [6, 7], which was extended from the soliton laser invented by Mollenauer [8, 9], has proved to be a simple, versatile, and economic mode locking technique. This mode locking scheme has been applied to a variety of laser systems including Ti:Sapphire [10], Nd:YAG [11], Nd:YLF [12], Nd:Glass [13], and Fibre lasers [14], allowing the generation of ultrashort light pulses over a wide range of the electromagnetic spectrum with previously unavailable durations. The self-mode-locked Ti:sapphire laser and related solid-state lasers have allowed the generation of powerful femtosecond pulses with an unprecedented stability, reliability, and reproducibility [15]. Pulse compression utilising self-phase-modulation in optical fibres has allowed the generation of 6 fs pulses [16].

Among the various mode-locked laser systems, the KCl:Tl colour centre laser still retains the predominant source for lasers working at wavelengths of around 1.5 μm in the research laboratories. This spectral region is for particular interest in optical communication research, because of the corresponding lowest-loss window of silica-based fibres over this spectral region [17]. The significant characteristics of the colour-centre laser are its wide tunability over a bandwidth in excess of 100 nm and the generation of pulses with duration of less than 100 fs, in combination with a high output

peak power. Using a KCl:Tl colour-centre laser, extensive studies have been conducted in linear and nonlinear propagation of ultrashort pulses in optical fibres and semiconductor devices. This has resulted in the demonstration of various all-optical switching devices based on fibres [18], and semiconductor waveguides. [19].

Application of ultrafast optical techniques ranges from such diverse areas as basic physical and biological sciences as well as technology [20]. Notably in the optoelectronics research area, nonlinear processes based on the third-order susceptibility $\chi^{(3)}$, such as self-phase modulation (SPM), stimulated Raman scattering (SRS), four-wave-mixing (FWM), etc. in optical waveguides have been extensively studied. Consequently, the exploitation of such nonlinear effects is gaining considerable attention. The SPM has found practical applications in picosecond-pulse compression and amplification [16]. Soliton formation due to the combined effect of SPM and anomalous group-velocity-dispersion in optical fibres has the potential application prospect in optical communications [21]. Optical switching has been successfully demonstrated in semiconductor waveguides by exploiting the third-order nonlinear effect [19]. Raman scattering, essentially undesired in optical fibres, has been successfully exploited in tuneable fibre Raman lasers [22]. Two-photon absorption in semiconductor waveguides working at the half-bandgap energy proved to be a limiting factor for the implementation of all optical switching devices. However, by operating at a wavelength slightly lower than the two photon energy band, the two-photon related absorption may be reduced [23].

In this introductory chapter, firstly the generation of ultrashort light pulses is overviewed, followed by a brief introduction to the characterisation of ultrashort pulses, then the linear and nonlinear propagation of ultrashort pulses is outlined.

1.2 Generation of ultrashort laser pulses

For the generation of ultrashort light pulses, the technique termed as laser mode locking is generally employed. The first demonstration of a mode-locked laser was in the mid-1960's [for example, see Refs. 24, 25], since then considerable progress has

been achieved. There have been a number of review papers concerning the generation of ultrashort light pulses [26-30]. In this section of the chapter, a brief introduction of the different mode locking techniques is presented.

1.2.1 Characteristics of free-running lasers

A laser basically consists of a gain medium within an optical resonator, as illustrated in figure 1.1. The resonator is usually composed of a set of mirrors that reflect the light beam back and forth through the gain medium. The gain medium is pumped through external excitation either optically (as in solid-state lasers) or electrically (as in gas, and semiconductor lasers), in such a way that the atoms normally sitting in the lower energy state of the gain medium will be excited onto a higher energy state. As a consequence of continuous pumping a population inversion might be set up. Without any external stimulation, atoms at the high energy state decay spontaneously back to the lower state again, accompanied by an emission of photons corresponding to the energy difference between the two states, $E_h - E_l$. When a light beam passes through the gain medium, however, it stimulates the atoms at the high quasi-steady state to return back to a lower state in the form of stimulating emission that adds to, or amplifies, the light beam. As a consequence of the accumulative process, an intensive coherent light (laser) beam is produced.

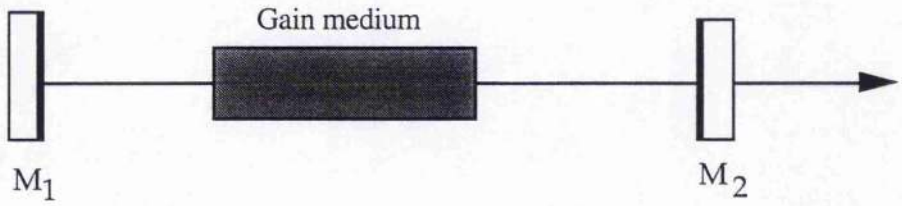

Figure 1.1. A schematic of laser resonator.

Normally, the light beam from such a laser is composed of a number of discrete wavelengths corresponding to different resonant frequencies, or resonator modes. Such resonator modes are literally defined as the longitudinal modes of the resonator, and satisfy the standing wave condition $n\lambda = 2L$. Therefore, the frequency of the longitudinal modes is given by

$$\nu = \frac{nc}{2L} \tag{1.1}$$

where c is the speed of light, L is the optical path length of the resonator, and n is an integer representing the mode number. The separation between neighbouring modes is expressed as

$$\Delta\nu = \frac{c}{2L} \tag{1.2}$$

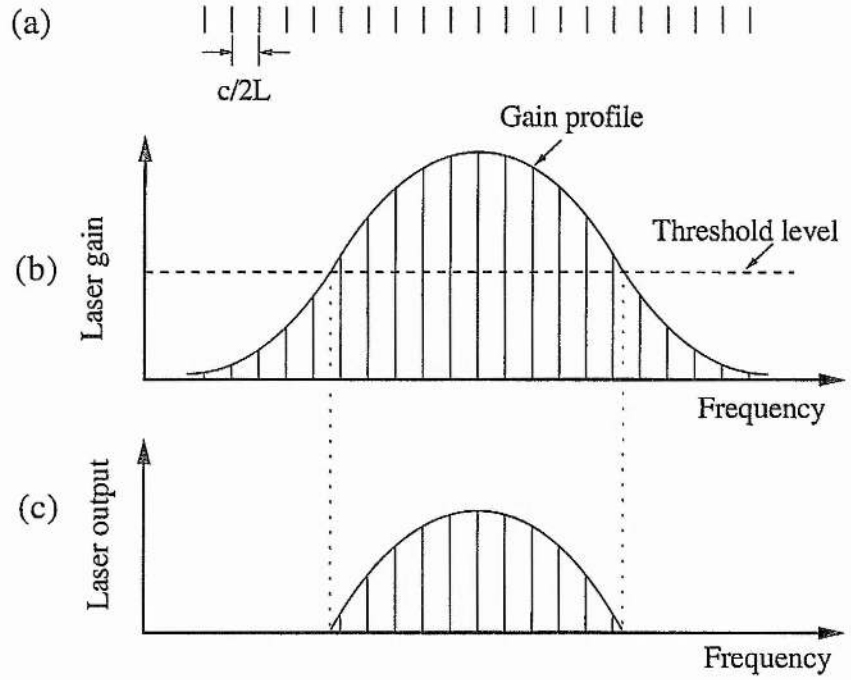

Figure 1.2. (a) Longitudinal modes of laser resonator; (b) Laser gain spectral profile; (c) Oscillating modes of laser output.

Usually, the gain bandwidth of a laser medium is over a wide range of spectra, and is much broader than the cavity mode spacing, $\Delta\nu = c / 2L$, as shown in Figure 1.2(b). Therefore, for a real laser system there are always a number of longitudinal modes that are above lasing threshold, and are built up as the laser output, as illustrated in figure 1.2(c). However, because these longitudinal modes oscillate in the laser cavity with random phase and amplitude, the output of the laser fluctuates arbitrarily in time owing to random interference between those modes [31,32].

There are two ways in which the fluctuation problem can be tackled. The first is by inserting frequency selecting elements into the cavity, (for example, optical etalon), or shortening the resonator length to allow only one longitudinal mode to oscillate, so that the output is light with high coherence and good spectral quality. The second approach is to force the modes to oscillate with a fixed phase relationship, which leads to an output periodically modulated as a train of short pulses with a period of cavity round trip time $2L/c$. This is what is commonly termed laser mode locking, and will be of concern in most of this thesis.

Essentially, there are two type of mode locking: longitudinal mode locking and transverse mode locking. However, in most cases the multi-transverse mode operation is undesirable and the laser is usually operated at the fundamental transverse mode. Therefore, the longitudinal mode locking is referred to in this thesis. The transverse mode locking can be found in a number of reports in the literature [for example, see Ref. 33]. In principle, the longitudinal mode locking technique can also be subdivided into two categories: active mode locking and passive mode locking. In active mode locking, a modulator, which is driven by an external power source in the period corresponding to cavity round-trip time, is inserted within the laser resonator. In passive mode locking scheme, the modulation is accomplished by a nonlinear optical element that is driven by the mode locked pulses themselves.

1.2.2 Description of mode locked laser pulses

Suppose that the optical strength of the mth longitudinal mode can be expressed as a complex function.

$$E_m(t) = E_m e^{i(\omega_m + \phi_m)} \tag{1.3}$$

The total optical radiation strength, therefore, can be represented by the sum of such longitudinal modes

$$E(t) = \sum_m E_m e^{i(\omega_m + \phi_m)} \tag{1.4}$$

where E_m, ϕ_m are the amplitude and initial phase of mth mode, respectively, and the summation extends over all oscillating modes. The instantaneous optical intensity is given by

$$I(t) \propto [\mathrm{Re}E(t)]^2 = \sum_m E_m^2 \cos^2(\omega_m t + \phi_m) + \sum_m \sum_n E_m E_n \cos(\omega_m + \phi_n)\cos(\omega_n + \phi_n) \tag{1.5}$$

In reality, the intensity received by optical receiver is the average intensity over a period of time which is much longer than an optical cycle. Therefore, we have

$$\langle I(t)\rangle \propto \left\langle [\mathrm{Re}E(t)]^2 \right\rangle = \frac{1}{T}[\sum_m \int E_m^2 \cos^2(\omega_m t + \phi_m)dt + 2\sum_m \sum_n \int E_m E_n \cos(\omega_m + \phi_n)\cos(\omega_n + \phi_n)dt] \tag{1.6}$$

which indicates that the received average intensity is the summation of all individual mode intensities. It also implies that for a free running laser the instantaneous intensity fluctuates randomly around this average intensity.

Now, we consider the case of a laser that is mode-locked. For simplicity, assuming that all longitudinal modes have same amplitude and same initial phase (as the ideal case of mode locked lasers), i. e.

$$E_m = E_0$$
$$\phi_m = \phi_0$$

Therefore, the frequency difference between neighbouring modes is given by

$$\Delta\omega = \omega_m - \omega_{m-1} = \frac{\pi c}{L} \tag{1.7}$$

Taking the central frequency as ω_0, then we have

$$\omega_m = \omega_0 + m\Delta\omega \tag{1.8}$$

For N modes oscillating, substitution of above ϕ_m, ω_m, E_m into equation (1.4), gives

$$E(t) = E_0 e^{i(\omega_0 t + \phi_0)} \frac{\sin\left(\frac{N\Delta\omega t}{2}\right)}{\sin\left(\frac{\Delta\omega t}{2}\right)} \tag{1.9}$$

Therefore, the output power

$$P(t) \propto {E_0}^2 \frac{\sin^2\left(\frac{N\Delta\omega t}{2}\right)}{\sin^2\left(\frac{\Delta\omega t}{2}\right)} \tag{1.10}$$

It is easy to see from this equation that the output takes the form of a pulse train which has a period of

$$T = \frac{2\pi}{\Delta\omega} = \frac{2L}{c} \tag{1.11}$$

The peak power equals N times the average power. The pulse duration Δt (FWHM) is given approximately by

$$\Delta t = \frac{T}{N} = \frac{2\pi}{N\Delta\omega} = \frac{1}{\Delta\nu} \tag{1.12}$$

Where N and $\Delta\nu$ are the oscillating mode numbers and lasing bandwidth, respectively. It is clearly shown that shorter pulse width demands a wider lasing bandwidth, i.e., more longitudinal modes.

1.2.3 Mode locking techniques

1.2.3.1 Active mode locking

Active mode locking can be achieved by modulating either the amplitude (loss or gain) or the phase of the optical radiation in the cavity. In each case it is known as amplitude modulation (AM) mode locking and phase modulation (PM) mode locking, respectively.

Principle of AM mode locking

In the frequency domain approach , this mode locking scheme can be described as follows. Suppose that the amplitude and frequency of the central mode at the gain profile are E_0 and ω_0, respectively. Then, the optical strength, which can be simply expressed as

$$E_0(t) = E_0(\cos\omega_0 t) \tag{1.13}$$

when the modulation is involved, becomes

$$E_0(t) = E_0(1 + M\cos\omega_m t)\cos\omega_0 t$$
$$= E_0\cos\omega_0 t + \frac{E_0 M}{2}\cos(\omega_0 - \omega_m)t + \frac{E_0 M}{2}\cos(\omega_0 + \omega_m)t \qquad (1.14)$$

where M is the modulation depth, ω_m is the modulation frequency which is chosen to be the same as the optical round trip of $c/2L$, or its integer $nc/2L$.

Equation (1.14) shows that apart from the original frequency ω_0 two new sideband frequencies at $\omega_0 + \omega_m$ and $\omega_0 - \omega_m$ are introduced. When such three frequencies pass the modulator again, the sideband frequencies $\omega_0 + 2\omega_m$ and $\omega_0 - 2\omega_m$ will be generated. As a result of the oscillation in the resonator, a lot of new frequency components will be generated. These frequencies coincide with the adjacent mode frequencies of the resonator, and thus leads to the modes becoming strongly coupled and cause phase-locking of the longitudinal modes.

Mode locking by loss modulation

In this mode locking scheme, the modulator is usually an acoustooptic modulator driven by a radio frequency (rf) generator. The acoustooptic modulator is presented in such a way that an ultrasonic standing wave is formed within the modulator crystal. The refractive index of the modulator varies accordingly with the amplitude of the standing wave, leading to the light signal passing through the modulator experiencing a periodical loss due to the diffraction thereby introduced. The minimum diffraction loss occurs at the time when the amplitude of the applied signal is zero. Twice in every radio frequency period the diffraction loss of the modulator happens to be minimum and the modulator appears transparent to the incident light. Therefore, by setting the radio frequency at half of the intermode spacing of the resonator, mode locking may be established, and a pulse train with a period of 2L/c might be achieved. A schematic of the mode locking process is shown in Fig. 1. 3.

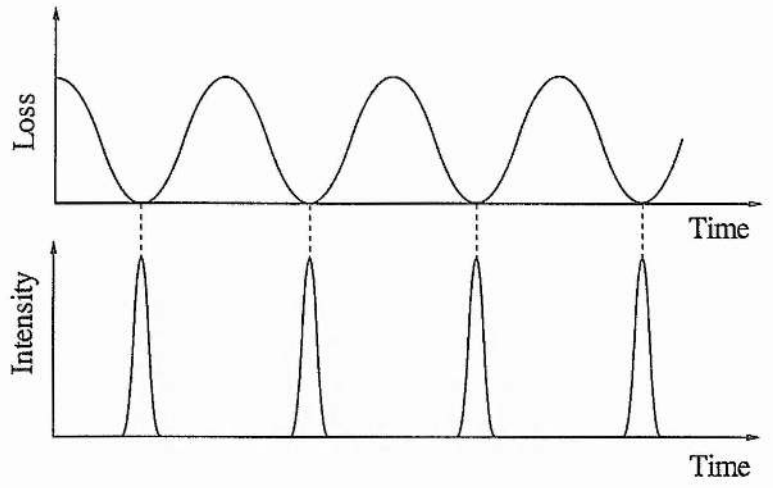

Figure. 1.3. Mode locking mechanism by loss modulation

Mode locking through gain modulation by synchronous pumping

Mode locking by modulating the active of the gain medium is usually applied to lasers which are pumped by another laser or to semiconductor lasers that are pumped electrically. In semiconductor lasers, gain modulation is accomplished by applying a radio frequency signal, at a repetition rate corresponding to the laser cavity period, directly to the bias current [34]. The pulse duration achieved with mode locked diode laser is of the order of a few tens of picoseconds. In the case of a laser being pumped by another laser the gain modulation is achieved by modelocking the pumping laser. For this mode-locking to work, it is generally required that the cavity length of the second laser has to be equal to or is an integer of that of the pumping laser. The mode locking achieved through this mode locking scheme is commonly referred to as mode locking by synchronous pumping.

The pulse shortening in synchronously pumped lasers is caused by a combination of gain modulation (due to pump pulses) and gain saturation. Referring to Fig. 1.4, which is a result of the theoretical analysis on the synchronously pumped colour-centre lasers, the pulse shortening mechanism can be discussed as follows. Before the arrival of the pump pulse, the gain of the colour-centre laser medium is zero. After the pump pulse arrives at the gain medium, the gain starts to build up and eventually exceeds the

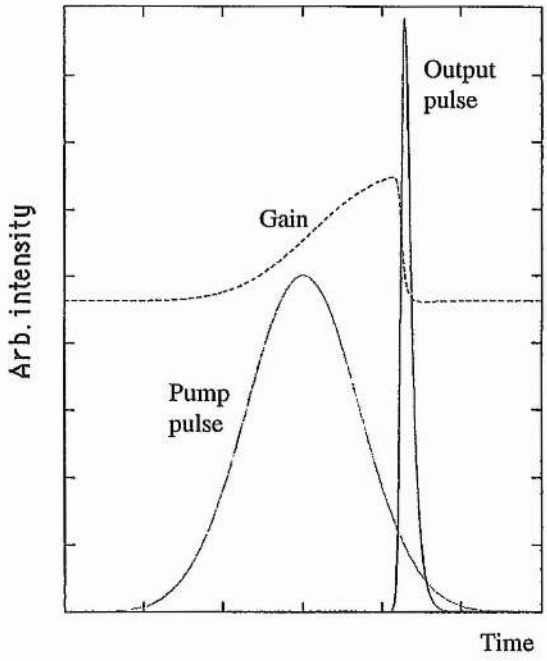

Figure 1.4. Schematic illustrating the dynamics of synchronously mode-locked colour-centre lasers.

loss in the resonator. Subsequently, the colour-centre laser pulse arrives, and begins to extract energy from the gain medium through the process of stimulated emission (amplification). As a result of this process, the gain is saturated and is brought back below the loss again, thus turning off the laser pulse. After the passage of the pump pulse, the gain slowly relaxes back to zero. For proper mode locking, the resonator lengths of the two lasers have to be properly matched. When the colour-centre laser cavity is too short, the colour-centre laser pulse arrives too early at the gain medium; this would allow the gain to recover after saturation and to exceed the loss for a second time, resulting in the formation of a satellite pulse. If the colour-centre laser cavity is too long, the colour-centre laser pulse arrives late at the gain medium; thus the spontaneous emission may be amplified prior to the arrival of the colour-centre laser pulse, resulting in a broad and noisy pulse shape. For this mode locking scheme to work, the decay time of the inversion must be fast enough so that the corresponding gain can be significantly modulated.

Mode locking by phase modulation (PM)

In this mode locking scheme, the modulation is applied to the phase of the light. In the time domain description, the frequency of the light passing through the phase modulator is up- or down-shifted by a value proportional to the Doppler frequency shift $d\varphi / dt$. Referring to Figure 1.5, when $d\varphi / dt \neq 0$ the successive passes through the modulator will eventually shift the optical field out of the gain profile. Only the optical fields passing through the modulator at the time $d\varphi / dt = 0$ will experience no frequency shift, and thus be amplified and form a mode locked pulse train after successive reflection between the two mirrors. Note that there are two stationary points, which may result in double pulse trains and cause instability.

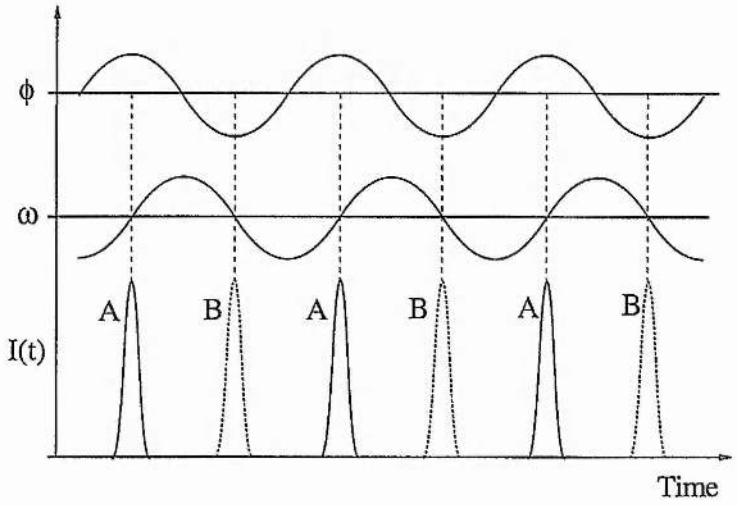

Figure 1.5. Schematics showing the mechanism of active mode locking by phase modulation.

In the frequency domain approach, when modulation is applied to the phase of the optical radiation, the modulated signal can be represented by

$$E(t) = E_0 \cos(\omega_0 t + \varphi_c \cos \omega_m t) \qquad (1.15)$$

Where φ_c is the modulation index, ω_m is the modulation frequency. Mathematically, this equation can be expressed as

$$E(t) = E_0 \sum J_m(\varphi_c) \cos(\omega_0 + m\omega_m) \qquad (1.16)$$

where J_m is Bessel function. From this equation it can be seen that the resultant radiation contains a number of sideband frequencies. The neighbouring frequencies have the identical frequency difference ω_m. In this way, the mode locking condition is obtained.

1.2.3.2 Passive mode locking

Passive mode locking has been the means for generating the shortest pulses. It led to the first sub-picosecond pulses [35] and can now be used to produce pulses in the order of tens of femtosecond [36]. This kind of mode locking is generally achieved by including a saturable absorber in the laser cavity. Since no external modulation is applied, contrasted to its counterpart - active mode locking, it is commonly referred as passive mode locking. The saturable absorber has the characteristics of low transmission when the optical radiation is low and becomes high transmission when the optical radiation reaches a threshold power level point I_{th}. In practice, the saturable absorber falls into two categories: slow and fast saturable absorber.

Slow saturable absorber

A slow saturable absorber [37] is a lossy element that becomes more transparent with intense light but with a recovery time longer than the time scale of the ultrashort pulse. It was proposed by New [38] that the pulse shortening with the slow saturable absorber was made possible by dynamic saturation of the gain. The absorber preferentially absorbs the leading edge of the pulse, while gain depletion causes losses at the trailing edge. At each round trip, the wings of the pulse experiences the loss while the peak of pulse receives gain. As a result, the pulse is shortened. The modulation dynamics of this mode locking process is illustrated in Figure 1.6. In simple term, the pulse shortening can be expressed as follow. When the pulse arrives at the absorber, the leading edge of the pulse is absorbed. This process, in turn, saturates the absorber, so that the central portion and the trailing edge of the pulse experiences less attenuation when passing through the absorber. As a result, the leading edge of the pulse is truncated. Now concerning the case when the pulse travels to the gain medium. The

intense central portion of the pulse is amplified sufficiently to saturates the gain, such that when the trailing edge arrives no gain is left. Thus, through the processes of absorber saturation and gain saturation the pulse is shortened.

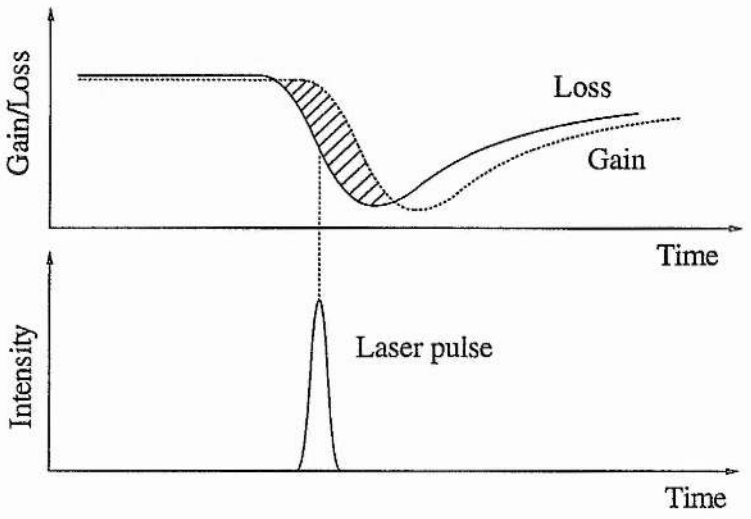

Figure 1.6. Pulse shaping dynamics for slow saturable absorber mode locking.

Fast saturable absorber

A fast saturable absorber is an element that responds essentially instantaneously to the light intensity. That is, it recovers its initial absorption in a time scale shorter compared to the pulse duration. Thus, it shapes the pulse on both the leading and trailing edges of the pulse. Figure 1.7 shows the pulse shaping dynamics with a fast saturable absorber.

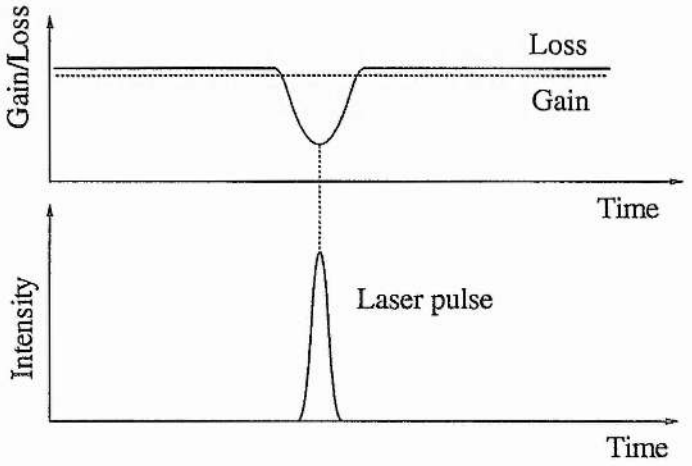

Figure 1.7. Pulse shaping dynamic with a fast saturable absorber.

Coupled-cavity mode locking

A coupled-cavity mode locking [39] scheme is basically composed of the main laser cavity where the gain medium is located, in conjunction with an adjacent auxiliary cavity containing a nonlinear element. This mode locking scheme has also been termed additive-pulse mode locking (APM) [40], and interferential mode locking (IML) [41] according to the mechanism being explained. Essentially, three different type of configuration can be arranged; namely, Fabry-Perot, Michelson, and Ring-cavity configurations, as the schematics shown in figure 1.8. For the nonlinear Fabry-Perot cavity configuration, the auxiliary cavity is formed by the output coupler of the main laser and an extra retroreflector M_2, as shown in figure 1.8(a). The output is derived from a beam splitter inserted in the external cavity. The proper operation of CCM mode locking requires that the optical length of the external cavity should be well matched with the main cavity or being the integer of it. A Michelson cavity configuration, in one sense, is basically a Michelson interferometer formed by inserting a beam splitter in the main cavity, as shown in figure 1.8(b). One arm of the interferometer is essentially part of the main cavity composed of the main cavity end mirror and the beam splitter; and the other arm consists of the beam splitter and a retroreflecting mirror M_2, between them the nonlinear element is contained. The output is again derived from the beam splitter. It is required that the optical length of the two arms should be the same. For the Ring cavity configuration, as shown in Figure 1.8(c), it is required that the nonlinear process should only occur to the light beam propagating in one direction while it has no effect on the beam travelling in the other direction. In this way, one of the counter-travelling beams experiences essentially no loss and self-phase-modulation so that the laser operation can be built up; while the other beam acquires the self-phase-modulation induced spectral broadening that is necessary for the pulse shortening in CCM lasers. In practice, it has been observed that the Fabry-Perot type has the capacity of producing shorter pulses than that of Michelson configuration whereas Michelson type is superior to the Fabry-Perot type with regard to stability [42]. For the Ring type, the interfering beams travel

along identical paths but in different direction, and so the cavity length stabilisation is not required [43]. However, the requirement of the nonlinear element is too critical to be satisfied.

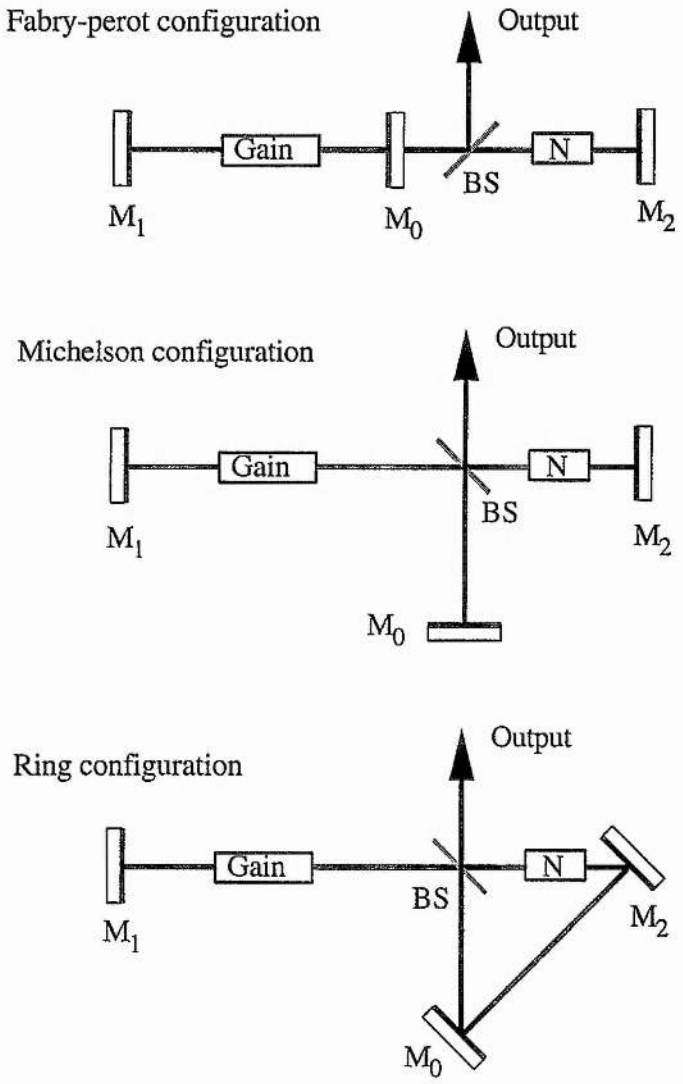

Figure 1.8. Diagrams illustrating the three types of cavity configurations.

This mode locking scheme was first implemented by Mollenauer and Stolen in 1984 in a synchronously pumped KCl:Tl colour-centre laser, whereby a Fabry-Perot cavity configuration was employed and the nonlinear element was a piece of optical fibre having anomalous group-velocity-dispersion. Compared with pulses of tens of picosecond by the synchronously pumped KCl:Tl colour-centre alone the pulse duration of this laser was dramatically reduced. The shortest pulses given by this laser were 60

fs. The pulse duration could be varied just simply by altering the length or the group-velocity-dispersion of the fibre. During this early stage of the CCM mode locked lasers, it was commonly accepted that the mechanism responsible for the mode locking process was mainly due to the pulse shortening resulting from the combined effect of self-phase-modulation and anomalous group-velocity dispersion in the solitonic fibre, and therefore it was termed the soliton laser. The interpretation was that the rejection of a temporally shortened pulse from the control cavity into the main cavity caused the generation of femtosecond pulses. However, it was verified experimentally [6] and numerically [7] that the solitonic fibre was not the only choice for this mode locking scheme, fibres with positive group-velocity-dispersion which instead of supporting solitons but broadening the pulse duration, and semiconductor amplifier could also be used to implement this mode locking process. Subsequent theoretical analyses [44.45] indicated that the key mechanism responsible for the mode locking process is the interferometric superposition between the pulses in the main cavity and that returned from the external cavity. While the self-phase-modulation in the nonlinear element is necessary for the shortening of output pulses, it provides the mean of generating new spectral components needed for mode-coupling [46]. By choosing an appreciable phase difference between the two cavities, it is possible to make the interferential feature constructive at the centre of the pulse, while in the wings it becomes destructive. In this way the centre of the pulse is amplified whereas the intensity in the wings is decreased.

The CCM mode locking scheme can be applied to lasers that are either already mode locked or in a continuous wave (CW) operation. In the former case, the main laser itself is mode locked, and the addition of the nonlinear external cavity tends to shorten and shape the pulses [for example, see Ref. 6]. In the latter case, the main laser is in a CW operation, and the CCM mode locking operates solely in a passive manner - without the need of any active gain or loss modulation of the main laser. This later case is often referred to as self-starting CCM mode locking. Self-starting CCM operation has been

demonstrated in a number of laser systems, such as Ti:Sapphire [47], Nd:YAG [48], Nd:YLF [49], Nd:Glass [50], etc.

The advantage of coupled-cavity mode locking lies in the fact that the generation of ultrashort laser pulses can be achieved in a wide range of solid state lasers. This technique is applicable to both high power as well as low power lasers and has been demonstrated in diode pumped systems [51]. Since no active modulator is required in the mode locking, the repetition of the laser can be scaled by adjusting the cavities' length. The nonlinear element can be of such elements as optical fibres (both normal and anomalous group-velocity-dispersion) [6], semiconductor amplifiers [6, 52], quantum wells [53], and semiconductor waveguides [54]. Such elements are cheaper and much easier to operate with, compared with active modulators as in actively mode locked lasers and dye saturable absorbers for passively mode locked lasers.

One drawback, however, of the coupled-cavity mode locking scheme is the requirement for a cavity length stabilisation system. To keep proper CCM mode locking the cavity length has to be controlled within a fraction of wavelength. A small variation of the cavity length, due to any external perturbation, will destroy the CCM mode locking process. Usually the stabilisation of the cavity is accomplished by a feed back loop system. In stabilisation, part of the laser output or the signal returned from the nonlinear elements is fed to an optical detector which converts the optical signal into electrical signal. The electronic signal is amplified by an electronic system, and used to drive a PZT that is attached to one of the mirrors in the cavity (usually the end mirror of the external cavity). The idea of the stabilisation scheme evolved from the observation that the time averaged power varied over a considerable range with the mirror motion [55]. A small shift of the cavity length will result in a variation in the output power level. This power variation, when detected, will be transferred to the change in the voltage applied to the PZT by the electronic system, which then will force the cavity back to its original again. The optical detector is commonly a photo diode. In case strong modulation is required a photonmultiplier can be used [54].

Kerr-lens mode locking

This mode locking technique utilises the optical Kerr effect in a laser cavity. This Kerr effect can be generated either from the gain medium itself, as in the case of Ti:Sapphire laser [15]; or a nonlinear element being inserted in the laser cavity when the optical Kerr effect of the gain medium is not sufficient, as the case of NaCl:OH- colour laser [56]. At high intensity, the self-focusing, due to the optical Kerr effect, of the laser beam causes a change of the beam diameter in the cavity. By putting an aperture in the cavity at the position where the beam diameter decreases with increasing intensity, then the self-focusing feature is transferred to an amplitude modulation. In operation, the low intensity CW radiation is blocked by the aperture, while only the intense beam (as in the case of an ultrashort pulse) is sustained. By using this technique pulses as short as 11 fs has been produced directly from a Ti:Sapphire laser [36].

1.3 Characterisation of ultrashort light pulses

The measurement of light pulses can be implemented in different methods depending on the time scale of the pulses to be measured. The most convenient and simplest approach is to use a photo diode in combination with a fast oscilloscope. However, this method is generally limited by the response time of the detector and the bandwidth of the oscilloscope. The alternative way of directly measuring the pulse duration is the electro optical streak camera which has a resolution of around 300fs at present in the research laboratory [57]. Whereas, the most widely employed method in measuring sub-picosecond pulses is the second harmonic autocorrelator, which offers the best temporal resolution.

1.3.1 Streak camera

Pioneered by Zevoisky and Franchenko [58], the streak camera has become a standard technique for the measurement of ultrashort pulses in picosecond regime [59]. With reference to Fig. 1.9 a streak camera consists of input optics, streak image tubes, electrical deflection signal generator, and readout system. The input optics is composed of a narrow input slit and an optical lens. A streak image tube typically consists of a

photocathode, acceleration mesh, electron-optical focusing lens, deflection system, and phosphor screen.

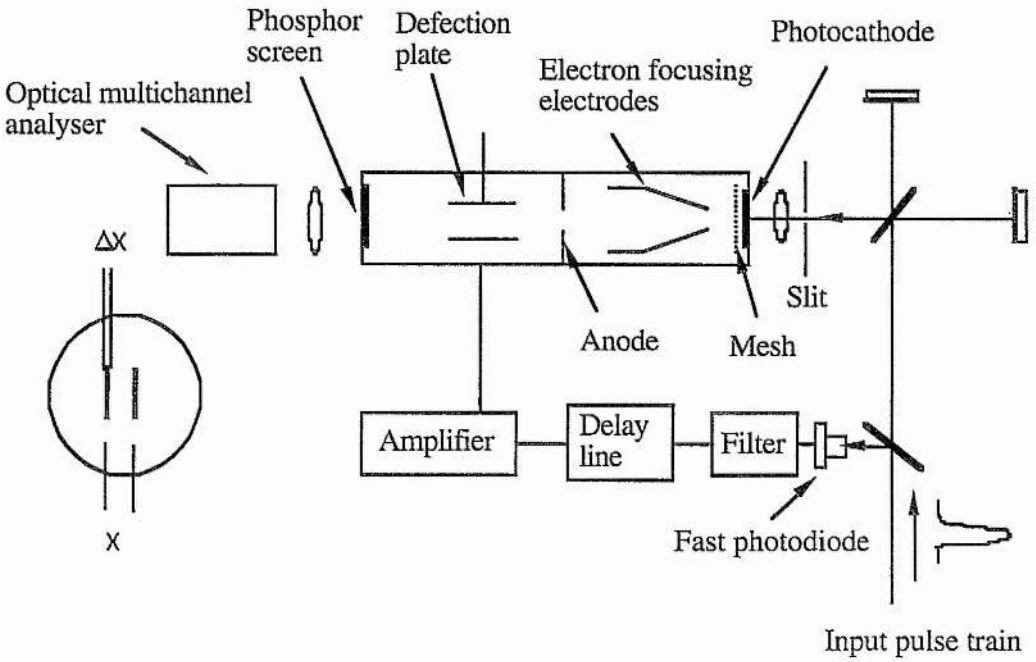

Figure 1.9. Arrangement of the synchronous operating streak camera.

For the pulse duration measurement, the pulses to be measured are first injected into either a Michelson interferometer arrangement or a glass plate with calibrated thickness, which divides a single pulse into two replicas. The time delay between the two replicas can be then easily deduced from the difference of the two arms' length in the Michelson arrangement, or from the thickness of the glass plate. These pulses are then incident on the slit and imaged by the optical lens onto the photocathode of the image tube. The slit image is converted by the photocathode into a packet of photon electrons that replicates the spatial and temporal information of the input light signal. These emitted photoelectrons are accelerated and focused by the electron optical lens onto the phosphor screen where the photoelectron signal is reconverted into a light signal for subsequent processing. To record the temporal characteristics of the electron pocket, a linear time-varying voltage ramp is applied to the deflection system which is synchronised with the arriving of the photoelectrons packet such that the photoelectrons arriving at different time are deflected correspondingly at different position on the phosphor screen. The

deflection direction is chosen perpendicular to the orientation of the slit length direction. In such way the temporal information of the input pulses is recorded by the spatial profile of the slit image onto the phosphor screen. Therefore, the temporal distribution of photoelectrons is converted to spatial distribution and a pair of "streaks" images of the pulse appears on the phosphor screen. Because the number of produced photoelectrons is proportional to the input signal intensity, the temporal profile of the pulse is recorded. The measured pulse duration can be deduced to be

$$\Delta t = \frac{\Delta x}{x}\tau \qquad (1.17)$$

where Δx is the spatial displacement of the pulse image, x is the spatial separation of the two pulse images, and $\tau$is the time delay between the two replicas.

The streak camera may be operated in either single shot or in synchronisation with the mode locked laser. In the latter case a small fraction of the signal is incident on to a biased photo diode, so that the output of the diode is a sine wave at the exact repetition frequency of the pulse trains. The sine wave or the harmonic of which is then applied to the deflection plates. By correct adjustment of the electrical delay line the electrons produced by the light pulse pass the deflection plates during the linear section of the deflecting voltage ramp.

1.3.2 Second harmonic autocorrelator

As implied by its name, this technique is based on the process of second harmonic generation in a nonlinear crystal [59-62]. Essentially two types of autocorrelator can be arranged, depending on the phase matching requirement. In Type I, the two beams incident on the crystal are polarised in the same direction. In type II, the two beams are orthogonally polarised, and the second harmonic signal is generated only when the two pulses are overlapped. Therefore, Type II gives a background-free autocorrelation trace. Type I on the other hand, allows second harmonic generation for either pulse alone, leading to autocorrelation traces having a background level. However, when the two beams are incident on the crystal in non-collinear manner, a background-free autocorrelation trace can also be obtained for Type I. In the work presented in this

thesis, all the pulse duration measurement was conducted by the Type I collinear method, and therefore is more concerned in the discussion of this subsection.

A schematic diagram of the autocorrelator is shown in Figure 1.10. In essence, it is a Michelson interferometer with a SHG crystal, a lens and a filter. The filter serves to cut the unconverted fundamental light from the crystal. The intensity of each pulse from the mode locked pulse train is split into two subcomponents by a beamspliter. These two subcomponents travel the different arms of the Michelson interferometer and are reflected back by the retroreflecters M_1 and M_2 respectively. Then they recombine and are focused onto the SHG crystal. A photomultiplier is used to detect the signal at 2ω from the SHG crystal. One of the retroreflectors, M_1, was mounted on a loudspeaker which was driven by the output of a triangle wave oscillator. The translation of the retroreflector ensures that one subcomponent pulse arrives slightly later (or earlier) at the crystal. The result is that the instantaneous intensity incident on the crystal is a function of the overlap of two subcomponent pulses. By suitable adjustment of the interferometer two arms length and correct control of the speaker's oscillation frequency and amplitude, a real-time display of the SHG autocorrelation trace can be obtained on a oscilloscope.

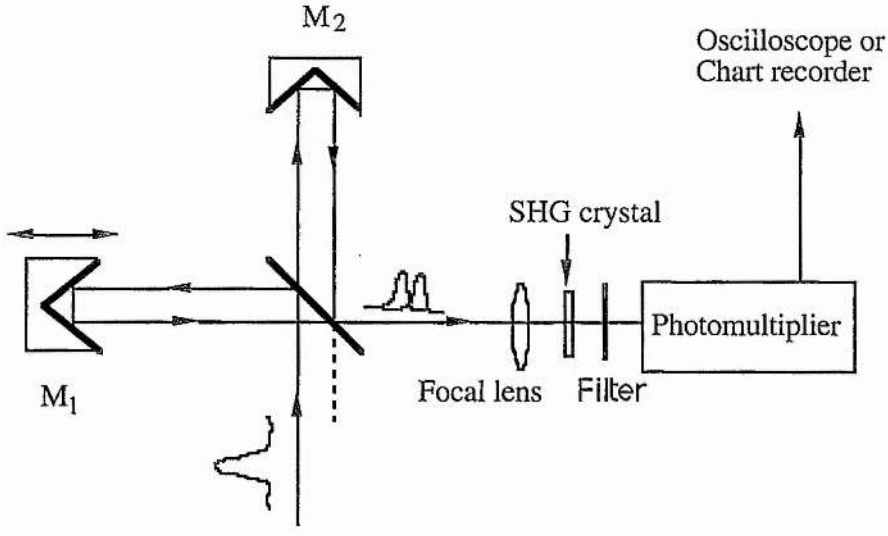

Figure 1.10. A schematic diagram of the SHG autocorrelator

The output from the photomultiplifer represents the correlation of the two sub-pulses, the localised value of which can be expressed as

$$I_d(\tau) = G_2(\tau) + s(\tau) \tag{1.21}$$

where $G_2(\tau)$ is the second-order intensity correlation function, $s(\tau)$ is the rapidly varying interference term related with $\cos(\omega\tau)$ and $\cos(2\omega\tau)$. If the response time of the detector system is chosen to be too slow to follow the constructive and destructive feature (which is dependent on both the oscillation frequency and amplitude of the speaker) of the interferometric autocorrelation traces, the second term $s(\tau)$ will average to zero, and only $G_2(\tau)$ is recorded. This case is commonly referred as intensity autocorrelation. The intensity correlation function can be expressed as

$$G_2(\tau) = 1 + \frac{2\int_{-\infty}^{\infty} I(t)I(t+\tau)dt}{\int_{-\infty}^{\infty} I^2(t)dt} \tag{1.22}$$

where $I(t)$ is the pulse intensity. It can be easily deduced that when the two sub-pulses are not overlapped the intensity correlation function $G_2(\tau)$ equals unity, while as the two sub-pulses are overlapped at the centre of the pulse the intensity correlation function $G_2(\tau)$ is 3, i.e.

$$\tau >> \Delta\tau \Rightarrow G_2(\tau) = 1$$
$$\tau = 0 \Rightarrow G_2(\tau) = 3$$

where $\Delta\tau$ is the pulse width being measured. As can be seen that the intensity correlation has a peak to background ratio of 3 : 1. The presence of the background in conjunction with the shape of the autocorrelation traces offers a useful and convenient check for the quality of mode locked laser pulses. Figure 1.11 provides autocorrelation traces for three different situations of light sources. Figure 1.11(a) represents the autocorrelation of well-defined mode locked pulses, the peak-background ratio of 3 : 1 is clearly explicated. Figure 1.11(b) is the autocorrelation of a noise burst corresponding to that of free-running laser output. The peak-shoulder-background ratio of which is 3:2:1. Figure 1.11(c) represents the autocorrelation of a CW radiation, a peak-background ratio of 3 : 2 is obtained.

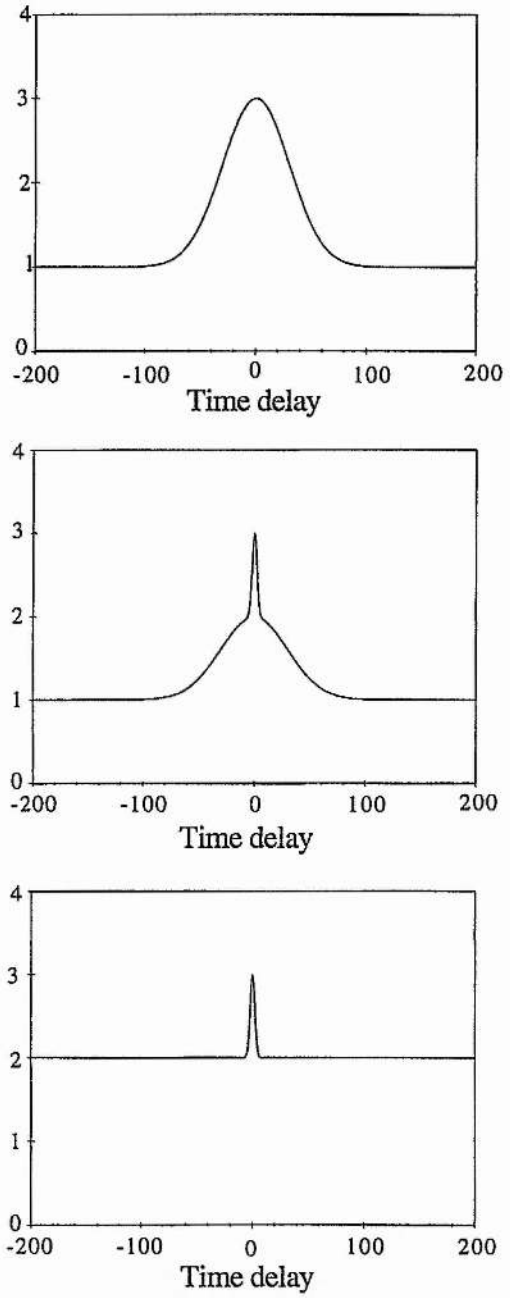

Figure 1.11. Intensity autocorrelations for (a) mode locked pulses, (b) noise burst, and (c) CW radiation.

The determination of actual pulse width $\Delta\tau_p$, from the recorded autocorrelation traces requires an assumption of the pulse profile. The actual pulse width $\Delta\tau_p$ and the autocorrelation trace width Δt are related through a constant k

$$k = \frac{\Delta t}{\Delta\tau_p} \tag{1.23}$$

the value of which depends on the pulse profile. Table 1.1 gives the expression and the value of k for three standard pulse shapes. Also shown for each case is the bandwidth-duration product $\Delta\nu\Delta\tau$ for bandwidth limited pulses. The validity of the pulse shape assumption can be cross-checked by comparing the experimentally measured bandwidth-duration product with the calculated value. If the bandwidth-duration product is larger than that calculated, frequency chirped pulses might be inferred. A smaller one, compared with the calculated value, might imply that the pulse profile is not symmetric. For pulses that are not bandwidth limited, the interferometric autocorrelation, as will be discussed later, provides the frequency chirp information. For asymmetric pulses, a different autocorrelation technique: cross-correlation, can be used [63].

Table 1.1 Correction factor and bandwidth-duration products (at bandwidth limited situation) for three standard pulse shapes.

Pulse type	I(t)	k	$\Delta\nu\Delta\tau_p$
Gaussian	$\exp(t^2)$	$\sqrt{2}$	0.414
Sech2	$\sec h^2 t$	1.543	0.315
Symmetric two-side exp	$\exp(-2\|t\|)$	2.421	0.142

As the scanning speed of the shaking mirror is reduced or alternatively, the response time of the electronic detection system is increased, it is possible to resolve the interference feature arising from the second term $s(\tau)$ in equation (1.21). In this case, the second-order autocorrelation is given by [64-66].

$$G_2(\tau)+s(\tau)=1+[2+\cos(2\omega\tau)]\times\frac{\int_{-\infty}^{\infty}I(t)I(t+\tau)dt}{\int_{-\infty}^{\infty}I^2(t)dt} +2\cos(\omega\tau)\times\frac{\int_{-\infty}^{\infty}\sqrt{I(t)I(t+\tau)}\times[I(t)+I(t+\tau)]dt}{\int_{-\infty}^{\infty}I^2(t)dt} \tag{1.24}$$

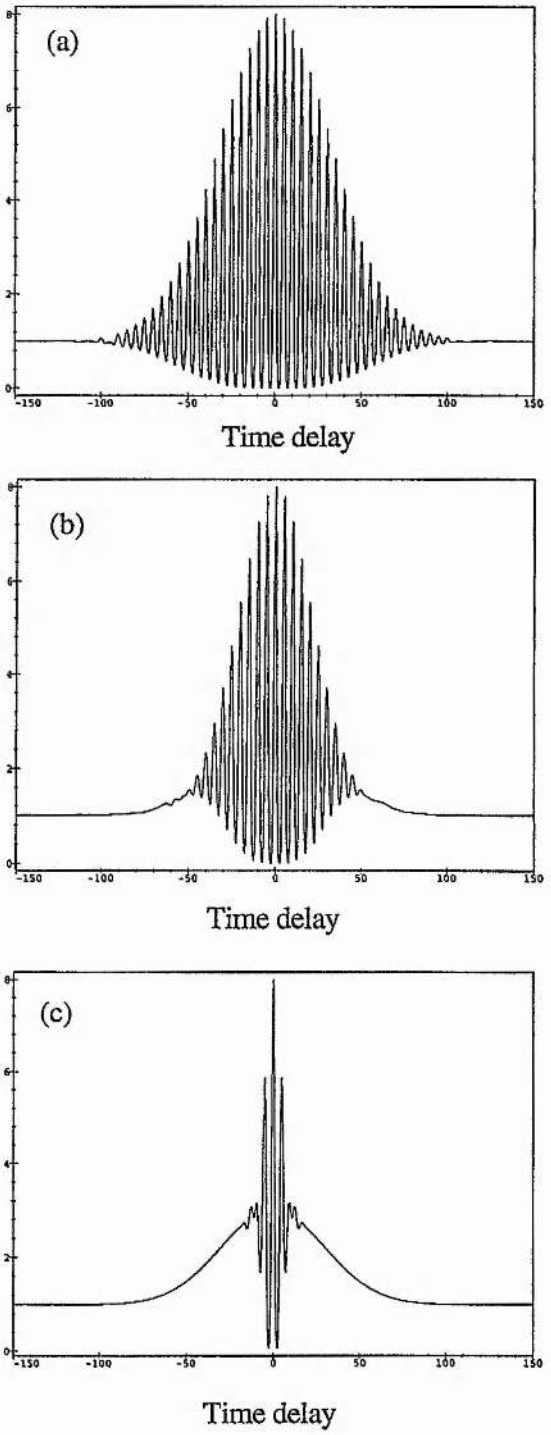

Figure 1.12. Interferometric autocorrelations for 70 fs pulses of (a) bandwidth-duration product limited; (b) chirped with chirp parameter C=2; and (c) chirped with C=15.

It is not difficult to show that the peak-background ratio of the interferometric autocorrelation is 8:1. The fringes have maxima when $\omega\tau = 2n\pi$ and minima at

$\omega\tau = (2n+1)\pi$. The time delay between the two maximal corresponds to one optical cycle of the carrier, which is $2\pi / \omega$. This feature of the interferometric autocorrelation can be used to calibrate the time scale on the oscilloscope screen by counting the number of the fringes in each division. Figure 1.12 shows the interferometric autocorrelations for three pulses with different chirp parameters. Figure 1.12(a) represents the autocorrelation of chirp-free pulses. As can be seen a well-defined autocorrelation trace is generated. Figure 1.12(b) and Figure 1.12(c) show the autocorrelation traces when frequency chirp is present in the pulses. It can be seen that the visibility at the wings is lost, and it is a clear indication of the presence of frequency chirp.

In practice, both the intensity and the interferometric autocorrelations along with the corresponding spectral width of the pulse are taken all together, so that a cross-check can be conducted. The intensity autocorrelation can not give any phase information about the pulses, but it provides the mean for the determination of the pulse duration. While the interferometric autocorrelation can present the frequency chirp information of the pulses. The bandwidth duration product indicates the degree of chirp.

1.4. Pulse propagation

Pulse propagation in optical waveguides, such as fibres, has been extensively studied [67-84], mainly promoted by the motivation of possible exploitation in optical communication and various practical applications. Pulses essentially manifest itself in two ways when propagating in a nonlinear medium, one is the variation in pulse width, and the another is the shift in frequency. The group-velocity-dispersion of the medium gives rise to the process of temporal broadening or shortening of the pulse. The nonlinear effects, however, resulted in the shift of the pulse frequency or the extension of the spectral width. In optical fibres the long interaction length and the confined core area make the observation of various nonlinear effects become much easier. Nonlinear effects such as self-phase-modulation [69,70], Modulation instability [71-73], Four-wave-mixing [74-77], Raman scattering [78-84], etc. have been observed. In this section, a brief introduction of such linear and nonlinear effects will be presented.

1.4.1 Linear propagation

The material dispersion, defined as the variation of refractive index of the material with respect to the wavelength of incident waves, is generally described through the Sellmier equation given by

$$n^2(\lambda)-1=\sum_{j=1}^{k}\frac{B_j\lambda^2}{\lambda^2-\lambda_j^2} \tag{1.25}$$

where n represents the refractive index, λ is the wavelength, and λ_j is the jth resonant wavelength of the material, B_j is a coefficient related with the jth resonance. λ_j and B_j can be determined by fitting the experimentally obtained $n(\lambda)$.

The large spectral bandwidth associated with ultrashort light pulses makes the dispersion feature become a detrimental factor in optical waveguides (fibres). Even without any nonlinear effect, the dispersion alone might severely change the temporal feature of the pulse. In this case, the description of the pulse propagation by using the propagation constant $\beta(\omega)$, seems more straightforward, and therefore is more frequently used. The propagation constant $\beta(\omega)$ can be expanded into a Taylor series, which is

$$\beta(\omega)=\beta(\omega_0)+\beta'\times(\omega-\omega_0)+\frac{1}{2}\beta''\times(\omega-\omega_0)^2+\frac{1}{6}\beta'''\times(\omega-\omega_0)^3+\cdots\cdots \tag{1.26}$$

where ω_0 is the central frequency of the pulse, and

$$\beta^m=\left.\frac{d^m\beta}{d\omega^m}\right|_{\omega=\omega_0} \tag{1.27}$$

The coefficients β, β', and β'' in the first three terms are related to the phase velocity, group velocity, and group velocity dispersion respectively. The physical meaning of which is summarised as follow

$$\beta=\beta(\omega)\big|_{\omega=\omega_0}=\frac{\omega_0}{v_\phi(\omega_0)}=\frac{\omega_0}{Phase\ \ velocity}$$

$$\beta'=\left.\frac{d\beta}{d\omega}\right|_{\omega=\omega_0}=\frac{1}{v_g(\omega_0)}=\frac{1}{Group\ \ velocity}$$

$$\beta''=\left.\frac{d^2\beta}{d\omega^2}\right|_{\omega=\omega_0}=\frac{d}{d\omega}\left(\frac{1}{v_g(\omega_0)}\right)=Group\ \ velocity\ \ dispersion$$

Some useful expressions relating the above coefficients to the refractive index and wavelengths are listed below

$$\begin{aligned}\beta &= \frac{2\pi\lambda}{c} \\ \beta' &= \frac{1}{c}\left(n - \lambda\frac{dn}{d\lambda}\right) \\ \beta'' &= \frac{\lambda^3}{2\pi c^2}\frac{d^2n}{d\lambda^2} \\ \beta''' &= \frac{-\lambda^4}{4\pi^2c^3}\left(3\frac{d^2n}{d\lambda^2} + \lambda\frac{d^3n}{d\lambda^3}\right)\end{aligned} \tag{1.28}$$

For most optical media, the group velocity dispersion β'' is positive in the visible region but changes sign in the near infrared. The wavelength at which the sign is altered is called zero-dispersion wavelength λ_D. For fused silica, zero GVD occurs at a wavelength of 1.3 μm. At zero GVD, pulses propagate in a medium essentially with no variation in pulse shape and duration. However, in such case the higher dispersion (for example β''') might take action. Commonly, the case of $\beta'' > 0$ is specified as normal dispersion, while the case of $\beta'' < 0$ is referred to as anomalous dispersion.

In some cases, the GVD is described through D, which is defined as the pulse spreading per unit length and per unit wavelength, and is related with β'' through the expression

$$D = -\frac{2\pi c}{\lambda^2}\beta'' \tag{1.29}$$

Because of the GVD, pulses propagating in a solely dispersive medium will experience temporal broadening no matter whether the sign of the GVD is positive or negative. In the region of normal GVD, where $\beta'' > 0$, the longer wavelength components of the pulse propagate faster than the shorter wavelength components, and therefore the longer wavelength components moves to the front part of the pulse while the shorter wavelength components are dragged to the rear part of the pulse. As a result, a positive frequency chirp (up-chirp) is built up along the pulse profile and the pulse becomes temporally broadened. At the region of anomalous GVD, where $\beta'' < 0$, temporal broadening of the pulse will also happen but which is associated with a

negative frequency chirp (down-chirp). A schematic diagram illustrating three pulses with different chirp parameters is shown in Figure 1.13, where (a) shows a chirp-free pulse, (b) is an up-chirped pulse, and (c) represents a down chirped pulse.

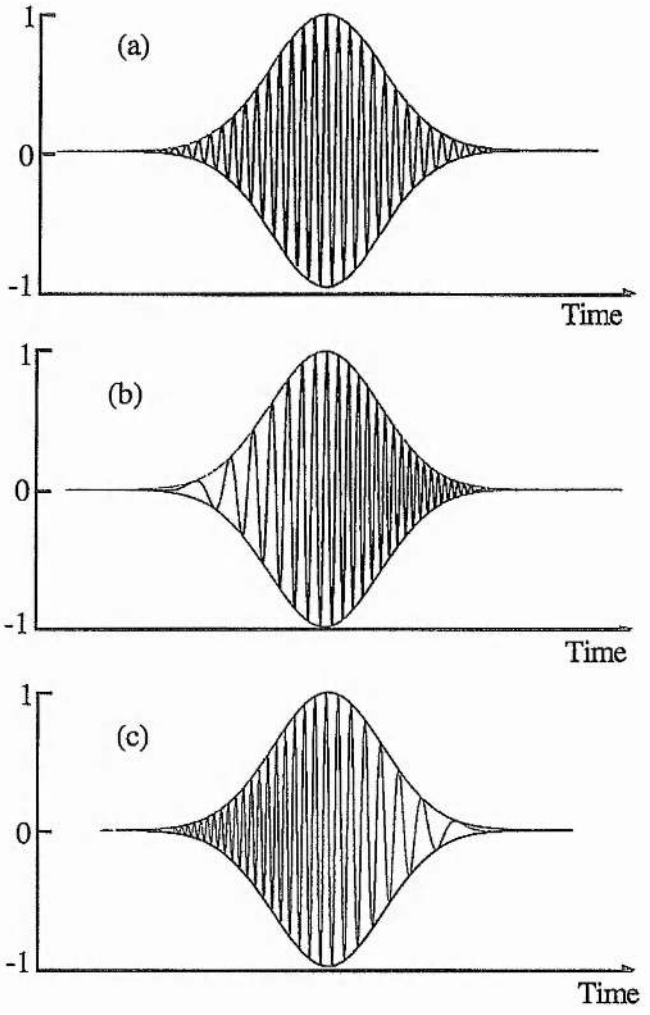

Figure 1.13. Schematics illustrating three pulses with different chirp parameters. (a) Chirp-free pulse; (b) Up-chirped pulse; (c) Down-chirped pulse.

If a Gaussian pulse is assumed, the pulse duration $\Delta\tau_{out}$ (FWHM), after passing a distance z through the dispersive medium is given by the expression

$$\Delta\tau_{out} = \Delta\tau_{in}\sqrt{\left(1+2\sqrt{\ln 2}\frac{C\beta'' z}{\Delta\tau_{in}^2}\right)^2+\left(2\sqrt{\ln 2}\frac{\beta'' z}{\Delta\tau_{in}^2}\right)^2} \qquad (1.30)$$

where C is the frequency chirp parameter, presented in the expression of the pulse field in a manner of

$$E(t) = \exp\left(-\frac{(1+iC)}{2} \times \frac{t^2}{T_{in}^2}\right)\exp(-i\omega_0 t) \tag{1.31}$$

with T_{in} being the half-width at 1/e-intensity point of the incident pulse. For up-chirped pulses, $C > 0$, down-chirped pulses, $C < 0$, and chirp-free pulses, $C = 0$. The relation between $\Delta\tau$ (Full width at half-maximum, FWHM) and T (half-width at 1/e-intensity point) is given as follow

Gaussian $$\Delta\tau = 2(\ln 2)^{1/2} T = 1.665T \tag{1.32}$$

Sech2 $$\Delta\tau = 2\ln(1+\sqrt{2})T = 1.763T \tag{1.33}$$

If the pulse is initially unchirped, i.e. $C = 0$, equation (1.30) becomes

$$\Delta\tau_{out} = \Delta\tau_{in}\sqrt{1+\left(\frac{4\ln 2}{\Delta\tau_{in}^2}\beta'' z\right)^2} = \Delta\tau_{in}\sqrt{1+\left(\frac{z}{z_D}\right)^2} \tag{1.34}$$

where

$$z_D = \frac{T_{in}^2}{\beta''} = \frac{\Delta\tau_{in}^2}{4\ln 2} \times \frac{1}{\beta''}, \tag{1.35}$$

defined as the dispersion length. From equation (1.34), it can be seen that for a given length of the dispersive medium, shorter pulse broadens faster because of a smaller dispersion length associated. At $z = z_D$, an Gaussian pulse broadens by a factor of $\sqrt{2}$.

Equation (1.30) shows that when the pulse chirp parameter C and the GVD parameter β'' of the medium have the same sign, i.e. $\beta'' C > 0$, the pulse broadens monotonically with z; if $\beta'' C < 0$, it first experiences a temporal narrowing until a minimum value and then broadens again. This latter case can be used for compression of chirped pulses by passing the pulse through an appropriate length of dispersive medium with opposite sign of β''. The length required for the optimum compression is given by

$$z_{opt.} = \frac{C}{1+C^2} z_D \tag{1.36}$$

The pulse duration at the optimum length is expressed as

$$\Delta\tau_{\min} = \frac{\Delta\tau_{in}}{(1+C^2)^{1/2}} \tag{1.37}$$

In experimental research, it is customary to use the bandwidth-duration product $\Delta\nu\Delta\tau$ to show the degree of chirp imposed on a pulse. By doing a Fourier transform of the optical field and some simple deduction, the relation between the bandwidth-duration product $\Delta\nu\Delta\tau$ and the chirp parameter C can be expressed as follows

$$P_{\Delta\nu\Delta\tau} \equiv \Delta\nu\Delta\tau = \frac{2\ln 2}{\pi}\sqrt{1+C^2} \tag{1.38}$$

Therefore, the optimum length for pulse compression and minimum pulse duration obtained are re-expressed as

$$z_{opt.} = z_D\left(\frac{2\ln 2}{\pi P_{\Delta\nu\Delta\tau}}\right)\sqrt{1-\left(\frac{2\ln 2}{\pi P_{\Delta\nu\Delta\tau}}\right)^2} \tag{1.39}$$

$$\Delta\tau_{mim} = \frac{2\ln 2}{\pi}\frac{\Delta\tau_{in}}{P_{\Delta\nu\Delta\tau}} \tag{1.40}$$

1.4.2 Nonlinear propagation

The interaction between electromagnetic fields and matter is commonly through the relation of the induced polarisation $\vec{P}$ with respect to the applied field $\vec{E}$. Previous to the invention of lasers, it was reasonable to consider that a linear relationship held very well between the induced polarisation and the electromagnetic fields, i.e.

$$\vec{P} = \varepsilon_0\chi^{(1)}\vec{E} \tag{1.41}$$

where ε_0 is the vacuum permitivity, $\chi^{(1)}$ is the linear susceptibility of the material. However, in the presence of high intensity optical fields, such linear response is no longer holds, but satisfies the more general relation [78]

$$\vec{P} = \varepsilon_0\left[\chi^{(1)}\vec{E} + \chi^{(2)}\vec{E}\vec{E} + \chi^{(3)}\vec{E}\vec{E}\vec{E} + \cdots\right] \tag{1.42}$$

where $\chi^{(j)}$ is the jth order susceptibility which is a tensor of the rank of j+1, with $\chi^{(1)}$ being the dominant contribution to the polarisation. In theory, most of the nonlinearity can be derived from this equation. The linear refractive index and the attenuation

coefficient is related to the linear susceptibility $\chi^{(1)}$. The second-order susceptibility $\chi^{(2)}$ is responsible for such effects as second-harmonic generation and sum-frequency generation. However the second-order susceptibility $\chi^{(2)}$ becomes zero for a medium that has inversion symmetry, i.e. isotropic. For the study in this thesis, apart from the KDP crystal used for the autocorrelator most of the nonlinear media concerned, such as optical fibres and semiconductor waveguides, have a symmetric feature, and therefore $\chi^{(2)}$ term vanishes. The third-order term $\chi^{(3)}$ is responsible for phenomena such as third-harmonic generation, four-wave-mixing, self-phase-modulation, self-focusing, and two-photon-absorption.

Nonlinear refractive index

For an isotropic material, such as fused silica where $\chi^{(2)}=0$ and if neglecting terms higher than $\chi^{(3)}$, the refractive index of the medium becomes intensity dependent and is given by the relation

$$n = n_0 + n_{2I} I \tag{1.43}$$

where n_0 is the refractive index at low intensity level, I is the optical intensity of the incident signal, and

$$n_{2I} = \frac{12\pi^2}{n_0 c}\chi^{(3)} \tag{1.44}$$

is the so-called nonlinear optical Kerr coefficient. For fused silica, the nonlinear optical Kerr coefficient $n_{2I} = 3.2 \times 10^{-16} cm^2/W$.

Self-phase modulation (SPM)

Self-phase modulation arises from the combination of nonlinear refractive index and a time-varying amplitude of the incident field [69, 70]. Since the refractive index depends on the optical intensity, the phase shift of an optical field after propagating through a distance z in an optical medium is then given by

$$\phi(t) = \omega_0 t - kz = \omega_0 t - \frac{2\pi}{\lambda} n_0 z - \frac{2\pi}{\lambda} n_{2I} I z \tag{1.45}$$

For an optical pulse, the intensity varies over the pulse envelope, i.e. it changes with time. Thus, the instantaneous frequency of the pulse at a distance z is given by

$$\omega(t) = \frac{\partial \phi}{\partial t} = \omega_0 - \frac{2\pi}{\lambda} n_{2I} z \frac{\partial I}{\partial t} \tag{1.46}$$

It can be seen that the instantaneous frequency of the light pulse differs across its envelope from the central frequency ω_0 by

$$\delta\omega(t) = -\frac{2\pi}{\lambda} n_{2I} z \frac{\partial I}{\partial t} \tag{1.47}$$

Because the instantaneous intensity at the leading edge of the pulse increases with time, but decreases in time at the trailing edge, the leading edge of the pulse experiences a "red" shift while the trailing edge of the pulse sees a "blue" shift. This can also be viewed as frequency chirp induced by the SPM. As the pulse travels further, the chirp becomes greater.

If an input pulse with a Gaussian profile ($I = I_0 \exp\left[-(t/T)^2\right]$) is assumed, as shown in Figure 1.14 (a), then the instantaneous frequency shift is given by

$$\begin{aligned} \partial\omega(t) &= \frac{2\pi}{\lambda} n_{2I} z \left\{ 2I_0 \frac{t}{T^2} \exp\left[-(t/T)^2\right] \right\} \\ &= \frac{2\phi_{\max} t}{T^2} \exp\left[-(t/T)^2\right] \end{aligned} \tag{1.48}$$

where $\phi_{\max} = \frac{2\pi}{\lambda} n_{2I} z I_0$, is the maximum phase shift; T represents the half width of the pulse at $1/e$ intensity point. The full-width at half-maximum (FWHM) $\Delta\tau$, is related with T by the relation $\Delta\tau = \left(2\sqrt{\ln 2}\right)T$ for Gaussian pulses. Figure 1.14(b) shows the instantaneous frequency shift associated with the Gaussian pulse. As we can seen, over the central region of the pulse, the chirp is approximately linear and is positive (i.e. frequency increases with time). The frequency in the leading edge of the pulse is down shifted while in the trailing edge is up chirped. The maximum frequency shift happens at the point where $t/T = 1/\sqrt{2}$, and which is given by

$$\begin{aligned} \partial\omega_{\max} &= \pm\frac{2\phi_{\max}}{T}\sqrt{\frac{1}{2e}} \\ &= \pm\frac{2\phi_{\max}}{\Delta\tau}\sqrt{\frac{2\ln 2}{e}} \end{aligned} \tag{1.49}$$

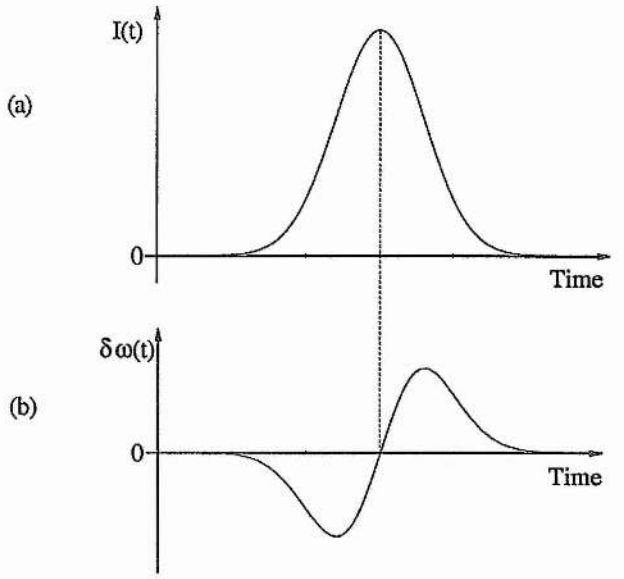

Figure 1.14. Diagram showing (a) a Gaussian pulse profile; (b) frequency shift due to the SPM.

Modulation instability

Modulation instability (MI) is a nonlinear process resulting from the interplay between the nonlinearity and the dispersion effect. It has been studied in such diverse fields as fluid dynamics, plasma physics, and also in optical fibres. In the context of optical fibres, the nonlinearity comes from the optical Kerr effect, and the modulation instability requires an anomalous group velocity dispersion. The modulation instability manifests itself, in the time domain, as break-up of the input pulse (or CW radiation) into a train of well-separated pulses. In the frequency domain, sidebands spectra are generated at both side of the input carrier frequency. The interaction among these equally spaced spectral components gives rise to the generation of a pulse train.

The maximum gain occurs at frequencies that are separated from the carrier frequency by $\pm\Omega_c$ on both sides of the input spectrum. This separation is given by the expression [71]

$$\Omega_c = \left[\frac{2\gamma P_0}{|\beta''|}\right]^{1/2} \tag{1.50}$$

where P_0 is the peak power inside the fibre, β'' is the GVD of the fibre, and $\gamma = n_2\omega / cA_{eff}$, with A_{eff} being the effective mode area of the laser beam. In practice, by knowing the peak power inside the fibre and the experimentally measured sideband

separation Ω_c, the GVD of the fibre can be deduced. This will be presented in the experiment in Chapter 6.

The maximum gain of MI at Ω_c is independent of fibre dispersion, it increases linearly with the input power. This can be expressed as

$$g_{\max} = 2\gamma P_0 \tag{1.51}$$

In practice, the MI can be achieved by perturbation of the pump signal in the way that a small signal at frequency $\omega_0 \pm \omega_c$ co-propagates together with the pump signal [72]. In this case the small signal acts as a probe for the MI process. It can also be initiated from the noise signal in picosecond pulses [73].

The MI, in fibre communication systems, is an undesired effect. However it was proposed by Hasagawa [73] that by utilising the MI in optical fibres, short optical pulses with ultrahigh repetition rate can be produced. This would be very useful in ultrahigh-bite-rate communication, optical computing systems, and many other scientific areas.

Four-wave mixing

Four-wave mixing is a parametric process that involves the interaction among four optical waves via the third-order nonlinear susceptibility. One case is the third-harmonic generation in which three photons at frequency ω transfer their energy to a single photon at frequency 3ω. However in optical fibres it is generally difficult to satisfy the phase-matching condition for such process to occur in high efficiency. One particular case that has been extensively studied in optical fibres involves the simultaneous creation of two photon at frequencies ω_3 and ω_4 through the annihilation of two photons at frequencies ω_1 and ω_2 [74-77]. The energy conservation requires that

$$\omega_3 + \omega_4 = \omega_1 + \omega_2 \tag{1.52}$$

The phase-matching requirement for this process to occur is that

$$\Delta K = K_3 + K_4 - K_1 - K_2 = 0 \tag{1.53}$$

For the degenerate case where $\omega_1 = \omega_2 = \omega_0$, equation (1.52) becomes

$$2\omega_0 = \omega_3 + \omega_4 \tag{1.54}$$

Physically, a strong pump wave at ω_0 creates two side bands located symmetrically at frequencies ω_3 and ω_4 with a frequency shift given by

$$\Omega = \omega_0 - \omega_3 = \omega_4 - \omega_0 \tag{1.55}$$

where the relation $\omega_3 < \omega_4$ has been assumed. In general, the low-frequency side band at ω_3 and the high-frequency side band at ω_4 are referred to as the Stokes and anti-Stokes bands and denoted by ω_s and ω_a respectively.

Raman Scattering

Stimulated Raman scattering is a nonlinear process that is broadly defined as the interaction of incident light with the molecular vibration modes in a medium [78]. Essentially, a photon at frequency ω_P is annihilated and a photon at the Stokes frequency $\omega_s = \omega_P - \omega_v$ is generated, leaving the molecular (or atoms) in an excited state with energy $\hbar\omega_v$. This process is illustrated in Figure 1.15.

In silica fibres, the Raman process has been extensively studied, and the exploitation of which has been successfully demonstrated [79, 80]. Because of the amorphous nature of the fused silica the molecular vibration frequencies spread out into bands which overlap and create a continuum. Therefore, the Raman gain in silica fibres extends continuously over a broad spectral range.

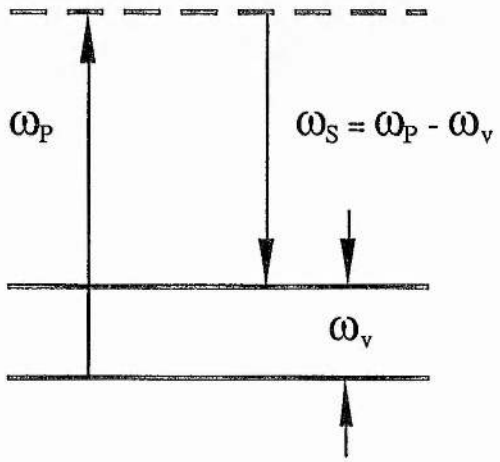

Figure 1.15. Energy structure representing the Raman scattering process.

The intensity of the Stokes signal after a distance z can be expressed by the relation

$$I_s(z) = I_p(0)e^{gI_p z} \tag{1.56}$$

where g is Raman gain coefficient, Ip is the pump intensity. In principle, there is no actual threshold power level for Raman scattering to happen. However, due to the exponential nature of the Raman gain, there is little difference in pump intensity between negligible Raman generation and nearly total conversion. A threshold condition was defined by Smith [81], at which the Stokes power is equals to that of pump,

$$P_{th} = \frac{16A}{gL} \tag{1.57}$$

where A is the effective core area of the fibre, g is the Raman gain, and L is the interference length. For fused silica, the Raman coefficient g_R as a function of the frequency shift at a wavelength of 1.5 μm is shown in Figure 1.6 [82]. It can be seen that the Raman gain coefficient g_R extends over a large frequency range up to 40 THz with a dominant peak at 13.2 THz.

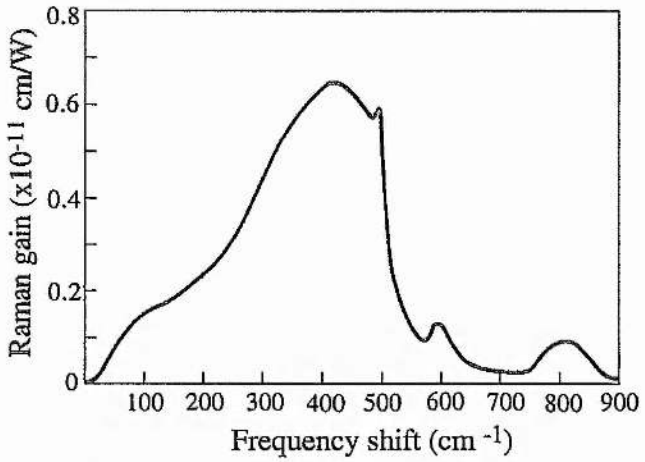

Figure 1.16. Raman gain spectrum in fused-silica (See Ref. 82).

For femtosecond pulses propagating in the anomalous GVD regime of optical fibres, a Raman process termed soliton self-frequency-shift [83], is encountered. Phenomenally, this effect manifests as a continuous downshift of the incident pulse

frequency. It was explained by Gordon [84] that the physical mechanism responsible for such down-frequency shift is due to the Raman effect. Because of the broad, continuous Raman gain spectrum in silica fibres, it is possible that the shorter wavelength components of the incident pulse acts as a Raman pump for the longer wavelength components. Thus a continuous downshift of the pulse frequency occurs when the pulse propagates along the fibre. Theoretical analysis has indicated that the amount of frequency shift per unit length is inversely proportional to the fourth power of the pulse duration, which can be expressed as [84]

$$\frac{d\nu_0}{dz} \propto \frac{1}{\Delta t^2} \tag{1.58}$$

It can be seen that the frequency shift is larger for shorter pulses. This is also understandable in terms of spectral width of the incident pulses, as that the shorter pulses have a broader spectrum.

1.5 Summary

In this chapter, an introduction on the generation, characterisation, and propagation of ultrashort laser pulses has been presented. Different mode-locking techniques have been outlined. A general description on the optical streak camera and the second-harmonic autocorrelator has been provided. Nonlinear effects, including the self-phase-modulation, modulation instability, four-wave mixing, and Raman scattering, etc. have been discussed.

References

1. *Ultrafast Phenomena* VII, C. B. Harris, E. P. Ippen, G. A. Mourou, and A. H. Zewail, eds. (Springer-Velay, Berlin, 1990).
2. *Ultrafast Phenomena* VIII, Technical Digest Series Vol.7, 1994, (Danapoint, Coliforia, 1994).
3. *Ultrashort Laser Pulses and Applications,* W. Kaiser, ed. (Springer-Verlag, Berlin, 1988).
4. E. P. Ippen, Appl. Phys. B 58, 159 (1994).
5. W. Sibbett, R. S. Grant, D. E. Spence, Appl. Phys. B 58, 171 (1994).
6. P. N. Kean, X. Zhu, D. W. Crust, R. S. Grant, N. Langford, and W. Sibbett, Opt. Lett. 14, 39 (1989).
7. K. J. Blow, and B. P. Nelson, Opt. Lett. 13, 1026 (1988).
8. L. F. Mollenauer and R. H. Stolen, Opt. Lett. 9, 13 (1984).
9. L. F. Mollenauer and R. H. Stolen, In *Ultrafast Phenomena IV* (Springer-Verlag, 1984), Page 2-6.
10. D. E. Spence, and W. Sibbett, J. Opt. Soc. Am. B 8, 2053 (1991).
11. J. Goodberlet, J. Jacobson, J. G. Fujimoto, P. A. Schulz, T. Y. Fan, Opt. Lett. 15, 553 (1990).
12. J. M. Liu, J. K. Chee, Opt. Lett. 15, 685 (1990).
13. F. Krausz, Ch. Spielmann, T. Brabec, E. Wintner, A. J. Schimidt, Opt. Lett. 15, 737 (1994).
14. K. Tamuro, C. R. Doerr, L. E. Nelsson, H. A. Haus, and E. P. Ippen, Opt. Lett. 19, 46 (1994).
15. D. E. Spence, P. N. Kean, and W. Sibbett, Opt. Lett. 16, 42 (1991).
16. R. L. Fork, C. H. Brito Cruz, P. C. Berker, and C. V. Shank, Opt. Lett. 12, 483 (1987).
17. G. P. Agrawal, *Nonlinear fibre optics,* (Academic Press, Boston, 1989).
18. S. R. Friberg, A. M. Weiner, Y. Silberberg, B. G. Sfez, and P. S. Smith, opt. Lett. 13, 904 (1988).
19. K. Al-hemyari, J. S. Aitchison, C. N. Ironside, G. T. Kennedy, R. S. Grant, and W. Sibbett, Electro. Lett. 28, 1090 (1992).
20. A. Miller, and W. Sibbett, J. Mod. Opt. 35, 1871 (1988).
21. L. F. Mollenauer and K. Smith, opt. Lett. 13, 675 (1988).
22. C. Lin, *Fiber Raman Lasers,* In *Tuneable Lasers* [Applied Physics, 59, 1987; Springer-Verlag], eds. Mollenauer and J. C. White,
23. C. C. Yang, A. Villeneuve, G. I. Stegeman, C. H. Lin, H. H. Lin, Electron. Lett. 29, 37 (1993).
24. M. Jr. DiDomenico, J. Appl. phys. 35, 2870 (1964).
25. H. W. Mocker, and R. J. Collins, Appl. Phys. Lett. 7, 270 (1965)
26. G. C. H. New, IEEE J. Quantum Electron. QE-10, 115 (1974).
27. A. E. Siegman, *Lasers,* (University Science Books, Mill Valey, California).

28. D. J. Bradly, *Methods of Generation*, Pape 17-81, In *Ultrashort light pulses,* (Topics in Applied Physics, Vol 18, Springer-Verleg), ed S. L. Shapiro, Berlin.
29. P. W. Smith, Proc. IEEE 58, 1342 (1970).
30. D. J. Bradly and G. C. H. New, Proc. IEEE 62, 313 (1974).
31. A. J. Demaria, Prog. Opt. IX, 33 (1971).
32. W. Koechner, Solid-state laser engineering, Third edition, (Springer series in Optical Science, Springer-Verley, 1992).
33. P. W. Smith, A. M. Weiner, *Mode-locking of lasers,* In Encyclopaedia of *Lasers and Optical technology,* (Academic Press, 1991), ed Robert A. Meyers.
34. D. Burns, Phd Thesis, (University of St. Andrews, 1991).
35. A. J. DeMaria, D. A. Atetsen, H. Heyman, Appl. Phys. Lett. 8, 22 (1966).
36. M. T. Asaki, C. P. Huang, D. G. Harvey, Z. Zhou, H. C. Kapteyn and M. Murnane, Opt. Lett. 18, 977 (1993)
37. R. L. Fork, C. V. Shank, R. Yen, and C. A. Hirlimann, IEEE J. Quantum Electron. QE-19, 500 (1983).
38. G. H. C. New, opt. Commun. 6, 188 (1972).
39. W. Sibbett, "Hybrid and passive mode locking in coupled-cavity lasers," in *Ultrafast Phenomena* VII, C. B. Harris, E. P. Ippen, G. A. Mourou, and A. H. Zewail, eds. (Springer-Velay, Berlin, 1990).
40. J. Mark, L. Y. Liu, K. L. Hall, H. A. Haus, E. P. Ippen, opt. Lett. 14, 28 (1989).
41 M. Morin, M. Piché, Opt. Lett. 14, 1119 (1989).
42. R. S. Grant and W. Sibbett, Opt. Commun. 86, 177 (1991).
43. T. F. Corruthers and I. N. Duling III, Opt. Lett. 15, 804 (1990).
44. F. Ouellette and M. Piché, Can. J. Phys. 66, 903 (1988).
45. E. P. Eppen, H, A, Haus, and L. Y. Liu, J. Opt. Soc. Am B 6, 1736 (1989).
46. W. Sibbett, Inst. Phys. Conf. Ser. 126, 1 (1992).
47. J. Goodberlet, J. Wang, and J. G. Fujimoto, opt. Lett. 14, 1125 (1989).
48. L. Y. Liu, J. M. Huxlay, E. P. Eppen, and H. A. Haus, opt. Lett. 15, 553 (1990).
49. J. M. Liu and J. K. Chee, Opt. Lett. 15, 685 (1990).
50. F. Krausz, Ch. Spieimann, T. Brabec, E. Wintner, and A. J. Schmidt, Opt. Lett. 15, 1082 (1990).
51. G. P. A. Malcolm, A. I. Ferguson, opt. & Quantum Electro. 24, 705 (1992).
52. R. S. Grant, P. N. Kean, D. Burns and W. Sibbett, Opt. Lett. 16, 384 (1991).
53. U. Keller, G. W. 'tHooft, W. H. Knox, and J. E. Cunningham, Opt. Lett. 16, 1022 (1991).
54. R. S. Grant, Z. Su, G. T. Kennedy, W. Sibbett, and J. S. Aitschison, Opt. Lett. 18, 1600 (1993).
55. F. M. Mitschke, and L. F. Mollenauer, IEEE J. Quantum. Electro. QE--22, 2242 (1986).
56. G. T. Kennedy, R. S. Grant, and W. SIbbett, Opt. Lett. 18, 1736 (1993).

57. A. Finch, G. Chen, W. E. Sleat, and W. Sibbett, J. Mod. Opt. 35, 345 (1988).
58. E. K. Zavoiskii, and S. D. Fanchenko, Sov. Phys. Doklady 1, 285 (1956).
59. Y. Liu, PhD Thesis, (University of St. Andrews, 1992).
60. E. P. Eppen and C. V. shank, *Techniques for measurement,* In *Ultrashort light pulses,* (Topics in Applied Physics, Vol 18, Springer-Verleg), ed S. L. Shapiro, Berlin.
61. D. J. Bradlay, and G. H. C. New, Proc. IEEE, 62, 313 (1974).
62. R. Trebino and C. G. hayden, Opt. Lett. 15, 1079 (1990).
63. A. Finch, PhD thesis, (university of St. Andrews, 1989).
64. K. L. Sala, G. A. Kennedy-Wallace, and G. E. Hall, IEEE J.. Quantum Electro. QE-16, 990 (1980).
65. J.-C. M. Diels, J. J. Fontaine, I. C. McMichel, and F. Simoni, Appli. opt. 24, 1270 (1985).
66. X. Zhu, PhD thesis, (University of St. Andrews, 1991).
67. G. P. Agrawal, *Nonlinear fibre optics*, (Academic press, San Diego, 1989).
68. Sigman, *Lasers,* Chapters 9 & 10, (University Science books, 1986).
69. R. H. Stolen and C. L. Lin, Phys. Rev. A, 17, 1448 (1978).
70. E. P. Ippen, C. V. Shank, and T. K. Gustafson, Appl. Phys. Lett. 24, 190 (1974).
71. A. Hasegawa and W. F. Brinkman, IEEE J. Quantum. Electron. QE-16, 694 (1980).
72. G. P. Agrawal, Phys. Rev. Lett. 59, 880 (1987).
73. K. Tai, A. Hasegawa, and A. Tomita, Phys. Rev. Lett. 56, 135 (1986).
74. R. H. Stolen and J. E. Bjorkholm, IEEE J. Quantum Electro. QE-18, 1062 (1982).
75. R. H. Stolen, M. A. Bösch, and C. L. Lin, Opt. Lett. 6, 213 (1981).
76. C. L. Lin, W. A. Reed, A. D. Pearson, H.-T. Shang, P. F. Gladis, Opt. Lett. 6, 493 (1981).
77. R. H. Stolen and W. N. Leibolt, Appl. Opt. 231 (1976).
78. R. W. Boyd. Nonlinear Optics, (Academic Press, INC, 1993).
79. C. Lin and P. F. Glodis, Electron. Lett. 18, 696 (1982).
80. L. F. Mollenauer, R. H. Stolen, and M. N. Islam, Opt. Lett. 10, 229 (1985).
81. P. G. Smith, Appl. Opt. 11, 2489 (1970).
82. R. H. Stolen and E. P. Ippen, Apl. Phys. Lett. 22, 276 (1972).
83. F. M. Mitschke and L. F. Mollenauer, Opt. Lett. 11, 659 (1986).
84. J. P. Gordon, Opt. Lett. 11, 662 (1986).

Chapter 2

Coupled-Cavity Mode Locking of KCl:Tl Colour-Centre Laser with Optical Fibre

Since the demonstration of the soliton laser [1] - the original version of coupled-cavity mode-locking scheme, extensive theoretical and experimental studies have been conducted regarding its underlying mechanism and the operational optimisation [2-12]. The continuous trend of this study has resulted in the generation of laser pulses over a wide spectral extension with duration previously unavailable in a number of laser systems [5, 13-17]. Optical fibre was the first and still the dominant nonlinear element used in this mode locking scheme, and proved to be versatile and economic. Although the use of which has been well established, the optimisation of the CCM mode locking is still beyond reach at the start of this project [18, 19]. Therefore, a further study of the coupled-cavity mode-locked KCl:Tl colour-centre laser with optical fibre as the nonlinear element in the control-cavity was conducted. It was found that two operational regimes existed in the coupled-cavity mode-locked KCl:Tl laser. Optimised operation of the laser has resulted in routine generation of pulses having duration as short as 63 fs. It is believed that such short pulses are among the shortest ever generated directly from colour centre lasers working at the wavelength of around 1.5 μm.

This chapter is organised as follows. Firstly, a brief introduction of the colour-centre laser is provided. Then, some of the characteristic features of the coupled-cavity mode-locked KCl:Tl colour centre laser are presented, followed by the exploration of pulse chirp-compensation using pair of prisms in the main laser cavity. At last the optimised operation of the CCM laser is investigated.

2.1. Introduction to the KCl:Tl colour centre laser

Before the discussion of the couple-cavity mode-locking of KCl:Tl colour-centre laser, a brief introduction of the colour-centre laser itself is necessary. Details can be found in a number of literature [20-22].

2.1.1. Basic physics of colour centres

F-centre

Colour centres are simply point defects in crystal lattices. It may consist of one or more electrons trapped at anionic vacancies in the lattice. In general, these defects have the effect of giving rise to the absorption of the host material (normally transparency) within a wide range of spectral band in the visible region (and thus the term of colour-centre). In alkali halide crystal lattices, colour centres have been intensively studied, bringing about a number of lasers that cover a wide spectral range of 0.8-4.0 μm. Basically, there are two methods by which the colour-centre can be created. One is the additive colouration method in which the colour centres are created by diffusing an excess amount of the alkali metal into an alkali-halide crystal. Another method is radiation damage of the alkali-halide crystal so that electron-hole pairs can be generated.

In aklali halide crystal lattices, there are more than 15 different type of colour centres that have been developed. The most fundamental colour centre, F centre ("F" comes from the German word Farbe, means colour), consists of a single electron trapped at a vacancy surrounded by an essentially undisturbed lattice, as shown in the diagram of Figure 2.1(a). Although F centre itself does not give lasing action, but it forms the building block for more complex, laser-active centres. If one of the neighbouring alkali ions is a substitutional alkali impurity, say Li^+ in a KCl crystal, the centre is called F_A centre, as shown in Figure 2.1(b). Similarly, the F_B centre is formed by an F centre beside two substitutional impurities, as shown in Figure 2.1(c). There are also many other colour centres, such as F_2 centre, F_2^+ centre, $(F_2^+)_A$ centre, etc.. These centres formed the basis for various colour-centre lasers.

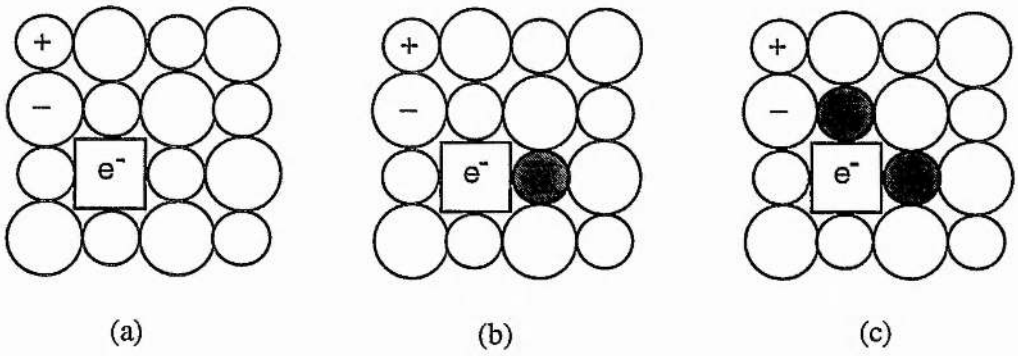

Figure 2.1. Diagrams illustrating the structure of some of the colour-centres. (a) F centre, (b) F_A centre, (c) F_B centre. (the shaded cycles represent the substitutional alkali impurities.)

Although the F centre itself is not laser-active, the optical properties of which are important in understanding the laser physics of other colour centres. By using a highly simplified quantum mechanical model, the optical absorption and emission of the F centre can be understood on a qualitative basis. This model regards that the F centres are essentially electrons trapped in a three-dimensional square well. This well is formed by the electrostatic potential of the positive ions surrounded the electron. By using this model, the energy between the ground state and the first excited state is given by [see Ref. 22]

$$E_{2p} - E_{1s} = \frac{3h^2}{8ma^2} \tag{2.1}$$

where $1s$ denotes the ground state, $2p$ represents the excited state, h is the Planck's constant, a is the box dimension, and m is the mass of the electron.

For most alkali halides, it was found experimentally that if distance a is taken as the nearest neighbour separation, the F-band energy can be related to a as [see Ref. 22]

$$E_F = 17.7a^{-1.84} \tag{2.2}$$

In this equation, a is in unit of angstroms and E_F is in electron volts. It is also known as "Mollwo relation". In the alkali halide crystals, the lattice vibrations (phonons) will result in the variation of the actual dimension of the square well at a period of less than 10^{-13} sec. From relation (2.2), it can be seen that this variation will, in turn, cause the energy levels to vary on the same time scale. Since this happens randomly and occurs at

all F centres in a rate which is faster than the excited state lifetime of the centre, homogeneously broadened absorption and emission bands are therefore assured.

$Tl^0(1)$ centre

The laser-active centre used in this work was $Tl^0(1)$ centre in KCl crystal. Basically, the $Tl^0(1)$ centre is formed by a neutral Tl atom perturbed by the field of an adjacent single anion vacancy, as the diagram shown in Figure 2.2. The formation of the $Tl^0(1)$ centre requires the use of the radiation damage method. The first step is to form the KCl crystal with 0.2 mol% Tl^+ dopant. Then, the KCl crystal is irradiated by electron beams so that the F centres are generated. Next, the crystal is exposed to light from a microscope lamp for about 10 minutes at a temperature of ~30^0C, allowing the creation of $Tl^0(1)$ centres.

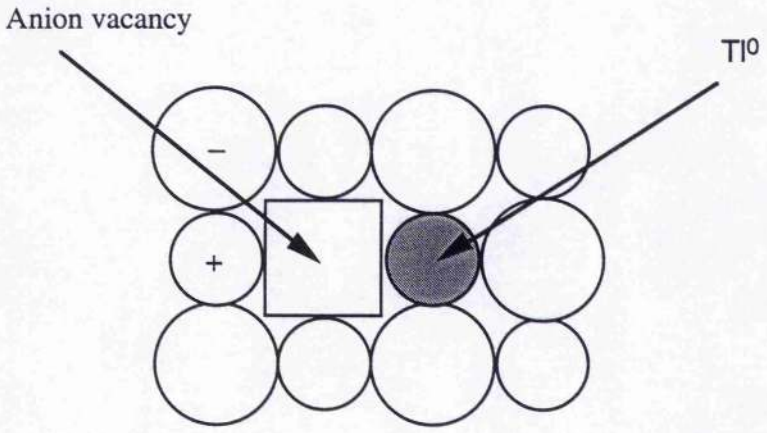

Figure 2.2. Diagram showing the structure of Tl^0 (1) colour centre.

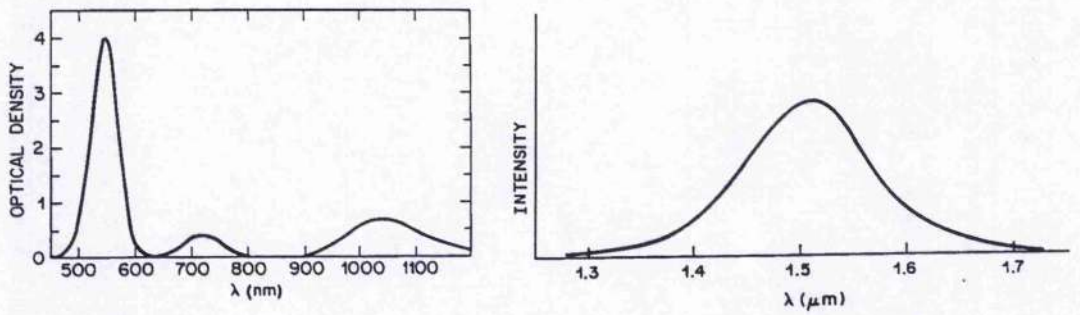

Figure 2.3. Absorption and emission bands of the KCl:Tl. (adopted from Ref.21)

Figure 2.3 represents the absorption and emission bands of the KCl:Tl laser crystal. Essentially, the pumping band of the laser is peaked at the wavelength of 1.04 μm, and the emission band is centred at 1.51 μm. The KCl:Tl colour centre laser can be tuned from 1.4 to 1.63 μm, and output power up to 1 W can be produced. Some parameters related to the KCl:Tl colour centre lasers are summarised in Table 2.1.

Table 2.1. Some parameters of KCl:Tl colour-centre laser.

Parameters	Values
Refractive index of the KCl	1.47
Peak absorption wavelength (λ)	1.04 μm
Absorption band	650 cm^{-1}
Peak emission wavelength (λ)	1.51 μm
Tuning range ($\Delta\lambda$)	1.4 - 1.63 μm
Gain cross section (σ)	1.3×10^{-17} cm^2
Laser upper level lifetime (t)	1.6 μs

Three characteristics make the colour-centre lasers unique in practical applications. In the first case, the colour centre lasers cover an entire spectral range of 0.8 - 4 μm, that is where the dye laser stopped. Secondly, the homogeneously broadened absorption and emission bands of the laser-active centres allow for the single-mode laser operation over the entire tuning range of the laser. Thirdly, the large cross section combined with the large homogeneous bandwidths makes it suitable for the generation of ultrashort laser pulses. It is the last feature that is most interested in this work.

One drawback of the colour centre laser, however, is that the operation of the laser requires the laser crystal being cooled at cryogenic temperature (~77 K). Failing to meet this condition will lead to fading of the output power. At room temperature, the centres may either thermally dissociate or become mobile and transform into non-lasing centres through attachment to other defects. In practical laser system, the crystal is cooled by anchoring to a cold finger which is usually maintained at ~77 K by a storage Dewar of liquid nitrogen.

2.1.2. KCl:Tl colour-centre laser

The laser used in this study was based on a Burleigh F-centre laser system modified by stretching the cavity length to about 1.8 m to match the length of the Nd:YAG pump laser [23]. A schematic representation of the laser is shown in Figure 2.4. Essentially, the laser crystal is clamped in a gold-coated cassette which is connected to a cold-finger. The cold-finger itself is maintained at cryogenic temperature by thermal attachment to a liquid nitrogen dewar located above the chamber housing the laser crystal. The chamber is retained at vacuum condition (~10^{-6} Torr), that provides thermal insulation for the crystal and prevents condensation on the crystal surfaces. Mirror M_1 can be adjusted mechanically along the beam axis. With the modified laser cavity, mirror M_4 has a focal length of 0.5 m, and the output coupler M_O has a reflection of 78%. The tuning of the output was completed by a birefringent filter.

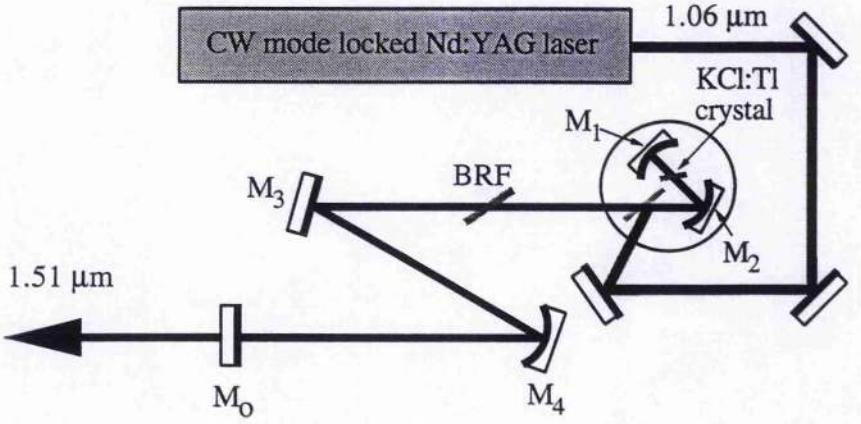

Figure 2.4 Schematic diagram of the KCl:Tl colour-centre laser.

The KCl:Tl colour-centre laser crystal was pumped by a Nd:YAG laser beam using coaxial pumping technique. In this pumping scheme, a Brewster angled beamsplitter with coating that transmits the laser radiation (1.5 μm) while reflects the pump radiation (1.06 μm), was used, as the diagram shown in Fig. 2.4. The crystal itself was also oriented at Brewster's angle to minimise the reflectivity losses.

For synchronous mode-locking, the pump laser itself was mode-locked, and the colour-centre laser cavity was adjusted to match the pumping laser cavity length. The pump laser, a Spectra Physics Series 3000 Nd:YAG Laser System, typically generated

pulses having duration of around 100 ps, and an average output power up to 7 W in single transverse mode could be produced. In the situation of synchronous mode-locking, the KCl:Tl colour-centre laser could produce pulses at few tens of picosecond. The output power of the colour-centre could be as high as few hundreds milliwatts depending on the pumping power level. The output power of the laser as a function of pump power is shown in Figure 2.5. The slope efficiency was derived to be about 8% with a output coupler of 22%. The tuning of the output could be obtained by a birefringent filter inside the colour centre laser cavity. A typical tuning curve of the colour centre is shown in Figure 2.6. It can be seen that the laser operates over a spectral range in excess of 80 nm at a pump power of about 1.5 W. It is expected that at higher pump power and with a relatively lower transmission of the output coupler the tuning range would be much wider.

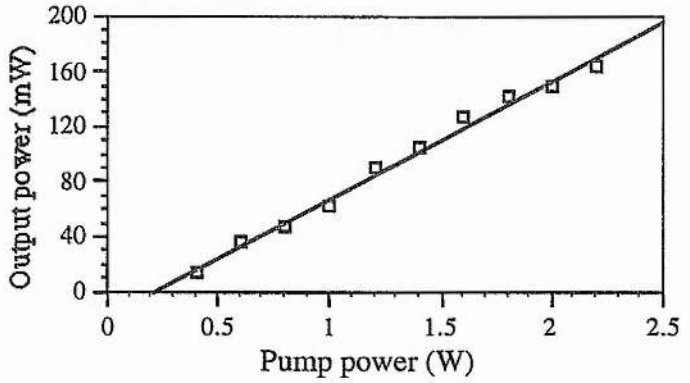

Figure 2.5. Output power of the KCl:Tl centre laser as a function of pumping power.

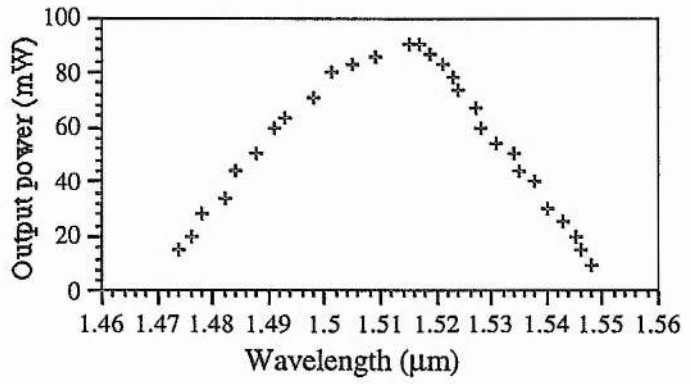

Figure 2.6. A typical tuning curve of the KCl:Tl colour centre laser.

2.2. Operational characteristics of the CCM KCl:Tl colour-centre laser

As mentioned in Chapter 1, three kind of coupled-cavity mode-locking configurations can be arranged, namely Fabry-Perot, Michelson, and Ring cavity configuration. In comparison, the Michelson arrangement has the advantages of having a relatively stable output characteristic and a compact cavity assembly [24]. Therefore, throughout most of the work in this project a Michelson cavity arrangement was employed.

In the experiment of this chapter, the nonlinear element used in the control-cavity for the coupled-cavity mode-locking of the KCl:Tl colour-centre laser was a 28 cm long erbium-doped monomode optical fibre with zero dispersion located at about 1.43 μm. Some of its characteristic parameters are shown in Table 2.2.

Table 2.2. Parameters of the Er-doped fibre used in the experiment

Parameters	**Values**
Dopant concentration	1.6×10^{18} (cm^{-3})
Δn	16×10^{-3}
Core diameter	4.6 (μm)
Zero dispersion wavelength	1.43 (μm)
D at 1.5 μm	4.1 (ps/km/nm)

2.2.1 Experimental Set-up

The schematic diagram of the experimental set-up is shown in Fig. 2.7-(1). The main laser cavity is formed through mirrors M_1, M_2, M_3, M_O, M_4 to M_5. If we term the arm, of the Michelson arrangement, containing the optical fibre as the nonlinear branch, and the another the linear branch. Then, it can be seen that the linear branch in the arrangement here is composed of M_O, M_4, and M_5. The nonlinear branch is formed by M_O, M_6, M_7, the optical fibre, and M_8. M_O acted as both the output coupler and the beam splitter of the CCM laser, and had a transmission of T = 12%. Because there are two parts of output, in reality M_O had a intensity transmission equivalent to 24%. One

part of the output from M_O was coupled into the nonlinear branch, and another part was taken as the laser output. The coupling of the laser beam into and out of the fibre was accomplished by using two x20 microscope objectives (AR coated over the spectral range of the laser output). A variable neutral density filter enables the variation of the power in the fibre. A small fraction of the output or that returned from the fibre was used as reference signal of the stabilisation loop system.

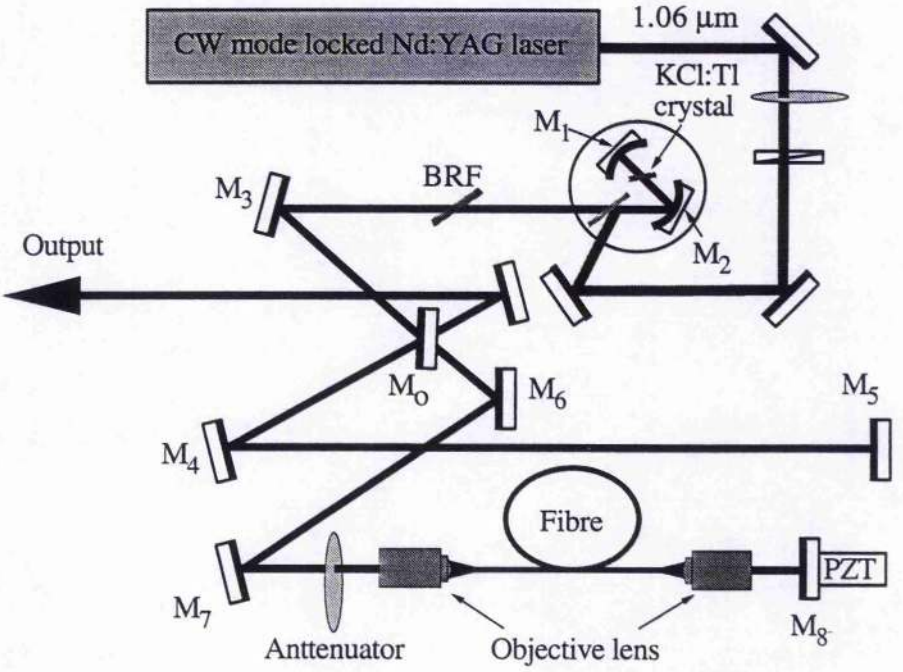

Figure 2.7-(1) Experimental set-up of the CCM KCl:Tl colour centre laser with a Michelson configuration.

A diagram of the typical stabilisation electronic loop system is shown in Fig. 2.7-(2) [3, 19]. Essentially, the photodiode is illuminated by a portion of laser radiation. The amplified signal of this photodiode output is then compared with an empirically set reference voltage. The error signal of these two signals is amplified and drive the piezoelectric transducer (PZT).

The procedure on the alignment of the CCM laser was conducted as follows. Firstly, with the nonlinear branch blocked, the KCl:Tl colour-centre laser was adjusted

for proper synchronous mode-locking, meanwhile the control cavity length was set roughly equal to that of the main cavity. Secondly, using a photo-detector in front of mirror M_8 to optimise the coupling of laser beams into and out of the fibre. Thirdly, the optimum feedback was achieved by detecting the signal returned from the fibre through the adjustment of mirror M_8 and the focal length of the second objective lens. Finally, the matching position of the two cavities is determined through the variation of the position of M_8 by using a translation stage. The matching point can be predicted when a dramatic enhancement of the mode-locking behaviour appears on the second harmonic autocorrelation traces. At this stage, owing to the random vibration of the mirrors, caused from the unstable environment, the laser operation occurs to switch randomly between CCM mode-locking operation and synchronous mode-locking process. When the stabilisation loop system is involved, through the adjustment of the error signal applied to the PZT, the optimum coupled-cavity mode-locking operation can be achieved.

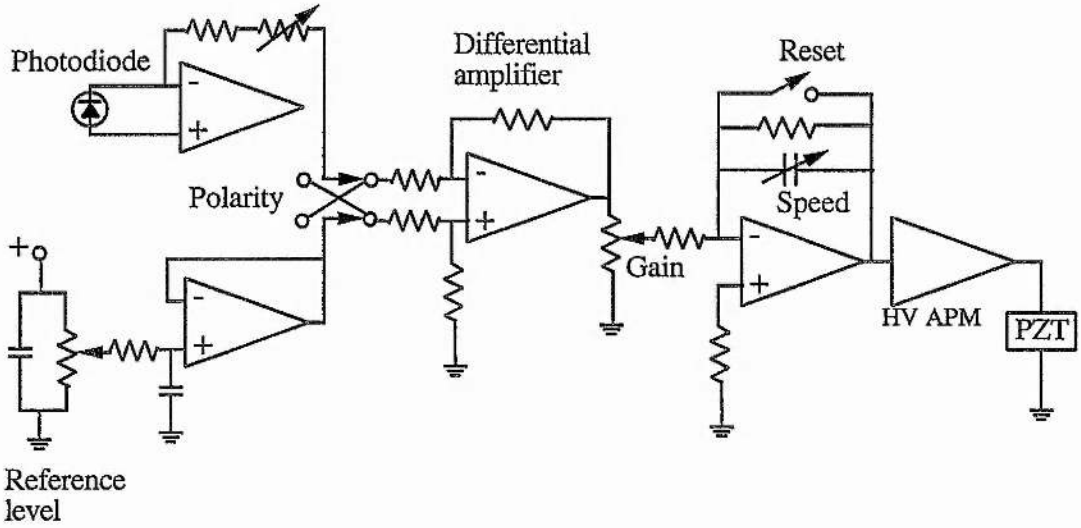

Figure 2.7-(2). Diagram of the stabilisation electronic loop system.

2.2.2. Two operational regimes

The foremost experiment was conducted without any bandwidth limiting element (frequency tuning birefringent filter) inside the laser cavity. The output spectrum of the

KCl:Tl colour centre laser was essentially centred at a wavelength of 1.52 μm. Without the involvement of the control cavity, the KCl:Tl colour centre alone typically produced pulses at few tens of picosecond, and continuous mode locked pulse train could be generated. A clear evidence of the stable mode locking operation is shown in Figure 2.8.

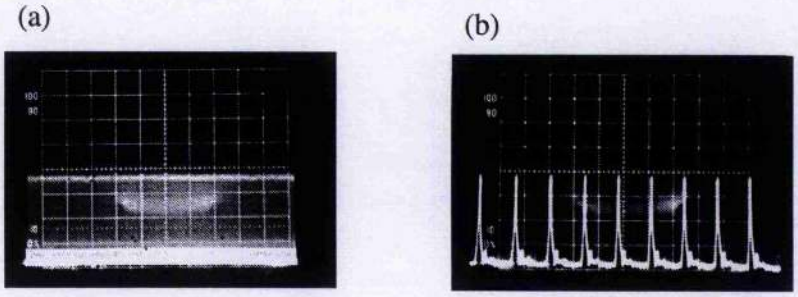

Figure 2.8. Output pulse train of the synchronously mode-locked KCl:Tl colour-centre.

As the feedback from the control cavity was introduced, however, it was found that two operational regimes were presented. These two regimes corresponded to different phase settings of the two cavities, and could be achieved subsequently from Regime 1 to Regime 2 or the opposite simply by altering the error signal applied to the PZT. Without any external perturbation, either of the two operational regimes could run for hours without failing. The output power in the two operation regimes were quite different as well. It was found that the output power in Regime 2 was about 3 mW higher on average than in Regime 1.

In Regime 1, a clean and relatively stable output pulse train could be obtained, but pulse duration was longer. The interferometric autocorrelation trace indicated that a strong frequency chirp existed over the pulse envelope. In Regime 2, relatively shorter and less-chirped pulses could be obtained, but in this case the CCM mode locking process was accompanied by a self Q-switching effect manifested in such a way that the output pulse train was modulated in a period of about 2 μs. An experimental result illustrating this Q-switching effect is shown in Figure 2.9. They were recorded from a fast oscilloscope in conjunction with a fast photodiode. Simply, the output of the laser

was incident upon the fast diode and then the output electric signal of which was fed to the oscilloscope. It can be clearly seen that within the envelope of the much longer Q-switched pulses the laser was still mode locked. However, a broader CW back ground signal was presented, which can be clearly seen from Figure 2.9 (b) - (e). The Q-switched pulse was estimated to be about 1.2 μs in duration, and therefore there would be about 100 mode locked pulses under each Q-switched pulse.

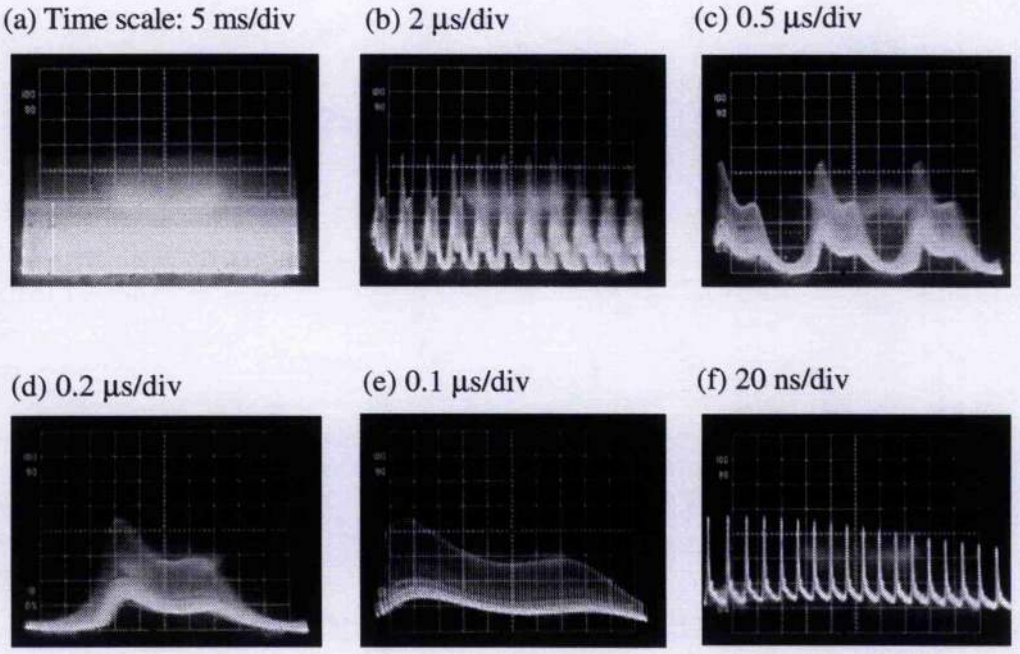

Figure 2.9. Experimental results illustrating the Q-switching effect of the CCM laser. (These results were recorded from a fast oscilloscope).

It has also been found that between these two regimes, there was a third unstable operational regime. In this regime, the performance of the laser appeared to switch between Regime 1 and Regime 2 randomly. A typical autocorrelation of the output pulses in such case is shown in Figure 2.10. The jumping up and down of the autocorrelation trace is a clear indication of the unstable operation of the laser. The case of higher amplitude corresponded to Regime 2, while the lower one represented the case of Regime 1.

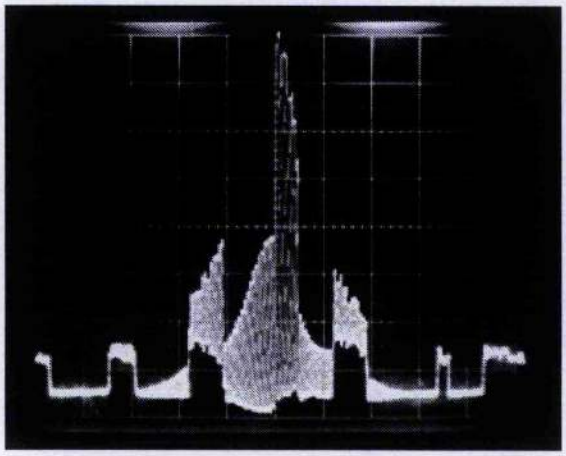

Figure 2.10. Autocorrelation trace illustrating the switching of the output between the two regimes.

Regime 1

With proper mode-locking operation in Regime 1, the intensity and interferometric autocorrelation traces and the corresponding spectrum of typical output pulses are shown in Figure 2.11. This set of result was obtained by setting the pumping power of the Nd:YAG at 1.5 W, and the useful output power of the CCM laser was about 30 mW. The power coupled into the external fibre was maintained at about 20 mW. Under such experimental conditions, the pulses obtained was about 170 fs with a spectral width of 28 nm. The bandwidth-duration product of 0.73, which is much larger than 0.32 of transformed limited sech^2 pulses, indicates that the pulse was highly frequency chirped. From the elevated wings of the interferometric autocorrelation trace, this frequency chirp of the output pulses can also be inferred.

As the power coupled into the fibre was varied, the pulse duration and chirp feature changed as well. At lower power level, relatively shorter and less chirped pulses could be obtained. When the power level was increased, broader and stronger chirped pulses tended to be produced. Diagrams illustrating these relationship is shown in Figure 2.12, where (a) shows the variation of the pulse duration and spectral widths of the output pulses as functions of power level in the fibre, (b) indicates the bandwidth-duration product as a function of power in the fibre. It can be seen that pulses as short as 140 fs can be generated when power level in the fibre was as low as 12 mW, and in this case

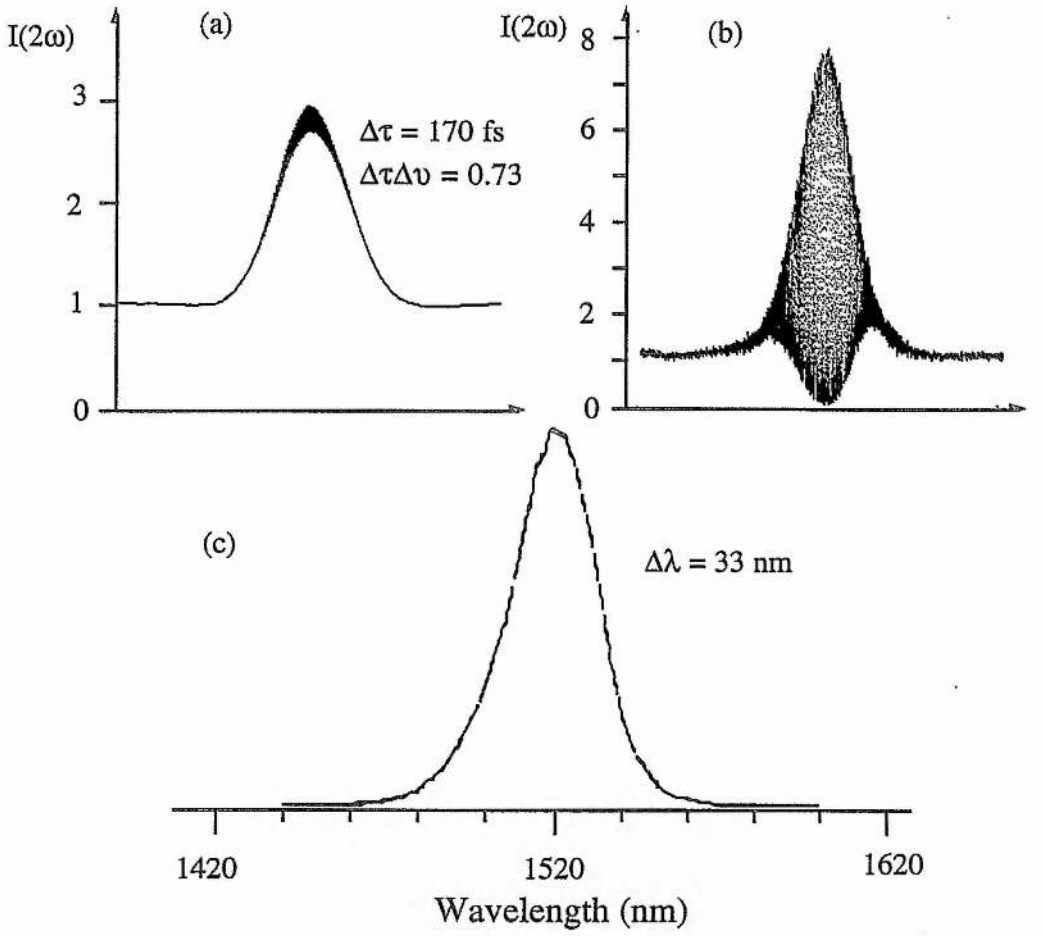

Figure 2.11. Typical output autocorrelations and spectrum of the CCM laser. (a) Intensity autocorrelation, (b) Interferometric autocorrelation, and (c) Spectrum.

the bandwidth duration product was about 0.40. When the power in the fibre reached to 25 mW, pulse duration increased to 190 fs, and the bandwidth-duration product of 0.96 indicates that a strong chirp existed across the pulse envelope. It also can be seen that as the power in the fibre was increased from 12 mW to 25 mW the output spectral widths increased from 22 nm to 39 nm. This could be attributed to the SPM induced spectral broadening in the fibre, since the SPM effect gives rise to broader spectrum at higher power level.

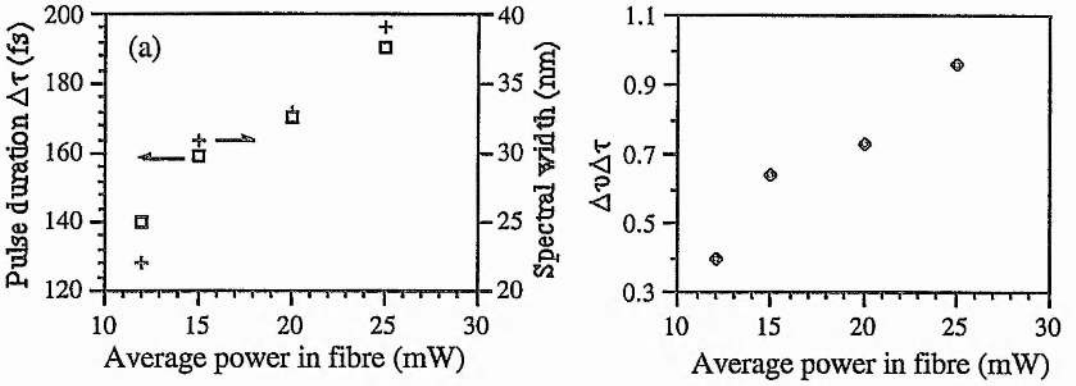

Figure 2.12. (a). Variation of pulse duration and spectral widths as a function of power level in the external fibre; (b) Bandwidth-duration products as a function of power level in the external fibre.

Regime 2 (Self Q-switching effect)

In Regime 2, although the output pulse train was modulated, but relatively shorter and less chirped pulses could be generated. Figure 2.13 shows the variation of output pulse duration, spectral widths and the bandwidth-duration products as functions of intra-fibre power level. As can be seen that, contrary to Regime 1, the pulse duration of Regime 2 decreased as the increase of the intra-fibre power level. At relatively lower power level, say 13 mW, the pulse duration was about 150 fs. As the power in the fibre reached to about 25 mW, pulses as short as 90 fs were produced, and in such case the bandwidth-duration product was about 0.47. Although the spectral widths varied notably from 21 nm at an average power of 13 mW to 40 nm at the power of 25 mW, the bandwidth-duration product remained at about 0.4 (comparing to the data in Figure 2.12 (b), where the bandwidth-duration was as high as 0.96 at the same power level). A typical interferometric autocorrelation of such modulated output pulses is shown in Figure 2.14. The Q-switching feature may also be inferred from the vague fringes of the interferometric autocorrelation traces.

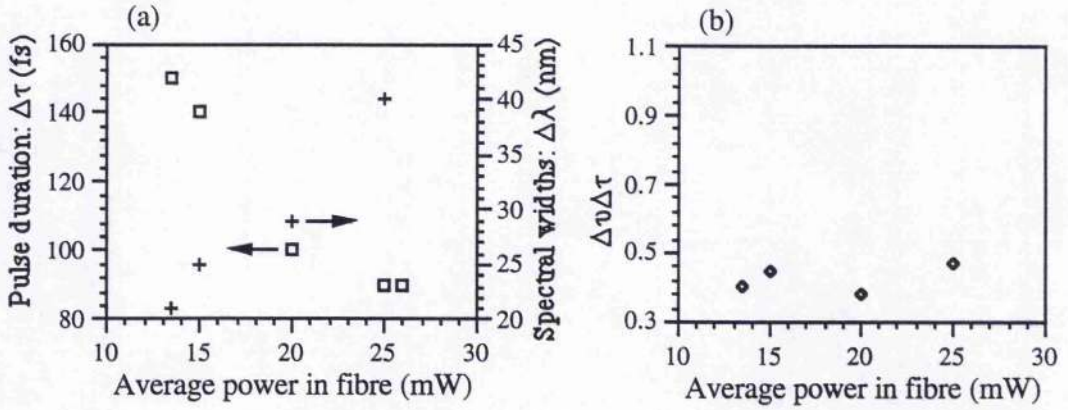

Figure 2.13. Variation of pulse duration, spectral widths (a), and the bandwidth-duration products (b) as a function of power level in the external fibre (Regime 2).

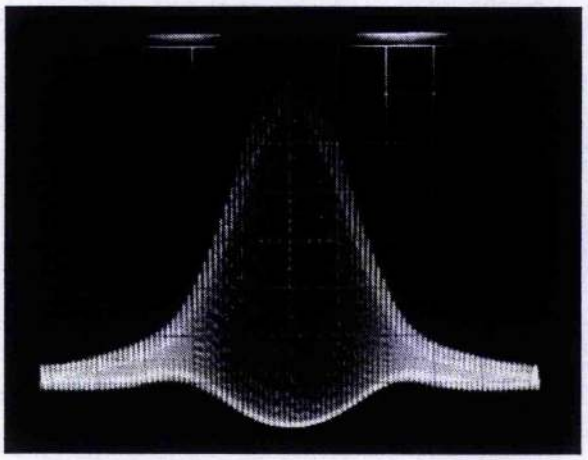

Figure 2.14. Interferometric autocorrelation of output pulses (Regime 2).

When the power in the optical fibre was changed, the modulation period varied as well. It was found that the modulation period increased with the increase of the power in the fibre, a diagram showing this tendency is illustrated in Figure 2.15. It can be seen that the modulation period varied in a time scale from about 1.4 μs to 2 μs. As the average power in the fibre was lower than 13 mW, the Q-switching effect no longer existed, and at this stage the laser was very sensitive to external perturbation (slight vibration of the table may eliminate the CCM operation). When the power level was lower than 9 mW, coupled-cavity mode locking was very hard to achieve.

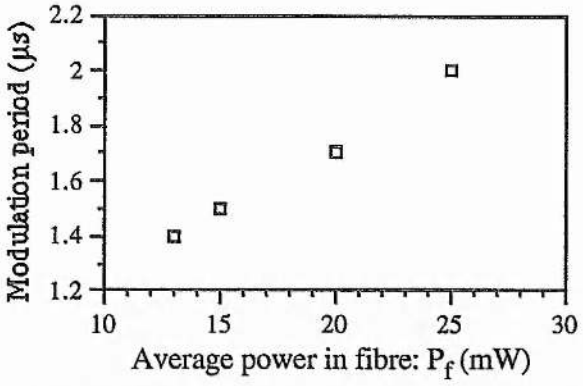

Figure 2.15. Variation of modulation period with optical power level in the fibre.

Figure 2.16 shows the spectra of the CCM laser output for the two regimes. For the purpose of comparison, the spectra of the two regimes were overlaid together. The higher one corresponds to the case in Regime 2, the lower one represents the case of Regime 1. It can be seen that in both cases the spectra became asymmetric as the power level in the fibre was increased. Notably, the centre of the spectrum for the two regimes were in quite a difference. This difference became large when the power in the fibre was increased. The spectrum at Regime 2 located at the longer wavelength side respected to the spectrum at Regime 1. The spectral widths in both cases became large when the power in the fibre was increased.

Discussion

A theoretical work performed by Kelly [25], where an empty external cavity was presumed, showed a same result as presented here. In that paper, it was indicated that if the pulses returned from the external cavity and that being circulated in the main cavity had the opposite phase (anti-phase) when adding at the common mirror, the laser would exhibit a series of intermittent large scale intensity fluctuations, which is casually defined as Q-switching or pulse train modulation here.

The Q-switching behaviour probably can be conceived as follow. It is known that the shortest pulse is generated at a phase difference of $-\pi/2$ between the pulses returned from the control cavity and that being circulated in the main cavity [8]. The nonlinear phase shift resulted from the SPM in the fibre is proportional to the instantaneous

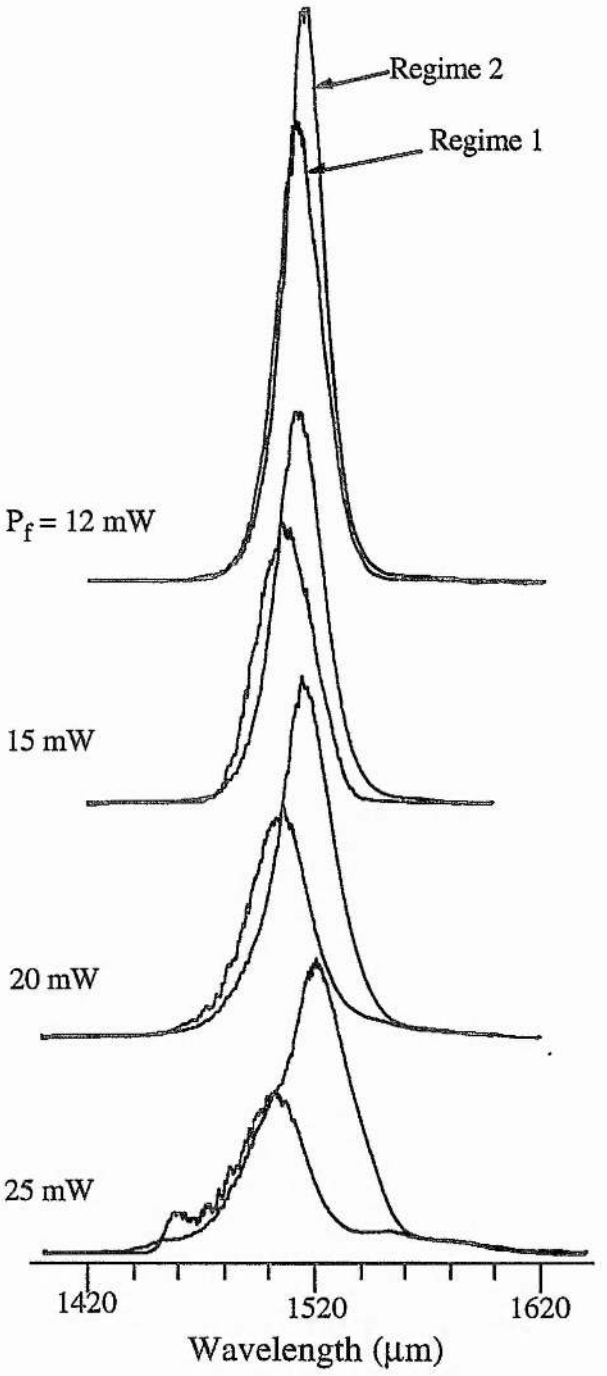

Figure 2.16. Output spectra of the two regimes at different power level in the fibre. The lower one corresponds to Regime 2, higher one represents Regime 1. (Referring to Fig 2.12 (a) and Fig. 2.13 (a)).

intensity of the pulse, and therefore is different across the pulse envelope - largest in the pulse centre and becomes smaller towards the wings. Assuming, now, that the two pulses are overlapped at a phase difference of about $-\pi/2$ in the pulse centre. When the

laser is turned on and the external cavity is involved, the coupled-cavity mode-locking process will eventually built up. As the evolution continuous, the pulse is becoming shorter, and thus the instantaneous intensity becomes greater. As a result, the nonlinear phase shift introduced from the SPM is becoming larger. At some stage, the phase difference between the two pulses in the centre may reach beyond $-\pi/2$. In such case, the addition of the two pulses in the centre is no longer constructive but characterised by a destructive feature. The consequence would be a collapse of the CCM process. However, at this stage, the colour-centre is still synchronously mode-locked, and the external cavity is still in action. After some recovery time, the coupled-cavity mode-locking process will be built up again. The time interval between the two Q-switched pulses is in fact correspondent to the build-up time of the CCM laser. In the experiment here, it was about 0.8 μs, which was in good agreement with the experimental result (~1 μs) obtained by Zhu [26].

2.2.3 Dispersion compensation by using pair of prisms

The chirp feature of the output pulses, as illustrated in Figure 2.11, was examined by passing the output pulses through a length of glass rod. It was found that the pulse duration was reduced from 170 fs to about 140 fs after passing through 30 cm long glass rod, and the chirp was largely reduced. It was known that the glass rod used in the experiment had a anomalous GVD at wavelength of 1.5 μm, therefore, it could be concluded that the output pulse of the laser was positive chirped. This chirp is believed to be predominantly resulted from the self-phase-modulation in the fibre.

Frequency chirp compensation in CCM lasers has been performed in a number of laser systems. The chirp can be compressed by inserting additional dispersion element in either the control cavity or the main laser cavity. With a length of glass rod in the control cavity of a CCM KCl:Tl colour centre laser, Zhu [27] has observed a reduction of pulse duration from 140 fs to 90 fs. By using pair of prisms in the main laser cavity of a CCM Ti:Sapphire laser, chirp compensation has also been implemented [28]. In the following

experiment, the exploitation of prism pair in the main laser cavity of the CCM KCl:Tl laser will be investigated.

The experimental arrangement is similar to Figure 2.7, except that a prism pair was inserted in the main laser cavity. Figure 2.17 shows the arrangement of the prism pair in the main cavity. Essentially, the prism pair was located close to the end mirror of the main cavity so as to reduce beam distortion thus introduced. Each of the prisms was mounted on a three dimensional translation stage, so that the distance between the two prisms and the optical path length of the laser beam within the prisms could be easily varied.

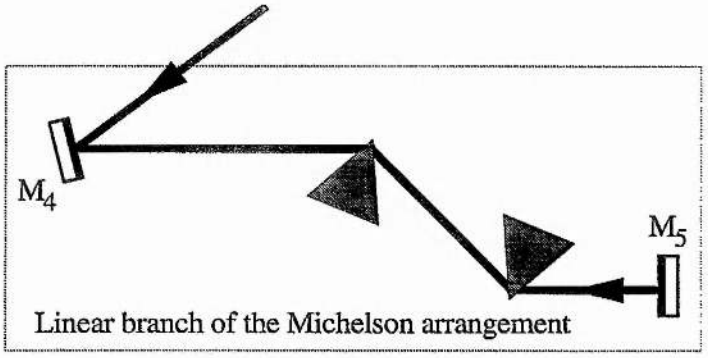

Figure 2.17. Experiment arrangement of the prism pair in the main laser cavity. (Refer to Fig. 2.7).

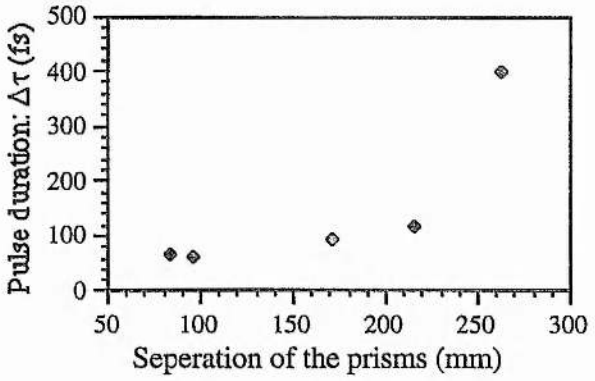

Figure 2.18. Variation of pulse duration as a function of the two prisms' separation.

Figure 2.18 shows the variation of the pulse duration as a function of relative distance between the two prisms. As can be seen that when the separation of the two prisms was very large, the negative dispersion thus introduced might be too big, instead

of shortening the output pulse was greatly broadened. For example, when the separation of two prisms was about 263 mm the pulse duration was as large as 400 fs. As the separation of the two prisms was reduced, the pulses was decreased as well. Reduction of the two prisms' separation to 96 mm lead to the generation of pulses having duration of 64 fs and a bandwidth-duration product of 0.35. The interferometric autocorrelation and the spectrum of the 64 fs pulses are shown in Figure 2.19. The broader shoulder appeared at the wings of the autocorrelation trace might indicate that the output pulses had an asymmetric profile. While the undesired sub-feature appeared on the spectrum implies a noisy output. By further decrease of the two prisms' separation to less than 96 mm, not much change in the pulse duration was observed. Due to the restriction of the prism's mount, the separation of the two prisms could not be tuned to less than 60 mm. At last it should be mentioned that the above results were obtained in the case of an intra-fibre power level of 20 mW.

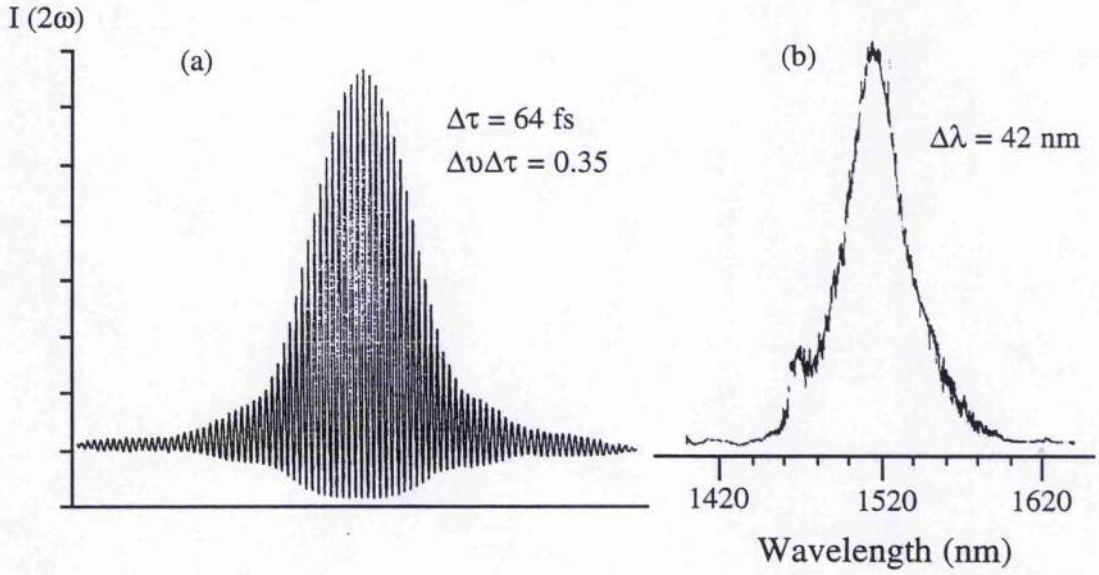

Figure 2.19. Interferometric autocorrelation and spectrum of 64 fs pulses, obtained when the separation of the two prisms was 96 mm.

As the power coupled into the fibre was varied, it was found that the output pulse duration and the pulse profile changed as well. At higher power level, autocorrelation traces that appeared having extended wings, as shown in Figure 2.20, was frequently

observed. However as the power was relatively low, the CCM operation was liable to collapse. The optimum separation of the two prisms was also different at varied power levels. This might be related with the frequency chirp introduce in the fibre. At high power level, strong chirp could be induced, therefore to compensated for this chirp larger separation might be needed. It should be indicated that a notable feature accompanied was the strong noise appeared on the output pulses, which can be inferred from the noisy feature appeared on the spectrum of Figure 2.19 (b). Measurement has indicated that the output power fluctuated randomly in time within a range of 3 mW. This fluctuation appeared on the autocorrelation trace to be a jumping -up and -down.

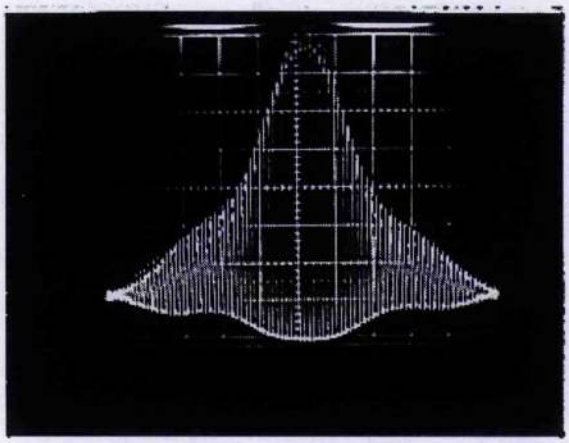

Figure 2.20. Typical interferometric autocorrelation of output pulses

Discussion

Although shorter pulses could be achieved, dispersion compensation with prism pair in the main laser cavity seems not quite suitable for the KCl:Tl colour centre laser. This can be reasoned as follow. First, the insertion of the prism pair has caused an unstable operation of the CCM laser, and the output pulses appeared having a strong noise feature. These undesired effects were most probably resulted from the alteration in the property of the transverse beam profile introduced by the prism pair. Second, the sign of the dispersion introduced by the prisms pair was the same as that of the laser crystal and the windows in the cavity at the lasing wavelength (all have a negative GVD at 1.5 μm), thus it seems un-practical to insert such an "huge" system in the main cavity

just for compensating the frequency chirp introduced in the control cavity. As for the case of Ti:Sapphsire lasers was concerned, the relatively longer crystal can introduce large frequency chirp to the laser pulses, and the sign of this chirp is contrary to the chirp introduced by the prism pair, therefore the prism pair is in fact acted to compensate the chirps introduced by both the laser crystal and the fibre in the external cavity.

2.2.4 Optimisation of CCM laser operation

As a birefringent filter was inserted in the main cavity, it was found that the CCM performance was significantly improved. In addition to the compression of the frequency chirp imposed on the output pulses, the Q-switching effect was also avoided. By orienting the optical axis of the filter parallel to the laser beam, pulses as short as 63 fs has been obtained.

The primary motivation of the insertion of the filter in the main cavity was to limit the lasing bandwidth and thus reduce the frequency chirp of the output pulses. Firstly, a 0.3 mm thick birefringent filter was inserted into the main laser cavity. It was found that apart from the reduction in frequency chirp, the Q-switching effect was also avoided. In such case, the noise feature occurred previously was largely removed and the performance of the laser appeared much more stable. However, the pulse duration was notably increased to above 200 fs, in the case that the operating wavelength was selected by the filter. Such increase in the pulse duration could be understood as a result of the restriction on the lasing bandwidth due to the insertion of the birefringent filter. The pulse duration as a function of operation wavelength is shown in Figure 2.21. It can be seen that as the wavelength was tuned toward longer wavelength side the pulse duration became shorter. This feature could be attributed to two factors: one is the dependence of the transmission bandwidth of the birefringent filter on the operating wavelength, the another is the dispersive feature of the optical fibre.

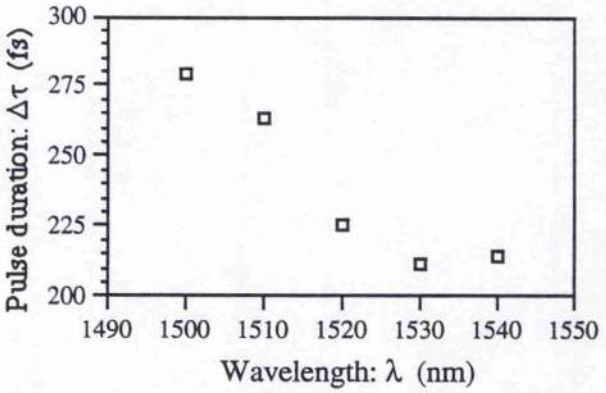

Figure 2.21. Pulse duration of CCM laser output at different working wavelengths (with 1 mm thick birefringent filter in main cavity).

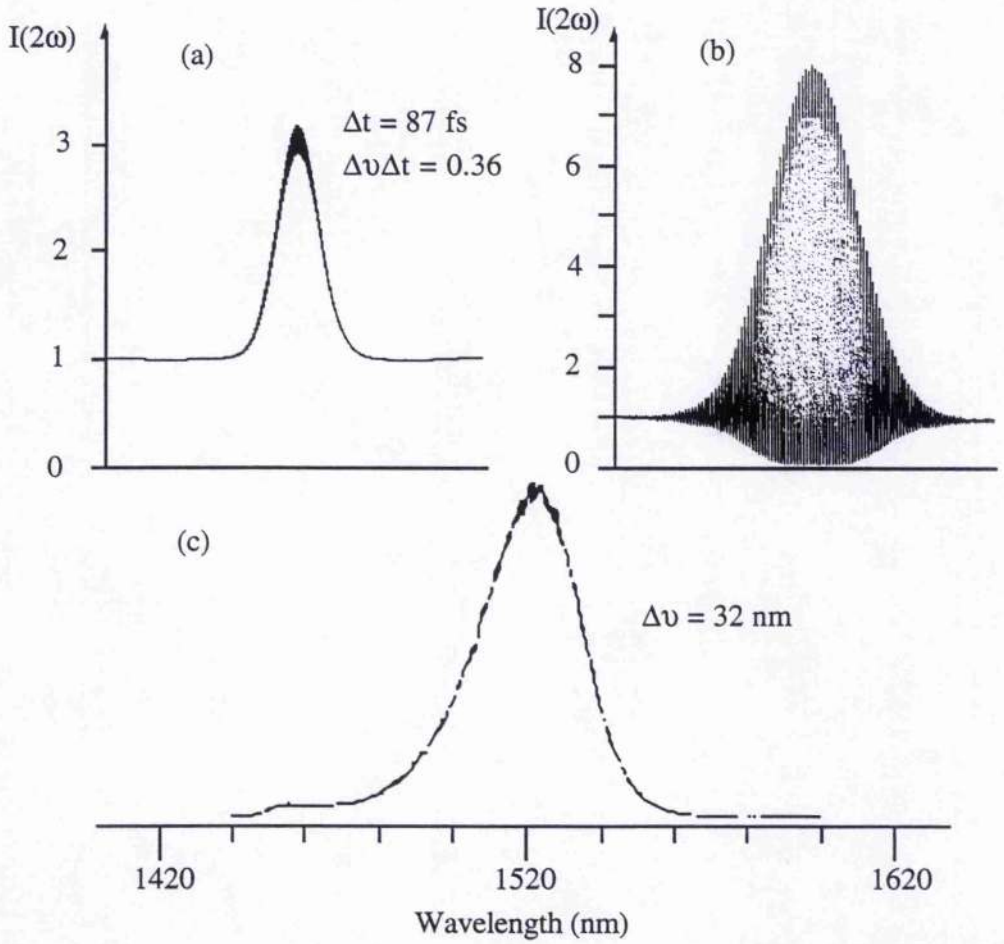

Fig. 2.22. Intensity and interferometric autocorrelation traces and spectrum of the output pulses, when the optical axis of a 0.3 mm birefringent filter in the main cavity was oriented parallel to the laser beam.

When the birefringent filter was tuned to the point where its optical axis was parallel to the laser beam, a large reduction in the output pulse duration was observed. In such case, the filter essentially had no limitation on the lasing bandwidth, but might introduced additional chirp to the laser pulses. Figure 2.22 shows the intensity and interferometric autocorrelation traces and the correspondent spectrum of the shortest pulses obtained with the 0.3 mm filter in the main cavity. The pulse duration of 87 fs is more than two folds shorter than that when the filter was oriented for restricting the lasing bandwidths. The bandwidth-duration product of 0.36 indicates that the pulse was nearly transformed limited ($sech^2$ pulse profile assumed). This result was obtained with a power level of about 16 mW in the fibre and an useful output power of 25 mW from the CCM laser.

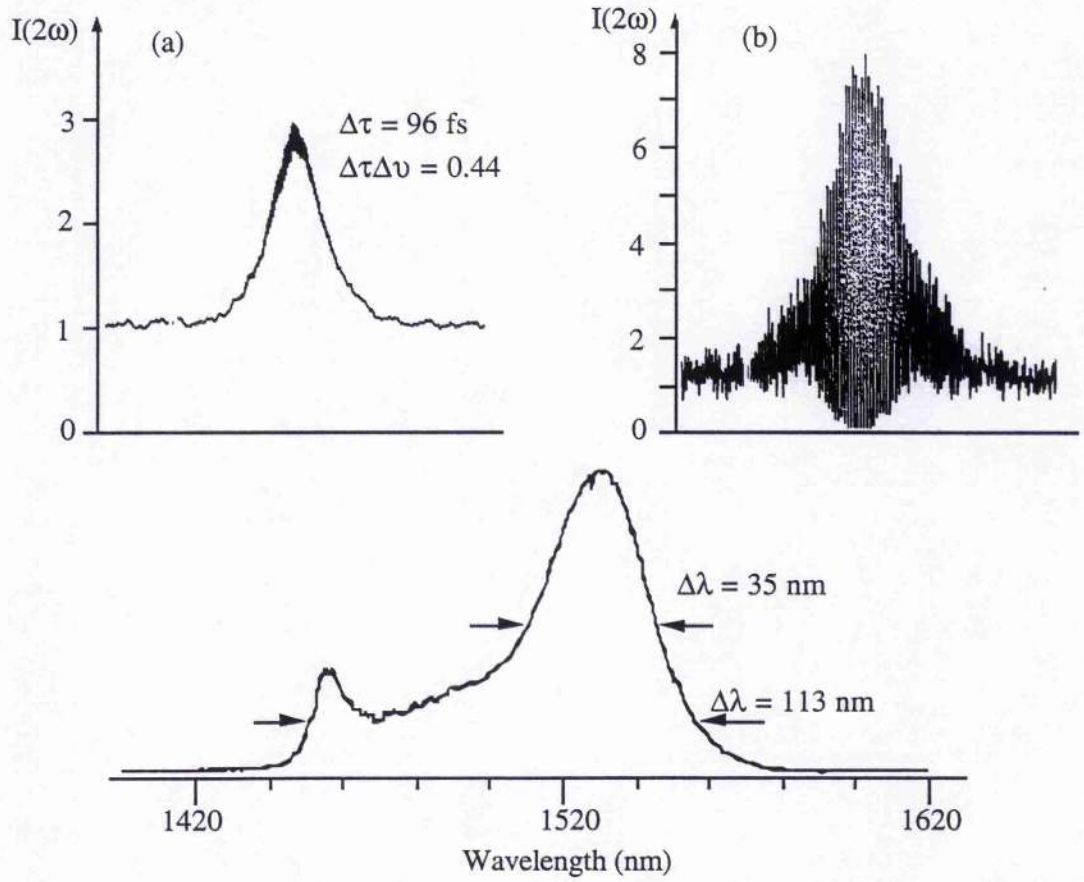

Fig. 2.23. Intensity and interferometric autocorrelation traces and spectrum of pulses returned from the fibre (corresponding to Fig. 2.22).

The autocorrelation and spectrum of the pulses returned from the external cavity is shown in Figure 2.23. Compared with Fig. 2.22, the pulse duration of about 96 fs was slightly greater than that of the output pulses, while the spectrum of which was greatly extended. This large spectral extension was believed to be mainly resulted from the SPM effect in the fibre.

To further reduce the pulse duration, the 0.3 mm thick filter was replaced by a 1 mm thick filter. It was observed that at appreciate intra-fibre power level transform limited output pulses having duration of less than 70 fs could be produced. Figure 2.24 shows the second-harmonic interferometric autocorrelation and the correspondent spectra of the output pulses at different intra-fibre power level. It can be seen that the output pulse duration decreased as the power in the external fibre was increased. When the power level in the fibre reached to 20 mW, pulses having duration of 63 fs was generated and the output spectral width in this case was as large as 45 nm. At higher intra-fibre power level (> 16 mW), a notable feature of the spectrum was the long tail appeared at the shorter wavelength side, which was transferred from the pulses returned from the external cavity and probably resulted from the higher-order dispersion term in the fibre. The diagram showing the variation of output pulse duration, spectral width and the bandwidth-duration products as function of power level in the fibre are shown in Figure 2.25.

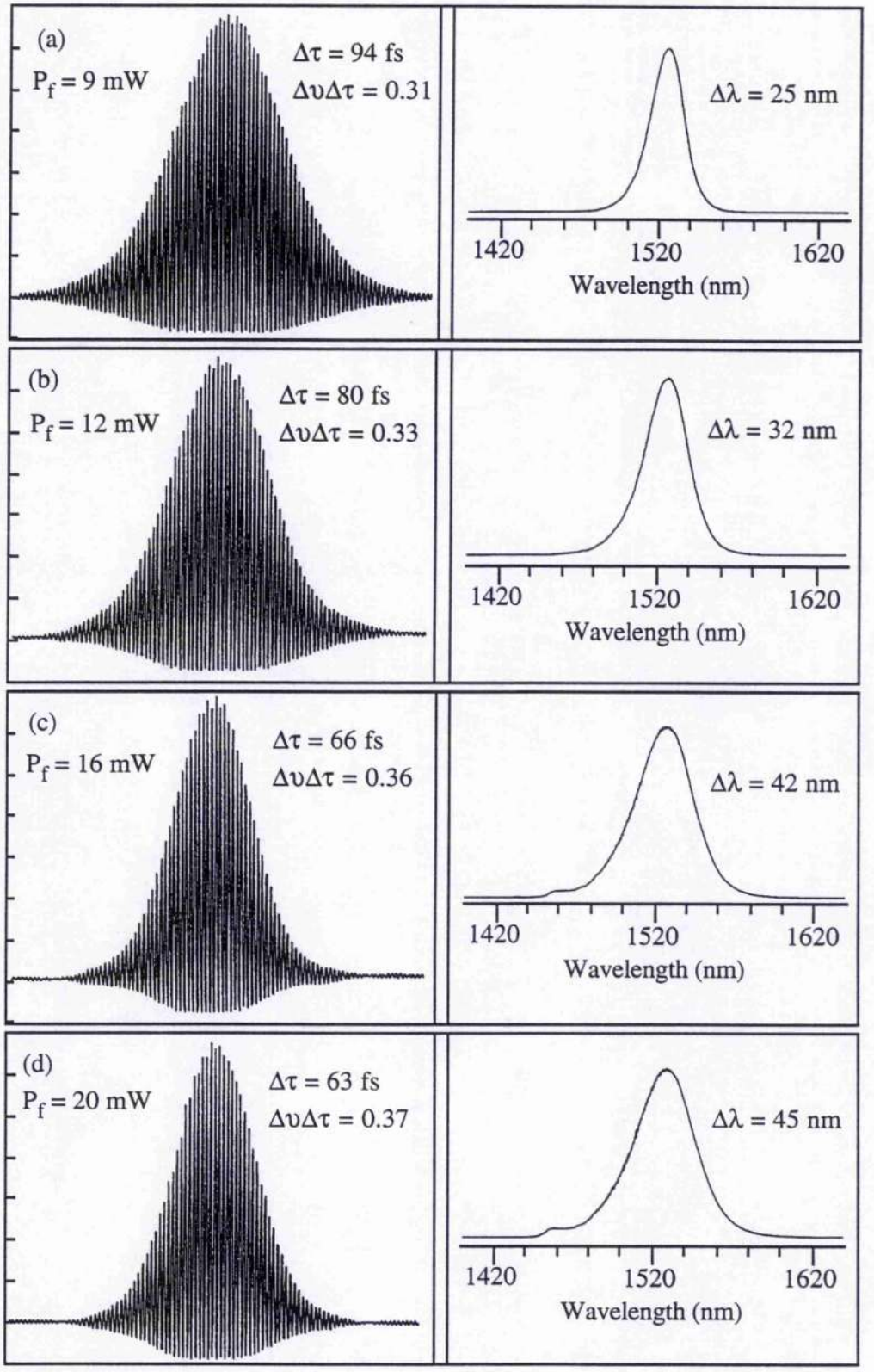

Figure 2.24 Second-harmonic interferometric autocorrelation and spectra of output pulses at different intra-fibre power level.

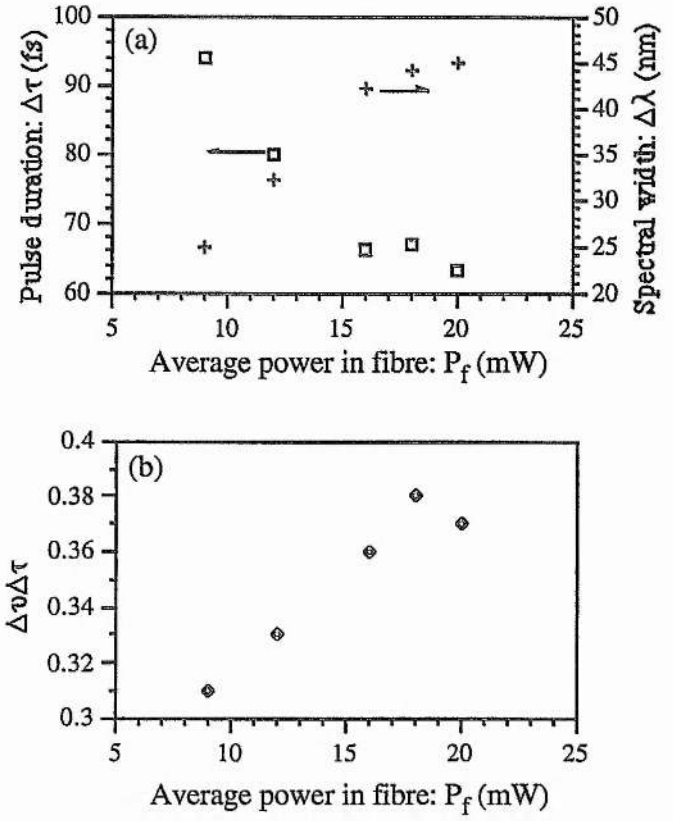

Figure 2. 25. Variations of pulse duration, spectral width (a); and the bandwidth-duration products (b) as a function of power level in the fibre.

For different power level in the external fibre, the spectra returned from the fibre is shown in Figure 2.26. At low power levels, say lower than 12 mW, the spectrum was symmetrically broadened. However, when the power level in the fibre was higher than 12 mW, the spectrum became asymmetric. The spectral profiles seem very different from the purely self-phase modulation induced spectral broadening in the way that depletion and large frequency shift occurred at the short wavelength side. By further increasing of the power in the fibre to above 16 mW, a spectral peak at the short wavelength side was gradually built up. It is believed that this depleted spectral profile was probably resulted from the involvement of the third-order dispersion term, because, as the pulses propagating in the fibre was relatively shorter, the higher-order dispersion terms could become important. In the experiment here, the duration of the output pulses

was less than 70 fs and the average power level in the fibre was higher than 16 mW, it is necessary to take account of the third-order dispersion effect.

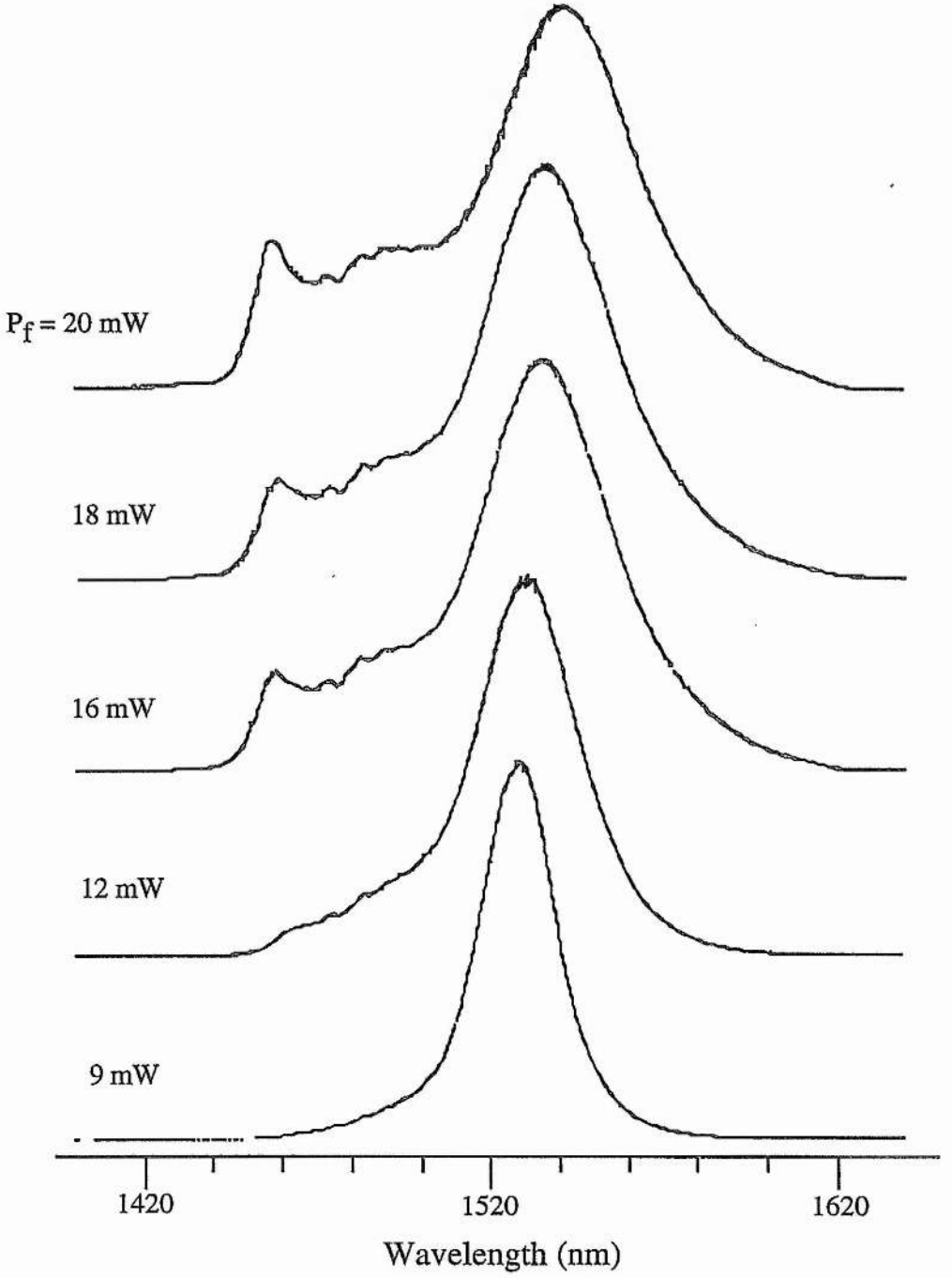

Figure 2. 26. Spectra of pulses returned from the external cavity at different power levels in the fibre.

2.3. Summary

In this chapter, the coupled-cavity mode locking of KCl:Tl colour centre laser with a 28 cm long optical fibre as the nonlinear element in the Michelson cavity arrangement has been presented. Two operational regimes were observed when there were no bandwidth limiting element (for example, a birefringent filter) in the main laser cavity. In Regime 1, clear CW mode-locked pulse train could be generated, whereas in such case the output pulse was relatively broader and was heavily chirped. In Regime 2, shorter and less chirped pulse could be obtained, however, the output pulse train was modulated with much longer Q-switched pulses. These two regimes could be obtained subsequently from Regime 1 to Regime 2 or the opposite by simply altering the reference signal applied to the PZT (i.e. varying the phase difference of the two cavity pulses).

Examination of the chirp feature in Regime 1 by passing the output pulse through a length of glass rod revealed that the output pulses were positive chirped, therefore dispersion compensation by using prisms' pair in the main laser cavity was explored. Pulses as short as 64 fs has been produced when the two prisms separated at 96 mm. It was found that although the pulse was shortened and the chirp was compressed, but the laser suffered an unstable operation.

In the motivation of restricting the lasing bandwidth and thus reducing the output pulse chirp, a 0.3 mm thick birefringent filter was inserted into the main cavity. It was found that in addition to the chirp compression the Q-switching effect was also avoided. However, in such case, the pulse duration was increased to above 200 fs. By orienting the optical axis of the filter parallel to the laser beam, transform limited pulses having duration of 87 fs was produced. As a 1 mm thick filter was used to replace the 0.3 mm filter, pulses as short as 63 fs has been generated.

References

1. L. F. Mollenauer and R. H. Stolen, Opt. Lett. 9, 13 (1984).
2 F. M. Mitschke and Mollenauer, opt. Lett. 12, 407 (1987).
3. F. M. Mitschke and Mollenauer, IEEE J. Quantum Electro. QE-22, 2242 (1986).
4. W. Sibbett, "Exploitation of optical nonlinearity for enhanced mode locking in coupled cavity lasers" Paper FQ-1, In the Technical Digest of CLEO'89, (Baltmore, USA, 1989).
5. P. N. Kean, X. Zhu, D. W. Crust, R. S. Grant, N. Landford, and W. Sibbett, Opt. Lett. 14, 39 (1989).
6. K. J. Blow and D. Wood, J. Opt. Soc. Am. B5, 629 (1988).
7. E. P. Ippen, H. A. Haus, and L. Y. Liu, J. Opt. Soc. Am. B6, 1763 (1989).
8. M. Morn and M. Piché, Opt. Lett, 14, 1119 (1989).
9. P. A. Bélanger, J. Opt. Soc. Am. B8, 2077 (1981).
10. J. Mark, L. Y. Liu, K. L. Hall, H. A. Haus, and E. P. Ippen, Opt. Lett. 14, 48 (1989)
11. G. Sucha, Opt. Lett. 16, 922 (1991).
12. H. A. Haus, J. G. Fujimoto, E. P. Ippen, J. Opt. Soc. Am. B8, 2068 (1991).
13. D. E. Spence, and W. Sibbett, J. Opt. Soc. Am. B 8, 2053 (1991).
14. J. Goodberlet, J. Jacobson, J. G. Fujimoto, P. A. Schulz, T. Y. Fan, Opt. Lett. 15, 553 (1990).
15. J. M. Liu, J. K. Chee, Opt. Lett. 15, 685 (1990).
16. F. Krausz, Ch. Spielmann, T. Brabec, E. Wintner, A. J. Schimidt, Opt. Lett. 15, 737 (1994).
17. K. Tamuro, C. R. Doerr, L. E. Nelsson, H. A. Haus, and E. P. Ippen, Opt. Lett. 19, 46 (1994).
18. X. Zhu, PhD Thesis (University of St. Andrews, 1991).
19. R. S. Grant, PhD Thesis (University of St. Andrews, 1991).
20. L. F. Mollenauer, "Colour centre laser," Chapter 2, in Laser Handbook, Vol. 4, eds. M. L. Smith and M. Bos, (Elsevier Scirence, Amsterdam, 1985).
21. L. F. Mollenauer, "Colour centre lasers," in Tunable lasers, (Topics in Applied Physics, Sringer-Velay, 1987).
22. C. R. Polock, "Color Center Lasers" In "Encyclopedia of Lasers and Opical Technology", Ed. R. A. Meyers, (TRW, Inc. 1991).
23. P. N. Kean, PhD Thesis, (University of St. Andrews, 1989).
24. R. S. Grant, and W. Sibbett, Opt. Commun. 86, 177 (1991).
25. S. M. J. Kelly, Opt. Commun. 70, 495 (1989).
26. X. Zhu, W. Sleat, D. Walker, and W. Sibbett, Opt. Commun. 82, 406 (1991).
27. X. Zhu, Finch, and W. Sibbett, J. Opt. Soc. Am. B7, 189 (1990).
28. D. E. Spence, and W. Sibbett, J. Opt. Soc. Am. B8, 2055 (1991).

Chapter 3

Pulse propagation in passive AlGaAs waveguides

3.1. Introduction

The exploitation of third-order susceptibility in passive semiconductor waveguides has attracted much interest during recent years, predominantly promoted by their potential application in optical communication systems [1, 2]. Based on their third-order susceptibility, a number of all-optical signal processing devices have been reported. These include the nonlinear directional coupler [3], nonlinear Mach-Zehnder interferometer [4], and nonlinear mode sorter [5]. Compared with glass fibres, the Kerr nonlinearity in AlGaAs waveguides working at the half-band gap is two orders of magnitude larger [6]. This large nonlinearity makes the waveguide a suitable alternative as the nonlinear element in a coupled-cavity mode locked colour centre laser. To investigate the potential of this nonlinear device as the nonlinear element in the control cavity of such a laser, an examination of the waveguide parameters was performed as described in this chapter. This was done through a study of the propagation of ultrashort laser pulses in the waveguide, and some of the fundamental concepts concerning particular waveguide characteristics will be emphasised.

3.1.1. Band structure of semiconductors

Analogous to most of the semiconductors, the passive AlGaAs waveguides possess an electron energy band structure that consists of a conduction band and the valence band, as shown in Fig. 3.1. At low temperature and in the absence of any external excitation (for example, optical pumping or electrical bias), the conduction band is normally empty and the valence band usually has a full occupancy with

electrons. The conduction band is separated from the valence band by an energy gap E_g. For compound semiconductors, such as AlGaAs, the band gap energy can be varied by changing the composition ratio of the three constituents, Al, Ga, and As [7].

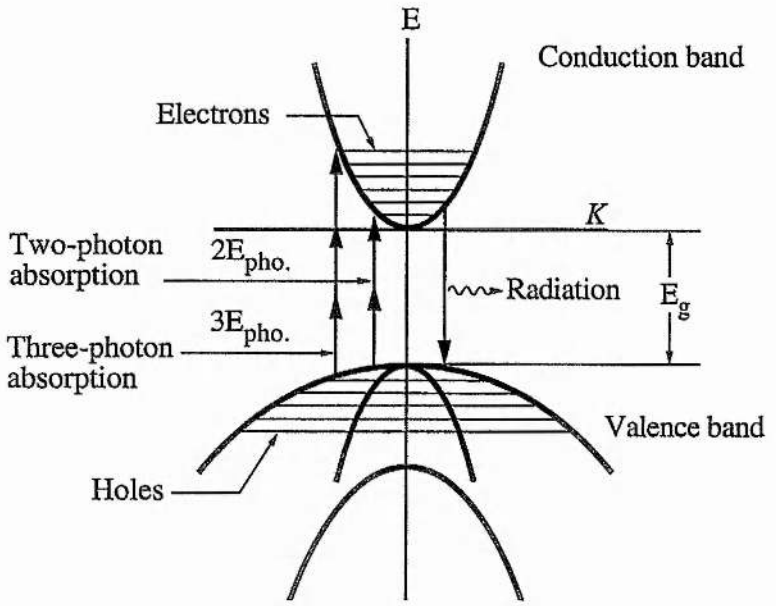

Figure 3.1. Diagram showing the typical band structure of semiconductors and the illustration of two- and three- photon absorption.

The quantum property of the semiconductor material can be characterised by a threshold wavelength, which is related to the bandgap energy, Eg, by the expression [8]

$$\lambda_{th} = \frac{hc}{E_g} = \frac{1.24}{E_g}[\mu m] \tag{3.1}$$

where h is the Planck's constant, c is the light speed in vacuum, and the E_g is in unit of eV. When the incident optical wavelength satisfies $\lambda < \lambda_{th}$ (frequency $\upsilon > \upsilon_{th}$), the quantum interaction between the optical field and the valence band electrons dominates the loss mechanisms and gives rise to a rapid attenuation of the optical signal. This quantum interaction generally excites an electron across the band gap and thus an electron-hole pair is created. As the optical wavelength λ exceeds λ_{th}, the direct band-to-band excitation becomes impossible, other attenuation mechanisms, such as multi-photon absorption, scattering, in this case may become dominant. That is the reason why all semiconductor detectors have a cut-off wavelength (beyond this

wavelength the electromagnetic wave is undetectable). In the inverse process, the recombination of electrons and holes can result in the emission of radiation. The fundamental mechanism of LEDs and semiconductor lasers is based on this latter process. The study of this chapter is mainly concerned with the propagation of ultrashort light pulses in passive AlGaAs waveguides and thus absorption associated with the multi-photon absorption effects will be discussed.

3.1.2. Introduction to the passive AlGaAs waveguides

The AlGaAs waveguides used throughout the experiments described in this thesis were fabricated by researchers in the University of Glasgow. They were produced by using MBE growth on a GaAs substrate. The 1.5 μm thick $Al_{0.18}Ga_{0.82}As$ guiding layer was sandwiched between a 4 μm thick buffer layer and a 1.5 μm thick cladding layer, both with 24% Al composition. Guiding ribs having widths between 3 and 5.5 μm were revealed in the upper cladding layer to a depth of approximately 1.3 μm using reactive ion etching. A cross-section of the AlGaAs waveguides is illustrated in Figure 3.2.

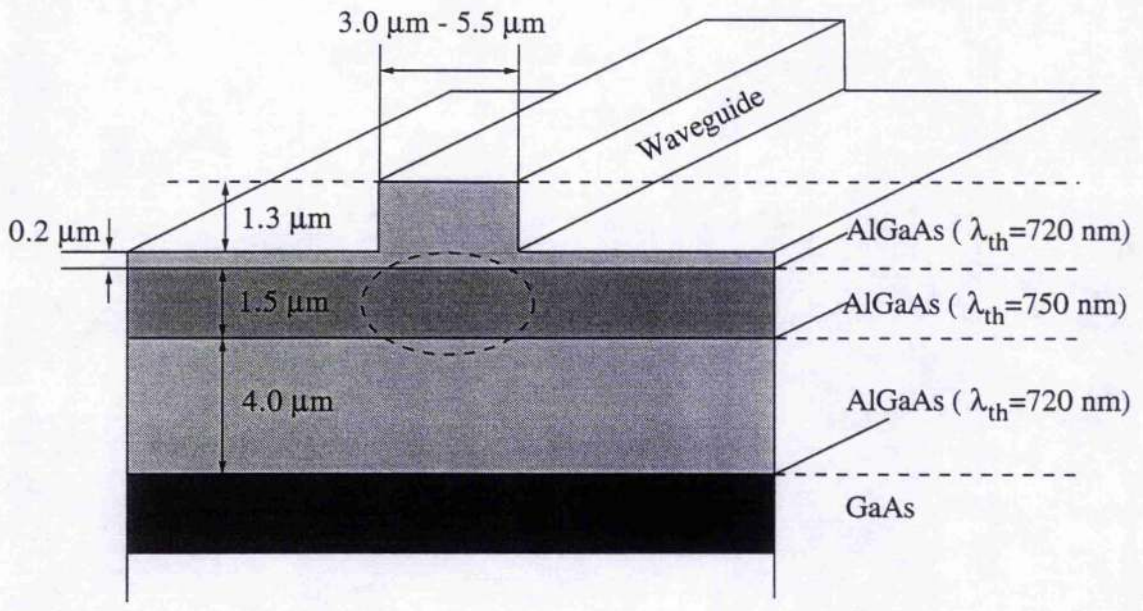

Figure 3.2. Cross-section of the waveguide used in the experiments.

For all the measurements described in this chapter, a 3.03 mm long waveguide having its two facets cleaved normal to the ridge line was used. The ridge of the waveguide was 4 μm wide, and etched to 1.06 μm deep.

3.2. Attenuation and absorption in semiconductor waveguides

3.2.1. Linear attenuation

The total loss of the waveguides to an optical field can be expressed as [9]

$$\frac{dI(z)}{dz} = -\alpha I - \beta_2 I^2 - \beta_3 I^3 - \cdots \tag{3.2}$$

where α represents the linear loss coefficient, β_2 and β_3 are the two-photon and three-photon absorption coefficients respectively. At low optical intensity, in the case before the appearance of laser, the higher-order absorption effects are very weak and can be neglected, and the linear term α in this case is in dominant. However, as the light intensity becomes higher, the effects of two- and three-photon absorption can be very significant and could become a limiting factor for the implementation of practical optical devices [10].

If only the linear loss is considered, the intensity I after travelling a distance L within the medium relates to the incident intensity I_0 and linear loss coefficient α

$$I = I_0 e^{-\alpha L} \tag{3.3}$$

The linear coefficient α in the equation is in unit of cm^{-1}. In an optical communication system, a more commonly used expression in units of dB/cm, is given below [11]

$$\begin{aligned} \alpha'(dB/cm) &\equiv \frac{10}{L}\log_{10}\left(\frac{I}{I_0}\right) \\ &= \frac{10}{\ln 10}\alpha = 4.343\alpha \end{aligned} \tag{3.4}$$

Direct interband transitions, scattering and thermal effects all could contribute to the linear loss of the waveguides. In the study here, the optical photon energy of the incident light is near the half-band gap of the AlGaAs, and so the absorption associated with the direct interband transition is impossible. The main loss associated

with the linear term in Equation (3.2) would result mainly from the scattering due to the imperfections in the ridge structure, for example, by imperfect photolithography and etching steps. With development in such fabrication techniques, AlGaAs waveguides with linear losses as low as 0.15 dB/cm (0.035 cm^{-1}) at a wavelength of 1.52 μm has been reported [12].

3.2.2. Nonlinear loss: Multi-photon absorption (MPA)

Basic concepts

Multiphoton absorption processes have been extensively studied since the advent of the laser over three decades ago [13, 14]. Conceptually, the multiphoton absorption is readily understood. It involves the transition of an election from the low valence band to the higher conduction band due to the absorption of two or more photons of the incident light. The general theory of MPA process was initially treated by Goppert-Mayer in 1936 using a nth-order time-dependent perturbation theory and obtained an expression for the probability of the simultaneous absorption of n photons by a single atomic electron [15]. However, the quantitative calculation of the transition rate is not easy because it requires a knowledge of the eigenstates of the crystal and summation over all the energy bands [9].

In general, when the photon energy is above the band-gap energy, the fundamental absorption (single-photon transition or absorption) dominates the attenuation mechanism and therefore the material employed is said "*opaque* "to the radiation field. The multiphoton absorption in this case is comparatively much weaker. Wherever the photon energy falls below the bandgap energy, the single-photon absorption becomes no longer possible and the material is said to be of "*transparent* " to the radiation field. The multiphoton absorption in this case might become an apparent loss factor to the optical field and may affect the practical performance of optical devices, as for the case of all-optical switching in waveguides, especially at higher incident optical intensities.

Two-photon absorption

Two-photon absorption can be treated as the fundamental transition mechanism for excitation in the transparent region of the material. The simultaneous absorption of two photons of energies E_1 and E_2 produces an excitation of energy of $E_1 + E_2$, and the subsequent luminescence depends quadratically on the intensity of the exciting radiation. It has been shown by Van Stryland et al. that in direct bandgap semiconductors the two-photon absorption coefficient β_2 scales inversely with the cube of bandgap energy [13]. This relation can be expressed as

$$\beta_2 = K\sqrt{E_P}F(2\hbar\omega / E_g) / n^2 E_g^3 \tag{3.5}$$

K is a constant for all materials and has a value of 3100, E_P is a parameter of material dependence but is approximately constant, normally taken as 20 eV. The function $F(2\hbar\omega / E_g)$ is given by the relation

$$F(2\hbar\omega / E_g) = \frac{(2\hbar\omega / E_g - 1)^{3/2}}{(2\hbar\omega / E_g)^5} \tag{3.6}$$

where $\hbar\omega$ is the photon energy.

Victor Mizrahi et al. [10] demonstrated that two-photon absorption can place a fundamental limitation on the usefulness of any high $\chi^{(3)}$ material in all-optical switching schemes based on an intensity-dependent refractive index. This limitation was formulated in terms of a geometry-independent criterion. A general criterion for avoiding large TPA-induced loss is given by

$$\beta_2 I_0 L < 1 \tag{3.7}$$

assuming no linear loss. For a nonlinear directional coupler, the light-induced phase shift required is 4π, the criterion for switching is given as

$$4\pi = \frac{2\pi n_2 I_0 L}{\lambda} \tag{3.8}$$

where λ is the vacuum wavelength of light, L is the length of the waveguide, and I_0 is the required switching intensity inside the waveguide, taking into account the

waveguide mode profile. Combining relation (3.7) and Eq. (3.8), the criterion for a directional coupler is

$$T \equiv \frac{2\beta_2 \lambda}{n_2} < 1 \qquad (3.9)$$

where T is defined as the figure of merit, meaning that for effective switching a value of less than 1 is required.

Villeneuve et al. [16] have measured the nonlinear refractive index n_2 and two-photon absorption coefficient β_2 near half the bandgap in a MBE-grown, AlGaAs waveguides. It was shown that the two-photon absorption coefficient of the waveguides was in a range from 0.1 cm/GW to 1.2 cm/GW within the wavelength scale from 1660 nm to 1490 nm. The figure of merit T deduced exhibits a trend in which it decreases with increasing wavelength. The value of figure of merit was less than one at the longer wavelengths beyond 1500 nm. This shows promise for efficient nonlinear interaction.

3.3. Intensity-dependent refractive index in semiconductor waveguides

There have been been extensive studies of the third-order nonlinear susceptibility $\chi^{(3)}$ related nonlinearity in semiconductor waveguides. These are actively pursued because of two motivations. In the first instance, the optical waveguide geometry offers a means of avoiding the unattractively high pumping power generally required for conventional bulk nonlinear optics. Secondly, it has been recognised that the passive and active guided-wave optical devices could be incorporated into compact monolithic optical circuits capable of complex functions which mimic some aspects of integrated electronics. In practice, the confinement of optical light in the semiconductor waveguide makes it a suitable element for all-optical processing devices based on the third-order nonlinear susceptibility, $\chi^{(3)}$.

Nonlinear optical processes are often limited by their time response, heating, or loss which relates to the excitation of charge carriers in the material. It is an advantage for many photonic applications if the nonlinear process is dominated by a refractive change that promptly follows the pump field without significant loss in the material.

Unfortunately nonlinear index changes are intrinsically connected with nonlinear loss. Resonant nonlinearity can be extremely large, but recovery time are slow because they are limited by the carrier recombination. Nonresonant nonlinearities (such as Kerr effect) have a rapid recovery time because they are not associated with any population transfer. Different mechanisms can contribute to the third-order nonlinearity and these will be briefly discussed below.

3.3.1. Kerr effect

The Kerr effect, or bound electron nonlinearity, offers the fastest response to the optical light pulses. This effect can be described as harmonic oscillations of bound electrons which yields a nonlinear index change without the absorption of energy. Since no electron bonds are broken, carriers are not generated, and the relaxation time to an intense pulse of light can be extremely rapid, of the order 10^{-14} s [2].

In general, the Kerr nonlinear refractive index n_2 of a semiconductor waveguide can be obtained by measuring the self-phase-modulation induced phase shift of ultrashort, high intensity light pulses travelling through the waveguide. It is known that the maximum nonlinear phase shift imposed on a pump pulse propagating in a material having third-order optical nonlinearity n_2 is given by

$$\Delta\phi = \frac{2\pi}{\lambda} L n_2 I \qquad (3.10)$$

where L is the interaction length, I is the light intensity at the temporal peak of the pulse averaged over the spatial beam mode, and λ is the wavelength. It can be seen that if the nonlinear phase shift, waveguide length and the peak intensity in the waveguide are known then the nonlinear refractive index can be derived as discussed later.

Equivalent to Equation (3.5), for the intensity-dependent refractive index n_2, a corresponding scaling law also exists, which was derived from the application of Kramers-Kronig relation to the scaling law given by Eq. (3.5) and has the form of [17]

$$n_2(esu) = K' \frac{G_2(\hbar\omega)/E_g)}{n_0 E_g^4} \tag{3.11}$$

where $K' = 3.4 \times 10^{-8}$, $G_2(\hbar\omega / E_g)$ is the dispersion function obtained from a Kromers-Kronig transform on $F(2\hbar\omega / E_g)$ given in Equation (3.6). It can be seen that the nonlinear refractive index n_2 scales inversely as the fourth power of the band-gap energy.

For the half-bandgap AlGaAs waveguide used here, the nonlinear refractive index is estimated to be in the order of 10^{-13} cm^2/W at wavelength of around 1.5 μm. This value is more than two orders magnitude larger than that in glass fibres. Glass fibres have one of the lowest optical nonlinearities because of their large band gap. A notable feature for optical fibres is that one is able to make low-loss optical fibres many kilometres in length so that despite the low nonlinearity, large phase shifts can be obtained. However, using semiconductor waveguides less than one centimetre in length one can achieve a large phase shift, if operating at photon energies just below half of the band-gap energy so as to avoid two-photon absorption. Phase shift, resulting from the Kerr nonlinearity, as large as 4.5 π have been observed by Ho et al. in $Al_{0.2}Ga_{0.8}As$ waveguides for wavelengths below the two-photon absorption edge. [18].

3.3.2. Effect of free carriers to the third-order nonlinearity

Carriers generated from the multiphoton absorption will also contribute to the refractive index changes of waveguide material. This can be understood as the result of intensity-dependent change in the first-order susceptibility, $\Delta\chi^{(1)}$, owing to the carrier populations. It can be described by quoting an effective third-order susceptibility, $\chi_{eff}^{(3)}$, and the induced polarisation could be expressed as

$$P(\omega) = (\chi^{(1)} + \chi_{eff}^{(3)}|E(t)|^2)E(\omega) = (\chi^{(1)} + \Delta\chi^{(1)})E(\omega) \tag{3.12}$$

where E(ω) is the magnitude of incident light field [14].

3.3.3. Thermal effect on the refractive index

The dissipation of absorbed energy will inevitably lead to heating of the crystal lattice. The rise in temperature in turn could lead to the refractive changes of the waveguides. The reason for refractive index changes can be understood as a result of the bandgap variation at different temperatures. The magnitude of this is related to the material absorption coefficient, heat capacity, thermal conductivity, and temperature dependence of the linear refractive index [2, 14].

3.3.4. Electrostrictive nonlinearity

Electrostrictive nonlinearity is one of the mechanisms responsible for the self-trapping of intense laser beams. It was originally encountered when dealing with self-focusing effect of Q-switched laser pulses propagated through liquids [see, for example, Ref. 19]. This effect arises from the strain field induced by the laser pulse and is proportional to the gradient of the laser intensity. The strain fields causes a position-dependent variation of the density of the material, thus giving rise to the focusing of laser beam. This characteristic is a slow nonlinear effect where the response time is typically in the nanosecond regime [20]. For pulses with picosecond and femtosecond durations, this effect is very weak and can therefore be neglected.

3.4. Dispersion in semiconductor waveguides

As in all materials, the refractive index of semiconductor waveguides is wavelength-dependent and so the different spectral components of optical pulses travel at different group velocities. Therefore, after passing through the waveguide, ultrashort light pulses with a broad spectrum may well acquire some appreciable temporal broadening. Such pulse broadening could become a limiting factor for the implementation of practical all-optical devices. Furthermore, when it is combined with the spectral broadening effect due to SPM, this effect could be more severe. It has been reported that pulses with duration of 430 fs are broadened to 650 fs after passing through a 2 mm long AlGaAs waveguide [21]. However, such effects have not yet been taken into account when dealing with practical waveguide devices. In this

chapter, some experimental results related to pulse broadening in AlGaAs waveguide will be presented. In Chapter 6, an experiment for measuring the GVD of the waveguide will be described.

3.5. Experimental measurement of the waveguide parameters

3.5.1. Linear loss measurement

Principle of measurement

The most commonly used method for determining the linear loss of a semiconductor waveguide is to utilise the transmission feature of a Fabry-Perot resonator structure. By measuring the transmission at resonance and anti-resonance of the resonator through varying the length of the waveguide, the linear loss can be obtained. Kaminow and Stulz were the first to use a waveguide Fabry-Perot structure to determine the loss of a nominal 4 μm strip guide [22]. The principle of the measurement is quite straight forward. It is known that the optical power transmitted from the Fabry-Perot (FP) waveguide resonators formed by the two cleaved opposite facets of the waveguides is given by

$$T(\phi)=\frac{(1-R)^2 e^{-\alpha L}}{(1-\tilde{R})^2+4\tilde{R}\sin^2(\phi)} I_0 \tag{3.13}$$

when a perfectly coherent, monochromatic incident light beam is assumed. In this equation, α represents the linear propagation loss coefficient, I_0 is the effective input intensity including losses due to input, L is the waveguide length, R is the facet reflectivity, and $\tilde{R}=\mathrm{Re}^{-\alpha L}$, $\phi=2\pi n_{eff}L/\lambda_0$ is the single-pass phase shift in the waveguide, n_{eff} is the effective mode index. It can be seen that the transmission factor $T(\phi)$ varies periodically as the phase term ϕ. The maximum and minimum transmission occur when the phase term ϕ is 0, π and $\pi/2$, $3\pi/2$, respectively. The contrast of the transmission feature is given by

$$K=\frac{T_{\max}-T_{\min}}{T_{\max}+T_{\min}}=\frac{2\tilde{R}}{1+\tilde{R}^2} \tag{3.14}$$

By solving this equation, then:

$$\tilde{R} \equiv \mathrm{Re}^{-\alpha L} = \frac{1-\sqrt{1-K^2}}{K} \tag{3.15}$$

Therefore, the linear attenuation coefficient is given as

$$\alpha = \frac{1}{L}\left[\ln R - \ln\left(\frac{1-\sqrt{1-K^2}}{K}\right)\right] \tag{3.16}$$

From this equation, it can seen that the linear loss coefficient α can be obtained from a measurement of the fringe contrast K of the transmitted signal, provided that the facet reflectivity and waveguide length are known.

If the refractive index of the material is obtainable the facet amplitude reflectivity can be readily achieved from the Fresnel equation, which is given by [23]

$$r_{\parallel} = \frac{n_t \cos\theta_i - n_i \cos\theta_t}{n_t \cos\theta_i + n_i \cos\theta_t} \tag{3.17}$$

where n_i and n_t are the refractive index in the input space and output space, θ_i and θ_t are the incident and refractive angles respectively, and the polarisation of the light is assumed to be parallel to the incident plane. In normal incident situation, both θ_i and θ_t equal zero, and therefore the intensity reflectivity is given by $R = \frac{(n_t - n_i)^2}{(n_t + n_i)^2}$.

Normally, for linear loss measurement of a waveguide, the facets of the waveguide is cleaved perpendicular to the ridge line. Therefore, the facet reflectivity can be expressed as

$$R = \frac{(n_{eff} - 1)^2}{(n_{eff} + 1)^2} \tag{3.18}$$

where n_{eff} is the effective refractive index of the waveguide (assuming that the input space is the free space, where $n_i \approx 1$).

A more accurate measurement of the linear loss is to measure the resonance and anti-resonance transmission of waveguides at different lengths [12]. By fitting the data at different guide lengths, both the linear loss and facet reflectivity can be determined. However, this method requires that the waveguide facets in each case are cleaved in the same manner, so that an identical facet reflectivity can be assigned.

Linear loss measurement of AlGaAs waveguides

The experimental arrangement is shown in Figure 3.3. A KCl:Tl colour centre laser, as discussed in Chapter 2, was employed for this evaluation. The Nd:YAG pump laser was switched to CW output operation from the original mode locked operation, so as to obtain a narrow linewidth output. A three-stage birefringent filter was used in the colour-centre laser cavity to select the output wavelength, as well as to restrict the output bandwidth. The output of the laser was polarised in the horizontal direction (TE). The output of the laser was coupled in and out of the waveguide by using two X20 objectives. An attenuator was used to change the power coupled into the waveguide. To avoid feedback from the waveguide facets, an optical isolator was included within the laser beam. A photo diode was used to detect the transmitted signal from the waveguide, and the output of this was fed into an storage oscilloscope. During the initial coupling procedure, an infrared CCD camera monitored the mode profile of the laser beam out of waveguide, so as to ensure an optimised coupling.

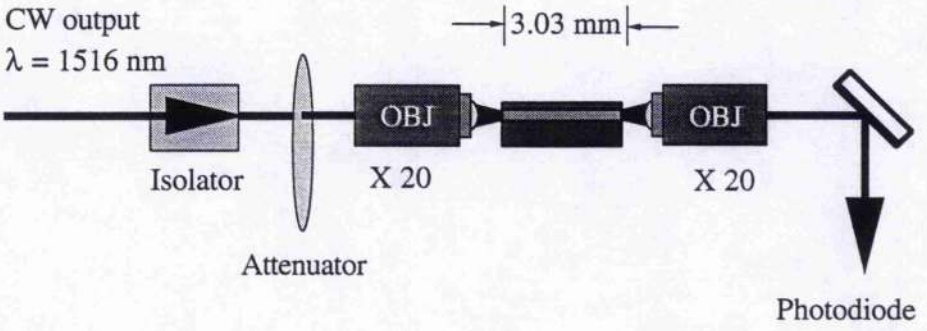

Figure 3. 3. Layout illustrating the experimental arrangement for the measurement of the linear attenuation of the waveguide.

The measurement could be conducted either by varying the laser output wavelength through the birefringent filter in the cavity, or by varying the waveguide length through altering the temperature, so as to change the phase term in Eq. (3.13). In practice both methods were employed and both of them gave a similar result. In the discussion here, only the latter case will be discussed.

The measurement was conducted with the colour-centre laser output setting at a wavelength of 1516 nm. To vary the temperature and thus alter the waveguide length and the phase shift of the laser beam within the waveguide, a liquid-nitrogen-soaked cotton ball was brought closs to the waveguide. At the same time, the variation of the waveguide transmission was recorded by using the storage oscilloscope. One key point is that the zero-reference level must be recorded at every time, although the assessment of the absolute value of the transmission is not necessary.

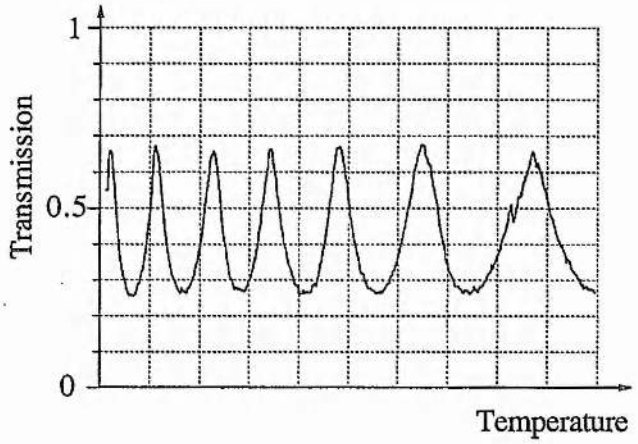

Figure 3.4. Experimental result showing the variation of transmission of a 3.03 mm long AlGaAs waveguide as a function of temperature.

Figure 3.4 shows the experimental result of the variation of transmission as a function of temperature, taken from an oscilloscope. It needs to be noted that the high transmission of 0.67 at resonance and the low transmission of 0.26 at anti-resonance shown in the diagram do no represent the real values of the waveguide transmission, they only give a relative value of the waveguide transmission. The fringe contrast K was given by

$$K = \frac{0.67 - 0.26}{0.67 + 0.26} = 0.44$$

It is known that the effective refractive index of the waveguide in the guiding region is 3.32 and so if this value is teken into Equation (3.18) the facet reflectivity is deduced to be 0.29. Following the discussion of the preceding section, if by taking the facet

reflectivity R = 0.29, waveguide length L= 0.303 cm, and the fringe contrast $K = 0.44$ into Equation (3.16); the linear loss coefficient of the waveguide can be calculated to be 0.74 cm^{-1}, which is equivalent to 3.21 dB/cm.

Discussion

The main factor affecting the accuracy of this measurement is the evaluation of the reflectivity of the waveguide facets. In the experiment, the reflectivity was taken from the Fresnel equation (3.17), which gives a upper limit and is a good approximation of perfect waveguide facets. Any defect on the facets, such as contamination, damage, or imperfect perpendicularity between the waveguide facets and the ridge line will all inevitably lower its reflectivity. Therefore, equation (3.16) always yields an attenuation coefficient that is higher than the real value when the imperfections are taken into account. The main advantages of the Fabry-Perot method is its immunity to the drift of input intensity. Whatever the cause of the change of input intensity, the value of the contrast K of the fringe will not be affected, and thus does not affect the accuracy of the measurement.

3.5.2. Measurement of two-photon absorption

Principle of measurement

The two-photon absorption coefficient can be obtained from transmission measurements at various incident intensities [24]. As described in Equation (3.2), if only up to two-photon absorption is considered, the attenuation of the light propagating through the waveguides can be expressed as

$$\frac{dI}{dz} = -\alpha I - \beta_2 I^2 \tag{3.19}$$

The evaluation of this equation yields the transmission

$$I_{trans} = \frac{(1-R)^2 \eta e^{-\alpha L}}{1+\beta_2 (1-R)\eta I_{inc}(1-e^{-\alpha L})/\alpha} I_{inc} \tag{3.20}$$

where η is the coupling efficiency into the waveguide, R is the Fresnel reflectivity of the facets and L is the waveguide length.

Rewriting Equation (3.19) as the inverse of the transmission factor $T = I_{trans} / I_{inc}$ gives

$$\begin{aligned} T^{-1} &= \frac{I_{inc}}{I_{trans}} = \frac{1+\beta_2(1-R)\eta I_{inc}(1-e^{-\alpha L})/\alpha}{(1-r)^2\eta e^{-\alpha L}} \\ &= \frac{1}{(1-R)^2\eta e^{-\alpha L}} + \frac{\beta_2(1-e^{-\alpha L})}{(1-R)\alpha e^{-\alpha L}} I_{inc} \\ &= \frac{1}{T_0} + \frac{\beta_2(1-e^{-\alpha L})}{(1-R)\alpha e^{-\alpha L}} I_{inc} \end{aligned} \tag{3.21}$$

where T_0 is the linear transmission factor. From this equation, it can be seen that the inverse transmission factor T^{-1} is the linear function of incident intensity. Thus, the plot of T^{-1} vs. I_{inc} should be a straight line with a slope directly proportional to the two-photon absorption coefficient β_2. The two uncertain factors in the measurement are the coupling efficiency and the linear absorption coefficient. However, the coupling efficiency is extracted from the Equation (3.21), and the linear absorption coefficient can be obtained by Fabry-Perot method described previously.

If the experimentally obtained slope of T^{-1} vs. I_{inc} is S_I, from Equation (3.20), it follows that

$$S_I = \frac{\beta_2(1-e^{-\alpha L})}{(1-R)\alpha e^{-\alpha L}} \tag{3.22}$$

Therefore, the two-photon absorption coefficient is

$$\beta_2 = \frac{(1-R)\alpha e^{-\alpha L}}{1-e^{-\alpha L}} S_I \tag{3.23}$$

In the evaluation of two-photon absorption, some other expressions can be encountered in the literature. Following the discussion by Agrawal [11], the pulse duration T_0, defined as the half-width at the 1/e intensity points, is related to the pulse duration τ_p, designated as the pulse-width at half intensity points, as

Gaussian pulse $\tau_p = 1.665 T_0$ (3.24)

Sech2 pulse $\tau_p = 1.763 T_0$ (3.25)

Therefore, the peak power can be expressed as

For Gaussian Pulses: $$P_p = \frac{E}{2T_0} = \frac{P_{ave.}}{2T_0 f_p} = \frac{P_{ave.}}{1.065\tau_p f_p} \quad (3.26)$$

For Sech^2 pulses: $$P_p = \frac{E}{2T_0} = \frac{P_{ave.}}{2T_0 f_p} = \frac{P_{ave.}}{1.134\tau_p f_p} \quad (3.27)$$

where E represents the pulse energy and is given by $E = P_{ave.}/f_p$, $P_{ave.}$ is the average power in the waveguide, f_p is the repetition rate of the laser pulses. The peak intensity in the waveguide may be expressed as

$$I_p = \frac{P_p}{A_{eff.}} = \frac{P_{ave}}{1.134\tau_p f_p A_{eff.}} \quad (3.28)$$

where $A_{eff.}$ is the effective mode area of the waveguide.

In most cases, the experimentally measured slope represents the inverse of transmission against average incident power. If expressed as S_p, then by using Equation 3.23 the two-photon absorption coefficient can be expressed as

$$\beta_2 = \frac{1.134\tau_p f_p A_{eff.}(1-R)\alpha e^{-\alpha L}}{1-e^{-\alpha L}} S_p \quad (3.29)$$

assuming a Sech^2 pulse profile.

From Equation (3.20), it can be seen that the intercept of the fitted line with the y-axis should be the inverse of the linear attenuation ($1/T_0$). This feature can be used as a cross-reference for the reliability of the two-photon absorption measurement. If the intersection point is far from the inverse of the experimentally measured linear loss, it might imply that some experimental errors are present. Alternatively, it could signify that other nonlinear effects (such as three-photon absorption) may exist.

For the evaluation of the two-photon-absorption, the laser pulse profile should be considered. The linear relationship between the inverse of transmission and the incident power is only valid for a square pulse shape in both temporal and spatial domains. Therefore, the raw data obtained for the Gaussian (or Sech2) pulse profile should be referenced to the square pulse shape [25], so that a linear relationship between the inverse of the transmission and the incident power can be assumed.

Two-photon absorption measurement of AlGaAs waveguides

The experimental set-up is shown in Fig. (3.5). Picosecond and femtosecond laser pulses could be readily obtained from the synchronously or coupled-cavity mode locked KCl:Tl colour-centre laser, as discussed in Chapter 2. The output of the laser was polarised in the horizontal direction. The wavelength of the output pulses was centred around 1516 nm. Similar to the case of linear loss measurement, an optical isolator was included within the laser beam to prevent the feedback from the waveguide facets. An attenuator wheel was employed to vary the power level coupled into the waveguide. To make the variation of the power smooth, the attenuator wheel was driven by a small electric motor. A mirror with 90% reflectivity was used to split the laser beam intensity into two parts, where one part went to the waveguide and the other was directed to a photo diode (named photo diode 1). The coupling of the laser beam into and out of the waveguide was accomplished by two X20 objectives, and an infrared CCD camera was frequently used to monitor the profile of the beam out of the waveguide during the original stage of the coupling procedure. The laser signal transmitted through the waveguide was detected by photo diode 2. To record the variation of the transmission as a function of input power, a chart recorder was used. The output electronic signal from the photo diode 1 was fed to the X axis of the chart recorder, and the output electronic signal from photo diode (2) was connected to the Y axis of the chart recorder; so that a plot illustrating the relationship of transmitted power and incident power could be recorded.

The incident and transmitted power level corresponding to different position of the plotted chart was calibrated prior to the experimental measurement. This was done by measuring the power and marking the corresponding position of the X and Y axes of the coordinate. The procedure was conducted as follows: Firstly, with the laser beam blocked, the zero position was marked on the plotting paper of the chart recorder. Secondly, with the Y axis unconnected or the laser beam out of the waveguide blocked, the X axis of the coordinate was marked. Thirdly, with the X axis

unconnected or the beam leaking out of the reflection mirror blocked, the Y axis of the coordinate was marked. One important thing is that the photo diode should respond linearly to the incident optical power. This was achieved by choosing the appropriate photo diodes and setting up a suitable voltage bias on the photo diodes.

During the experiment, both picosecond and femtosecond pulses were employed. The femtosecond pulses could be achieved by coupled-cavity mode-locking of the KCl:Tl colour-centre laser with a piece of optical fibre, while a picosecond output could be obtained directly from the colour-centre laser alone with the external cavity blocked. First of all, prior to the experiment, the two photo diodes were calibrated with a CW output or with much broader pulses, ensuring that a linear response for the two photo diodes at the power levels involved.

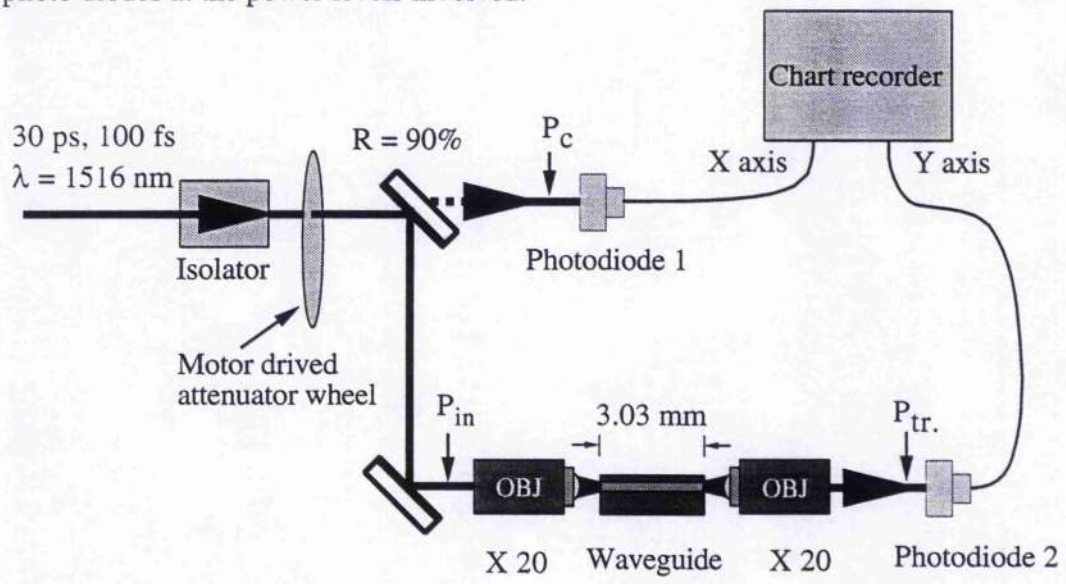

Figure 3. 5. Experimental set-up for the measurement of two photon absorption.

The experimental result is shown in Fig. (3.6), where the Y axis of the coordinate represents the transmitted average power and the X axis is the incident average power. It can be seen that for the 30 ps pulses the transmitted power is a linear function of incident power within the incident power range of 60 mw available in the experiment. This means that essentially no two-photon absorption occurred for the 30 ps pulse. For the 100 fs pulses, however, the distinctive curve indicates that a strong two-photon absorption occurred.

From the linear relationship of the transmitted and incident power for the 30 ps pulses, the effective total linear transmission of the waveguide could be estimated. This was about 22%, given simply by the gradient of the straight line. This linear transmission is expressed as

$$T_{Lin.} = \eta(1-R)^2 e^{-\alpha L} \tag{3.30}$$

As mentioned earlier, η is the total coupling efficiency of waveguide, R is the facet reflectivity, α is the linear loss of the waveguide, and L is the waveguide length. By taking the measured value of the linear loss α= 0.74 cm^{-1}, and facet reflectivity R=0.29 into this equation, then the coupling efficiency η can be deduced. This gave a value of about 55% in the experimental work prepared.

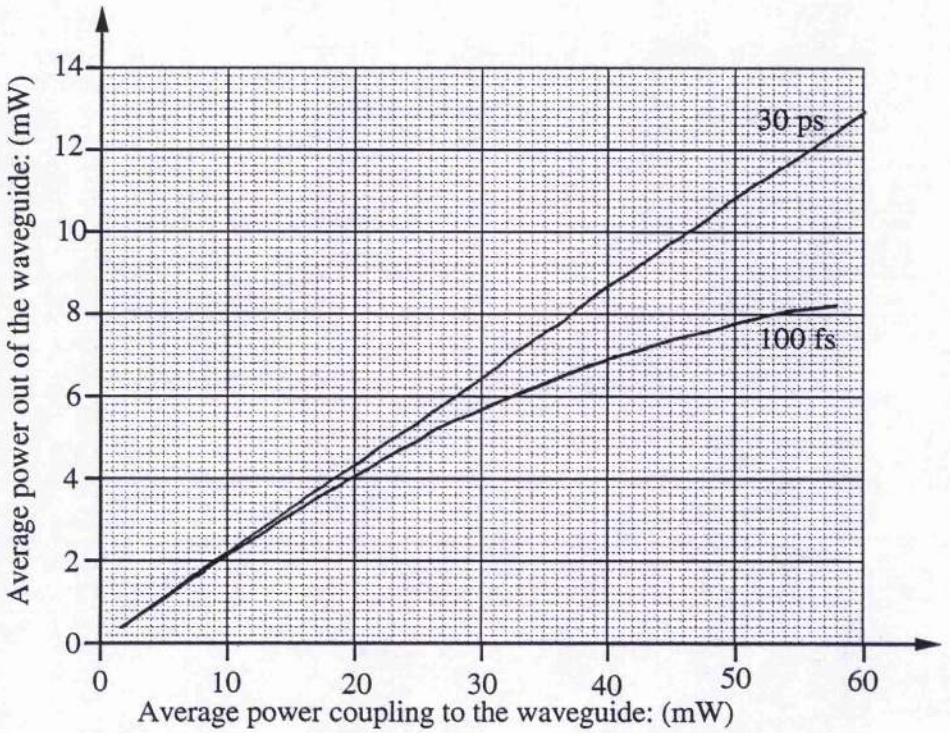

Figure 3.6. Experimental result showing the variation of the average power out of the waveguide as a function of the input power for the 30 ps and 100 fs laser pulses.

For the 100 fs pulses, the inverse of the transmission 1/T ($P_{tran.}/P_{in}$) as a function of incident power (P_{in}) is shown in Figure 3.7. The lower dotted curve is obtained from the raw data, while the upper dotted curve is corrected to square pulse profile

assuming that the original pulse was Gaussian shaped in both space and time. It can be seen that, instead of being a linear function, the inverse of the transmission as a function of the incident power was a curve with positive curvature. This feature of the curve was most likely to have resulted from the presence of three-photon-absorption. As discussed earlier, if only the linear loss and two-photon absorption are considered, a straight line should be simply assumed for the function of transmission inversion versus the incident power. However, as three-photon-absorption is involved, this linear relationship no longer holds and a curve with positive curveture would be obtained, because of the reduction in the transmission at increased incident power levels.

To limit the influence of three-photon effect in the evaluation of the two-photon-absorption coefficient, linear fitting of the experimentally obtained data was performed within the range of incident power level lower than 30 mW. As the formula in the inset of Figure 3.7 shows, for the corrected data the slope of the linear fitted line was 0.088. The intercept point of this fitted line with the y-axis was 4.034. As discussed earlier, the inverse of this intercept point should give the linear transmission, which was 25% in this case, slightly larger than the measured value of 22%.

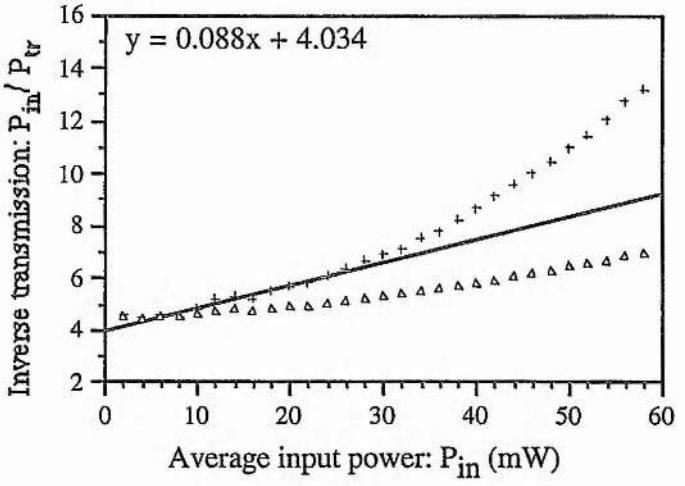

Figure 3.7 . Variation of the inverse transmission as a function of incident power level. The lower one is the raw experimental result, the upper one corresponds to the case after being corrected to square pulse shape [25].

Table 3.1. Parameters used in the evaluation of two-photon-absorption coefficient.

τ_p (fs)	f_p (Hz)	$A_{eff.}$ (cm^2)	R	L (cm)	α (cm^{-1})	S_p (mW^{-1})
100	84×10^6	6×10^{-8}	0.29	0.303	0.74	0.088

For the calculation of the two-photon absorption coefficient, the parameters involved are summarised in Table 3.1. The effective mode area was taken as 6 μm^2, which was chosen as the geometric area of the ridge width (4 μm) times the height of the guiding layer (1.5 μm). By taking the data of Table 3.1 into Eq. (3.29), the two-photon-absorption coefficient is calculated to be

$$\beta_2 = 0.1 \ \ cm/GW$$

Any error mainly originated from the uncertainty in the assumption of the pulse profile and the presence of three-photon-absorption.

Discussion

There were a few factors that affected the accuracy of the measurement. Experimentally, a laser producing femtosecond pulses is not an ideal choice, because the pulse shape factor makes the inverse transmission against the input power vary from the assumed straight line as predicted theoretically for the square pulses in the previous section. A better choice would be pulses with few tens picosecond in duration. However, in the experiments here the relatively low laser output power restricted the observation of two-photon observation in the picosecond regime, and so the femtosecond pulses were employed. The smooth rotation of the attenuator wheel and linear response of the photo diodes all could affect the accuracy of the measurement. Theoretically, the involvement of three-photon-absorption should be considered in the evaluation of absorption parameters. However, this would need a more complex modelling procedure to be applied.

3.5.3. Measurement of the nonlinear refractive index

The nonlinear refractive index of semiconductors can be obtained in varieties of techniques by measuring the nonlinear refractive index related effects [25], such as the

nonlinear phase shift experienced by the optical pulses [18, 26, 27]. It has been shown that the most reliable and straightforward method to determine the nonlinear refractive index is to measure the phase shift of light pulses after passing through the waveguide. As presented in Chapter 1, the nonlinear phase shift $\Delta\phi$ is related to the peak intensity I_p through the nonlinear refractive index n_2 by the relationship:

$$\Delta\phi = (2\pi L_{eff} / \lambda) n_2 I_p \qquad (31)$$

where $L_{eff.}$ is the effective length of the waveguide and λ is the wavelength in vacuum. If the phase shift and optical intensity are known, then the nonlinear refractive index can be determined.

The experimental set-up for the measurement of the passive AlGaAs waveguide was similar to Figure 3.5; except that the transmitted signal was split into two parts, in which one part was fed to a second-harmonic autocorrelator and the another approached to a monochrometer.

The experimental result is shown in Figure 3.8, where the spectral and temporal characteristics of the transmitted pulses are depicted. The left column shows the input spectrum (a), and the transmitted spectra (b) - (d) at different intra-waveguide power level; the middle and right columns correspond to the interferometric and intensity autocorrelation respectively for the input pulses (a), and transmitted pulses (b) - (d). It can be seen that both the spectral width and the pulse duration were clearly broadened, and the higher the power, the larger the amount of broadening would be. It is believed that the spectral broadening resulted from the self-phase-modulation of the pulses in the waveguide, while the temporal broadening was predominantly caused by the positive GVD of the waveguide at this wavelength. (GVD measurement of the waveguide will be discussed in Chapter 6).

The nonlinear phase shift $\Delta\phi$ corresponding to Figure 3.8 (b), (c), (d) are approximately about π, 1.5π, and 2.5π respectively [28]. Asymmetry of the spectra resulted mainly from the asymmetries of the input pulse shape. The effective length of the waveguide was calculated to be 2.71 mm by using the measured linear attenuation

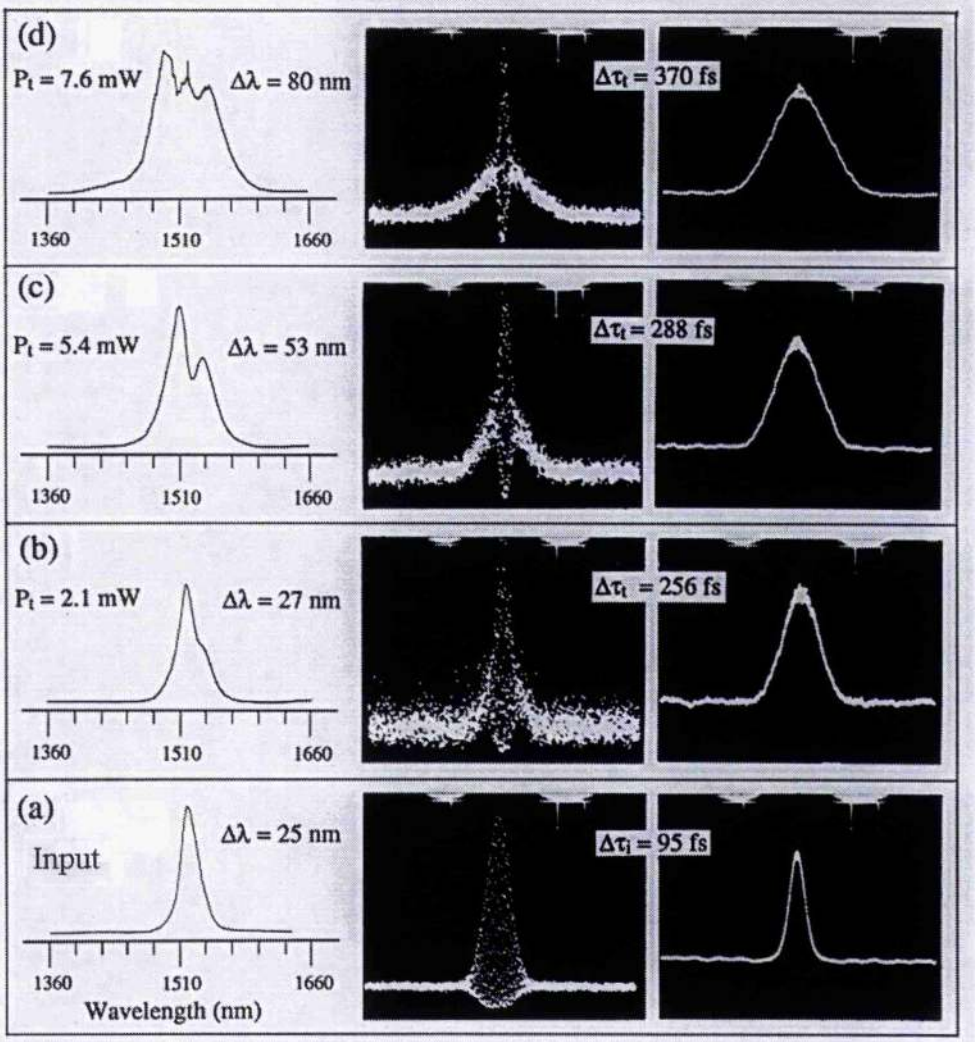

Figure 3.8. Spectra and autocorrelation traces of the input (a) and the transmitted pulses (b) - (d) at different power level.s

coefficient α. By taking the waveguide facet transmission of 0.71, then the average power within the waveguide corresponding to the cases in Figure 3.8 (b), (c), (d) were 3 mW, 7.6 mW, and 10.7 respectively. Therefore, the nonlinear refractive index for the three cases are estimated to be (b) 0.95 x 10^{-13} cm^2/W, (c) 0.6 x 10^{-13} cm^2/W, and (d) 0.85 x 10^{-13} cm^2/W. For this evaluation, the pulse duration was taken as the averaged value of the input and transmitted pulse duration, so as to take account of the pulse broadening factor involved. By averaging the three calculated values, a nonlinear refractive index of $n_2 = 0.8 (\pm 0.1) \times 10^{-13}$ cm^2/W has been estimated. This result is in

a reasonable agreement with the result of $n_2 = 5.8 \times 10^{-14}$ cm^2/W presented in Reference [4].

There were a few factors that affected the accuracy of the measurement. First of all, the peak intensity varied along the waveguide, owing to the pulse broadening effect. Secondly, the effective mode area used in the evaluation was an estimation and it might differ from the real value. Thirdly, the two-photon-absorption would reduce the peak power and thus to some extent would affect the accuracy of the measurement. However, this method clearly provides a quantitative knowledge of the nonlinear refractive index, and it represents a good approach for the estimation of the nonlinear refractive index in a waveguide geometry.

By taking the experimentally measured values of β_2 and n_2 into Eq. (3.9), the figure of merit of the waveguide at 1.515 μm was estimated to be 0.397. This satisfies the criterion of $T < 1$ for all-optical switching [10].

3.6. Summary

In this chapter, the nonlinear pulse propagation in passive AlGaAs waveguide has been described. Some background aspects of linear attenuation and multiphoton absorption have been presented. The measurement of the linear attenuation and two-photon-absorption coefficients of a 3.03 mm long AlGaAs waveguide were conducted and it was deduced that an AlGaAs waveguide has a linear loss coefficient of about 0.74 cm^{-1}, and a two-photon-absorption coefficient of 0.1 cm/GW. A single-pass evaluation for the propagation of 95 fs pulses in the waveguide revealed that both the spectrum and duration of the pulse were distinctively broadened. It has been concluded that the spectral broadening resulted from the self-phase-modulation effect in the waveguide, while the temporal broadening was mainly due to the group-velocity-dispersion in the waveguide. Evaluation of the experimental results implied that the nonlinear refractive index of the waveguide, n_2 was 0.8×10^{-13} cm^2/W and this result agrees closely with theoretical predictions.

References

1. G. I. Stegeman, E. M. Wright, Optical and Quantum Electronics, 22, 95 (1990).
2. I. Bennion and M. J. Goadwin, Chapter 8, In "Nonlinear Optics in Signal Processing," Ed. R. W. Eason, A. Miller, (Engineering Aspects of Laser Series, Series editor, Dr. T. A. Hall, Champman-Hall.)
3. A. Villeneuve, C. C. Yang, P. G. T. Wigley, G. I. Stegeman, J. S. Aitchison and C. N. Ironside, Appl. Phys. Lett. 61(2), 147 (1992).
4. K. Al-hemyari, J. S. Aitchison, C. N. Ironside, G. T. Kennedy, R. S. Grant, and W. Sibbett, Electronics Letters, 28, 1090 (1992).
5. Y. Silberberg and G. I. Stegeman, Appl. Phys. Lett. 50, 801 (1987).
6. M. N. Islam, C. E. Soccolich, R. E. Slusher, A. F. J. Levi, W. S. Hobson, and M. G. Yong, J. Appl. Phys., 71, 1927 (1992).
7. John Gowar, Chapter 7, "Optical Communication Systems," Prentice-Hall International Series in Optoelectronics.
8. John Gowar, Chapter 12, "Optical Communication Systems," Prentice-Hall International Series in Optoelectronics.
9. V. Nathan, A, H. Gueuther, S. S. Mitra, J. Opt. Soc. Am. B. 2, 294 (1985).
10. V. Mizrahi, K. W. Delongm, and G. I. Stegeman, M. A. Saii and M. J. Andrejco, Opt. Lett. 14, 1140 (1989).
11. G. P. Agrawal, "Nonlinear fibre optics," (Academic Press, Boston, 1989).
12. E. Kapon, R. Bhat, Apll. Phys. Lett. 50, 1628 (1987).
13. E. W. Van. Stryland, H. Vanheerzeele, M. A. Woodall, M. J. Soileau, A. L. Smirl, S. Guha, T. F. Boggess, Optical Engineering, 24, 613 (1985).
14. A. Miller, Chapter 3, In "Nonlinear Optics in Signal Processing," Ed. R. W. Eason, A. Miller, (Engineering Aspects of Laser Series, Series editor, Dr. T. A. Hall, Chapman-Hall.)
15. M. Göppert-Mayer, Ann. d. Phy. 9, 273 (1931).
16. A. Villeneuve, C. C. Yang, George I. Stegeman, Chen-Hui Lin and Hao-Hsiung Lin, Appl. Phys. Lett., 62, 2464 (1993).
17. M. Sheik-Bahae, D. J. Hogan, and E. W. Van Stryland, Phy. Rev. Lett. 65, 96 (1990).
18. S. T. Ho, C. E. Soccolich, M. N. Islam, W. S. Hobson, A. f. J. Levi, and R. E. Slusher, Appl. Phys. Lett., 59, 2558 (1991).
19. O. Svelto, in Progress in Optics XII, edited by E. Wolf, North-Holland, (1974).
20. W. Lee Smith, "Nonlinear refractive index", in "Handbook of laser science and technology", by Marvin J. Weber, CRC Press, Vol. III, Part I, 259 (1986).
21. M. J. LaGasse, K. K. Anderson, C. A. Wang, H. A. Haus, and J. G. Fujimoto, Appl. Phys. Lett. 56, 417 (1990).

22. E. P. Kaminow, L. W. Stulz, Appl. Phys. Lett. 33, 62 (1978).

23. E. Hecht, "Optics" Secon Edition, (Addison-Wesley Publishing, 1989).

24. A. Villeneuve, M. Sundheimer, N. Finlayson, and G. I. Stegemen, Appl. Phys. Lett. 56, 1865 (1990).

25. W.Lee Smith, "Two-photon absorption in condensed media," In Handbook of laser science and technology", by Marvin J. Weber, CRC Press, Vol. III, Part I 229 (1986).

26. M. J. Lagasse, K. K. Anderson, H. A. Haus, and G. W. Fujimoto, Appl. Phys. Lett., 45, 2068 (1989).

27. K. L. Hall, A. M. Darwish, E. P. Ippen, U. Koren, G. Raybon, Appl. Phys. Lett. 62, 1320 (1993).

28. R. H. Stolen and C. Lin, Phys. Rev. A 17, 1448 (1978).

Chapter 4

Coupled-cavity mode locking of KCl:Tl colour-centre laser with passive AlGaAs waveguides

4.1. Introduction

In Chapter 2, coupled-cavity mode-locking of KCl:Tl colour centre laser with a length of optical fibre has been discussed, where 63 fs pulses were generated. It has been shown that along with the optical fibres a number of nonlinear elements, such as semiconductor amplifiers [1, 2], quantum well structures [3, 4], also can be employed as the nonlinear element for the implementation of CCM lasers. One common feature of these elements is the high optical nonlinearity exhibited at the laser wavelengths [5, 6]. In Chapter 3, the propagation characteristics of ultrashort light pulses in passive AlGaAs semiconductor waveguides have been described. It was observed that the third-order nonlinearity is two-orders of magnitude higher than in silica fibres, and phase shifts in excess of 2π have been obtained with ridged waveguides as short as 3.03 mm long. This attainment offers the possibility for the exploitation of the waveguide as the nonlinear element for the coupled-cavity mode locked KCl:Tl colour-centre lasers. Accordingly, in this chapter, the implementation of coupled-cavity mode locking with the passive AlGaAs waveguides as the nonlinear element will be discussed. The principal advantage, as will be seen, in using the semiconductor waveguides over silica based optical fibres is their low power requirement and this affords considerable potential for miniaturisation.

The waveguides used in the experiment described here were similar to those studied in the research outlined in Chapter 3, except that a different guiding geometry was exploited. In the first instance, Brewster-angled waveguides with a straight guiding

geometry was used, as shown in the inset of Figure 4.1. The guiding ridges were cleaved in such a way that allows the incident light to be coupled into the waveguide at Breswter's angle, so that the facet reflectivity could be minimised and accordingly the transmission was maximised.

In the second case, a curved guiding geometry was used. The guiding ridges were curved in such a way that at the input facet the laser beam was incident at an appropriate angle to the normal of the front facet for good optical coupling, while at the output facet it is perpendicular to the facet surface. Ideally, a waveguide having its ridge line at the Breswter's angle incident would be the best choice, because then the facet reflectivity would be minimised. However, the original waveguide that was processed was fabricated with the radius of the curve being fixed at 20 mm, and because the waveguide crystal can only be cleaved in some particular orientation, instead of Brewster-angle, for different length of waveguides used in the following experiment a series facet-ridge angles were assessed. A schematic diagram of the waveguide guiding geometry is illustrated in the inset of Fig. 4.4. For this guiding geometry, instead of using an additional mirror and a micro-objective for the feed-back of the transmitted light as in the case with the straight waveguide; the back facet itself acts as a moderate reflectivity mirror, which gives an intensity reflectivity of about 0.29. A third option is that a curved guiding geometry was retained, but the back facet of the waveguide is gold-coated so that its reflectivity could be increased.

In the experimental work described here, each waveguide geometry was employed for the CCM KCl:Tl laser. Most of the research presented was concerned with the curved waveguide, due mainly to its higher coupling efficiency and the more effective coupling procedures involved.

4.2 Coupled-cavity mode locking with straight waveguides

4.2.1 Experimental set-up

The experimental set-up is illustrated in Figure 4.1. The coupled-cavity mode locking scheme was arranged in a conventional Fabry-Perot resonator configuration [7,

8], where the KCl:Tl colour-centre laser was synchronously pumped by a CW mode-locked Nd:YAG laser (series 3000) which has a repetition frequency of 82 MHz. With the external control cavity blocked pulses of tens of picosecond could be generated, and typical output power ranging from a few milliwatts to as high as 200 mW could be produced. The two cavities of the CCM scheme share the common mirror M1 (R = 78%), and the output was derived from a 50/50 beamsplitter (BS) inserted in the control cavity. The substrate of the waveguide was 4.15 mm long and 5.53 mm wide (see the inset of Fig. 4.1). This relatively large dimension of the substrate when presented at Brewster's angle prevented the use of lenses having working distances shorter than 2 mm, and therefore a $\times 10$ microscope objective lens (OBJ) was used to couple the input beam, and a diode collimating lens (DCL) (NA = 0.276) was used to collect the output. (It was expected that by using $\times 20$ objectives the coupling efficiency would be improved). The transmitted signal from the waveguide was then retroreflected by mirror M2, which was mounted on a piezoelectric transducer (PZT) driven by a length stabilisation system, back to the main cavity .

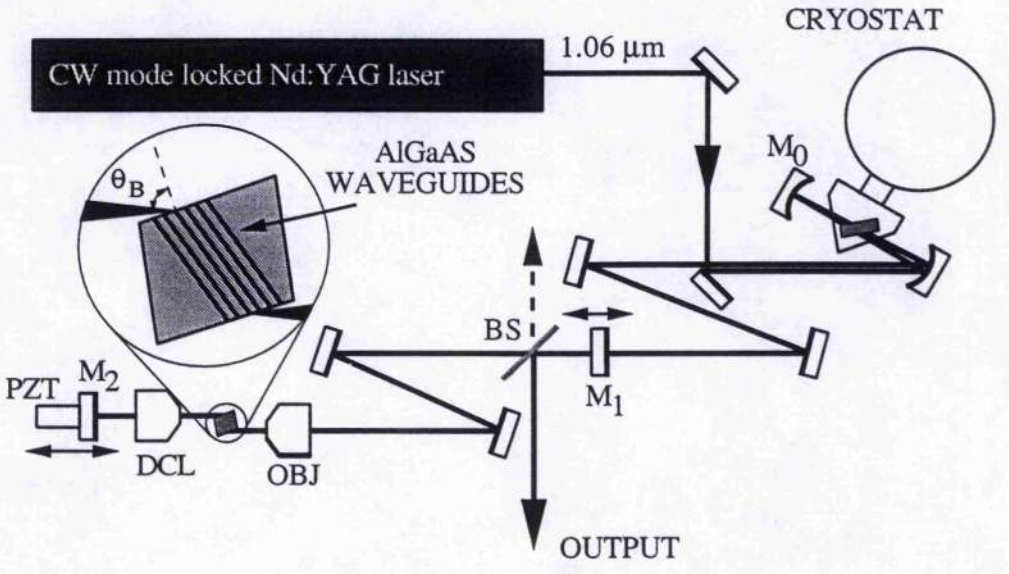

Figure 4.1. Experimental set-up of the CCM KCl:Tl colour-centre laser with a straight waveguide.

Similar to most of the coupled-cavity mode locking schemes, stabilisation of the cavity length was required [9]. This was implemented by an electronic feedback loop

system to control the position of mirror M_2, on which a piezo-electric translator was attached. This provided cavity tuning to within a fraction of wavelength. Owing to the insufficient feedback from the waveguide, large modulation of the output power was not possible. Therefore, for long term stability of the CCM process, instead of being derived directly from a photo-diode by detecting the average output power as in the case with optical fibres, the error signal was obtained from a second harmonic generator. In this way, although there might be some loss in the conversion from fundamental signal to the second harmonic, however, the modulation feature of the output was encouraged.

4.2.2. Experimental results

Measurements indicated that the throughput of the waveguide was typically about 15% of the incident power measured before the coupling objective. The effective total reflection from the waveguide was estimated to be only about 2%. Compared with an equivalent reflectivity of about 50% when optical fibres were used [10], this is clearly much poorer. For stable CCM operation, it is required that the intensity ratio between the signal returned from the control cavity and that being circulated in the main cavity has to reach a threshold level [11]. To increase the intensity ratio, the reflectivity of either mirror M_1 or the beamsplitter BS requires to be reduced, although both approaches do sacrifice some useful output power.

The procedure to achieve the CCM mode locking operation was conducted as follows. With the colour-centre laser being properly adjusted for synchronous pumping, the control cavity length was made roughly equal to that of the main cavity. The matching point of the two cavities for CCM operation could be found by varying the external cavity length gradually, while at the same time monitoring the second harmonic autocorrelator signal on an oscilloscope. The onset of the CCM operation appears as a dramatic enhancement of the second harmonic signal, resulting from the significant shortening in the output pulse duration and corresponding increase in pulse peak power. At this stage, without the stabilisation system, the output signal randomly jumped between the CCM and synchronous mode locking operation, due to random fluctuations

in the cavity lengths. When the servoloop system was applied (by altering the voltage applied to the PZT) a long-term stable CCM operation could be obtained.

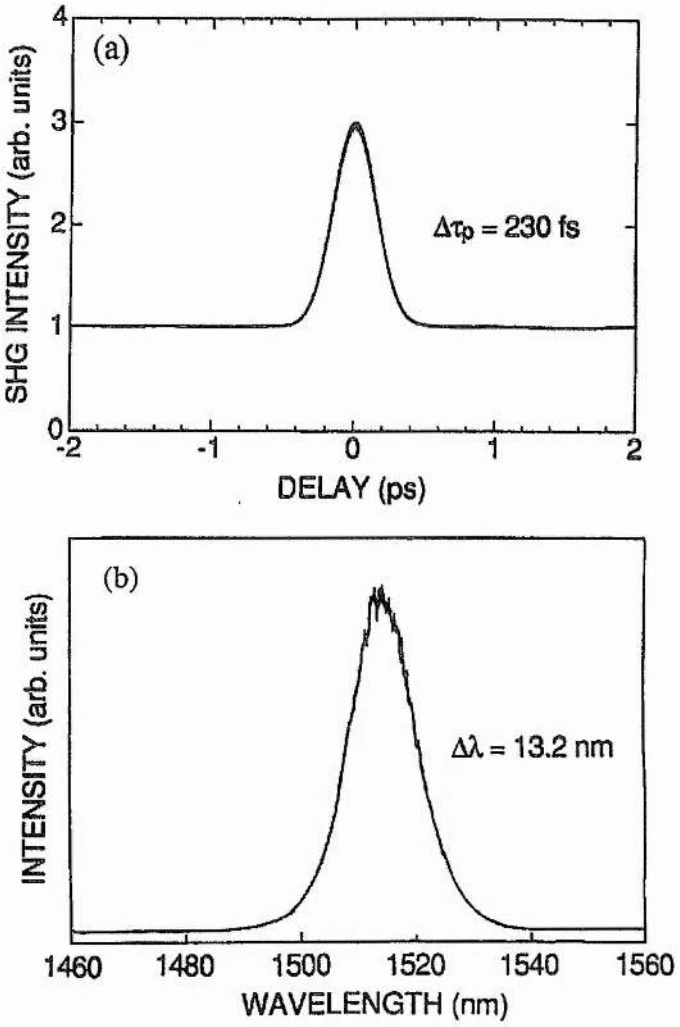

Figure 4.2. Intensity autocorrelation trace (a), and spectrum (b) of the output CCM pulses.

By using such an arrangement, pulses with durations of 230 fs were produced, as shown in Fig. 4.2, and the spectral widths were measured to be about 13.2 nm. Assuming a $sech^2$ pulse shape, a bandwidth-duration product of 0.39 was derived, which is slightly larger than that of the transform limited pulses (0.32). The pulses returned from the waveguide, illustrated in Figure 4.3, were measured to be appreciably broadened, both spectrally (30%) and temporally (120%). Given that the nonlinear attenuation was measured as low as 5%, this indicated that the temporal broadening was caused primarily by group-velocity dispersion.

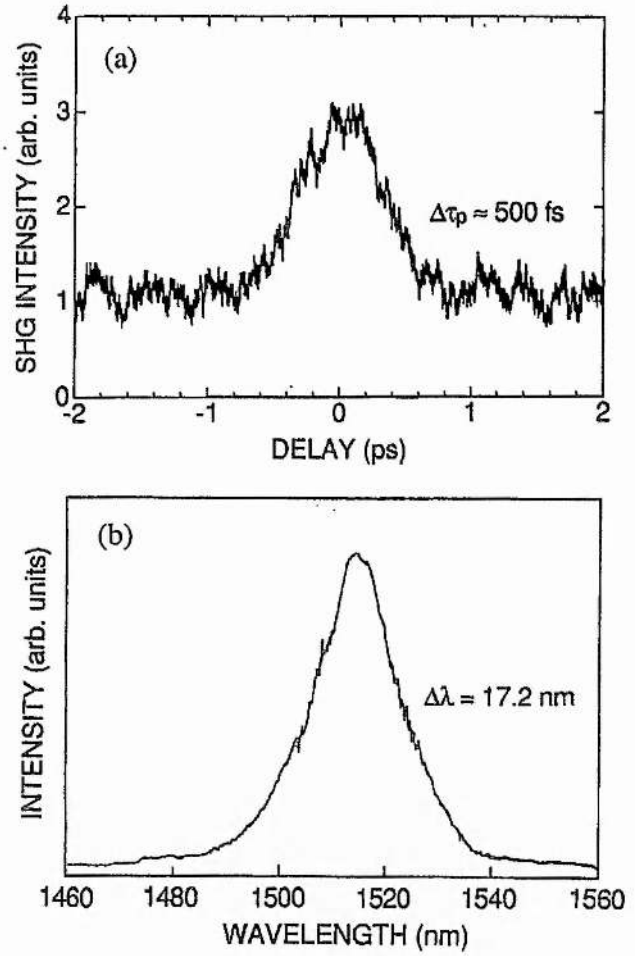

Figure 4.3. Intensity autocorrelation (a) and spectrum (b) of pulses returned from the waveguide.

The insufficient feedback from the waveguide restricted the versatility of the CCM laser, and made the spectral tuning and further shortening of the laser pulses impracticable. To eliminate such a drawback, waveguides with a different guiding geometry - curved waveguide, was employed, such that the coupling elements would be reduced and the coupling procedure was simplified. Consequently, the feedback from the waveguide would be increased, as discussed in the next section.

4.3 Coupled-cavity mode locking with curved waveguides

4.3.1 Experimental set-up

The schematic of the experimental set-up is shown in Fig. 4.4. As previously, the KCl:Tl colour-centre laser was synchronously pumped by a CW mode-locked Nd:YAG laser (series 3000). However, instead of being assembled as a Fabry-Perot resonator,

the CCM scheme was configured in a Michelson arrangement [7, 12], so that a relatively compact cavity could be configured. The linear and nonlinear branches of the Michelson cavity shared a common mirror M_{out} (R=93%), which also acted as the output coupler. Coupling of the laser beam into the waveguide was accomplished by a ×20 objective. As mentioned already, instead of using an objective to collect the transmitted signal and a mirror to reflect it back to the main cavity, the back facet of the waveguide itself acted as the end mirror of the control cavity.

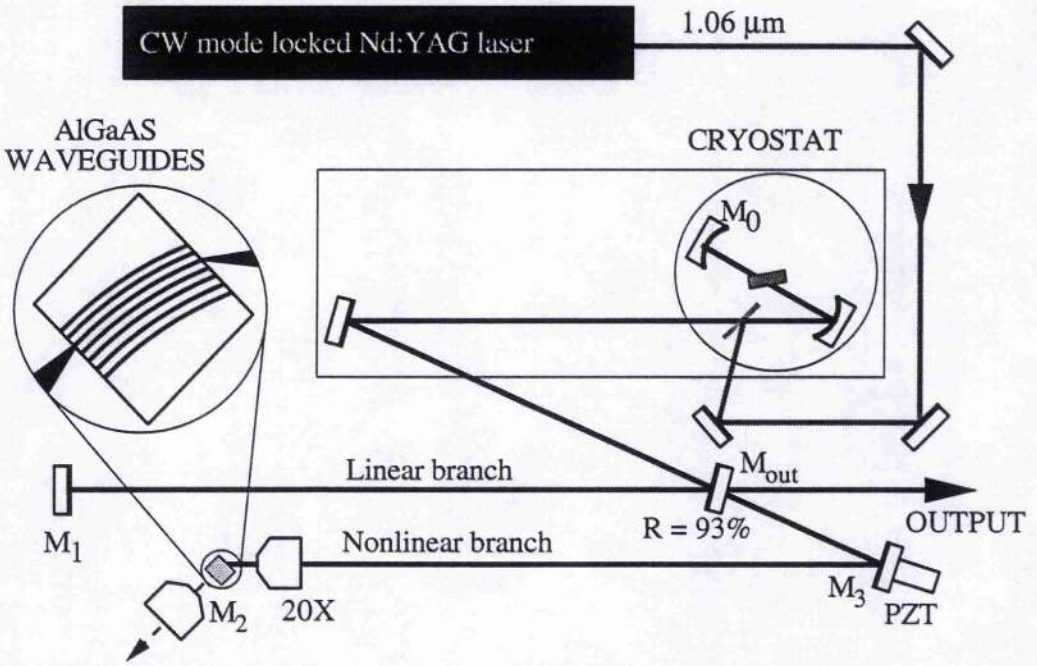

Figure 4.4. Schematic of the experimental set-up with a curved waveguide in a Michelson cavity configuration.

The stabilisation of the cavity was accomplished by a servo-loop system with a mirror M3 mounted on a PZT stage. The error signal could be derived either from the signal transmitted through the waveguide or from the second harmonic signal of the output pulses. It was observed that if the error signal was derived from the second harmonic of the output signal, the CCM process was more stable, mainly due to the relatively stronger modulation of the second harmonic signal [13]. Therefore, the latter option was selected for our cavity stability scheme, and all the results included here were obtained using this arrangement.

In the experiments, various lengths of waveguides have been used, and the associated results are discussed.

4.3.2 Typical laser output characteristics with the curved-waveguide as nonlinear element

First of all, a 3.49 mm long waveguide was used as the nonlinear element. It was found that the output pulses of the CCM KCl:Tl laser were generally frequency-chirped, and the shortest pulse duration was 240 fs. Both the pulse duration and the frequency chirp were dependent on the power level coupled into the waveguide. It was observed that when the power coupled to the waveguide was high the pulse duration would become broader and the frequency chirp became stronger.

Fig. 4.5 shows a typical autocorrelation and spectrum of output pulses having a duration of 300 fs. This set of results was obtained at an output power of about 34 mW. From the elevated wings of the interferometric autocorrelation, it can be seen that the

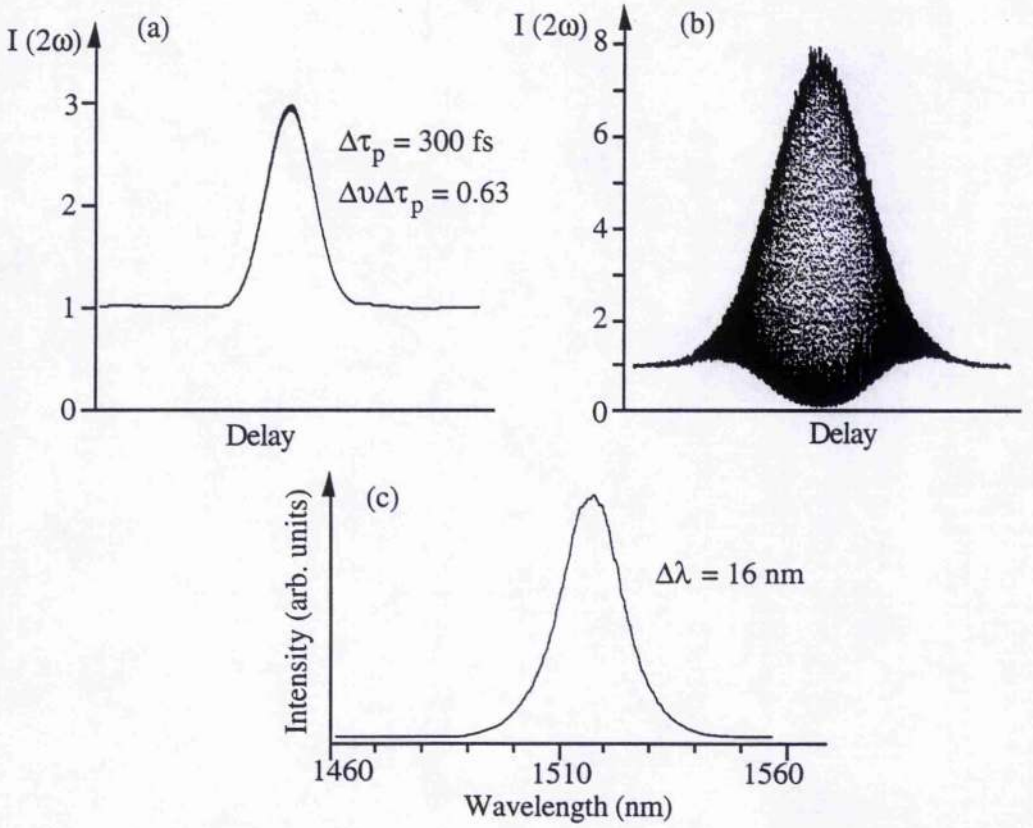

Figure 4.5. Typical autocorrelation and spectrum of output pulses with a 3.49 mm long waveguide.

output pulses were frequency chirped. The calculated bandwidth-duration product of 0.63 is significantly greater than 0.32 for the transform -limited pulses ($sech^2$ pulses).

The autocorrelation and spectrum of the transmitted pulses corresponding to Fig. 4.5 is illustrated in Fig. 4.6. The temporal duration and spectral width of the transmitted pulses were much greater than that of the output pulses. The bandwidth-duration product of 3.8 suggests that a very strong frequency chirp existed over the pulse evenlope. It is believed the spectral broadening was predominantly resulted from self-phase-modulation (SPM) in the waveguide, as discussed in Chapter 3. The temporal broadening of the transmitted pulses infers that the waveguide had a positive GVD around the wavelength of 1.5 μm, and this was verified by the GVD measurements described in Chapter 6, where a value of D=-1100 ps/nm/km has been deduced [14].

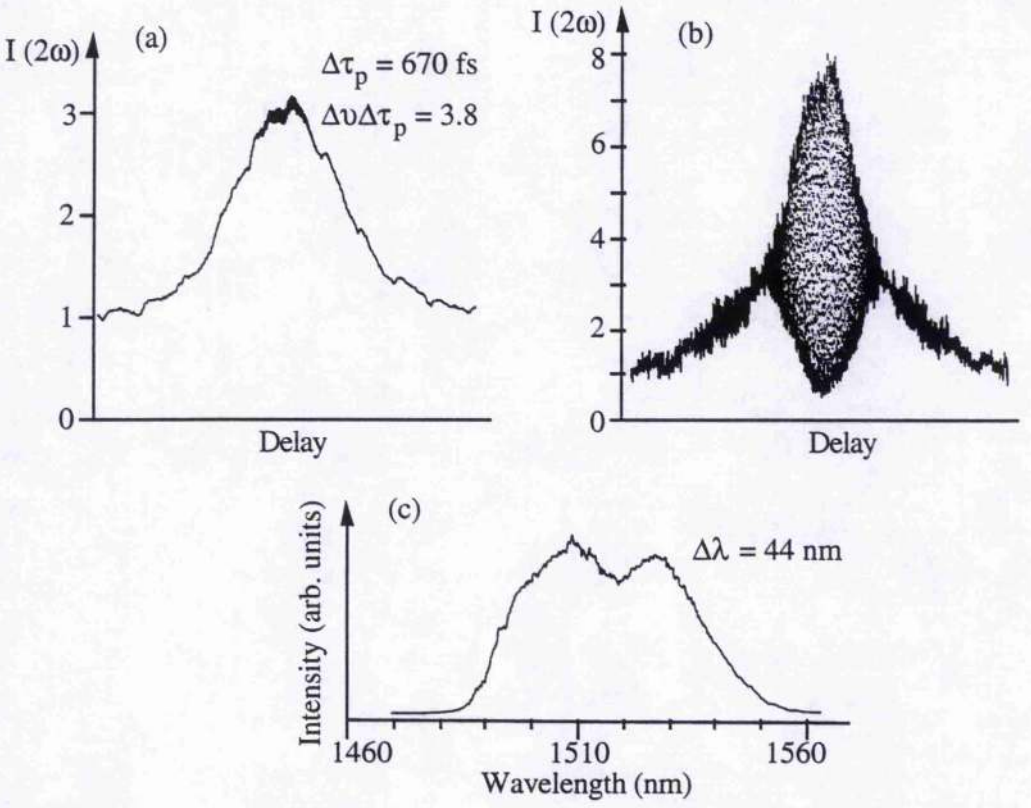

Figure 4.6. Autocorrelation and spectrum of the pulses transmitted from the waveguide (Corresponding to the output in Fig. 4.5).

One interesting feature was that the coupled-cavity mode-locking process could be maintained over a range of phase bias, defined as the phase difference between the

pulses returned from the control cavity and those being circulated in the main cavity. The output pulse duration could be varied continuously from around 250 fs to as large as 700 fs when the phase bias was varied. At the two ends of the tuning range of the phase bias the pulse duration was minimum and maximum respectively. To the experiment here, all the results obtained were taken with the minimum pulse duration. A further study of this characteristic will be presented in the next chapter.

4.3.3 Power dependence

Both the spectral broadening and frequency chirp of the returned pulses is directly related to the power coupled into the waveguide. The higher the power is, the larger the spectral broadening will be, and the frequency chirp is noticeably more pronounced. The consequence would be that the output pulse duration, spectral width and bandwidth duration product are all functions of the power level in the waveguide. The power dependence of the output characteristics was therefore studied as follows.

Firstly, by maintaining a constant coupling efficiency of the light beam to the waveguide (i. e. the power ratio between the signal returned from the external cavity and that being circulated in the main cavity kept constant), the output power (and the power coupled into the waveguide) was changed by varying the pumping power level. (In reality, the ratio is intensity-dependent due to the two-photon absorption in the waveguides. At higher power level, the two-photon absorption, TPA, effect will reduce the intensity ratio because of the stronger TPA effect). Fig.4.7 shows the variations of pulse duration, spectral width and bandwidth-duration product of the output pulses as functions of output power levels. It can be seen that when the output power was increased the output pulse duration, spectral width, and the chirp of the pulses were all enlarged.

In the experiment here, the total effective reflectivity from the waveguide was measured to be around 5%. It is more than two times higher than that with the straight waveguide (where total effective reflectivity was measured to be about 2%), although the intensity reflectivity of the back facet is only about 29%.

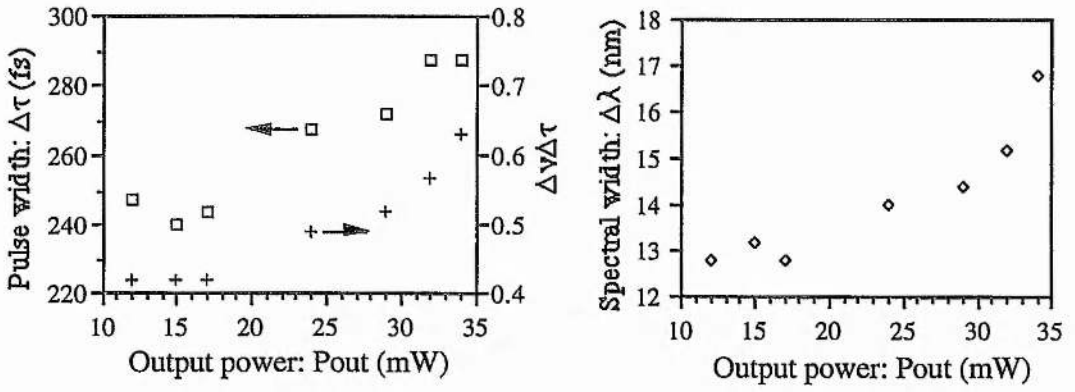

Figure 4.7. Pulse duration and spectral width of output pulse as a function of output power level.

The shortest pulses generated were about 240 fs and were obtained at an output power level of 15 mW. Below this power level, output pulse durations seemed to broaden again. This was perhaps due to insufficient SPM-induced spectral broadening of the returned pulses. However, even at the lowest power level in these experiments, the bandwidth-duration product of 0.42 was still higher than the 0.32 expected for transform-limited pulses ($Sech^2$ profiles), mainly due to the positive GVD of the waveguide. As the power increased to 34 mW, pulse duration reached to 285 fs and the spectral width increased to 16.8 nm.

The dependence of the above output characteristics on the pumping power may be explained on the following bases. At higher (lower) power level the SPM induced spectral broadening is relatively larger (smaller), therefore, under the same phase bias, more (less) spectral components of the returned pulses will be transferred to the main cavity pulses. (We mention phase bias here, because it represents a very important factor for the CCM mode locking process, as will be discussed in Chapter 5). Thus the spectrum of output pulses would be relatively broader. Due to the combined effect of the positive GVD and SPM induced spectral broadening, at higher power levels, the returned pulses would be comparatively broader and more heavily chirped than at lower power levels. As a result of this, much broader and more heavily chirped output pulses tended to be obtained at relatively higher power level.

In the second case, the pumping power (or output power) was kept constant while the power coupled into the waveguides was varied by using an attenuator wheel in front of the waveguide. It was found that, to establish coupled-cavity mode locking process, the power returned to the main cavity (or coupled into the waveguide) had to be above a specific threshold power level. In practice, because it was difficult to measure the power of returned signal, we chose to measure the power transmitted through the waveguide. [This is reasonably meaningful, because the power returned from the waveguide is directly proportional to the transmitted power.] Fig.4.8(a) shows the diagram of the variation of threshold power (transmitted from the waveguides), (b) is the power ratio between the signal returned to and circulated in the main cavity, at different output power levels. It indicates that as the output (or main cavity) power increased the threshold power increased as well. It implies that the threshold power level is not only related to the nonlinearity of the waveguide but also to the main cavity power levels. However, further evaluation indicated that the corresponding power ratio between the signal returned and that in the main cavity appeared, at the threshold condition, not to change to any significant extent. A constant value of about 0.5 X 10^{-5} was implied.

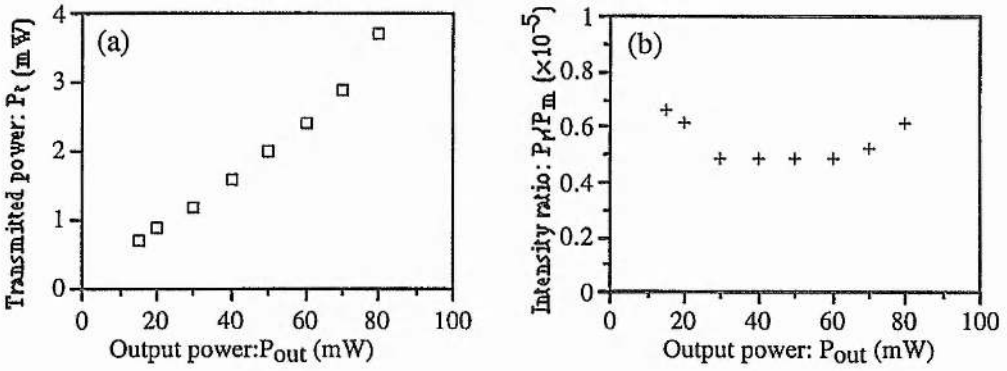

Figure 4.8. Variation of threshold power level (measured after the waveguide) coupled into the waveguide (a), and the power ratio between the signal returned to and circulated in the main cavity (b).

Fig.4.9 shows the variation of pulse duration as a function of the transmitted power. This set of results was obtained at an output power of about 35 mW. The power coupled into the waveguide was varied by a neutral-density wheel located in front of the

waveguide. Contrary to the case when the power ratio was kept constant as shown in Fig. 4.7, it appeared that the pulse duration firstly became shorter and then started to get broader again as the power coupled into the waveguide was increased. This seems to imply that an optimum power ratio existed. When the power coupled into the waveguide was lower, the SPM induced spectral broadening might be not sufficient; while as the power coupled into the waveguide was too high, the frequency chirp introduced by the combination effect of the SPM in and GVD of the waveguide might be too large. Therefore, both cases would not produce the shortest pulses. However, it was found that the CCM operation was much more stable at higher intra-waveguide power level than at lower intra-waveguide power levels, and this is also the reason that the relevant data about the spectra is not available here.

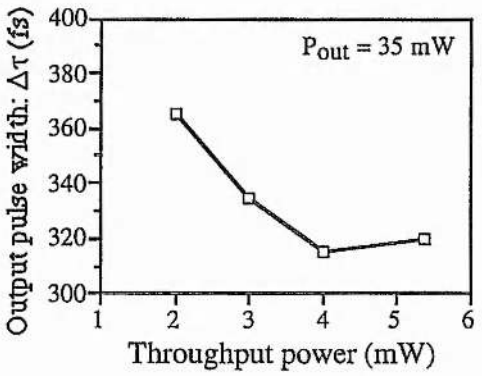

Figure 4.9. Variation of output pulse duration as a function of power level transmitted from the waveguide.

4.3.4 Frequency chirp compensation

4.3.4.1 Extra-cavity chirp compensation

As already mentioned, the waveguide introduces a positive frequency chirp on the returned pulses, due to the SPM effect in, and the positive GVD of, the waveguide. Thus, when such a positively chirped pulse is added to the main cavity pulse, it inevitably transfers the chirp features to the main cavity pulse through the interference-superposition of the two pulses. If a negative frequency chirp, that introduced by the KCl:Tl crystal and the output windows inside the main cavity, are relatively small, then

a net positive frequency chirp on the output pulses can be assumed. Therefore, if by passing the output pulses through an appropriate length of dispersion medium having a negative GVD at the laser wavelength (eg. silica based materials or a pair of prisms) then the chirp could be reduced.

To confirm the positive nature of the frequency chirp, the output pulses were passed through different lengths of glass rods (Heraeus: Suprasil I) which have an anomalous dispersion D = 13.8 ps/nm/km at wavelengths around 1.5 μm [15]. As expected, measured after the glass rod, the chirp of the pulses was indeed reduced and the pulse duration was also decreased. For output pulses having durations ~ 280 fs and a bandwidth-duration product of 0.61 the durations was reduced to about 230 fs, after passing through a 30 cm long glass rod.

There are practical limitations with chirp compensation outside the laser cavity. Firstly, for different degrees of chirp, the lengths of glass rod have to be optimised. For broader pulses, the compensation might require very long glass rods, so that makes the compensation impractical. Secondly, the introduction of the glass rod in the laser beam may also degrade the beam characteristics, such as polarisation and the spatial symmetry.

4.3.4.2 Chirp compensation in the nonlinear branch

Knowing that the chirp of the pulse is resulted from the SPM in and the positive GVD of the waveguide, an alternative approach involves locating the dispersion-compensation element in the nonlinear branch of laser cavity to directly compensate for the chirp of the returned pulses.

This was implemented in practice by inserting a length of glass rod in the nonlinear branch. Glass rods with different lengths have been employed. It was found that the best result was obtained when the 30 cm long silica rod (the longest one available) was used. The shortest pulses obtained were about 220 fs (see the autocorrelation and spectrum shown in Fig.4.10). It can be seen that the excess chirp was essentially removed, and the bandwidth-duration product of 0.35 was only slightly larger than

0.32, of transform-limited pulses. One additional point should be mentioned here. Because of the difference in the coupling efficiency each time a glass rod was changed, a valid relationship between the output pulse duration and the length of glass rod could not be obtained.

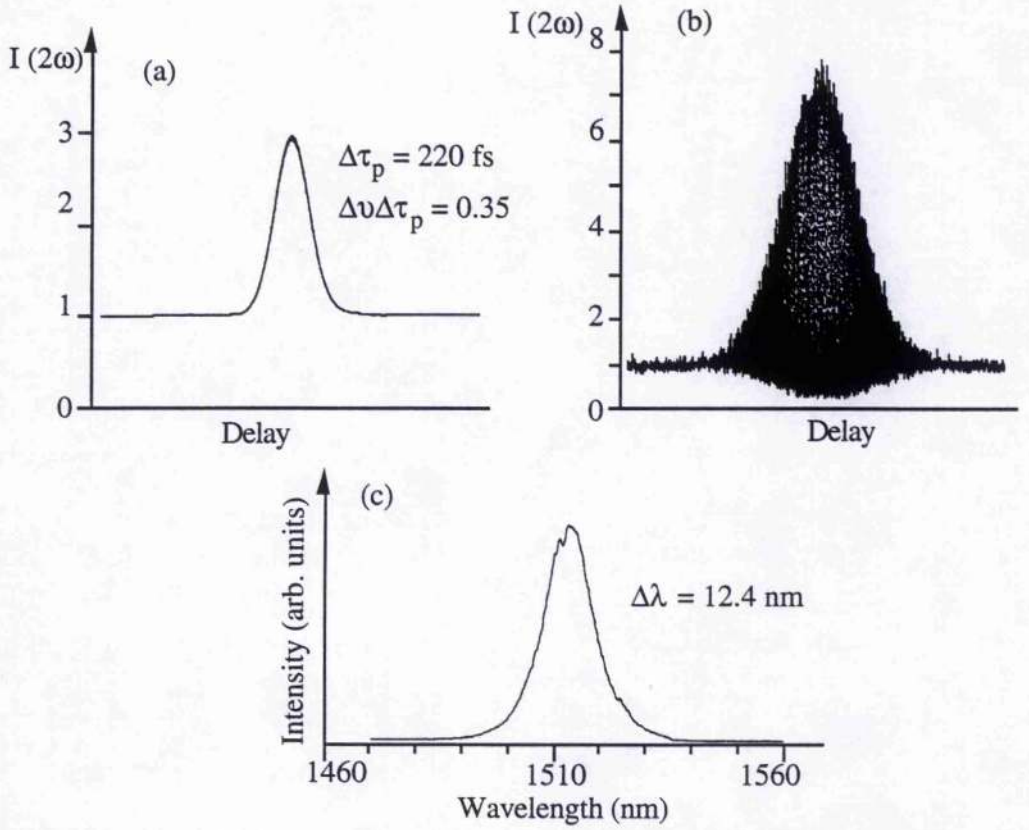

Figure 4.10. Autocorrelation and spectrum of 220 fs pulses obtained when 30 cm long silica rod was incorporated in the nonlinear branch.

4.3.4.3 Chirp compensation in main laser cavity

For chirp compensation in the main laser cavity, a pair of prisms [16, 17] represents the best choice. Therefore, as in the case of a Ti:sapphire laser [18], an attempt was made to include a pair of silica prisms in the main cavity to compensate for the positive chirp imposed on the main cavity pulses. It was found that, instead of shortening, the output pulses were broadened substantially. Reduction of the prism separation, (ie decrease of negative GVD of prism pair), resulted in somewhat shorter pulses. This might imply that the amount of negative chirp introduced by prism pair was too high (Both material and prism separation introduce negative GVD at wavelength of 1.5 μm).

Therefore, a subsequent approach was to insert an appropriate thickness of negative GVD element, such as silica discs, into the main cavity.

This was fulfilled by inserting a 2 mm thick silica disc at Brewster's angle into the main laser cavity. It was found that, after the insertion, the pulse duration was significantly reduced and the chirp was largely compressed. Nearly transform-limited pulses with duration of around 170 fs could be routinely obtained at an output power level of less than 35 mW. Fig 4.11 (a) and (b) are typical autocorrelation and spectral data for the output and transmitted pulses respectively. The clear autocorrelation trace and spectrum indicate that a stable mode locking process was established.

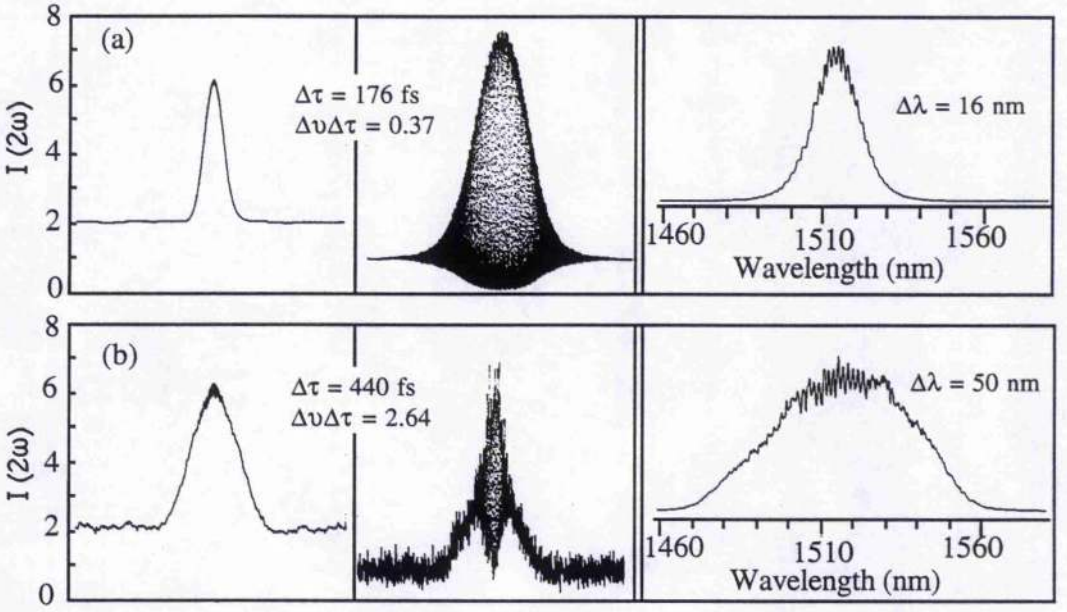

Figure 4.11. Typical autocorealtion and spectra of the output pulses (a), and transmitted pulses (b), with an additional 2 mm thick silica disc in the main laser cavity.

The shortest pulses, depicted in Fig. 4.12, were obtained at an output power level of about 40 mW. The bandwidth-duration product of 0.44 indicates that the pulses, in this case, were frequency-chirped. On the basis of the spectral width of 20 nm, transform-limited pulses having durations of 120 fs could be predicted. The slightly larger bandwidth-duration product might have resulted from the relatively higher power level in the waveguide. For 4 mm thick BRF with its optical axis oriented parallel to the laser beam in the main laser cavity, a similar result has been obtained. It was expected

that with the slightly thicker glass disc, further shortening of the output pulse would be possible. Unfortunately, the 2 mm thick disc was the only one available during the experiment.

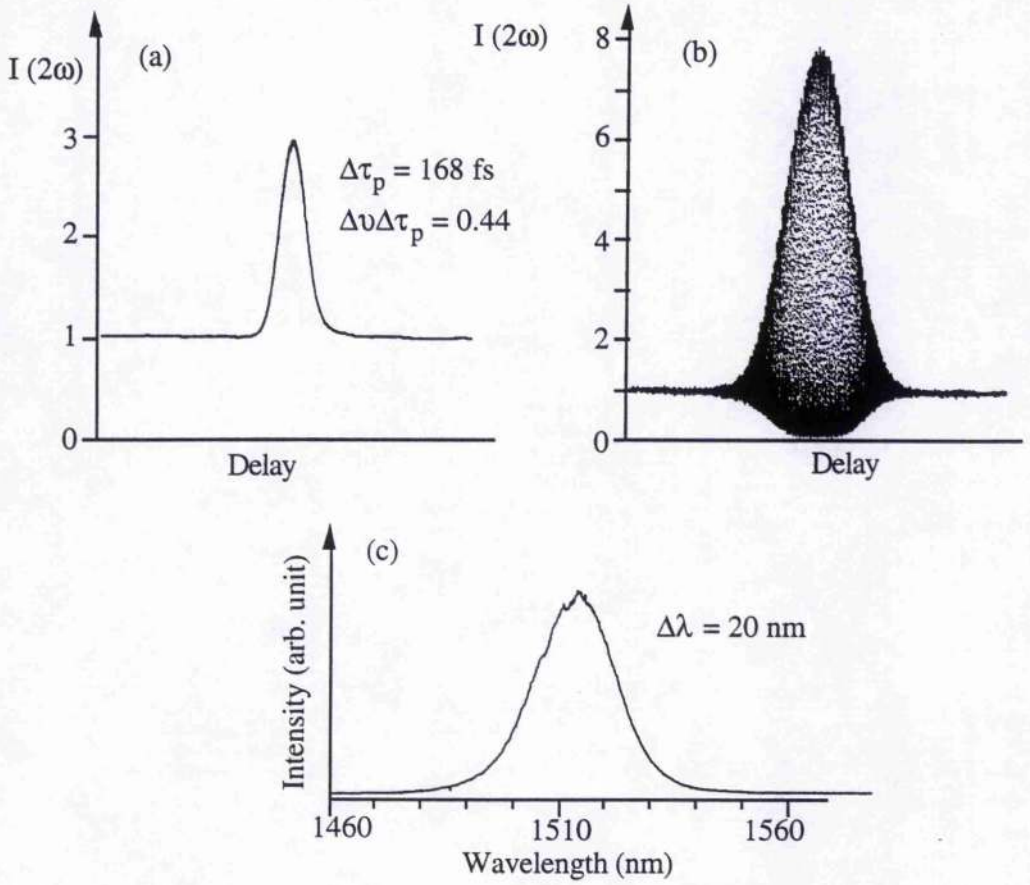

Figure 4.12. Autocorrelation and spectrum of 168 fs pulses obtained when a 2 mm silica disc was inserted in the main cavity.

Finally, it should be mentioned that, at higher power levels, multiple-pulsing was frequently observed when the silica disc was in the main laser cavity. This was probably caused by the etalon effect within the glass disc, owing to the slight disparity of the disc orientation from the Brewster's angle.

4.3.4.4 Discussion

In the case of chirp-compensation in the nonlinear cavity, the glass rod in fact acted to balance the positive chirp introduced within the waveguide. Because this chirp can be very high, longer glass rods are required. Whereas, for the case when the compensation is implemented in the main laser cavity, the silica disc acts to compensate for the

frequency chirp of the main cavity pulse. Because the chirp of the main cavity pulse is comparatively less, and probably more importantly, the compensation is possibly achieved over many round trips of main cavity pulse passing through the silica disc, therefore only a small piece of silica is required.

In practice, the optical components inside the main cavity, such as the gain medium, windows, etc. all have negative GVD at the wavelength of 1.5 μm. This negative GVD in the main cavity will in turn compensate partly for the positive chirp transferred from the returned pulses, and thus leads to the reduction of output pulse duration. However, if this chirp can not be fully compensated, the output pulse will still be chirped and this was the case when there was no additional silica disc inside the main cavity.

In contrast, with the Ti:sapphire laser [18], the gain medium, windows, etc. in the main cavity all have positive GVD at operating wavelengths of around 800 nm. The fibre incorporated in control cavity also has a positive GVD. Therefore, the combined effect of positive GVD within the main cavity and external cavity will make the chirp even stronger and pulses even broader after each round trip. The incorporation of a prism pair in the main cavity thus acted to compensate for the frequency chirp introduced from both the main cavity and the external cavity. As a result, a relatively larger dispersion would be required for the compensation of the chirped pulses.

4.3.5 Dependence on waveguide lengths

It is known that the combined effect of positive GVD and SPM in a waveguide will result in temporal broadening of the returned pulses. Therefore, an alternative way to reduce the pulse broadening effect was to use shorter waveguides. In the experiment, several lengths of waveguides have been used. Table 4.1 gives the output pulse duration for the lengths of waveguide that was available for evaluation. Fig.4.13 shows the dependence of pulse duration on the waveguide lengths, corresponding to the data in Table 4.1. It can be seen that the pulse duration decreased as the waveguide length was reduced.

Table 4.1 Dependence of output pulse duration on waveguide lengths.

L (mm)	3.49	2.75	2.7 *	2.51	1.22
$\Delta\tau$ (fs) **	> 240	> 190	> 190	>170	> 160
$\Delta\tau$ (fs) ***	~ 168	~ 160	~ 160	~ 160	~ 150

Note: * Waveguide with the end facet gold-coated.

** Without chirp compensation in either of the two cavities. The indicated output pulse duration, which was power dependent, was the shortest observed in each case.

*** The shortest pulse duration obtained when a 2 mm thick silica disc was included in the main laser cavity.

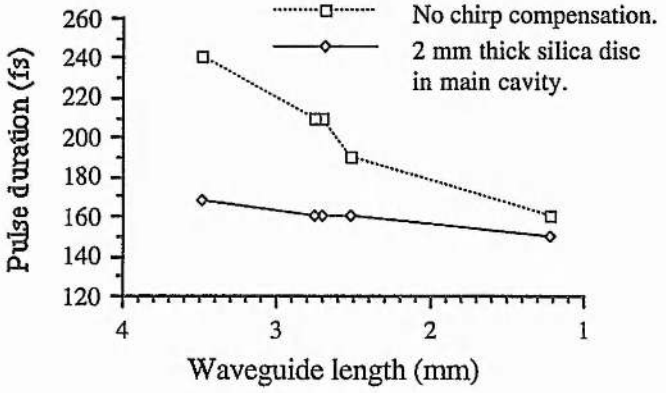

Figure 4.13. Dependence of output pulse duration on waveguide lengths.

It seems that by further shortening the waveguide length the output pulse duration would continually decrease. However, in practice the waveguide length can not be very short. Firstly, if it is too short (say less than 1 mm), the nonlinear spectral broadening may not be sufficient to establish the CCM process or the threshold power required for the CCM process will be too high. Secondly, the waveguide will become very difficult to handle. Therefore, the best approach is to use an appropriate length of waveguide and incorporate suitable dispersion compensation in the cavity.

With the 1.22 mm long waveguide, the shortest used in these experiments, pulses as short as 150 fs have been obtained - see the autocorrelation and spectrum shown in Fig. 4.14. The bandwidth-duration product of 0.34 indicates that the output pulse was almost transform-limited. The autocorrelation and spectrum of the transmitted pulses corresponding to Fig. 4.14 are reproduced in Fig. 4.15. It can be seen that after passing

through the waveguide, a 150 fs pulse was broadened to about 220 fs, and the spectrum was broadened from 17 nm to about 47 nm.

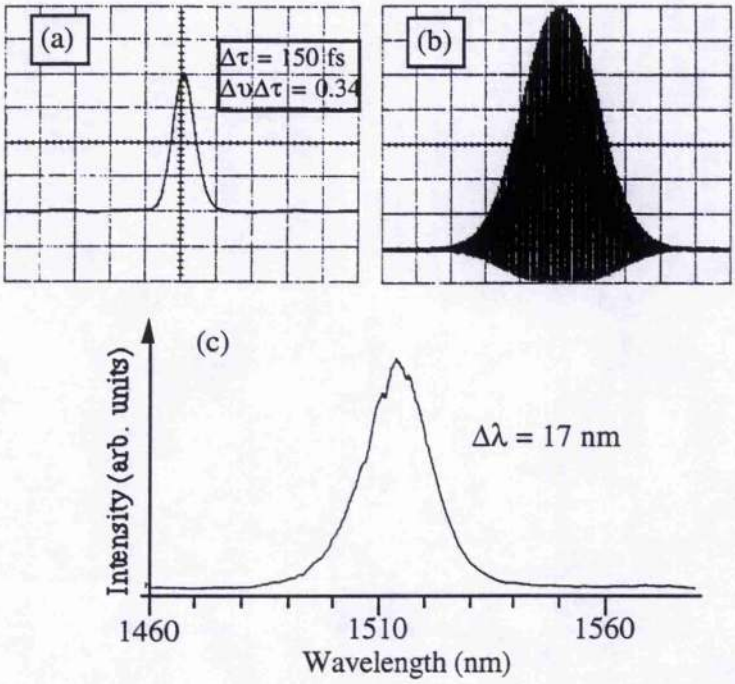

Figure 4.14 . Intensity (a), interferometric (b) autocorrelation traces and the spectrum (c) of the shortest pulses obtained for the 1.22 mm long waveguide.

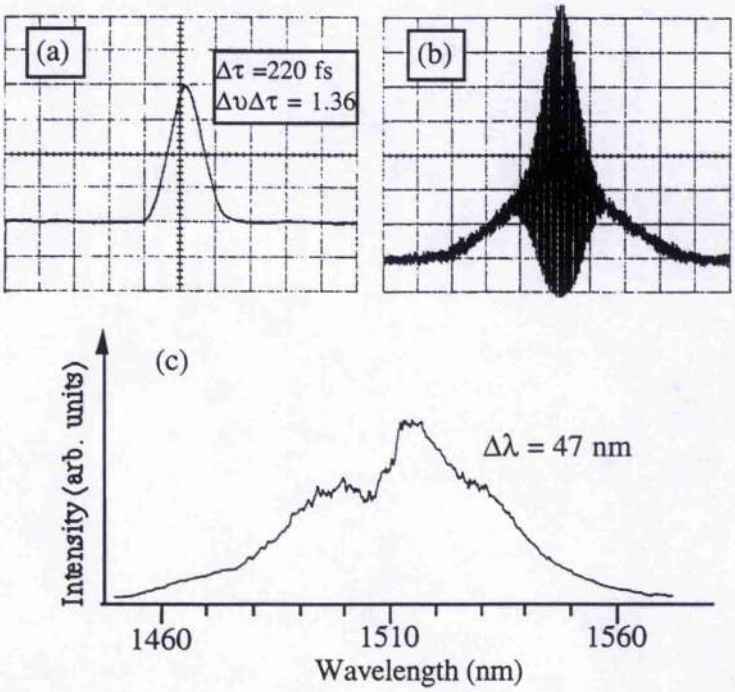

Figure 4.15. Intensity (a), interferometric (b) autocorrelation traces and the spectrum (c) of the pulses transmitted through the 1.22 mm long waveguide.

To increase the total effective feedback from the waveguide and reduce the threshold power required for the CCM mode locking process, a waveguide having its back facet gold-coated has been used. For this assessment, the waveguide was 2.7 mm long. It was found that by using this waveguide the total effective feedback from the waveguide was increased to about 15%, which is approximately three times higher than that of the non-gold-coated alternatives. Successful coupled-cavity mode locking was achieved at an output power level as low as 4 mW (Nd:YAG pumping power: 580 mW). Supposing that a coupling efficiency of 50% could be obtained, the power within the waveguide would be no more than 2 mW. This low-power requirement reinforces our optimism for the possibility of implementing integrated CCM schemes with semiconductor lasers.

The measured pulse duration with this waveguide was not as short as that with the 1.22 mm long waveguide. This was probably attributable to its longer length, because this imposes a greater temporal broadening on the returned pulses.

By comparing the emergent pulses in Fig.4.6, Fig.4.12 and Fig.4.15, an insight into the pulse broadening effects in the waveguide can be obtained. For convenience of discussion; Fig. 4.6, Fig. 4.12 and Fig. 4.15 are referred to as case 1, case 2, an case 3 respectively. The duration of the transmitted pulses for the three cases were 670 fs, 440 fs and 220 fs respectively, while the bandwidth-duration products were 3.8, 2.64 and 1.36. The pulse duration difference between case 1 and case 2, for the 3.49 mm long waveguide, was mainly caused by the difference in the initial pulse duration, whereas the pulse duration difference between case 2 and case 3 predominantly resulted from the difference in waveguide lengths. Although there were not much difference on the spectral width at the half-intensity for the three cases, the total spectral spreading with the 1.22 mm (case 3) waveguide was significantly greater than that of the other two. This feature indicates that the spectral broadening resulted primarily from the SPM effect, because a shorter pulse has a higher peak intensity and therefore the SPM induced spectral broadening is proportionally greater.

4.4. Involvement of two-photon-absorption and the observation of second and third harmonic generation

It was found that, when the power coupled into the waveguide was sufficiently high, red luminescence would radiate from the waveguide. This red light could be clearly seen to be distributed along the guiding line with greater intensity near the input facet. It is believed that this red light is related to the transition due two-photon-absorption (TPA) [19, 20], and/or the second-harmonic generation. Further evidence of the existence of two-photon-absorption is the variation in the transmitted power level at different pulse durations but for the same incident average power level (that is, different incident peak power). As mentioned already, and as discussed in the Chapter 5, the output pulse duration could be changed progressively from about 300 to about 700 fs, meanwhile the average output power was still kept unchanged, through the variation of the voltage level applied to the PZT. It was found that along with this alteration in the output pulse duration, the average power transmitted from the waveguide changed as well. With longer output pulses (the duration of the pulses incident to the waveguide is same to that of the output pulses), the transmitted power was higher than that with shorter output pulses. Because the average output power (or the average power incident to the waveguide) was not changed, the shorter pulse therefore had a higher peak power than the longer pulse. As the TPA was involved, the transmitted power from the waveguide would be lower with shorter pulses than with longer pulses. This is exactly what we have observed in these experiments.

An experimental result showing the dependence of the average power level on the pulse duration is presented in Fig. 4.16. It can be seen that as the pulse duration increased from 324 fs to 740 fs, the transmitted average power went from 3.4 mW to 3.8 mW. Corresponding to the data in Fig. 4.16, the variation of transmitted peak power as a function of the input peak power is shown in Fig. 4.17. Similar to the discussion in Chapter 3, the TPA coefficient can be obtained from the linear fitting of the inverse transmission. For the data obtained here, the TPA coefficient of the waveguide

was estimated to be about 0.3 cm/GW, which is three times larger than that deduced from the observations described in Chapter 3. This difference may be attributed to a few variable parameters in each case; such as the coupling efficiency, the error in the measurement of the average power, and also the waveguide samples were different in the two experiments.

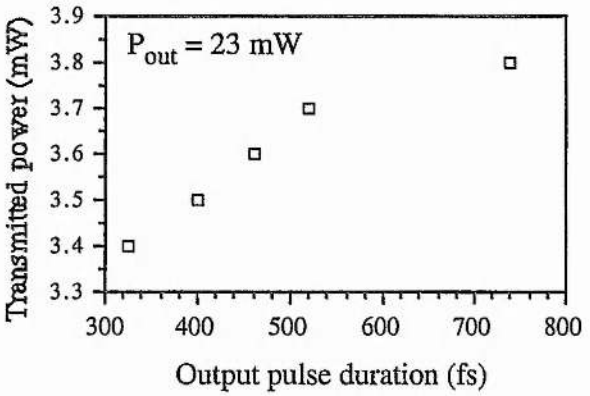

Figure 4.16. Dependence of transmitted power on the incident pulse duration. (average incident power constant: P_{out} = 23 mW.)

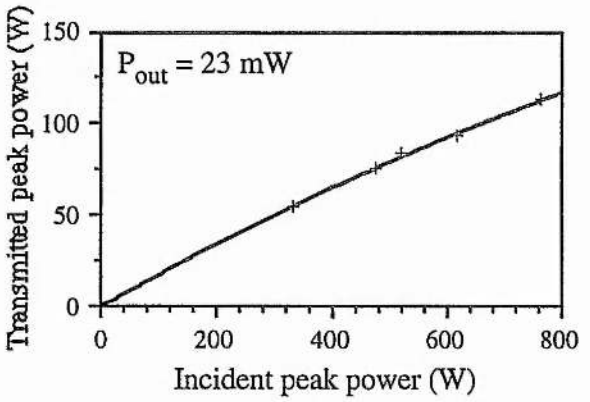

Figure 4.17. Transmitted peak power as a function of the input peak power.

By using a CCD camera to monitor the transmitted signal, two beam images, appearing as bright spot on the monitoring screen, were observed. These two images corresponded to different focal lengths of the microscope-objective that was employed to direct the transmitted signal into the CCD camera. One image was much brighter that the other. It is believed that the brighter image corresponded to the fundamental transmission and the dim one represented the signal of second-harmonic generation.

This can also be predicted by the difference in the focal lengths of the micro-objective in that the bright image had a longer focal length than the weaker one.

In order to obtain a clear picture about the spectrum of the transmitted signal, we measured the individual spectral component corresponding to the fundamental transmission, signals of the second and third harmonic generation respectively. This was done by using a 2.75 mm curved waveguide. Essentially, pulses having duration of approximately 200 fs from the CCM KCl:Tl colour-centre laser was passed through the waveguide. The spectrum of the transmitted signal was measured by using a monochrometer. Due to the limited spectral response, different photo diodes were used for the spectral regions involved. For the spectrum around the 1.5 μm region, a Ge photo diode was employed whereas for the spectra relating to the second and third harmonic signals, a Si photo diode was used.

Fig. 4.18 gives the experimental results, where (a) represents the spectrum of input signal, (b) shows the SPM broadened spectrum, and (c), (d) are the spectra of the second and third harmonic signals respectively. This result was obtained at an incident power of about 50 mW. The pulse duration was maintained at about 200 fs. It can be seen that the SPM broadened spectrum is almost five times larger than that of the input pulses. The spectrum of the second harmonic signal was centred at a wavelength of about 758 nm, exactly at the half wavelength of that of input pulses. The width of this transition spectrum was close to the half width of the SPM broadened spectrum. The spectrum of the third harmonic signal was centred at a wavelength of about 505 nm, one third of the input wavelength. The spectral width of 19 nm was about one third of the SPM broadened spectrum. From the relevance between the spectral widths of the SPM broadened spectrum and the spectra of the second and third harmonic signals, it may be expected that the second and third harmonic generation are directly associated with components of the SPM broadened spectrum.

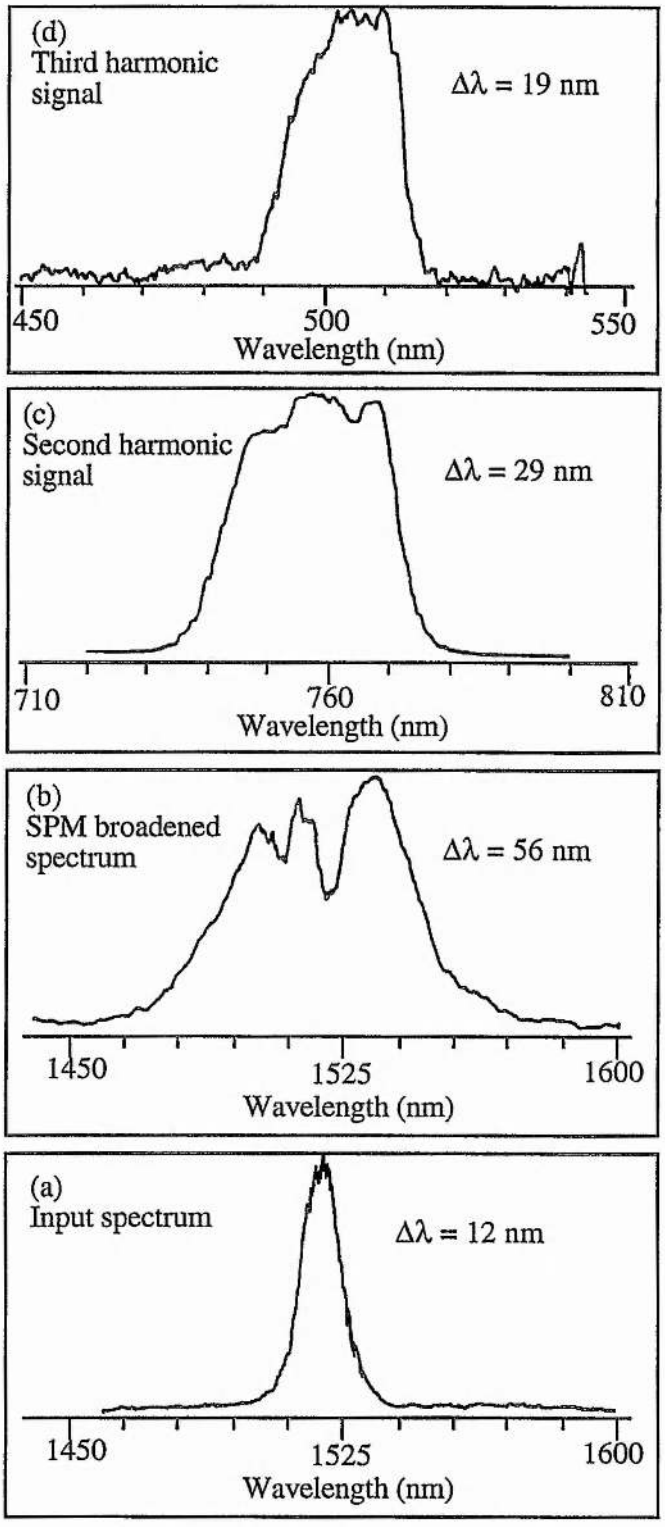

Figure 4.18. Measured individual spectral components. (a) Input spectrum; (b) SPM broadened spectrum; (c), (d) spectra of the second and third harmonic signals respectively.

4.5. Summary

In this chapter, the coupled-cavity mode locking of KCl:Tl colour-centre laser with passive AlGaAs waveguides illuminated at the half-band gap has been described. Two different guiding geometries - straight and curved waveguides - have been used in the experiments. With the straight waveguide as the nonlinear element, pulses having duration of 230 fs have been generated. However, it was found that the relatively large dimension of the waveguide substrate prevented the utilisation of objectives having focal lengths of less than 2 mm, and this thus limited the coupling efficiency into the waveguide. The insufficient feedback from the waveguide restricted the practicality of the CCM laser and made the further shortening of the output pulses difficult. To overcome this drawback, a curved guiding geometry was evaluated. Instead of using an objective and an additional mirror to retro-reflect the signal back into the main cavity, the back facet of the waveguide itself acted as the end mirror of the control cavity. By using a 3.49 mm long waveguide and employing the nonlinear Michelson cavity configuration, slightly broader pulses were generated. It was found that such pulses were generally strongly chirped. When chirp compensation was implemented in the nonlinear cavity with a 30 cm long glass rod, 220 fs pulses were recorded. Significant shortening of the output pulses was obtained when a 2 mm thick silica disc was inserted into the main laser cavity, and 168 fs pulses were generated. By using shorter waveguide, further shortening of the output pulses was achieved. With a 1.2 mm waveguide, pulses as short as 150 fs have been produced. By using a waveguide that was gold-coated on the back facet, successful coupled-cavity mode locking has been achieved at an output power level as low as 4 mW. This confirms our optimism for the possibility of making integrated CCM schemes for semiconductor diode lasers.

Compared with optical fibres, the use of AlGaAs waveguides offers some distinct advantages. Firstly, its high nonlinearity at the half-band gap affords a low power requirement for the CCM process. Secondly, the small dimension of the waveguides assured a compact cavity configuration. Thirdly, the output is much more stable than

with optical fibres because it is less affected by environmental and perturbative effects. Fourthly, it also provides the advantage of less-exacting coupling procedures required with the optical fibres, and only one microscope-objective is needed. Fifthly, because the guiding line is at an angle with the input facet, it avoids the feedback problem associated with fibres. At the moment, the pulse duration has not yet reached the level that with optical fibres. However, it is expected that by proper compensation of GVD both in the linear and nonlinear cavity branches this scheme will be comparable with optical fibres in terms of pulse duration.

References:

1. W. Sibbett, R. S. Grant, D. E. Spence, Apl. Phys. B 58, 171, (1994); P. N. Kean, X. Zhu, D. W. Crust, N. Langford, and W. Sibbett, Opt. Lett. 14, 39, (1989).
2. R. S. Grant, P. N. Kean, D. Burns and W. Sibbett, Opt. Lett. 16, 384 (1991).
3. U. Keller, W. H. Knox, and H. Roskos, Opt. Lett. 15, 1377 (1990).
4. H. A. Haus, U. Keller, and W. H. Knox, J. Opt. Soc. Am. B8, 1252 (1991).
5. K. J. Blow and D. Wood, "Mode-locking lasers with nonlinear external cavity," J. opt. Soc. Am B 5, 629 (1988).
6. W. Sibbett, "Exploitation of optical nonlinearity for enhanced mode locking in coupled cavity laser" Paper FQ-1, In Technical Digest of CLEO'89. (Baltamore, USA, 1989).
7. R. S. Grant and W. Sibbett, Opt. Commun. 86, 177 (1991).
8. H. A. Haus, J. G. Fujimoto, and E. P. Eppen, J. Opt. Soc. Am. B8, 2068 (1991).
9. F. M. Mitchsche and L. F. Mollenauer, IEEE J. Quantum Electron. QE-22, 2242 (1986).
10. X. Zhu, P. N. Kean, and W. Sibbett, IEEE J. Quantum Electron. QE-25, 2449 (1989).
11. X. Zhu and W. Sibbett, J. Opt. Soc. Am. B7, 2187 (9190).
12. F. Ouellette, M. Piché, Opt. Commun. 60, 99 (1986).
13. R. S. Grant, Z. Su, G. T. Kennedy, W. Sibbett, J. S. Aitchison, Opt. Lett. 18, 1600 (1993).
14. Z. Su, G. T. Kennedy, R. S. Grant, W. Sibbett, J. S. Aitchison, In the Technical Digest of Conference on Lasers and Electro-Optics, Volume 8, CLEO-94, 1994, Anaheim, California.
15. X. Zhu, A. Finch, and W. Sibbett, J. Opt. Soc. Am. B7, 187 (1990).
16. R. L. Fork, O. E. Martinez, and J. P. Gordon, Opt. Lett. 9, 150 (1984).
17. J. P. Gordon and R. L. Fork, Opt. Lett. 9, 153 (1984).
18. D. E. Spence and W. Sibbett, J. Opt. Soc. Am. B 8, 2053 (1991).
19. A. Villeneuve, C. C. Yang, G. I. Stegeman, C-H Lin, H-H Lin, Apl. Phys. Lett. 62, 2465 (1993).
20. C. C. Yang, A. Villeneuve, and G. I. Stegeman, J. S. Aitchison, Opt. Lett. 17, 710 (1992).

Chapter 5

Cavity-mismatch characterisations of the CCM KCl:Tl colour-centre laser

5.1. Introduction

It had been regarded, since the invention of the original version of coupled-cavity mode-locking scheme - the soliton laser by Mollenauear and Stolen in 1984 - that the mechanism responsible for the mode locking process was mainly due to the pulse shortening following solitonic effects in the control-fibres [1]. However, it was afterwards verified experimentally [2] and predicted theoretically [3] that solitonic fibre was not the only choice and fibres with normal group-velocity dispersion (GVD), which instead of supporting bright solitonic pulses gives rise to broadening of the incident pulses, could also be used in this type of mode-locking scheme. Subsequent theoretical studies [5] [6] [7] indicated that the key mechanism for this coupled-cavity mode-locking (CCM) process is the coherent superposition between the pulses returned from the control cavity and that being circulated in the main cavity.

The phase difference, or phase bias, between the pulses returned from the external cavity and that being circulated in the main cavity represents a very important factor for the CCM dynamics. (Here and in most part of this thesis the phase bias refers to the phase difference at the centre of the "main" and "control" cavity pulses). The maximum compression occurs when the phase difference is about $-\pi/2$ if the returned pulse is positively chirped (chirp parameter $C > 0$), and $\pi/2$ if it is negatively chirped (chirp parameter $C < 0$) [see Ref. 6, where C is donated by β_2 but with opposite sign]. To maintain proper CCM mode locking the relative phase of the two overlapped pulses has

to be properly adjusted and the two cavity lengths have to be maintained within an appropriate matching tolerance.

Chee, etc. has reported the cavity-detuning characteristics of a coupled-cavity mode locked Nd:YLF laser, where elegant experimental results were obtained [8]. In Chapter 4, the CCM, KCl:Tl colour-centre laser with passive AlGaAs control waveguide operating at the half-bang gap has been discussed. In this chapter, the experimental studies of the temporal and spectral characteristics of this CCM KCl:Tl colour-centre laser when operates at different cavity-detuning conditions will be presented. We refer the cavity-detuning within a fraction of wavelength as the fine cavity-detuning. Within this tuning range the output pulse duration and spectral profile could be continuously changed, as will be discussed later. For cavity-detuning beyond one wavelength (or 2π phase bias) different mode-locking regimes occur. We will refer to this as a large scale cavity-detuning.

This chapter is arranged as follow. Following a brief introduction, the fine fine-cavity-detuning characteristics are presented, followed by the third part - the large scale cavity-mismatching experiment. The waveguide used in this experiment was 3.49 mm long and with a curved guiding geometry. The back facet of the waveguide was set normal to the guiding ribs and thus gives an intensity reflectivity of about 29% assuming a refractive index of the waveguide material of 3.33. The normal of the front facet was at an angle of 10^{o} to the guiding rib.

5.2. Fine cavity-detuning characteristics

As mentioned in Chapter 4, the stabilisation of the CCM, KCl:Tl laser was accomplished by a servo loop-system and a PZT which is attached to mirror M_3 (see Fig. 4.4 in Chapter 4). A variation in the voltage applied to PZT will result in a change of the control cavity length within a fraction of wavelength. Therefore, the phase difference between a pulse returned and that being circulated in the main cavity can be tuned by simply varying the voltage applied to the PZT. In this investigation, this was accomplished by fine-tuning the voltage bias on our PZT control box. To monitor the

variation of the applied voltage, the output control signal from the control box for PZT was simultaneously connected to an oscilloscope. It was observed that the voltage could be varied within few tens volts while the CCM process was still maintained. It is estimated that the corresponding change of the external cavity length, or the phase bias, was less than one wavelength or 2π phase bias. The exact experimental value and sign of the phase bias was not easily determined.

It was found that proper couple-cavity mode locking could be maintained over a continuous range of phase bias. Within this tuning range the pulse duration and the spectral width could be continuously varied from narrower to broader or from broader to narrower dependent on the applied phase bias. At one extreme of the tuning range the output pulse duration and spectral width were both a minimum, while at the other limit of the tuning range they were both a maximum. Outside this tuning range the CCM mode locking operation was terminated. To simplify the discussion that is included latter in this section, we will refer to the regime that saw the side with shorter pulses as "side 1" and the regime with longer pulses as "side 2".

Fig. 5.1 shows typical autocorrelation traces of the output pulses when the phase bias was varied. This set of results was obtained at the output power of about 35 mW, and the total effective reflection from the waveguide was 5%. It shows that in different phase bias conditions the pulse characteristics were quite different. The interferometric autocorrelation and bandwidth-duration products clearly indicate that the chirp of the output pulses was increasing progressively when the pulse duration was becoming broader. The broadest pulses obtained at the extreme end of "side 2" in the experiment has durations in excess of 700 fs and with a bandwidth duration product of around 1.5, while the shortest pulses at the extreme end of "side 1" has durations of about 250 fs and with a bandwidth-duration product of around 0.47. These large differences explicitly indicate the importance of the phase bias for the CCM process. At "side 1" of the tuning range, less noise appeared on the output than at "side 2", but at "side 2" the CCM process was more stable than at "side 1". (At "side 1, the mode locking process

was more sensitive to the influence of the environment and could cease due to significant outside disturbance. While at "side 2" the mode locking process was less affected by local perturbation.).

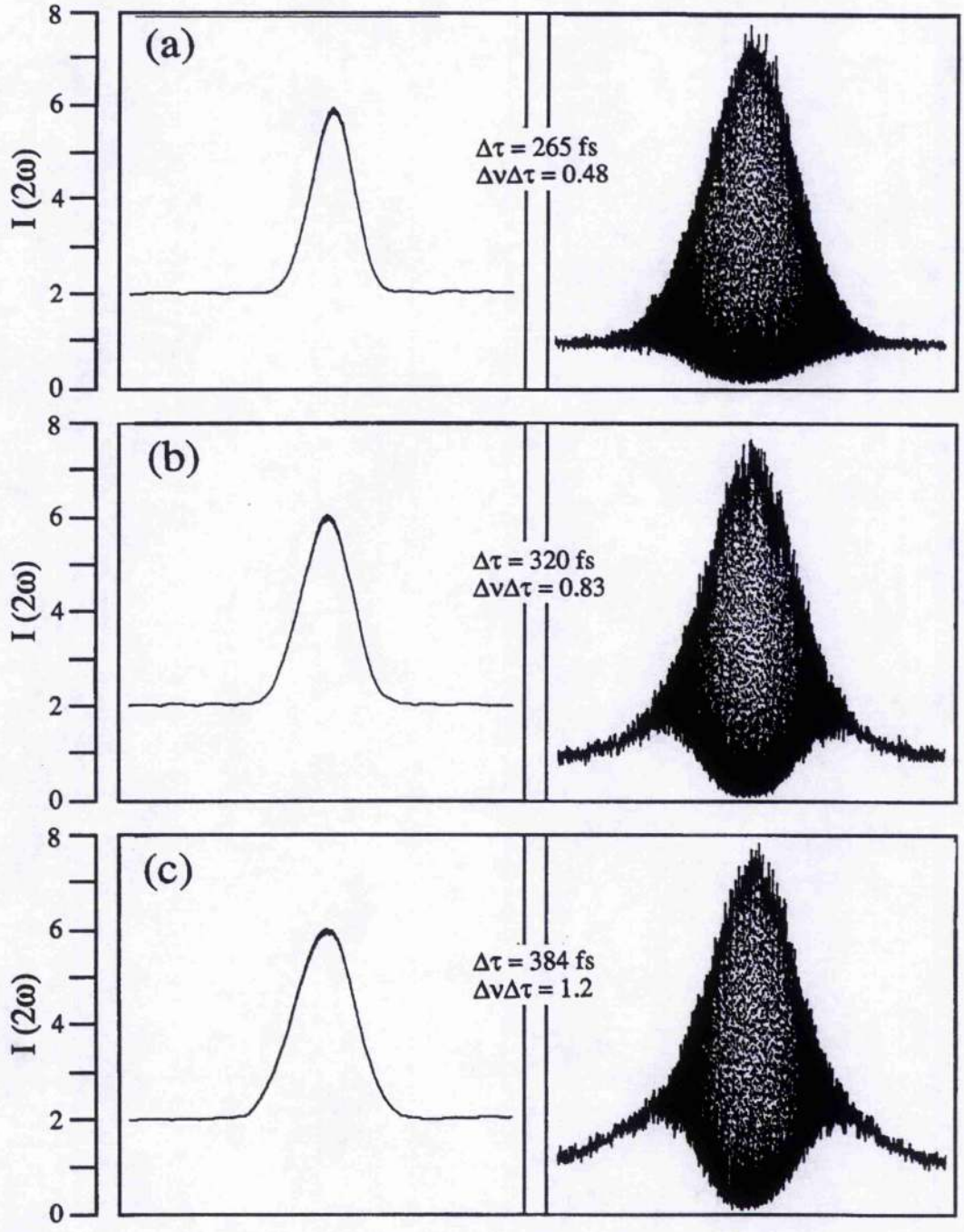

Figure 5.1. Autocorrelation traces of output pulses at three phase bias levels.

The corresponding spectra of Fig. 5.1 Are shown in Fig. 5.2. These clearly indicate that for different phase bias levels the spectral widths are also quite distinct. Shorter pulses correspond to narrower spectrum while longer pulses had broader spectra. A noticeable feature is that the peak intensity for a broader spectrum (longer

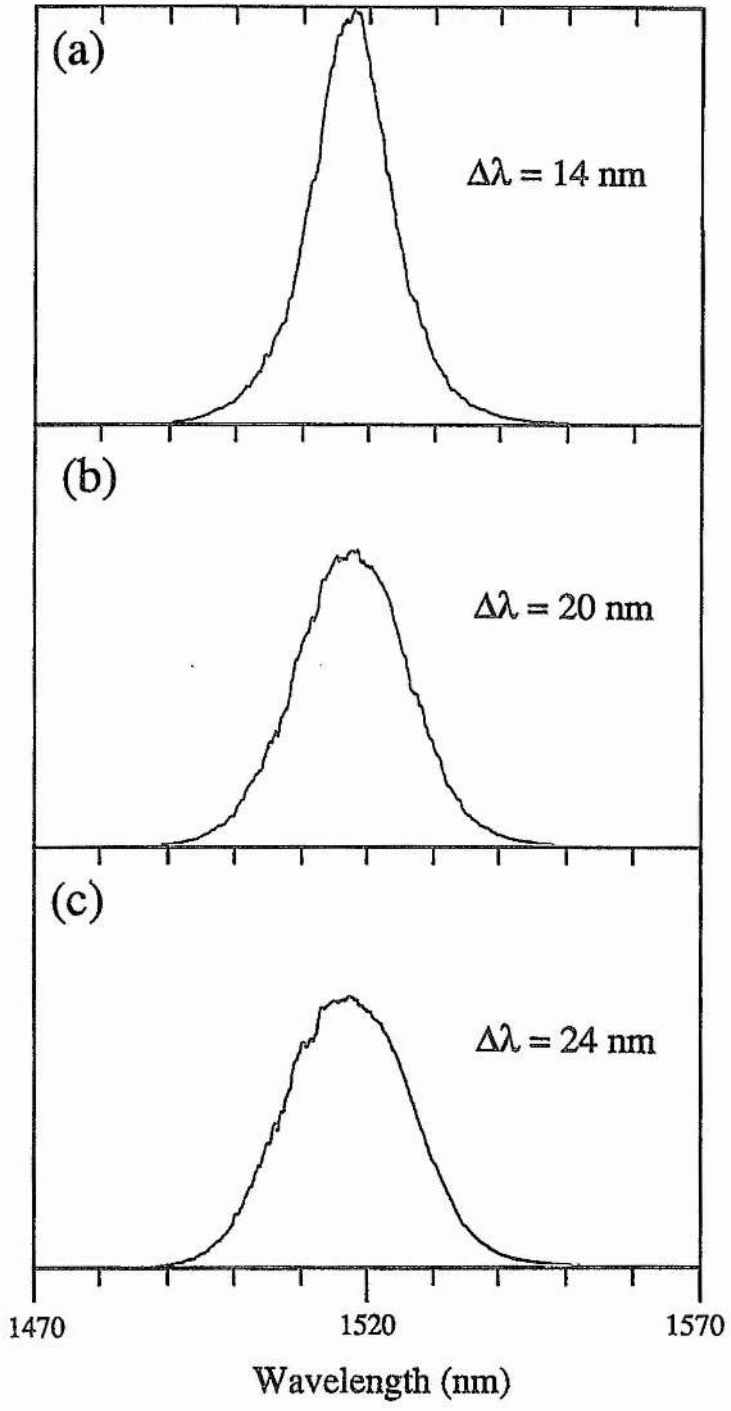

Figure 5.2. Spectra corresponding to the autocorrelations in Fig.5.1.

pulse duration) is relatively less than that for narrower spectrum. This indicates that, when the phase bias was varied towards "side 2", the power was shifted from the central part of the spectrum towards side bands. Another feature is that the spectral profile at all the phase bias levels shown here were all symmetric. This is because the two cavity lengths were approximately matched in large scale, as will be discussed in section 5.3 for large scale cavity-mismatch.

As a comparison, the spectra transmitted from the waveguide at the two extremes of the tuning range were also measured. Fig. 5.3 shows the autocorrelation and spectrum of the shortest pulses obtained at the extreme end of "side 1" and the corresponding spectrum of these transmitted pulses. It can be seen that due to self-phase-modulation in the waveguide the transmitted spectrum was significantly broadened from 13.6 nm of the incident pulses to 56 nm of the transmitted pulses. The duration of the transmitted pulses was measured to be 340 fs. This corresponds to a bandwidth-duration product of 2.0. Fig. 5.4 shows the autocorrelation and spectrum of the longest pulses obtained at the extreme end of "side 2" and the corresponding spectrum of transmitted pulses. Although the output spectrum of the output laser pulses was much broader (Fig. 5.4) than that for the bias level in Fig. 5.3, the spectrum of the pulses transmitted through the waveguide was narrower than that in Fig. 5.3. This was most possibly due to the longer pulse duration and the lower peak power would imply less SPM in the waveguide. Given that the duration of the transmitted pulses in this case was measured to be 628 fs, a bandwidth-duration product of 2.6 is derived. It can be predicted that the spectrum of the pulses returned to the main cavity was even broader than that of transmitted pulses due to double passing through the waveguide. From GVD in the waveguide the duration of the transmitted pulses were substantially broadened from 260 fs to 340 fs for the shortest output pulses and from 552 fs to 628 fs for the longest pulses. The near rectangular shape of the transmitted pulse spectrum in Fig.5.4 can also be interpreted to suggest that the profile of the transmitted pulses was essentially rectangular as well [9].

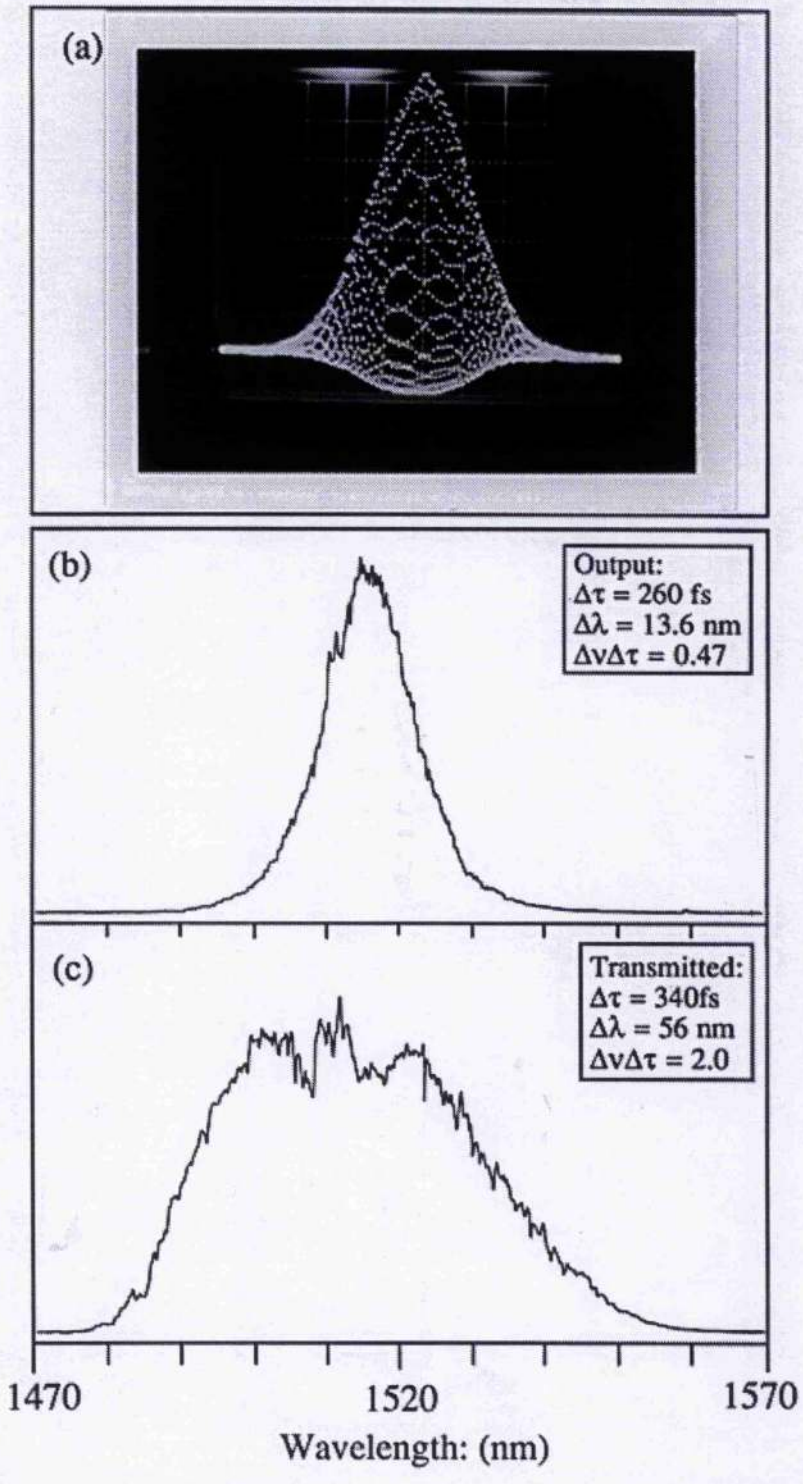

Figure 5.3. Interferometric autocorrelation (a) and spectrum (b) of output pulses, and (c) the corresponding spectrum of transmitted pulses obtained at the extreme end of "side 1".

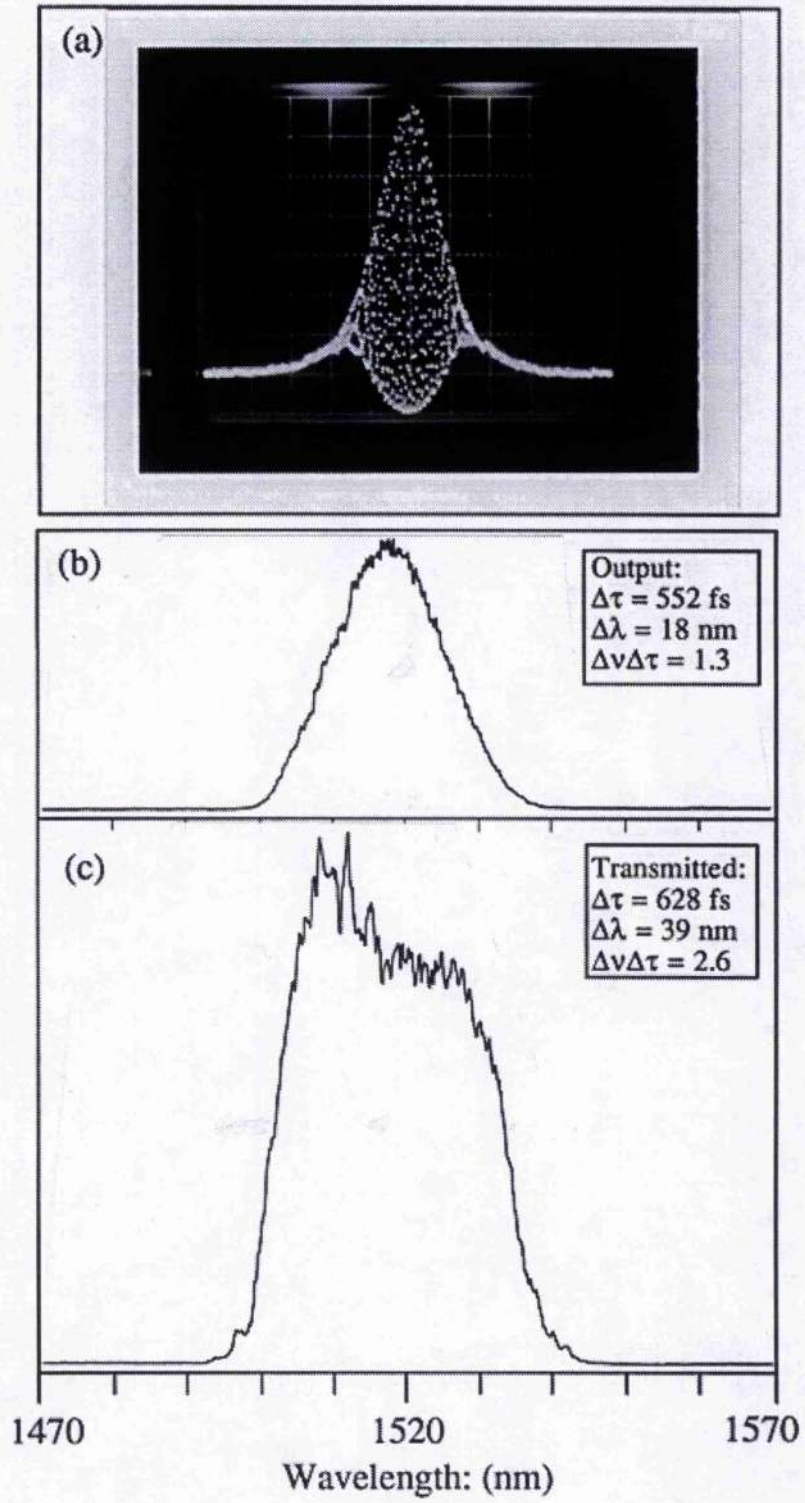

Figure 5.4. Interferometric autocorrelation (a) and spectrum (b) of output pulses, and (c) the corresponding spectrum of transmitted pulses obtained at extreme end of "side 2".

5.3. Discussion

The nonlinear phase shift resulting from the intensity-dependent refractive index is directly proportional to the instantaneous intensity of the incident pulse. The instantaneous intensity at different parts of the pulse profile is different, the central part being stronger and in the wings it becomes progressively weaker. Therefore, after propagating thorough the waveguide, the central part of the returned pulses will acquire more nonlinear phase shift than the wings. With regard to frequency characteristics, the frequency associated with leading edge shifts toward long wavelength and the trailing edge shifts towards short wavelength, the sign of the phase shift at the two wings is the same relative to that of the centre. When the phase-shifted pulse adds coherently with the main cavity pulse, different parts of the two pulses will have distinctive phase bias features. Therefore, particular parts of the pulse will have different destructive or constructive interference and this leads to the compression of the resultant pulses.

Following the theoretical discussion given in Ref. [6], the maximum compression ratio (i.e. where the shortest output pulses can be generated) occurs at a phase bias of $\pm \pi/2$ when the overlapped pulses are chirped. The sign of this phase bias should be opposite to the sign of the chirp parameter C of the pulses returned from the external cavity. (It is negative when the returned pulses are positively chirped and positively when the returned pulses are negatively chirped.). In the case here, the SPM effect and positive GVD of the waveguide made the chirp on the returned pulses positive. Therefore, at a phase bias of about $-\pi/2$ there is a maximum compressive superposition - and so the shortest pulses are generated. It also can be predicted that when the absolute value of phase bias is beyond about $\pi/2$, the superposition of the two pulses along the pulse profile will become destructive and so the couple-cavity mode locking process may not be permitted. When the phase bias is varied from $-\pi/2$ to $+\pi/2$, the destructive force at the wings becomes relatively weaker and this therefore results in broader pulses. From this analysis, it can be determined that "side 1" and "side 2" of the tuning range in this experiment correspond to the negative phase bias (external cavity length is

shorter than main cavity length) and to the positive phase bias (external cavity length is longer than main cavity length) respectively. The position of the zero phase bias is not readily predicted, however.

Experiments supported this expectation. We monitored the voltage applied to the PZT when the phase bias was changed. It was observed that when the phase bias was tuned from "side 2" to "side 1" (e.g. output pulses varied from broader to shorter), the voltage applied to PZT varied from relatively low to higher. Because the PZT responds to the increase of applied voltage as the expansion of the PZT, this expansion led to a shortening of the control cavity length, and thus a reduction of phase bias. Therefore, it confirmed that the pulse duration decreased as the reduction of the phase bias, within the limit of the tuning range.

Because of the positive nature of the nonlinear refractive index of the semiconductor waveguide at 1.5 μm, the SPM-induced frequency shift is negative near the leading edge (red shift) and becomes positive at the trailing edge (blue shift) of the pulses. The chirp due to the SPM is essentially linear and positive (up-chirp) over a large central region [9]. Therefore, the extent of the frequency shift within this linear range is proportional to the temporal locations relative to the centre of the pulse, e.g. the further away from the centre of the pulse, the larger the frequency shift will be. In another words, the returned pulses will have more "red" spectral component in the front edge and more "blue" component at the rear edge . Consequently, when the phase bias was varied toward "side 2" (positive phase bias), the destructive force at the wings becomes relatively weaker and therefore results in broader pulses. As a result, more "red" and "blue" shifted spectral components at the front and rear edges of the returned pulse will be coupled (or transferred) into the evolved laser pulses. Thus, the relatively broader and more strongly chirped output pulses with broader spectra are generated. Since the output power did not change, the power in the central part will shift to the sideband of the spectral profile when the phase bias is tuned from "side 1" towards "side 2". This is consistent with the experimental data indicated in Fig. 5.2.

In dispersion-compensation studies, we also observed that when a glass disc was inserted into the main cavity, at particular phase bias and relatively higher incident power level, generation of multiple pulses occurred. This can perhaps be explained to be the result of too much phase shift imposed on the returned pulses. The large phase shift on the returned pulses and the introduction of the extra glass in the main cavity resulted in even larger phase difference between the main cavity and the returned pulses. Therefore, over the pulse profile of the two overlapped pulses periodic constructive and destructive features can arise. As a result, the resultant pulse would be modulated and the output pulse would exhibit multiple-pulses.

It was also found that the power transmitted from the waveguide was a function of pulse duration. With shorter output pulses the transmitted power was higher, and similarly the transmitted power was lower when the output pulses tuned to longer pulse duration side (side 2). This effect is a direct result of two-photon-absorption (TPA) in the waveguide. Longer pulses had low peak intensity in the waveguide and thus experienced less TPA attenuation, while shorter pulses have high peak intensities and thus experienced more TPA attenuation in the waveguide. By measuring the transmitted power at different pulse durations, a two-photon-absorption coefficient has been estimated to be 0.3 cm/GW (see Chapter 4). This value is in reasonable agreement with that of the experimental results reported in Chapter 3 and with that published in the Reference [10] where a value of 0.14 cm/GW was presented.

5.4. Large scale cavity-mismatch characteristics

By defining the difference between the optical length of the external cavity and the main cavity as the cavity mismatching, $\Delta L = L_{ext.} - L_{mai.}$, we can divide the cavity-mismatching into three categories - positive, zero, and negative cavity-mismatches which refer respectively to the situation when the external cavity is longer, approximately the same, and shorter than the main cavity. In the experiment the cavity-mismatching was accomplished by a manual translation of mirror M3 which was mounted on a precision translation stage in the external cavity, e.g. by changing the

external cavity length while keeping the main cavity length constant. Due to the practical difficulty in determining the accurate zero cavity-mismatch condition, we intentionally assigns the zero-cavity-mismatch condition to the situation where the measured spectral and temporal profiles of the output pulses were most symmetric. As already mentioned, during the experiment, the temporal and spectral characteristics of the output pulses were monitored by a real-time second-harmonic autocorrelator and a real-time scanning Fabry-Perot etalon respectively. Therefore, the assumed zero-mismatching-condition could be deduced by moving the mirror attached to the PZT (shown in the experimental set-up in Figure 4.4) to the position where the monitored spectral profile of the output pulses were most symmetric.

Fig. 5.5 shows the measured spectra and second-harmonic autocorrelation traces of the output pulses for different cavity-mismatching conditions. It was observed that when the two cavities were not matched the output spectra were asymmetric and the larger the cavity-mismatch the more pronounced the asymmetric would be. For positive mismatches, a shoulder appeared at the shorter wavelength side of the output spectral profile; while for negative cavity-mismatch this feature appears at the longer wavelength side, as shown in Fig. 5.5 b, d. In the zero-mismatch condition, e.g. the optical lengths of the two cavities are taken to be approximately equal - and the output spectral profile was symmetric. Careful comparison of the autocorrelation traces at different situations indicates that the output pulse profile at matched condition was symmetric, while the elevated wings which appeared on the intensity autocorrelations at the mismatched regimes imply that the output pulse profile was asymmetric.

These results could be explained as follows. When the optical length of control cavity is longer than that of main cavity, e.g. positive mismatching, an overlap occurs between the trailing edge of the main cavity pulse and the front edge of the returned pulse. Thus, this overlap will result in the output pulses having a longer leading edge and a sharper trailing edge. In contrast, for negative-mismatch, the resultant pulses will have a longer trailing edge and a sharper leading edge. This phenomenon was also

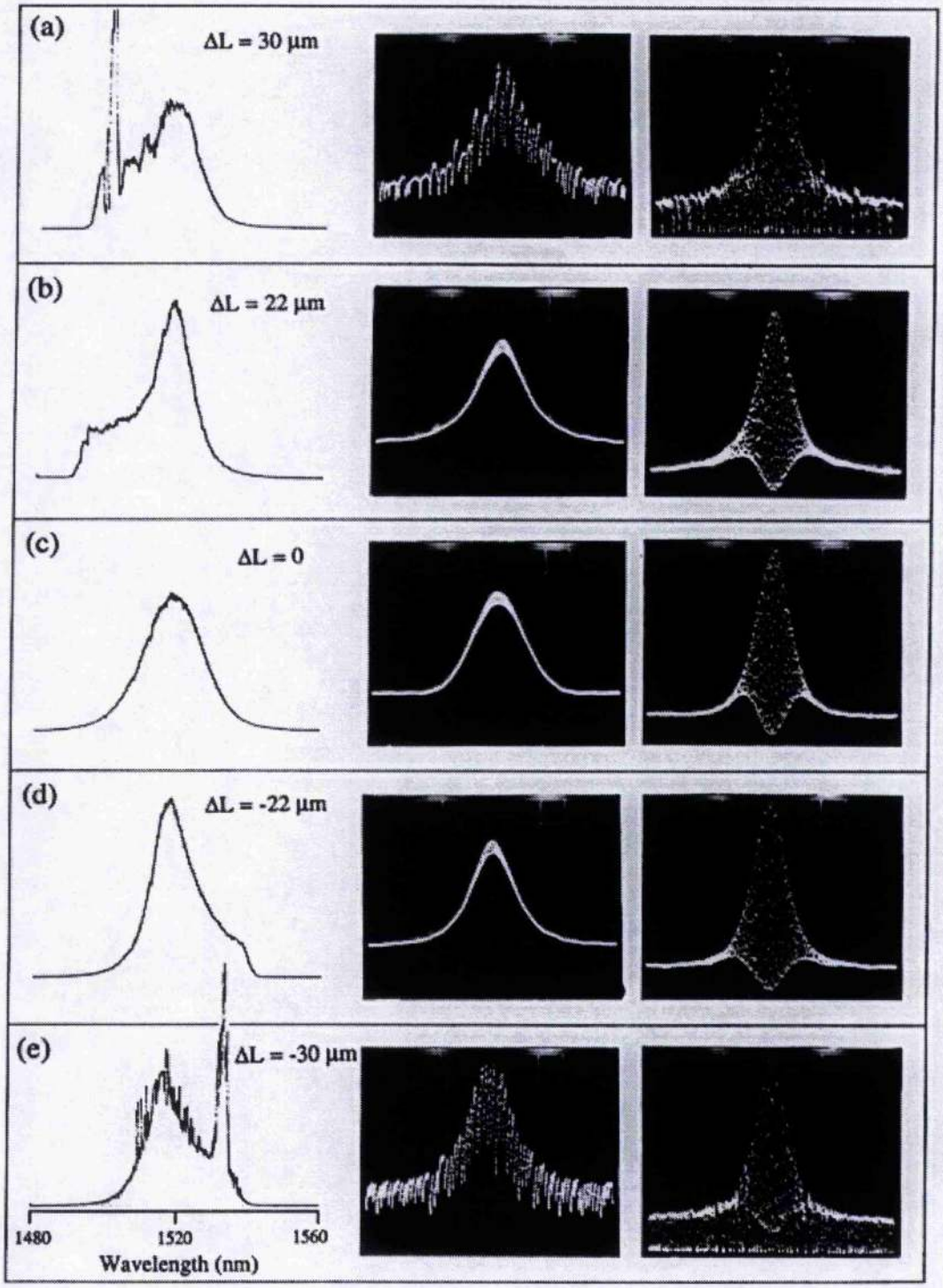

Figure 5.5. Spectra and autocorrelation traces of output pulses for different cavity-mismatch conditions.

observed and reported by Zhu and Sibbett when a piece of optical fibre was used as the nonlinear element [11]. It was more explicitly shown by Chee, et al in a CCM, Nd:YLF

laser through the cross-autocorrelation measurement of the output pulses [8], where analytical prediction are also studied by combining two chirped pulses together at different portion of the pulses.

When further away from the zero-mismatch position; $\Delta L = 30$ μm and $\Delta L = -30$ μm in the studies here; a peak feature appeared on the output spectrum and the autocorrelation traces exhibited a modulation structure. Measurement indicated that the isolated colour-centre laser output spectrum was in the middle of the broadened CCM output spectrum. Therefore the modulation characteristic can not be explained as the transient switching on and off of the CCM process. The origin of this spike feature which appeared on the output spectrum profile is not yet clear. The maximum detuning from the zero-mismatch condition is about 30 μm, and beyond this value the couple-cavity mode locking is prevented.

The transmitted spectra at different cavity-mismatch conditions were also measured, as indicated in Fig. 5.6, where for the reason of comparison, the output spectra are also shown. It was found that the output and transmitted spectral profiles were both symmetric at zero-mismatching , as confirmed in Fig.5.6 (b). When the two cavities were not matched, the transmitted spectral profile became asymmetric and shifted towards the shorter wavelength side at positive-mismatching, Fig. 5.6 (a), while at negative-mismatching it shifted more towards the longer wavelength side, Fig. 5.6 (c). This can be explained in terms of the SPM-induced spectral broadening in the waveguides. Due to the SPM effect, the leading edge of the pulse gives rise to a spectral broadening on the longer wavelength side and the trailing edge gives rise to spectral broadening on the shorter wavelength side. After passing through the waveguide, an asymmetric incident pulse will give rise to an asymmetric spectral profile of the transmitted pulse as well. Therefore, the asymmetric feature of the transmitted spectral profile in Fig. 5.6 indicates that the incident pulse shape was asymmetric. At positive mismatching, the "red" shift of the wavelength means that the incident pulses had a

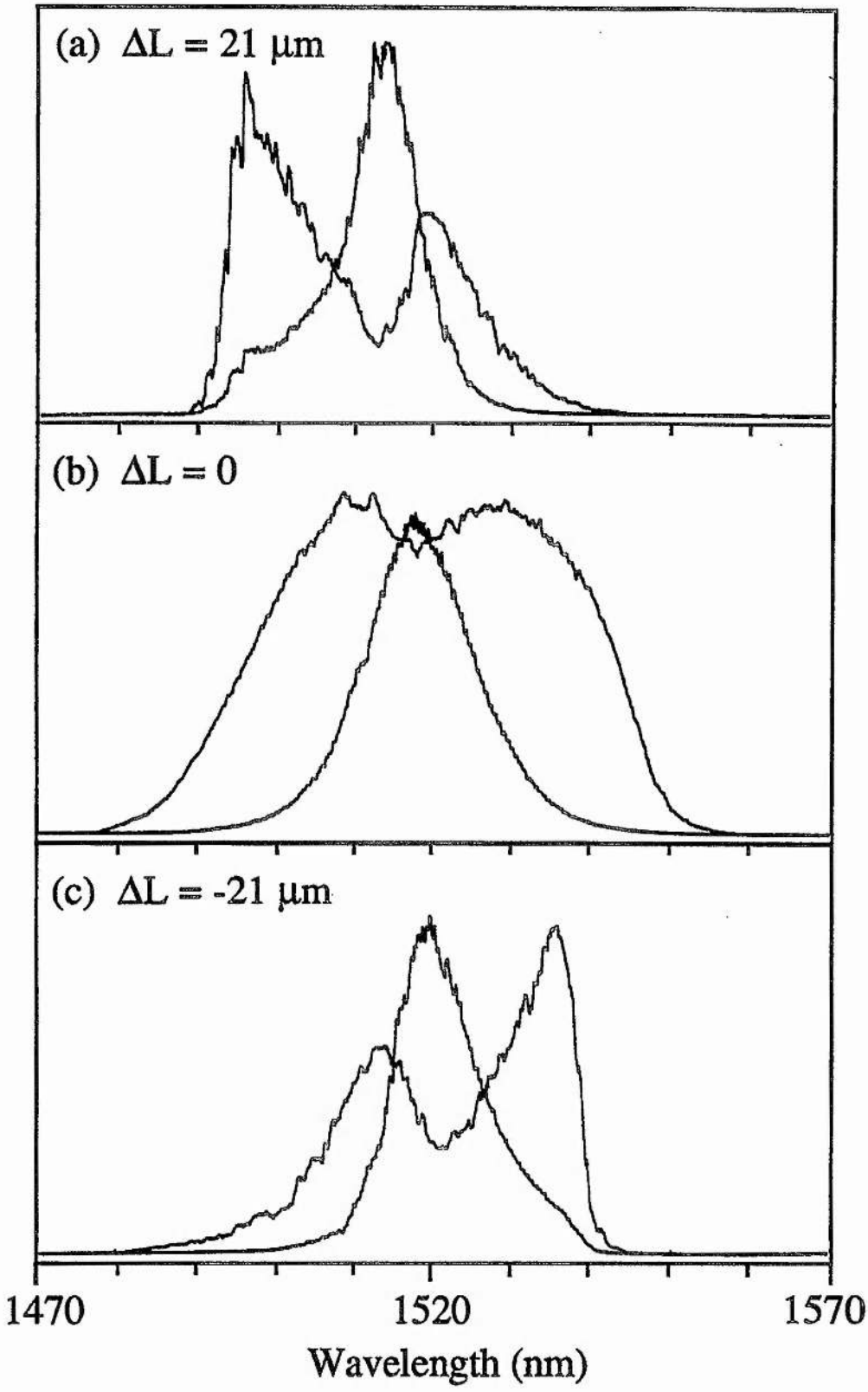

Figure 5.6. Output and transmitted spectra for different cavity-mismatching conditions.

sharper trailing edge and a longer leading edge,. These are consistent with the prediction of the output pulse shape for different cavity-mismatching conditions.

With reference to Fig. 5.6, it can be stated that as a positive cavity-mismatch, the pulses returned to the main cavity had more SPM-induced spectral components at the shorter wavelength side due to the asymmetric feature of the incident pulses. Therefore, when these returned pulses are overlapped with the main cavity pulses, relatively more shorter wavelength components will be transferred to the main cavity pulses. As a result, the output spectrum appeared with a shoulder at the shorter wavelength side and vice versa for negative cavity-mismatches.

Fig. 5.7 shows a diagram of the output pulse duration, spectral width and bandwidth-duration product as a function of the cavity-mismatching. It can be seen that when the two cavities were matched the pulse duration, spectral width and bandwidth-duration product were all maximum. Away from this matching point the pulse duration become shorter and the spectral width was reduced.

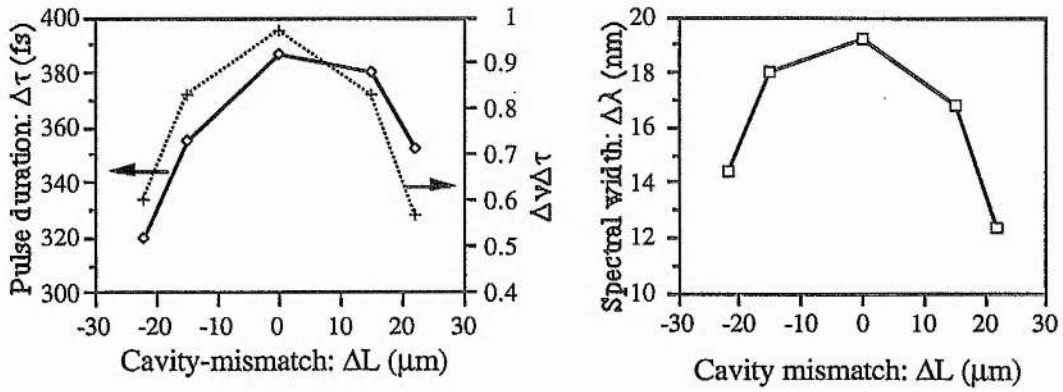

Figure 5.7.. Pulse duration, bandwidth-duration products and the spectral width of output pulses as a function of cavity-mismatch without any dispersion compensation element in either of the two cavities.

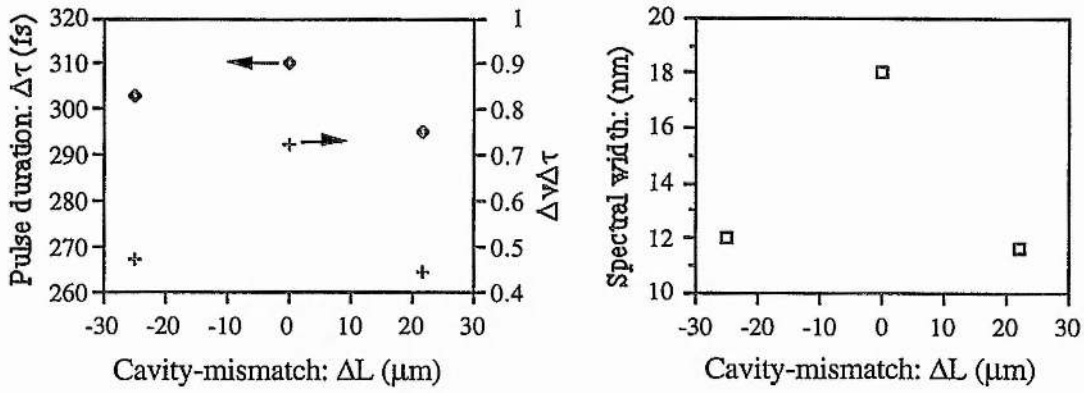

Figure 5.8. Pulse duration, bandwidth-duration products and the spectral width of output pulses as a function of cavity-mismatch when a 10 cm long silica rod was inserted in the nonlinear branch.

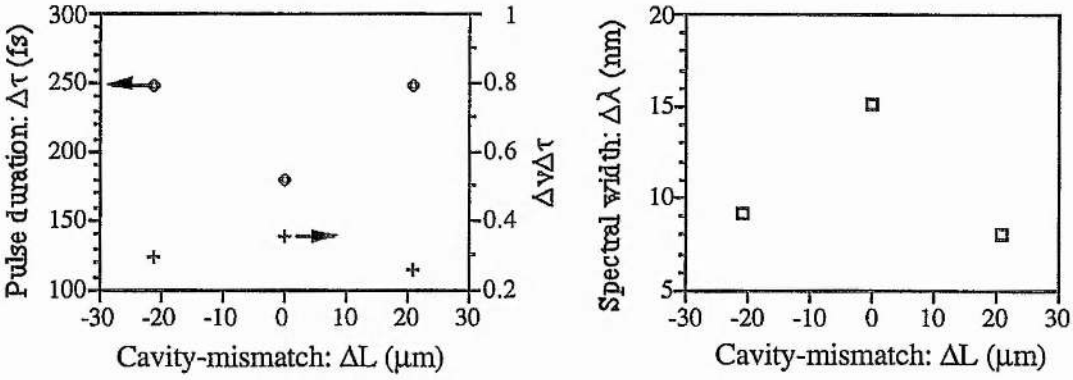

Figure 5.9. Pulse duration, bandwidth-duration products and the spectral width of output pulses as a function of cavity-mismatch when a 2 mm thick silica dick was inserted in the linear branch.

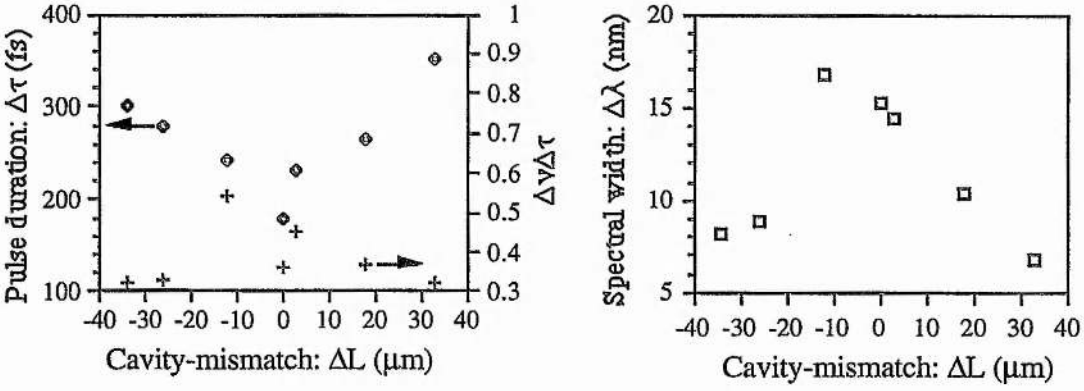

Figure 5.10. Pulse duration, bandwidth-duration products an the spectral width of output pulses as a function of cavity-mismatch when 30 cm long silica rod was inserted in the nonlinear branch.

The cavity-mismatch studies here also performed when frequency-chirp compensation was introduced in the cavity. An interesting feature is that the pulse duration at different cavity-mismatch for different chirp compensation. Without frequency-chirp compensation or with a 10 cm long silica rod inserted in the nonlinear branch, the pulse duration was longer at matched position than at mismatched position, as shown in Fig. 5.7 and Fig. 5.8. When 30 cm long silica rod was inserted in the nonlinear branch or a 2 mm thick silica disc was inserted in the linear branch the output was shorter at the matched position than at the mismatched position, as indicated in Fig. 5.9 and Fig. 5.10. When 30 cm glass rod was incorporated in the control cavity, referred to Fig. 10, the bandwidth-duration product at the mismatched position was smaller than 0.32 for the transform limited pulses ($sech^2$ profile assumed). This indicates and confirms again the pulse profile at mismatched position was asymmetric [9].

5.5. Summary

In this chapter, the cavity-detuning characterisations of the coupled-cavity mode-locked KCl:Tl colour-centre laser has been discussed. It was found that CCM process could be maintained over a significant range of phase bias. The experimental results indicated that the pulse duration could be continuously changed from around 240 fs to about 700 fs simply by varying the phase difference between pulses returned from the external cavity and that being circulated in the main cavity. At one side of the tuning range both the pulse duration and the spectral width of the output pulses were comparatively smaller, while at another side they were both larger. For practical applications of the CCM KCl:Tl colour-centre laser, it is appropriate to tune the laser to the condition where the shortest pulses are generated, because in such case the output pulse is less chirped and appears less noise than at another side of the phase-bias setting. Larger scale cavity-mismatching characterisations indicated that only when the two cavities were matched both the temporal and spectral profile of the output pulses were symmetric, and in this case the spectral width was a maximum.

References

1. L. F. Mollenauer and R. H. Stolen, Opt. Lett. 9, 13 (1984).
2. P. N. Kean, X. Zhu, D. W. Crust, N. Langford, and W. Sibbett, in Digest of conference on lasers and electro-optics (Optical Society of America, Washington D. C. 1988), Paper PD7; Opt. Lett. 14, 39 (1989).
3. K. J. Blow and D. Wood, J. opt. Soc. Am B 5, 629 (1988).
4. A. Miller and W. Sibbett, J. Mod. Opt. 35, 1871 (1988).
5. E. P. Ippen, H. A. Haus, and L. Y. Liu, J. Opt. Soc. Am. B 6, 1736 (1989).
6. M. Morin and M. Piché, Opt. Lett. 14, 1119 (1989).
7. J. Herrmann, M. Muller, in the Technical Digest of 4th European Quantum Electronics Conference, Italy, Paper USPaP 107, 451 (1993).
8. J. K. Chee, J. Liu, and M. N. Kong, IEEE J. Quantum Electron. 28, 700 (1992).
9. G. P. Agrawal, "Nonlinear Fibre Optics", (Academic Press, Boston, 1989).
10. K. Al-hemyari, J. S. Aitchison, C. N. Ironside, G. T. Kennedy, R. S. Grant, and W. Sibbett, Electro. Lett. 28, 1090 (1992).
11. X. Zhu and W. Sibbett, J. Opt. Soc. Am. B 7, 2187 (1990).

Chapter 6

Applications

The main concern in the previous chapters has been the generation of ultrashort laser pulses using the KCl:Tl colour-centre laser. In this chapter, some applications using the laser, conducted during the course of this project, will be described. The first section discusses the conversion of femtosecond pulses from the 1.5- to 1.3- μm region by self-phase modulation mediated four-wave mixing in an Er-doped optical fibre. The second section provides the experimental results on the measurement of the GVD of a passive AlGaAs waveguide. In the last section, experiment on pulse propagation in a long length (1.017 km) optical fibre will be presented.

6.1. Conversion of femtosecond pulses from the 1.5- to 1.3- μm region by self-phase modulation mediated four-wave mixing

6.1.1. Introduction

The generation of femtosecond laser pulses over a wide spectral range has been a key research topic in the area of ultrafast phenomena [1, 2, 3]. Two approaches commonly used to obtain ultrashort laser pulses at some desired wavelength have been to use of available mode-locked lasers or to exploitation of nonlinear effects, such as the Raman effect to wavelength-shift the pulses from one spectral region to another [4, 5]. In the experiment described here, femtosecond pulses from a 1.5 μm CCM KCl:Tl colour-centre laser are shifted to wavelengths near 1.3 μm in an erbium-doped, single-mode optical fibre by the process known as self-phase-modulation (SPM) mediated four-wave mixing.

SPM-mediated four-wave mixing is a nonlinear process first observed by Zhu and Sibbett in a study of femtosecond pulse propagation in Er-doped optical fibres [6]. In

this process self-phase modulation occurs first. Then, as the spectrum of the propagating pulses extends, part of the extended SPM spectrum reaches particular wavelengths at which the phase-matching condition for four-wave mixing is satisfied such that efficient four-wave mixing occurs. In particular, as was shown by the original results [6], for the incident pulses (having duration of ~ 130 fs, repetition rate of 82 MHz) centred at 1.51 μm the output radiation can have a spectrum with distinctive peaks at 1.36 μm (anti-Stokes) and 1.6 μm (Stokes), depending on the fibre length and the coupled optical power.

In the research presented here, a further study of this interesting nonlinear process was performed. The duration of the incident pump pulses have been reduced in duration to the sub-100 femtosecond range, which has led to enhanced frequency shifts toward both shorter and longer wavelengths for the propagating pulses at relatively lower average pump power levels. The shortest anti-Stokes wavelength so far obtained was centred at 1.33 μm, which, in combination with the previous results, gives a tuning range of 1.33 ~ 1.38 μm. (The wavelength tuning can be achieved by changing the average power or the duration of the incident pulses near 1.5 μm). Although the 1.5 μm incident pulses have an amplitude modulation of approximately 2% at frequencies ≤ 2 kHz, no noticeable fluctuations of the anti-Stokes wavelength was observed. With an average incident power (P_i) of 15 mW at 1.52 μm, the anti-Stokes signal(centred at 1.33 μm) had a power level of ~1.2 mW, which, when the coupling loss is taken into account, implies a typical energy conversion efficiency of 11% in the fibre. For a given average intrafibre power level, the energy conversion efficiency was observed to be not only related to the fibre length but also to the incident pulse duration. When the duration of the incident pulses centred at the wavelength of 1.52 μm was maintained around 80 fs the duration of anti-Stokes pulses varied from 100 fs to 300 fs, depending on the length of the fibre used. In general, provided the phase matching condition was met, the longer the fibre, the broader the anti-Stokes pulses.

6.1.2. Experiments and analyses

The pump laser used in these experiments was the coupled-cavity mode-locked KCl:Tl colour-centre laser, previously described in Chapter 2. By using an appropriate thickness of birefringent filter and by the appropriate adjustment of the optical power coupled into the nonlinear cavity, stable pulses having durations between 80 and 90 fs were produced. The output from the laser was coupled into and out of a single-mode Er-doped fibre through objectives O1 and O2 respectively (see Fig.6.1). Both objectives (20X) were coated with broadband anti-reflecting coatings, except for the outer surfaces near the fibre, where index matching liquid was used to reduce the surface reflectivity loss. An overall coupling efficiency (P_f/P_i - power after objective O2 divided by power before objective O1) of 70% was obtained. The exact optical power coupled into the fibre was controlled by incorporating a neutral-density wheel attenuator. The fibre (provided by the BNR Europe Ltd.) has an erbium dopant concentration of 1.6×10^{17} cm^{-3}, a refractive index difference of 16×10^{-3}, a core diameter of 4.6 μm, and a predicted zero-dispersion wavelength at 1.43 μm. At the output of the fibre a prism or a dichroic beamsplitter was used to discriminate between the spectral components of the exiting pulses.

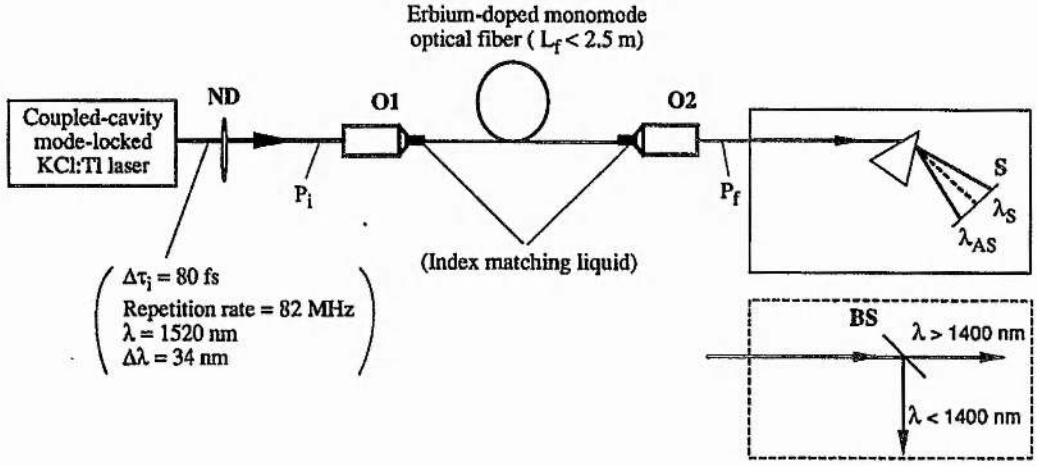

Figure 6.1. Experimental set-up for conversion of femtosecond pulses from 1.5 μm to 1.3 μm spectral region. ND: neutral density attenuator; O1, O2: objectives; BS: dichroic beamsplitter. (While the incident pulses are in the picosecond regime there is no four-wave mixing involved and the exiting beam after passing the prism will be in a direction as shown by the dashed line on the screen S).

Spectra for output pulses from 2.37 m fibre are reproduced in Fig. 6.2 (a) where the incident pulses had a duration of 80 fs and the average transmitted power was 12 mW (peak power in fibre = 2.2 kW). It can be seen that two distinct spectral features are evident, one peaked at 1.63 μm and another centred at 1.33 μm. This result should be contrasted with the spectrum of the incident pulses, which , as shown in Fig. 6.2(a) by

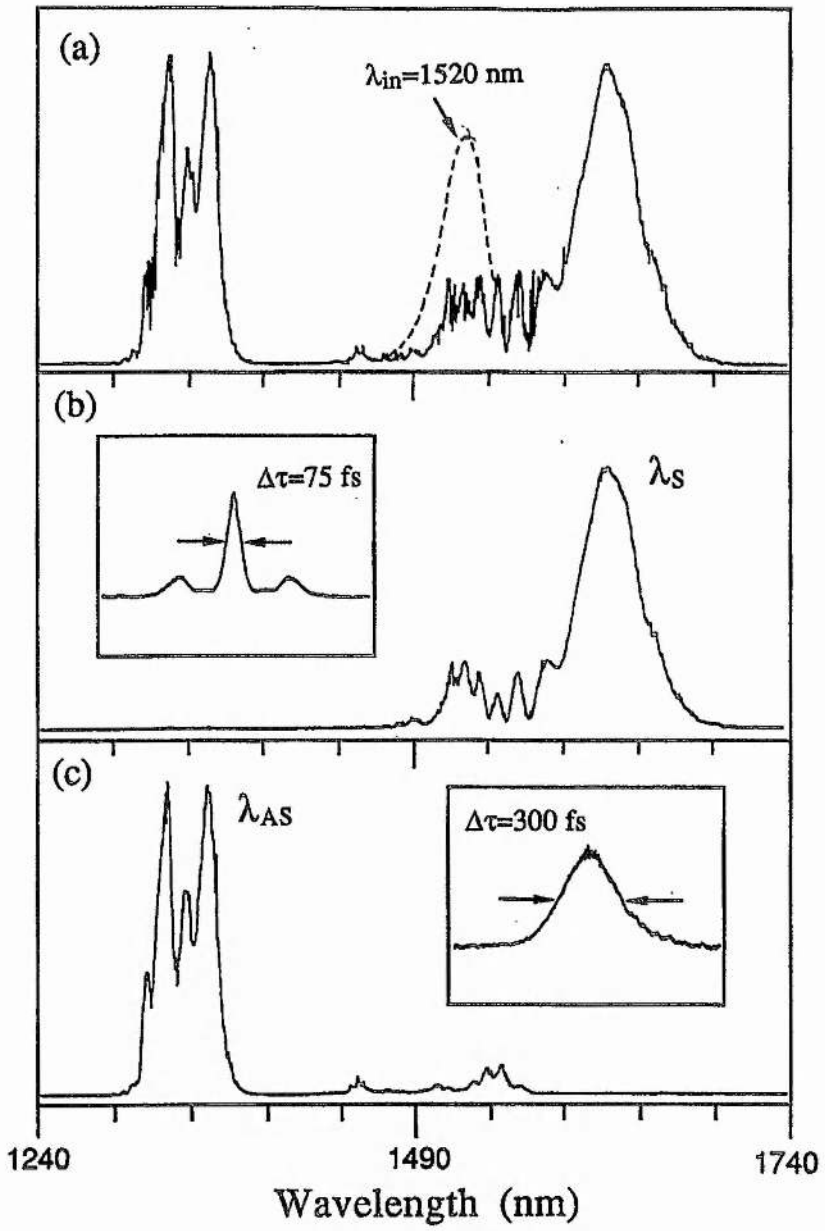

Figure 6.2. (a) Spectra for the pulses coupled into (dashed line) and exiting from (solid line) a 2.37 m erbium-doped fibre with P_f = 12 mW and $\Delta\tau_i$ = 80 fs; (b) (c) spectra for the spectrally discriminated Stokes and anti-Stokes signals, and the corresponding intensity autocorrelation traces.

the dashed curve, has a central wavelength of 1.52 μm and a bandwidth of 32 nm. When a dichroic beam splitter was used, the two dominant spectral components could be spatially separated in this way that the individual temporal features for each component were recorded, as shown in Fig. 6.2(b) and (c). [Note that the dichroic beamsplitter has a high reflectivity for the anti-Stokes signal and that the ringing on the reflectivity curve for the coating leads to the observed small amount of ripple in the spectral region beyond 1.4 μm - Fig. 6.2(c)]. The intensity autocorrelation trace for the Stokes signal (see the inset in Fig. 6.2(b)) shows a soliton-like feature. [Note that the component referred to here as the Stokes signal includes the residual spectral components at wavelengths near or longer than the incident laser wavelength; see Fig. 6.2(a), and (b)]. The central peak has an associated duration of 75 fs, which is slightly shorter than that of the incident pulses. In contrast, the anti-Stokes signal has a duration of 300 fs, which is significantly longer than the incident pulses and the corresponding Stokes signal.

In order to have some insight as to how the spectral characteristics of the propagating pulses change along the fibre, a cut-back experiment was performed. The monitored spectra for the pulses exiting from different lengths of fibre under approximately the same incident condition are shown in Fig.6.3. Interestingly, the shortest fibre length (L_f = 30 cm, trace (a) in Fig. 6.3) already shows a relatively large amount of spectral extension. Nevertheless, a significant anti-Stokes signal does not occur until the fibre length reaches 0.6 m (see Fig. 6.3(c)). This gives a clear indication of the region within the fibre where the four-wave mixing process is initiated. After the onset of the four-wave mixing, there is an associated spectral shift of the Stokes and anti-Stokes towards longer and shorter wavelengths. [Compare trace (d) with trace (c) in Fig. 6.3]. However, as the pulses propagate further in the fibre the central wavelength of the anti-Stokes remains essentially unchanged, as indicated by traces (d) - (f) in Fig. 6.3. This result is very different from the situation where the fibre length is fixed while the optical power of the incident pulses is varied [6] . As mentioned above, varying the optical power leads to the tuning of the anti-Stokes signal wavelength. The obvious

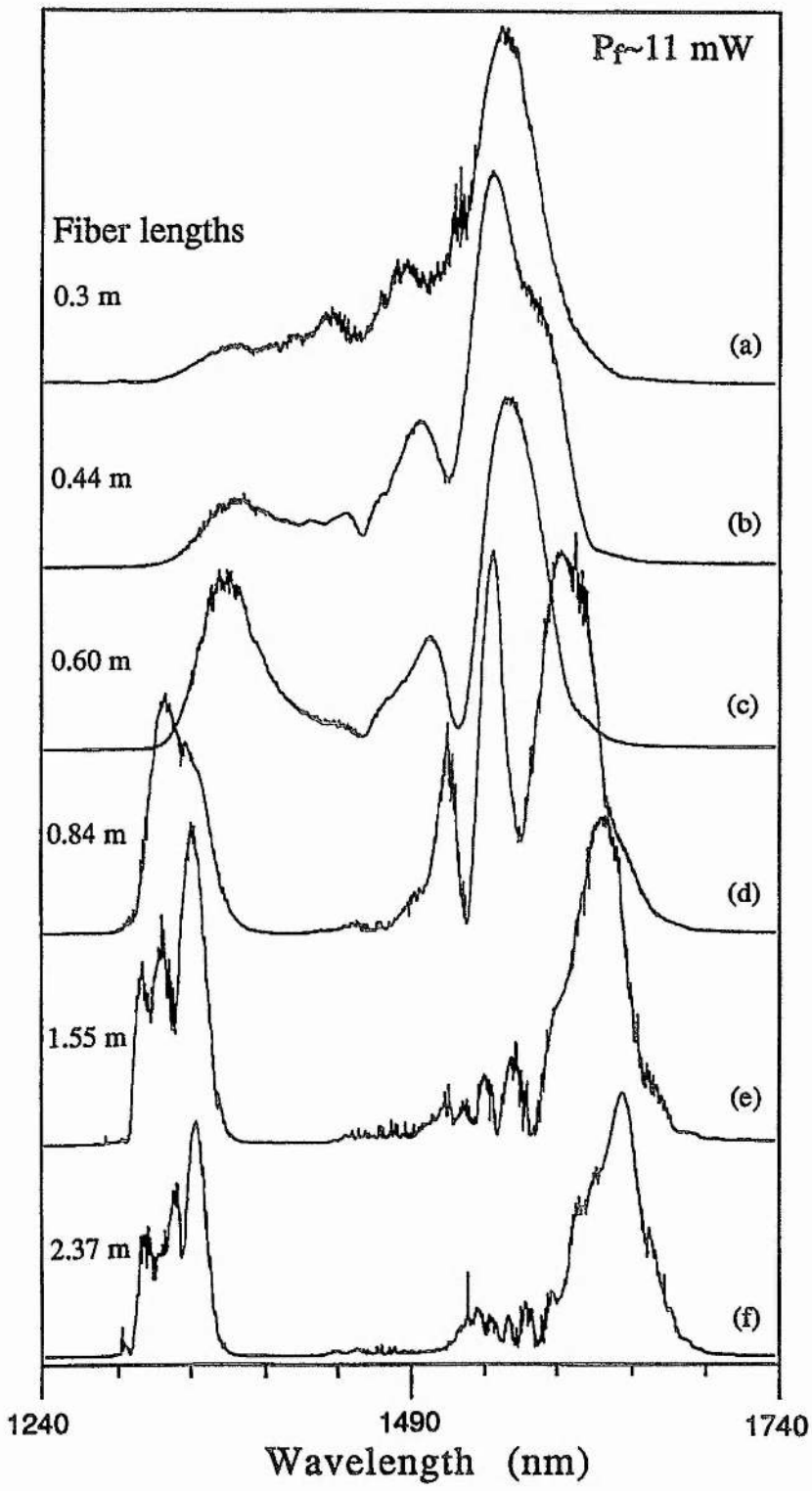

Figure 6.3. (a) - (f). Cut-back measurement of the spectrum of the propagating pulses for six different fibre lengths, where the incident conditions were maintained - P_f~11 mW, $\Delta\tau_i$: 80 ~ 90 fs.

modulation structure on the anti-Stokes spectra shown in the traces (e) and (f) reproduced in Fig. 6.3 indicates the involvement of SPM at these wavelengths. However, the spectral bandwidth of the anti-Stokes signal was not noticeably increased. For the traces (c) and (d) in Fig. 6.3, it can be seen that, in contrast to the anti-Stokes counterpart, the change of Stokes signal along the fibre is rather complicated. This change may be due to the mixture of and the interaction between the processes of four-wave mixing, self-phase modulation, and self-Raman effect.

The temporal features of the anti-Stokes signal exiting from different lengths of fibre were investigated by using a prism to separate it from Stokes wave (see Fig.6.1), and then using an autocorrelator to measure intensity and interferometric autocorrelation traces. Associated with the spectra shown in Fig.6.3 (c)-(f), the autocorrelation traces of the anti-stokes wave were recorded and are shown in Fig. 6.4. From Figs.6.4 (a), (c), (e), and (g), it can be seen that the duration of the anti-Stokes pulses increases monotonically with the fibre length (or the propagation distance). Correspondingly, the interferometric autocorrelation traces [(b), (d), (f), and (h) in Fig. 6.4] indicate an increased frequency chirp in the recorded pulses.

For the spectral and temporal data given in Figs. 6.3 and Fig. 6.4, the bandwidth-duration products for the anti-Stokes pulses can be deduced to be 0.82, 1.02, 1.49, and 2.35 for the 0.6-, 0.84-, 1.55-, and 2.37-m fibre lengths, respectively. Such values indicate the degree of frequency chirp associated with the anti-Stokes pulses. The relatively large frequency chirp within the initial anti-Stokes signal $\Delta\nu\Delta\tau = 0.82$ could be transferred from the chirped pump wave during the early stage of the four-wave mixing process, that is, a result of cross-phase modulation.

It is believed that the self-phase modulation of the incident 1.52 μm signal is responsible for producing the particular wavelength at which the phase-matching condition for four-wave mixing is met. In other words, the shorter-wavelength part of the SPM-extended spectrum acts as a pump wave in the four-wave mixing process. Thus, from an energy conservation point of view, only half of the incident signal can be

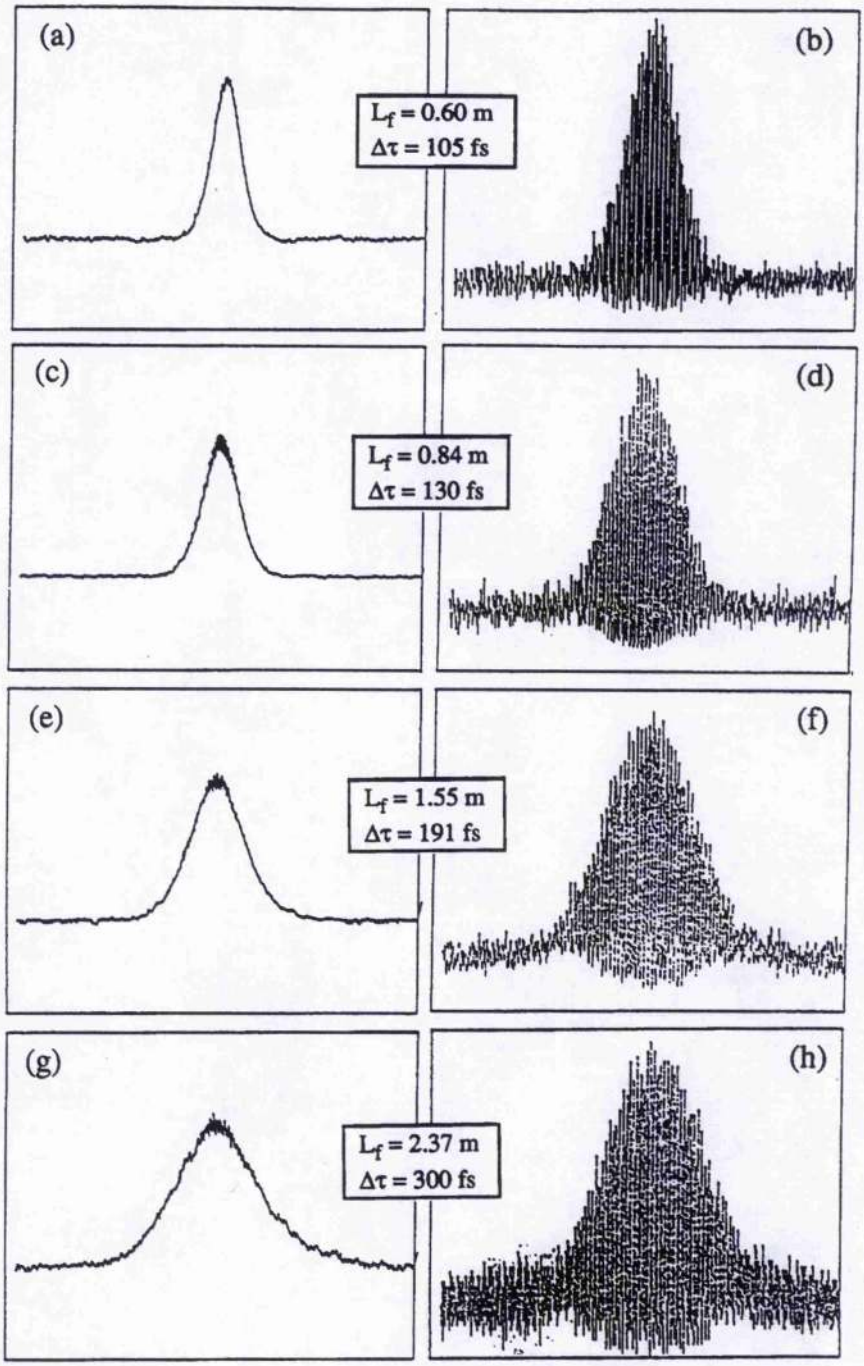

Figure 6.4. Intensity and interferometric autocorrelation traces for the anti-Stokes pulses as a function of fibre length [the corresponding spectra are the left part of the traces shown in Figs. 6.3(c)-(f)].

converted to the actual pump wave for four-wave mixing. If we take the conversion efficiency of this pump to four-wave mixing to be somewhere between 50% and 100%, say 75%, then the percentage of the total incident energy that contributes to the anti-

Stokes signal will be 1/2 x (75% x 1/2) = 3/16. Therefore, ignoring any loss inside the fibre, one can expect an energy ratio of the shorter wavelength (anti-Stokes) to the entire longer wavelength (Stokes) signals to be 3/16 : 13/16, that is, approximately 1:4. This simply means that if the average power of the spectral component around 1.33 μm is 1 mW measured by a power meter located after the dispersive prism in Fig. 6.1, then a similar measurement for the remaining spectral components (most having wavelengths ≥ 1.5 μm, for example, trace (f) in Fig 6.3.) would give an average power of 4 mW. In the experiment, the measured maximum ratio was approximately 1:5. This discrepancy could have arisen because we assumed too high a conversion efficiency or because we ignored the drain of energy to the Raman signal.

For the spectral data shown in Figs. 6.3 (c) - (f), the measured energy ratios of the anti-Stokes to Stokes for the four fibre lengths are as shown in Fig. 6.5, where the energy conversion efficiency from 1.52 μm to 1.33 μm is given. Interestingly a maximum conversion efficiency of ~ 14% exists for the 0.84-m-long fibre. When the incident pulse duration was varied while the average power was kept constant (that is, as the peak pulse power was varied), the optical power of the anti-Stokes wave also changed. An example of this is shown in Fig. 6.6, from which it can be seen that for a fibre length of 1.55 m the average power of the anti-Stokes wave increased as the incident pulses became broader. For the point that relates to $\Delta\tau_i$ = 122 fs in Fig. 6.6, the recorded anti-Stokes power level reaches 1.9 mW. In this case because the incident power P_i is 18 mW and the exiting power P_f is 13 mW, it can be deduced that the ratio of the anti-Stokes to Stokes signal is approximately 1:5, and the conversion efficiency from 1.52 μm to 1.33 μm is 16%. If we assume that the peak conversion observed for the 0.84 m fibre (Fig. 6.5) implies that such a fibre provides an interaction length that is close to the coherent length, then the tendency shown in Fig. 6.6 would indicate that, for the 1.55-m-long fibre to be close to a coherent length, the incident pulses should be broader. Hence an even higher conversion efficiency might be obtained if the system parameters are optimised. In general, for a chosen fibre length and a given coupling

power, an optimum incident pulse peak power will exist. With this optimum pulse duration a maximum conversion efficiency from 1.52 μm to 1.33 μm can be achieved.

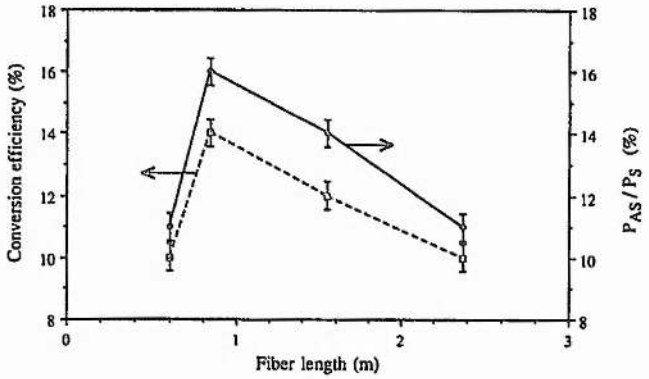

Figure 6.5. The energy conversion efficiency from 1.52 μm to 1.33 μm (dashed line) and the average power ratio of anti-Stokes wave to Stokes (solid line) as a function of fibre length.

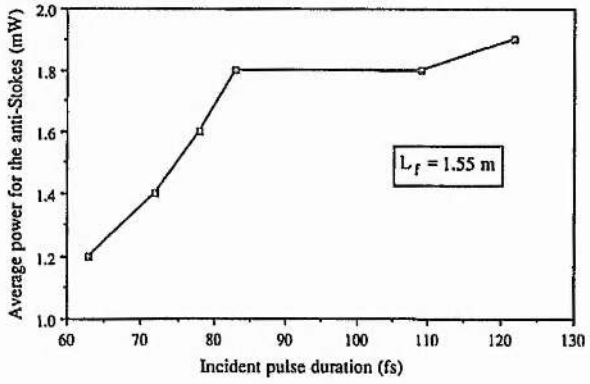

Figure 6.6. Variation of the average power of the anti-Stokes signal at exit of a 1.55-m-long fibre as a function of incident pulse duration (with P_i = 13 mW).

6.1.3. Conclusions

By pumping an erbium-doped monomode optical fibre with sufficiently powerful femtosecond pulses at 1.52 μm such that a self-phase-modulation mediated four-wave mixing process is initiated, we were able to produce femtosecond pulses near 1.33 μm. With the incident average power at a level of 10 mW, the average power of the anti-Stokes wave is typically 1-2 mW. The observed maximum up-conversion efficiency (from 1.52 μm to 1.33 μm) is 14% for 80-fs incident pulses and 16% for 122-fs incident pulses. The 16% value is close to a predicted value of 20% based on a simply analysis.

Being distinct from their Stokes counterparts, the anti-Stokes pulses have duration that exceed those of the incident pulses. Typically for 80-fs incident pulses at 1.52 μm, the duration of anti-Stokes pulses (which are found to be frequency-chirped) is ~ 100 fs at the fibre position where they are initiated. Because the anti-Stokes wave (centred at 1.33 μm) lies in the normal dispersive region of the fibre, these pulses broaden as they propagate.

6.2. Measurement of group-velocity-dispersion of the passive AlGaAs waveguides

6.2.1. Introduction

Recently, there has been much interest in the study of all optical switching in AlGaAs based semiconductor waveguides [7, 8] by utilising the enhancement of the nonlinear refractive index coefficient around half the bandgap energy. However, in most cases the group velocity dispersion (GVD) of the waveguides have been neglected. For broad optical pulses and relatively short waveguides, this assumption might be justified. When the waveguide is sufficiently long and subpicsecond pulses are used, the GVD effect can become significant. Therefore, it is necessary to have some knowledge about the GVD of the waveguide. In the experiment described here, direct measurement of the GVD of a passive AlGaAs waveguide was conducted.

The measurement was based on the synchronously-pumped, coupled-cavity mode-locked (CCM) KCl:Tl colour-centre laser, described in Chapters 4 and 5, in which the AlGaAs waveguide to be measured was used as the nonlinear element inside the control cavity. It is known that for proper CCM mode locking the optical lengths of the two cavities should be properly matched [9]. Mismatching of the two cavities will result in asymmetric features in both spectral profile and pulse envelope of the output pulses, as observed in Chapter 5 and discussed in Ref. [10]. Because of the difference in the GVD of the waveguide at different wavelengths, the transit time of pulses having different central wavelength are varied. Accordingly, it can be predicted that when the operating wavelength of the colour centre laser is changed, the round-trip time for pulses in the

control cavity varies as well. The length of the control cavity has to be re-adjusted so as to re-match the optical lengths of the two cavities. The change in the control cavity length is therefore a measure of the variation of the time delay versus wavelength that the pulses experience as they pass through the waveguide. Thus, by doing some simple calculation, the group velocity dispersion parameter D of the waveguide can be obtained. Utilising this principle, group-velocity-dispersion of an optical fibre has been successfully performed [11].

The AlGaAs waveguide to be measured was the one having a length of 3.49 mm, used in Chapter 4 and 5. Details of the waveguide structure can be found in Chapter 4.

6.2.2. Experiment and results

The experimental set-up was similar to that depicted in Fig. 4.4 of Chapter 4, except that a 2 mm thick birefringent filter was inserted in the main laser cavity (linear branch, see Fig. 4.4) to tune the output wavelength. The output wavelength could be varied from about 1.48 μm to 1.54 μm, and the output pulse duration was typically around 500 fs. The temporal features of the output pulse were monitored by a real-time autocorrelator, and the spectral feature were observed by a scanning Fabry-Perot interferometer. The main cavity length was varied by moving mirror M_1, which was mounted on a fine-translation stage; and the variation of the control cavity length was accomplished by moving the mirror attached to the PZT, which was also mounted on a fine-translation stage.

It was found that when the optical length of the two cavities were properly matched the spectrum of the output pulses would have a symmetric profile. But, if the two cavities were not properly matched the autocorrelation traces of the output pulse featured with long elevated wings, and an asymmetric output spectral profile was obtained, as evidenced in Fig. 5.5 of Chapter 5. These phenomena were initially considered to be a characteristic feature used for the correct judgement of the matching position.

In practise, it was found that, at a particular setting of the phase bias between the pulses in the two cavities, a peak feature appeared on the output spectrum, as shown in

Fig. 6.7. (Similar to that in Chapter 5, the setting of phase bias between the two-cavity pulses was accomplished by varying the signal level (voltage) applied to the PZT.) When the optical length of the control cavity was longer than that of the main cavity, the peak appeared at the short wavelength side of the spectrum, as depicted in Fig. 6.7-(a).The opposite occurred when the control cavity was shorter than that the main cavity, as illustrated in Fig. 6.7-(c). When the optical length of the two cavities were properly matched, the peak centred at the middle of the output spectrum, as depicted Fig. 6.7-(b). These characteristics were utilised in the determination of the matching position between the two cavities.

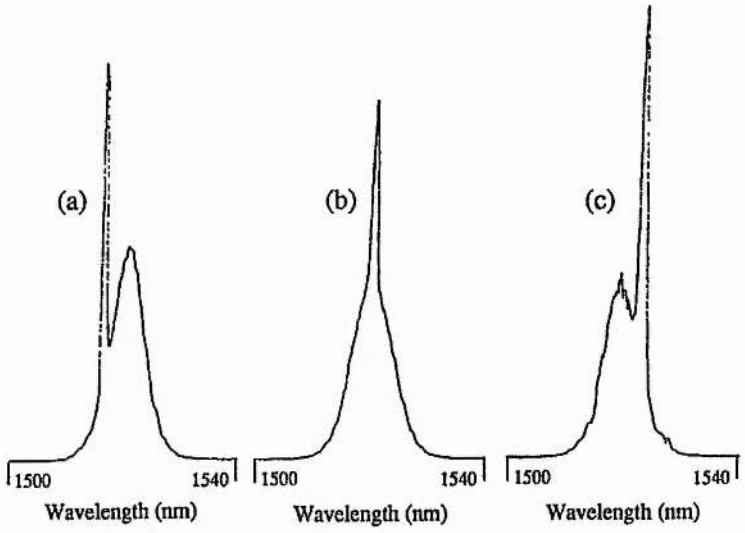

Figure 6.7. Spectra of the output pulses when the optical length of the control cavity is (a) longer than, (b) matched with , and (c) shorter than that of the main cavity.

The mechanism responsible for the peak which appears on the output spectrum under these condition is not well understood yet and requires further theoretical and experimental study. However, the matching position, when the peak was centred at the middle of the output spectrum, can be granted because in such case the output spectral profile was the most symmetric.

The measuring procedure was conducted as follows. Firstly, with the control cavity blocked, the end mirror M_1 of the main cavity was positioned to optimise the synchronous mode locking of the colour centre laser. The main cavity length was then

maintained constant during the whole measurement procedure. Secondly, the control cavity was unblocked and the mirror attached to the PZT was adjusted to obtain coupled-cavity mode-locking operation. Thirdly, the signal level applied to the PZT was varied until the peak feature appeared on the output spectrum (monitored by a real-time scanning FP interferometer). Fourthly, the laser wavelength was tuned using the BRF in the main laser cavity, and the spectral peak was centred in the middle of the spectral profile by moving the mirror attached to the PZT. Fifthly, the change in the control-cavity length was recorded for each wavelength chosen. Now by simple calculation, the change of the external length could be transformed to the variation of propagation time of the pulses through the waveguide.

Fig.6.8 shows the measured relative difference in transit time of pulses through the waveguide. It can been seen that at longer wavelength the transit time of pulses through the waveguide was less than that at shorter wavelength. This signifies that the waveguide had a normal group velocity dispersion around 1.5 μm. This is consistent with the previous observation that the pulses either transmitted through or returned from the waveguides were both temporally broadened. This was also verified by the single-pass experiment discussed in Chapter 3, where the transmitted pulses were temporally broadened.

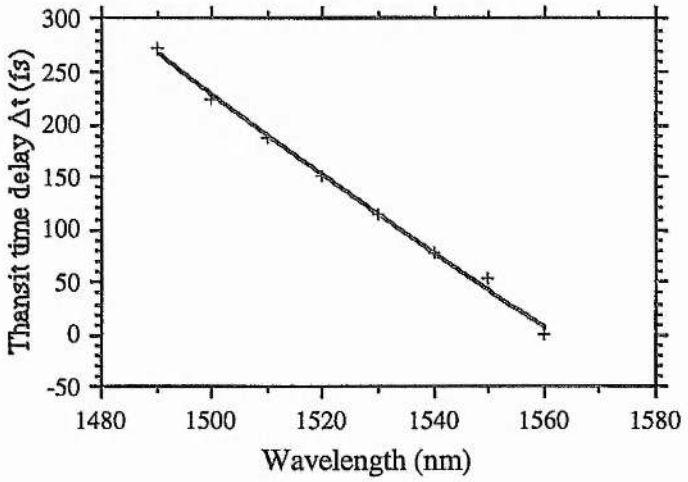

Figure 6.8. Relative difference in transit time of pulses through the waveguide for different wavelengths.

From a second order polynomial fit to the data in Fig. 6.8. the relative time delay Δt, of pulses through the waveguide, can be expressed as

$$\Delta t = 1.5385 \times 10^4 - 16.2811\lambda + (4.1177 \times 10^{-3})\lambda^2 \qquad (6.1)$$

where λ is the wavelength, expressed in nm.

The group velocity dispersion parameter D, defined as the pulse broadening per unit length of propagation and per unit wavelength, is given by

$$\begin{aligned} D &= \frac{1}{L}\frac{d(\Delta t)}{d\lambda} \\ &= \frac{1}{L}[-16.281 + (8.2354 \times 10^{-3})\lambda] \end{aligned} \qquad (6.2)$$

where L is the length of waveguide. On substituting L = 3.49 mm and λ = 1510 nm into the above equation, we get

$$D = -1100\, ps / nm / km$$

$$\text{or } \beta'' = -\frac{D\lambda^2}{2\pi c} = 1330 ps^2 / km$$

The GVD of the waveguide was also estimated by evaluating the effective refractive index data at wavelengths around 1.5 μm. Fig. 6.9 shows the variation of effective refractive index as a function of wavelength. Second-order polynomial fitting to the data gives

$$n_{eff} = 3.679 - 0.396\lambda + 0.107\lambda^2 \qquad (6.3)$$

In this equation, the wavelength λ is in μm. The group-velocity-dispersion is given by

$$\beta'' = \frac{\lambda^3}{2\pi c^2}\frac{d^2 n_{eff}}{d\lambda^2} \cong 1300 ps^2 / km$$

$$\text{or } D = -\frac{2\pi c}{\lambda^2}\beta'' = -1074 ps / nm / km$$

It can be seen that these two results were in good agreement.

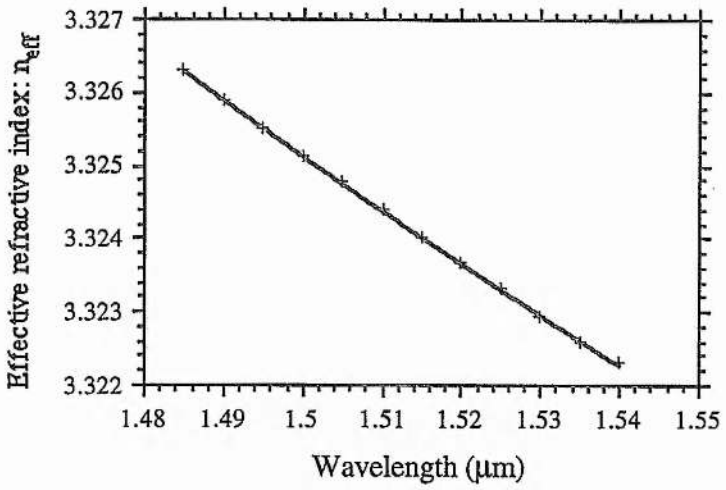

Figure 6.9. Dependence of effective refractive index on wavelengths.

Analogous to the case in optical fibres, a dispersion length can also be defined for the propagation of optical pulses in semiconductor waveguides [12], which is

$$L_D = \frac{2\pi c}{L^2|D|}\left(\frac{\Delta\tau_{in}}{1.736}\right)^2 \tag{6.4}$$

where $\Delta\tau_{in}$ is input pulse duration, D is the dispersion parameter and λ is the wavelength. The transmitted pulse duration $\Delta\tau_t$ is given by the equation

$$\Delta\tau_t = \Delta\tau_{in}\sqrt{1+\left(\frac{L}{L_D}\right)^2} \tag{6.5}$$

If we substitute the measured result of $D = -1100 ps/nm/km$, the input pulse duration $\Delta\tau_{in} = 100 fs$, and waveguide length L=3.49 mm into the above two equations, we get L_D=2.4 mm, and $\Delta\tau_t = 176 fs$. It can be seen that the pulse broadening resulting from the GVD is quite significant, and the dispersion length of the waveguide is comparable to the length of the waveguide. Therefore, it is necessary to consider the GVD effect for relatively longer waveguides and shorter optical pulses.

To confirm the measured result, a single-pass experiment was carried out. Here, transform-limited pulses were launched into the waveguide and the throughput pulse duration and spectrum were measured by an autocorrelator and a scanning FP interferometer respectively. For low input powers, the spectral broadening induced by

self-phase modulation could be neglected, so the pulse broadening could be considered to be that resulting solely from the group velocity dispersion. If both the input pulse duration and the throughput pulses duration were measured, from equation (6.4) and (6.5), the dispersion parameter D can be deduced. It was found that when 115 fs duration transform limited pulses were lunched into the waveguides, the transmitted pulses increased in duration to about 200 fs at low input powers (no significant spectral broadening was observed). Therefore, from Eq. 6.4 and Eq. 6.5, we get L_D=2.45 mm and $|D| = 1440$ ps/nm/km. Again these values are in good agreement with the measured result. The greater value of D obtained in the later case might be caused by the uncertainty in the determination of the pulse duration at very low power. As the autocorrelation traces were noisy which made the estimation of the pulse duration unreliable. When the launched power was high, the combined effect of the normal group velocity dispersion and the self-phase-modulation induced spectral broadening the transmitted pulse duration could be as high as 380 fs.

6.2.3. Conclusion

In conclusion, a measurement of the group velocity dispersion of an AlGaAs waveguide has been conducted. The result shows that the waveguide used here had a normal GVD at the wavelength around 1.5 μm and the value measured in this way was in good agreement with that calculated from the effective refractive index data.

6.3. Pulse propagation in optical fibres in the vicinity of zero-GVD

6.3.1. Introduction

In the first section of this chapter, the nonlinear pulse propagation in Er-doped fibres was discussed, with the emphasis on SPM-mediated four-wave-mixing. This section presents the experimental results pertinent to the propagation of ultrashort laser pulses in much longer optical fibres in the vicinity of zero-GVD. Attention will be focused on the spectral broadening effect of the transmitted pulses at different input wavelength. It has been found that different mechanisms are involved in the spectral

broadening, these include self-phase-modulation (SPM) [13, 14], modulation instability (MI) [15, 16], Raman scattering [17, 18], and the soliton-self-frequency-shift [19, 20].

In the experiment an AT&T fibre was used. The fibre was 1017 m long, and had an effective mode area of 80 μm^2. The wavelength of zero GVD of the fibre was specified as 1520 nm.

6.3.2. Experiments and results

The laser source used in this experiment was the synchronously mode-locked KCl:Tl colour centre laser, discussed in the previous chapters, which was tuneable from 1450 nm to 1570 nm. Typically, pulses having duration of 10 - 30 ps could be produced. With a newly installed crystal, output power of up to 200 mW could be obtained. The experimental set-up is illustrated in Fig. 6.10. The output from the laser was split into two parts by a beamsplitter, one part (~78%) was directed to the test optical fibre, with the another part going to the SHG autocorrelator to monitor the laser performance. An optical isolator was used to prevent the reflection from the fibre end disrupting the mode locking process. A variable neutral density (ND) wheel was used, before the coupling objective, to control the launched power to the fibre. Coupling of laser beam in and out of the fibre was accomplished by two 10X objective lenses. Typically, coupling efficiencies of about 60% were achieved. A portion of the transmitted signal was directed to a scanning monochrometer for spectral assessment. From time to time the pulses transmitted from the fibre was monitored by a SHG autocorrelator. For consistency, an effort was made throughout this experiment to ensure the pulse duration was maintained at about 14 ps.

As shown in Fig. 6.11, when the spectrum of the incident pulses was centred at a wavelength of 1515 nm, the spectral broadening was dominated by the SPM effect, within the experimentally limited power level (60 mW). The SPM induced spectrum became broader as the incident pump power was increased. However, the spectral profile became asymmetric at high power level.

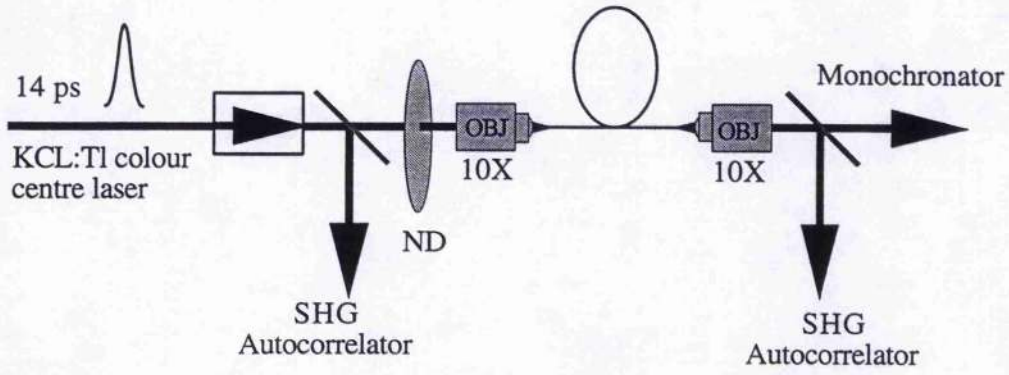

Figure 6.10. Experimental set-up for the single pass of pulses in the 1.017 km long optical fibre.

Fig. 6.12 shows the spectra of the transmitted pulses at an incident wavelength of 1520 nm. Pulse duration measurement has indicated that the transmitted pulses experienced essentially no temporal broadening. This implies that the zero-GVD wavelength of the fibre was in the vicinity of 1520 nm. From Fig. 6.12, it can be seen that the spectral broadening at this wavelength was still dominated by the SPM effect. Whereas, at higher power level (40 mW, 50 mW, and 60 mW) some evident spectral components emerged far beyond the SPM induced spectrum. It is believed that these spectral components are most probably resulted from the modulation instability, because part of the SPM induced spectrum may lie within the anomalous-dispersion region.

Comparing the SPM broadened spectra in Fig. 6.11 and Fig.6.12, it can be seen that, at the same incident average power level, the spectra in Fig.6.12 are broader than that in Fig.6.11 and are more asymmetric. This may be understood as a result of the pulse broadening effect at the wavelength of 1515 nm. Because the wavelength of 1515 nm lies within the normal GVD region, pulses at this wavelength will experience a temporal broadening when travelling in the fibre. Therefore, the peak power of the pulses will decrease as they propagate along the fibre. Whereas, at the wavelength of 1520 nm, the pulses experiences essentially no temporal broadening. As a result, the 1520 nm pulse will induce more spectral broadening than that of the 1515 nm pulse, due to its higher peak power.

Fig.6.13 shows the spectra of the transmitted pulses at the wavelength of 1526 nm, where the GVD becomes anomalous. It can be seen that a rather complicated spectral structure occurs. In this case, SPM, MI and self Raman scattering are all involved in the spectral broadening. At an average power level of less than 8 mW, the spectral broadening was dominated by the SPM effect. At a power of 8 mW, modulation instability began to appear, as evidenced by the typical spectral structure shown in Fig. 6.13 for the case of 10 mW incident power. When the power level was further increased, the spectral broadening involved a combination between SPM, MI and self-Raman effect.

When the input was further away from the zero-dispersion wavelength towards the longer wavelength side the self-Raman effect became the dominant nonlinear effect even at very low average power levels. This can be seen from the spectra shown in Fig. 6.14, Fig. 6.15 and Fig. 6.16. At higher power levels, self-Raman soliton generation has been obtained. Fig. 6.17 is an example showing the autocorrelations of typical transmitted pulses for the 1540 nm incident pulses, obtained at an average transmitted power of 60 mW. It can be seen that the 14 ps incident pulses have been compressed to about 210 fs after passing through the 1.017 km long fibre. One noticeable feature is that these transmitted pulses were highly chirped. The autocorrelation traces at large time scale indicates that a longer duration background pulse exists.

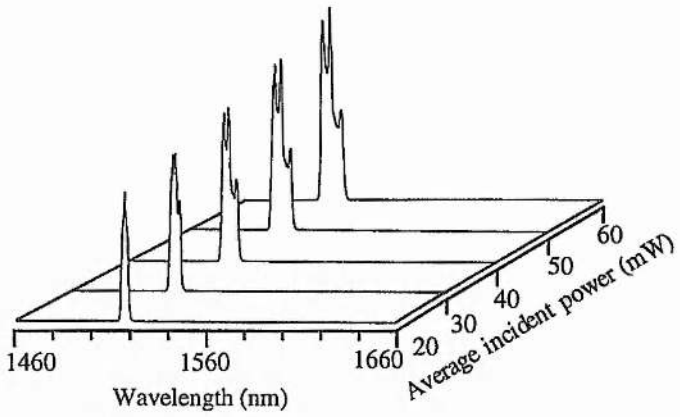

Figure 6.11. Spectra transmitted from the fibre at an incident wavelength of 1515 nm with different incident power level.

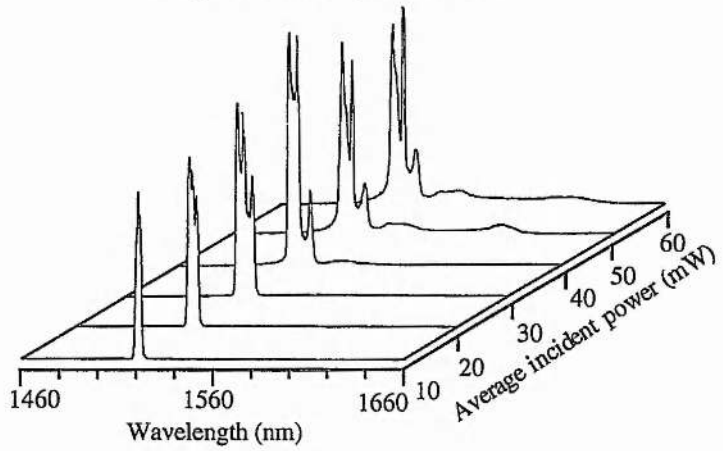

Figure 6.12. Spectra transmitted from the fibre at an incident wavelength of 1520 nm with different incident power level.

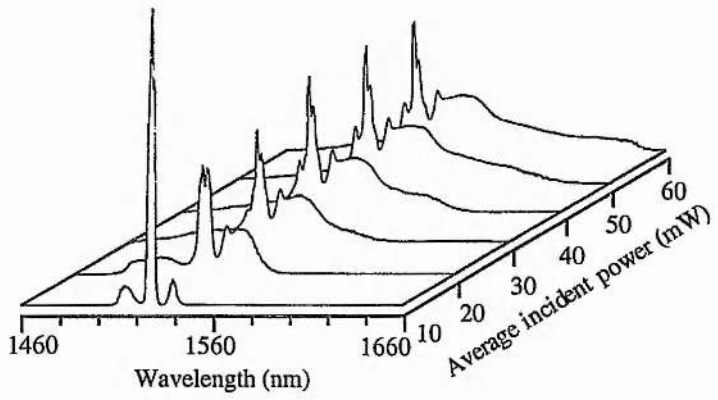

Figure 6.13. Spectra transmitted from the fibre at an incident wavelength of 1526 nm with different incident power level.

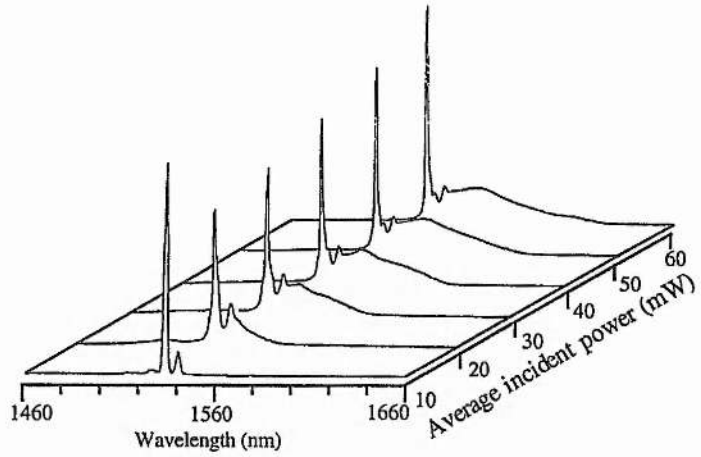

Figure 6. 14. Spectra transmitted from the fibre at an incident wavelength of 1530 nm with different incident power level.

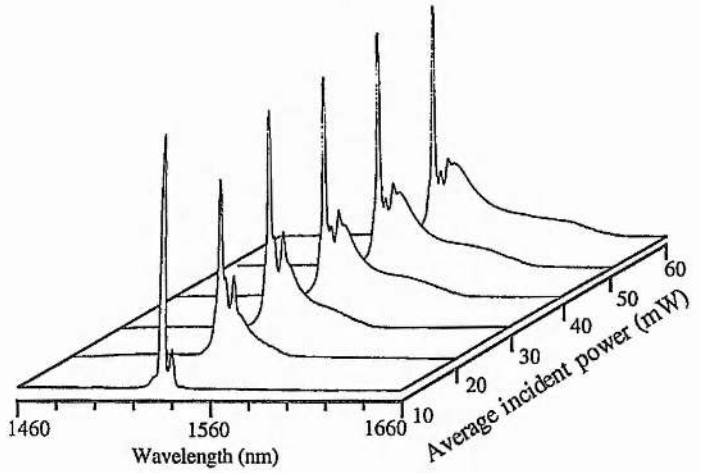

Figure 6. 15. Spectra transmitted from the fibre at an incident wavelength of 1535 nm with different incident power level.

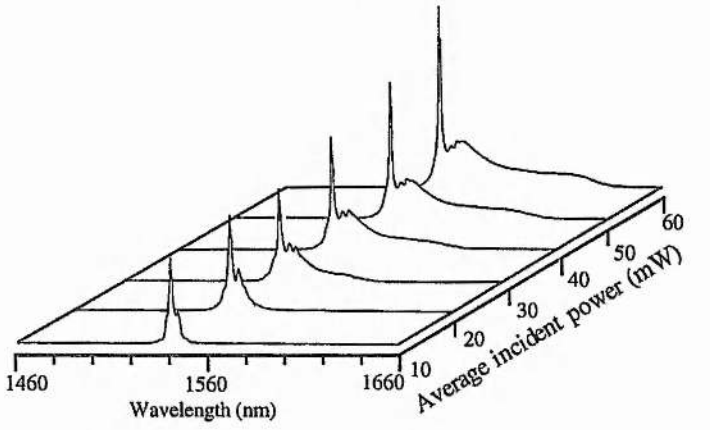

Figure 6.16. Spectra transmitted from the fibre at an incident wavelength of 1540 nm with different incident power level.

Soliton Raman generation in optical fibres has been extensively studied, some details of theoretical and experimental description can be found in a number of issued papers [17, 21]. The explanation of the soliton Raman generation process can be simply stated as follows: On propagating along the fibre the pulse firstly experiences the modulation instability effect. As a result, side-band spectra will be formed, as shown at the lower power level in Fig. 6.13. The "red" spectral component of the MI side band is well within the Raman gain band, and will act as a seed for the Raman scattering process on further propagation in the fibre. The result is that there is gain for the "red" component while shorter wavelengths experience absorption, or in another words there is an energy flow from short wavelengths into long wavelengths. If the power level is sufficiently high, the spectrum thus generated will cover a wide spectral region at the longer wavelength side, as observed in our experiment. Because such a broad spectrum is within the soliton regime, the pulse will be temporally compressed on further propagation along the fibre. At this stage, the soliton self-frequency-shift [20] may also take effect, which will shift the spectrum further toward the longer wavelength side.

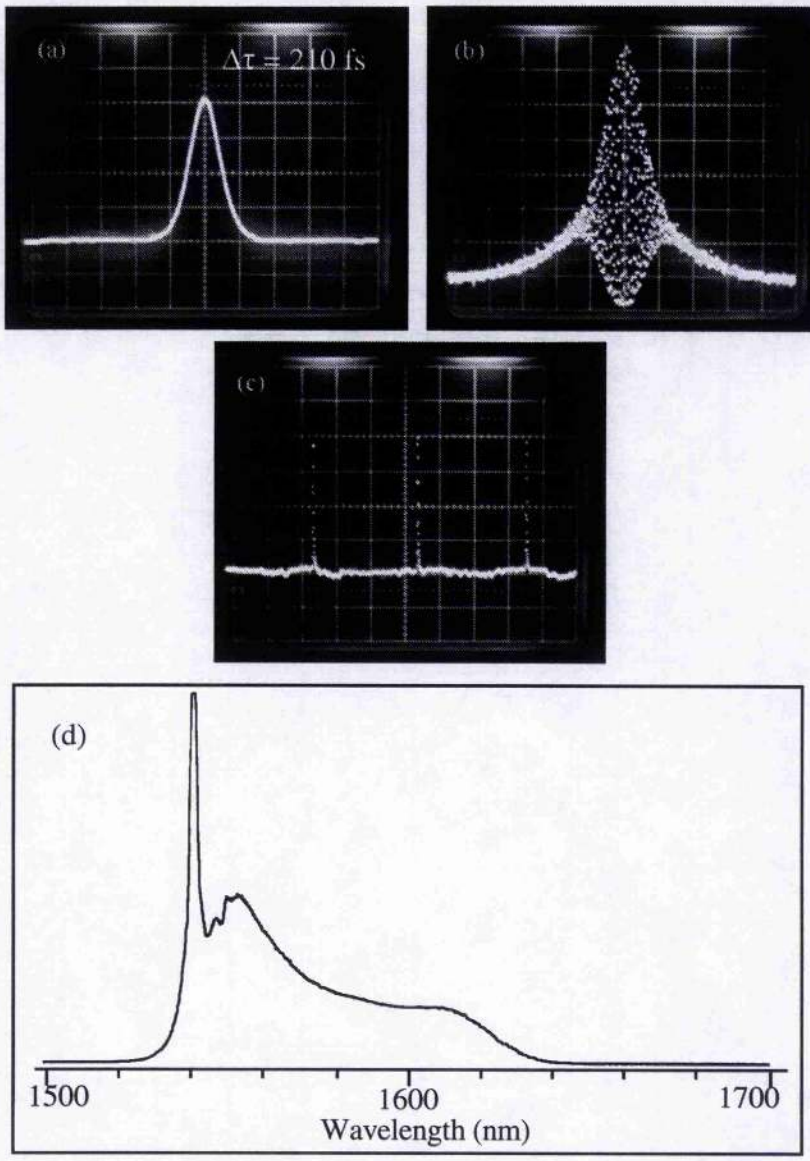

Fig.6.17. Typical autocorrelation traces and spectrum of the soliton Raman pulses obtained at an incident pulse duration of 14 ps and spectrum centred at 1540 nm. (a) Intensity autocorrelation; (b) Interferometric autocorrelation; (c) Intensity autocorrelation at relatively larger time scale; and (c) spectrum of the soliton Raman pulses. (Transmitted power measured to be 60 mW).

6.3.3. Estimation of GVD from the MI spectrum

As discussed in Chapter 1, the first side-band MI spectrum is separated from the incident spectrum by

$$\Omega = \left[\frac{2\gamma P_0}{|\beta''|}\right]^{1/2} \tag{6.6}$$

where P_0 is the peak power in the fibre, β'' is the GVD of the fibre, γ is a fibre parameter given by

$$\gamma = \frac{n_2 w}{c A_{eff}} \tag{6.7}$$

with n_2 the Kerr coefficient, and A_{eff} the effective mode area.

In term of wavelength, equation (6.6) can be restated as

$$\Delta\lambda = \frac{\lambda^2}{2\pi c}\left[\frac{2\gamma P_0}{|\beta''|}\right]^{1/2} \tag{6.8}$$

Therefore, if the GVD and peak power are known, the separation of the side-bands from the pumping spectrum can be calculated. It is obvious then that if we obtain $\Delta\lambda$ by experiment at a known peak power then the GVD parameter can be estimated. Transforming equation (6.8), the GVD parameter can be expressed as

$$\beta'' = -\left(\frac{\lambda^2}{2\pi c}\right)^2 \frac{2\gamma P_0}{(\Delta\lambda)^2}$$

or (6.9)

$$D = \left(\frac{\lambda^2}{2\pi c}\right)\frac{2\gamma P_0}{(\Delta\lambda)^2}$$

The minus sign for β'' in Eq. 6.9 is based on the fact that the modulation instability only occur at the anomalous dispersion regime.

Taking the case of incident average power of 10 mW as an example, and using the fibre parameters $A_{eff} = 80\ \mu m^2$, and $n_2 = 3.2 \times 10^{-16}\ (cm^2W^{-1})$; the calculated GVD of the fibre at the wavelengths of 1526 nm, 1530 nm, and 1535 nm are summarised in table 6.1.

Table 6.1. GVD estimated from the MI spectrum.

λ (nm)	Δλ (nm)	β'' (ps^2/km)	D (ps/nm/km)
1526	12	- 0.38	0.31
1530	7	- 1.13	0.91
1535	5	- 2.27	1.82

Note: Incident pulse width: Δt = 14 ps (Gaussian pulse assumed).

6.4. Summary

In this chapter, some applications of the ultrashort laser pulses generated from the mode-locked KCl:Tl colour-centre laser have been presented. The first section discussed the conversion of femtosecond pulses from the 1.5- to 1.3- μm region by the process of self-phase-modulation mediated four-wave mixing in an Er-doped optical fibre. By spectrally filtering the pulses at ~1.3 μm spectral region, pulses having duration of around 100 fs has been obtained. The second section provided the experimental results on the measurement of the GVD of a passive AlGaAs waveguide, based on the CCM mode locked KCl:Tl colour-centre laser. A GVD parameter of D = - 1100 ps/nm/km has been obtained. In the last section, pulse propagation in a long length (1.017 km) optical fibre has been examined. It was found that different mechanism were involved in the spectral broadening of the propagating pulses. Soliton Raman generation has resulted in pulse compression of the 14 ps incident pulses to a duration of 210 fs after propagating at ~1 km fibre.

References

1 W. Sibbett, on Ultrafast Processes in Spectroscopy (Bayreuth, Sept. 1991), Inst. Phys. Conf. Ser. No 126: Section I, 1 (1991).

2. R. L. Fork, C. V. Shank, C. Hirlimann, and R. Yen, W. J. Tomlinson, Opt. Lett. 8, 1 (1983).

3. J Squier and G Mourou, Laser Focus World, 28, 51 June issue, (1992).

4. A. S. Gouveia-neto, A. S. L. Gomes, and J. R. Taylor, IEEE J Quantum Electron. 24, 332 (1988).

5. P. N. Kean, K. Smith and W. Sibbett, IEE Proceedings, 134, Pt. J, 163 (1987).

6. X. Zhu and W. Sibbett, IEEE J. Quantum Electron. 27, 101 (1991).

7. J. S. Aitchison, A. H. Kean, C. N. Ironside, A. Villeneuve, and G. I. Stegeman, Electron. Lett. 27, 1709 (1991).

8. M. J. LaGasse, K. K. Anderson, C. A. Wang, H. A. Haus, and J. G. Fujimoto, Appl. Phys. Lett. 56, 417 (1990).

9. X. Zhu, P. N. Kean, and W. Sibbett, IEEE Journal of Quantum Electronics, Vol. 25, 2445 (1989).

10. J. k. Chee, J. M. Liu, and M. N. Kong, IEEE Journal of Quantum Electronics, Vol. 28, 700 (1992).

11. R. S. Grant, and W. Sibbett, Opt. Commun. 86, 177 (1991).

12. G. P. Agrawal, *Nonlinear fibre optics*, (Academic press, San Diego, 1989).

13. R. H. Stolon and C. Lin, Phys. Rev. A 17, 1448 (1978).

14. F. Shimizu, Phys. Rev. Lett. 19, 1097 (1967).

15. K. Tai, A. Hasegawa, and Tomita, Phys. Rev. Lett. 56, 135 (1986).

16. A. Hasegawa, and W. F. Brinkman, Opt. Lett. 9, 288 (1984).

17. A. S. Gouveia, A. S. L. Gomes, and J. R. Taylor, IEEE J. Quantum Electron. 24, 332 (1988).

18. T. Nakeshima. M. Nakashiwa, K. Nishi, and H. Kupota, Opt. Lett. 12, 404 (1987).

19. F. M. Mitschke and F. Mollenauer, Opt. Lett. 11, 659 (1986); J. P. Gordon, Opt. Lett. 11, 662 (1989).

20. M. N. Islam, G. Sucha, I. Bar-Joseph, M. Wegener, J. P. Gordon, and D. S. Chemla, Opt. Lett. 14, 370 (1989).

21. K. J. Blow and D. Wood, IEEE J. Quantum Electron. QE-25, 2665 (1989).

Chapter 7

General Conclusions

The main themes of the work presented in this thesis have been the generation of ultrashort laser pulses using a KCl:Tl colour-centre laser and the subsequent characterisations of their propagation in optical waveguides. Coupled-cavity mode locking of the KCl:Tl colour-centre laser with either monomode optical fibre or passive AlGaAs waveguides as the nonlinear element have been investigated. This work has shown that CCM, KCl:Tl laser having a fibre-based control cavity has the advantage of being able to generate relatively shorter pulses. However, this laser is more tolerant to the external disturbances when a short passive AlGaAs waveguide is used as the control-cavity nonlinear element. Also, when combined with a Michelson cavity configuration, there is the potential for greater miniaturisation of the CCM laser.

Temporal and spectral broadening have been observed when femtosecond pulses propagate in AlGaAs waveguides. It has been concluded that the temporal broadening results primarily from the group-velocity-dispersion of the waveguide, while the spectral broadening is caused mainly by the self-phase-modulation effect of the pluses in the waveguide. Two-photon-absorption in the waveguide has been observed and studied to provide date relating to the coefficient for two-photon absorption.

Optical fibre was the first and is still the dominant nonlinear element used in coupled-cavity mode-locked lasers, mainly due to its versatility and easy accessibility. Although a CCM, KCl:Tl colour-centre laser with optical fibres has been well established, the consideration for optimisation of practical laser performance was still required when this project was started [1, 2]. Therefore, as part of this work (Chapter

2), a re-examination of the characterisations of the CCM KCl:Tl colour-centre laser was carried out. It was found that two operational regimes existed for the CCM laser. In one regime the laser was properly mode-locked and distinct pulse train was generated, while in the other regime the mode-locked pulse train was modulated under longer Q-switched envelopes. By the insertion of a birefringent filter in the main cavity, the Q-switching effect could be eliminated. Optimisation of the laser performance was achieved when the birefringent filter was oriented in a direction parallel to the laser beam, and pulses as short as 63 fs have been generated.

Passive AlGaAs waveguides illuminated at the half-bandgap energy (1.5 μm) has been demonstrated to exhibit a large Kerr-type (non-resonant) nonlinearity [3] and thus nonlinear coefficient of the waveguide is two-orders larger than that in silica fibres [4]. Such a nonlinearity implied that a semiconductor waveguide would represent a suitable alternative of the optical fibres for the nonlinear element in the CCM KCl:Tl colour-centre laser. To explore the suitability of the AlGaAs waveguide as the nonlinear element, experiments on the pulse propagation in the waveguides have been conducted and the results are presented in Chapter 3. It was shown that waveguides used in this work have a linear loss coefficient of about 0.74 cm^{-1}. Two-photon-absorption coefficient of the waveguide was measured to be about 0.1 cm/GW. It was found that, after passing through the waveguide, pulses were broadened both temporally and spectrally. The temporal broadening was predominantly resulted from the positive GVD of the waveguide, while the spectral broadening was primarily caused by the self-phase-modulation of the pulses in the waveguide. Nonlinear phase shifts in excess of 2π have been measured. From the measurement of nonlinear phase shifts at different power levels, the nonlinear refractive index of the waveguide has been deduced to be 0.8×10^{-13} cm^2/W.

The main innovation of this project work is the coupled-cavity mode-locking with passive AlGaAs waveguides. In the experiments, two different guiding geometries have been employed. In the first case, a 4.15 mm long straight waveguide was used

and pulses having duration of 230 fs have been produced. However, the large substrate of the waveguide when presented at Brewster's angle prevented the use of lenses having focal length less than 2 mm, and this restricted the coupling efficient of light into the waveguide. It also made the further shortening of the output pulses impracticable. To overcome this drawback a curved guiding geometry was used. In this case, instead of using an objective and an additional mirror to return the exiting signal back into the main cavity, the rear facet of the waveguide itself acted as the end mirror of the control cavity. By using a 3.49 mm long waveguide and employing a Michelson-type cavity configuration, pulses having durations of about 250 fs have been produced. It was found that such pulses were in general highly chirped. This chirp is believed to be introduced from the positive GVD of, and SPM effect of pulses in, the waveguide. To eliminate the frequency chirp and thus reduce the pulse duration, dispersion compensation was implemented. When 30 cm long glass rod was inserted into the nonlinear branch of the Michelson cavity, 220 fs pulses were generated. However, further significant shortening of the pulse duration was achieved when a 2 mm thick silica disc was inserted into the main laser cavity. With this scheme, pulses as short as 168 fs have been recorded. By using shorter waveguides, some further shortening of the output pulses was achieved such that, with a 1.2 mm long waveguide, pulses as short as 150 fs have been observed.

To increase the feedback from the waveguide, a waveguide having its rear facet gold-coated has been used. With a 2.75 mm long gold-coated waveguide, successful coupled-cavity mode locking has been achieved at an output power level as low as 4 mW. This confirms an optimism for the possibility of making integrated coupled-cavity mode locking scheme applicable semiconductor lasers.

In Chapter 5, the cavity-detuning characterisations of the coupled-cavity mode-locked KCl:Tl colour-centre laser have been discussed. It was found that the CCM process could be maintained over a significant range of phase bias. The experimental results indicated that the pulse duration could be continuously changed from around

240 fs to about 700 fs simply by varying the phase difference between the pulses returned from the external cavity and those being circulated in the main cavity. At one extreme of the tuning range both the duration and the spectral width of the output pulses were comparatively small, while at the another extreme they were both large. For practical applications of the CCM KCl:Tl colour-centre laser, it is always appropriate to tune the laser to the condition where the shortest pulses are generated, because in such a case the output pulse is less chirped and appears less noisy. The larger scale cavity-mismatching characterisations indicated that only when the two cavities were properly matched did the temporal and spectral profiles of the output pulses appear symmetric, and in this case the spectral width was a maximum.

In Chapter 6, some applications of the mode locked KCl:Tl colour centre laser has been described. In the first instance, 120-fs pulses at the spectral region of 1.33 μm have been produced through the self-phase-modulation mediated four-wave-mixing process [5]. This was achieved by pumping an erbium-doped monomode optical fibre with sufficiently powerful femtosecond pulses at 1.52 μm, such that the self-phase-modulation mediated four-wave mixing process is initiated. The Stokes and anti-Stokes signals were well separated. By deploying a dichroic beamsplitter, the spectral component at 1.33 μm region was preferentially selected, so that ultrashort pulses at 1.33-μm spectral region were obtained. With the incident average power at a level of 10 mW, the average power of the anti-Stokes wave is typically 1 mW. The observed maximum up-conversion efficiency (from 1.52 μm to 1.33 μm) is 14% for 80-fs incident pulses and 16% for 122-fs incident pulses. This thus represented a method for obtaining femtosecond pulses in this -1.3 mm region but Cr:forsterite lasers are perhaps preferred alternative sources.

In the second section of Chapter 6, measurement of group-velocity-dispersion of the passive AlGaAs waveguide has been described. This measurement was based on the synchronously pumped CCM KCl:Tl colour-centre laser, where the waveguide to be measured was used as the nonlinear element in the control cavity. It is known that

coupled-cavity mode-locking requires a proper matching of the two-coupled cavities [6]. Mismatching of the two cavities will result in an asymmetric feature of both spectral profile and pulse envelope of the output pulses. Because of the difference in the GVD of the waveguides at different wavelength, the transit time of pulses having different central wavelengths varies accordingly. It can therefore be predicted that when the working wavelength of the colour-centre laser is changed, the round-trip time of the control cavity varies as well. To make the laser work properly, the period of the control cavity has to be re-adjusted so as to re-match the periods of the two cavities. The change in the control cavity period in fact corresponds to the variation of the time delay of the pulses that pass through the waveguide. Thus, by doing some related calculations, the group velocity dispersion parameter D of the waveguide can be obtained. For the waveguide used in this experiment, a GVD parameter of $D = -1100 ps / nm / km$ has thus been obtained. The result measured in this way was in good agreement with that calculated from the effective refractive index.

In the last section of Chapter 6, experiments on pulse propagation in a long span (1.017 km) of optical fibre have been performed. It was found that different nonlinear mechanisms, including self-phase-modulation (SPM), modulation instability (MI), Raman scattering, soliton Raman effect, have been involved in the spectral broadening of the propagating pulses. Soliton Raman generation in the anomalous GVD regime has resulted in pulse compression from 14 ps of the incident pulses to 210 fs of the transmitted pulses.

The pulse duration of the KCl:Tl colour-centre laser when coupled-cavity mode-locked using a passive AlGaAs waveguide is not yet as short as that obtained with optical fibres. However, it is possible that by using shorter waveguide elements and by applying appropriate dispersion compensation then the output pulse duration will be further reduced. A possible alternative approach towards reducing the output pulse duration would be to carefully control the GVD of the waveguide during its fabrication.

Finally, it should be mentioned that during the process of this work a room-temperature, mode locked laser source at 1.5 μm spectral region, the Cr^{+4}:YAG laser, has been demonstrated. From a practical viewpoint, it would be an advantage to replace the colour-centre laser with this newly developed room-temperature tuneable laser source, such that the low temperature requirement associated with the colour-centre laser would be avoided. However, to date, the tenability and reliability of the Cr^{+4}:YAG laser is not as good as the NaCl:OH^- colour-centre laser. It is nevertheless to be expected that room-temperature vibronic crystals will progressively replace colour-centre crystals in ultrashort-pulse near-infrared lasers.

References

1. X. Zhu, PhD Thesis, (University of St. Andrews, 1991).
2. R. S. Grant, PhD Thesis, (University of St. Andrews, 1991).
3. S. T. Ho, C. E. Soccolich, M. N. Islam, W. S. Hobson, A. F. J. Levi, and R. E. Slusher, Appl. Phys. Lett., 59, 2558 (1991).
4. M. N. Islam, C. E. Soccolich, R. E. Slusher, A. F. J. Levi, W. S. Hobson, and M. G. Yong, J. Appl. Phys., 71, 1927 (1992).
5. X. Zhu and W. Sibbett, IEEE J. Quantum Electron. 27, 101 (1991).
6. J. K. Chee, J. M. Liu, and M. N. Kong, IEEE J. Quant. Electron. 28, 700 (1992).

List of Publications

Journal Publications

Demonstration of polarisation rotation gate in GaAs/AlGaAs multiquantum well waveguides.

P. A. Snow, I. E. day, I. H. White, R. V. Penty, H. K. Tsang, R. S. Grant, Z. Su, W. Sibbett, J. B. D. Soole, H. P. Lebanc, A. S. Gozdz, N. C. Andreadakis and C. Caueau.

Electron. Lett. 28. 2346 (1992).

Conversion of femtosecond pulses from 1.5- to 1.3-μm region by self-phase modulation mediated four-wave mixing.

Z. Su, X. Zhu, and W. Sibbett.

J. Opt. Soc. Am. B10, 1050 (1993)

Al-optical modulation with ultrafast recovery at low pump energies in passive InGaAs/InGaP multiquantum waveguides

H. K. Tsang, P. A. Snow, I. H. White, R. V. penty, R. S. Grant, Z. Su, G. K. Kennedy and W. Sibbett.

Appl. Phys. Lett. 62, 1451 (1993).

Coupled-cavity mode locking with passive semiconductor waveguides,

R. S. Grant, Z. Su, G. T. Kennedy, W. Sibbett, J. S. Aitchison,

Opt. Lett. 18, 1600 (1993)

Conference Papers

Coupled-cavity mode locking using passive AlGaAs waveguides,

Z. Su, R. S. Grant, G. T. Kennedy, W. Sibbett, and J. S. Aitchison,

Paper, Page 109, Eleventh National Quantum Electronics Conference (QE 11), Belfast, August 1993.

Femtosecond pulse generation using passive Al GaAs waveguides at the half-bandgap.

Z. Su, R. S. Grant, G. T. Kennedy, W, Sibbett, and J. S. Aitchison,

Paper UPF2, page 395, 4th European Quantum Electronics Conference, Firenze, Italy, 1993.

Mode-locking using the half-bandgap nonlinearity in passive AlGaAs waveguides,

Z. Su, R. S. Grant, G. T. Kennedy, J. S. Aitchison, and W. Sibbett,

Paper MA3, OSA Topical Meeting on Nonlinear Guided-wave Phenomena, Cambridge, UK, September 1993.

Experimental determination of the group-velocity-dispersion of an AlGaAs waveguide at half the bandgap,

Z. Su, G. T. Kennedy, R. S. Grant, J. S. Aitchison, and W. Sibbett,

Paper CTHI8, CLEO' 94 (Conference on Laser and Electro-Optics), USA, 1994.

Acknowledgements

I would like to express many thanks to my supervisor, Wilson Sibbett, for his constant support, never-ending encouragement, and thoughtful guidance throughout the period of this project.

I am also indebted to Robert Grant and Xiaonong Zhu for their valuable discussion and helpful collaboration in this project.

I am grateful to: Dave Burns, Gordon T. Kennedy, and Gareth J. Valentine for kindly offering their enduring patience to proof-read parts of this thesis; Bill Sleat for his help with the electronics; Dave Hughes and Peter Roberts for their cheerful conversations; and all the members in the "Big W Squad" for their understanding and assistance.

Thanks are due also to all members of the technical staff in the Physics Department, in particular: Bob Mitchell for his help on the cryogenic aspects; Andy Barman for providing sufficient liquid nitrogen; Jim Lindsay, Reg Gavine and other members of the Mechanical workshop for making various bases and mounts.

I would also like to give thanks to Cui Yong and Tang Yan for providing the most essential support - the delicious meals, at the most appropriate moment.

Financial support from the Sino-British Technical Cooperation Training Programme is gratefully acknowledged.

Last but not least, many thanks to my wife, Huali, for taking over all of the burdens left at home.

Conversion of femtosecond pulses from the 1.5- to the 1.3-μm region by self-phase-modulation-mediated four-wave mixing

Z. Su, X. Zhu, and W. Sibbett

J. F. Allen Physics Research Laboratories, Department of Physics and Astronomy, University of St. Andrews, North Haugh, St. Andrews, Fife KY16 9SS, Scotland, UK

Received August 24, 1992; revised manuscript received January 15, 1993

By employing a femtosecond-pulse color-center laser, we were able to study quantitatively the process of self-phase-modulation-mediated four-wave mixing in an Er-doped optical fiber. It has been demonstrated that this scheme leads to the generation of femtosecond pulses in the 1.3-μm spectral region when a 1.5-μm mode-locked laser source is used.

INTRODUCTION

The generation of femtosecond laser pulses over a wide spectral range has been a key topic within research in the area of ultrafast phenomena.[1] Two approaches commonly used to obtain ultrashort laser pulses at the desired wavelengths have been the use of available mode-locked lasers and the exploitation of nonlinear effects such as the Raman effect to wavelength shift the pulses from one spectral region to another.[2] In this paper we report the generation of 100-fs pulses at wavelengths near 1.3 μm by the process of self-phase-modulation- (SPM) mediated four-wave mixing in an Er-doped single-mode optical fiber when we used a coupled-cavity mode-locked 1.5-μm laser as a pump source.

SPM-mediated four-wave mixing is a nonlinear process first observed by Zhu and Sibbett[3] in the study of femtosecond-pulse propagation in Er-doped optical fibers. In such a process SPM occurs first. Then, as the spectrum of the propagating pulses extends, part of the extended SPM spectral component reaches the particular wavelengths at which the phase-matching condition for four-wave mixing is satisfied such that four-wave mixing occurs. In particular, as was shown by the original results,[3] for the incident pulses (having a duration of ~130 fs and a repetition rate of 82 MHz) centered at 1.51 μm the output radiation can have a spectrum with distinctive peaks at 1.36 μm (anti-Stokes) and 1.6 μm (Stokes), depending on the fiber length and the coupled optical power.

In the research reported here we have made a further study of this interesting nonlinear process. The durations of the incident pumping pulses have been reduced to the sub-100-fs range, which has led to further frequency shifts toward both shorter and longer wavelengths for the propagating pulses at relatively lower average pump power levels. The shortest anti-Stokes wavelength so far obtained is centered at 1.33 μm, which, in combination with the previous results, gives a tuning range of 1.33–1.38 μm. (The tuning can be achieved by changing the average power or the duration of the incident pulses near 1.5 μm.) Although the 1.5-μm incident pulses have an amplitude modulation of approximately 2% at frequencies $\leq$2 kHz, no noticeable fluctuations of the anti-Stokes wavelength were observed. With an average incident power (P_i) of 15 mW at 1.52 μm, the anti-Stokes signal (centered at 1.33 μm) had a power level of ~1.2 mW, which, when we consider the coupling loss, implies a typical energy conversion efficiency of 11% in the fiber. For a given average intrafiber power level the energy conversion efficiency was observed to be not only related to the fiber length but also to the incident pulse durations. When the duration of the incident pulses centered at the wavelength of 1.52 μm was maintained at approximately 80 fs the duration of anti-Stokes pulses varied from 100 to 300 fs, depending on the length of the fiber used. In general, provided that the phase-matching condition was met, the longer the fiber, the broader the anti-Stokes pulses.

EXPERIMENTS AND ANALYSES

As shown in Fig. 1, the pump laser used in our experiments was a coupled-cavity mode-locked KCl:Tl color-center laser.[4] By using an appropriate thickness for the birefringent filter and by making a proper choice of optical power coupled into the nonlinear cavity, we controlled the laser to produce stable pulses with durations between 80 and 90 fs throughout these experiments. The output from the laser was coupled into and out of a single-mode Er-doped fiber through objectives O1 and O2, respectively. Both objectives (20×) were coated with broadband antireflecting coatings, except for the outer surfaces near the fiber, where index-matching liquid was used to reduce the surface reflectivity loss. An overall coupling efficiency (P_f/P_i, power after objective O2 divided by power before objective O1) of 70% was obtained. The exact optical power coupled into the fiber was controlled by incorporating a neutral-density wheel attenuator. The fiber (provided by the BNR Europe Ltd.) has a dopant concentration of 1.6×10^{17} cm^{-3}, a refractive-index difference of 16×10^{-3}, a core diameter of 4.6 μm, and an expected

0740-3224/93/061050-04$06.00

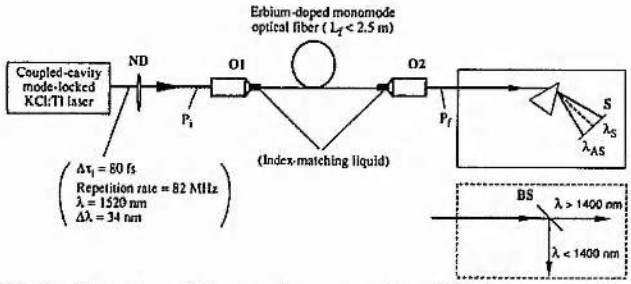

Fig. 1. Experimental setup for conversion of femtosecond pulses from the 1.5- to 1.3-μm spectral region: ND, neutral-density attenuator; O1, O2, objectives; BS, dichroic beam splitter; S, screen. Although the incident pulses are in the picosecond regime, no four-wave mixing is involved, and the beam after passing the prism will be in a direction as shown by the dashed line on the screen.

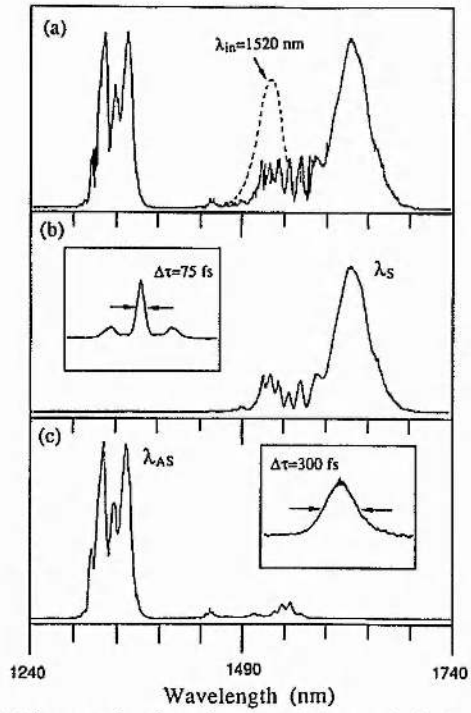

Fig. 2. (a) Spectra for the pulses coupled into (dashed curve) and exiting from (solid curve) a 2.37-m-long Er-doped fiber with $P_f = 12$ mW and $\Delta\tau_i = 80$ fs. (b), (c) Spectra for the spectrally discriminated Stokes and anti-Stokes signals, respectively, and the corresponding intensity autocorrelation traces.

zero-dispersion wavelength at 1.43 μm. At the output of the fiber a prism or a dichroic beam splitter was used to discriminate between the spectral components of the exiting pulses.

For a 2.37-m-long fiber and when the incident pulses have a duration of 80 fs and a transmitted average power $P_f = 12$ mW (that is, a peak power of 2.2 kW in the fiber), the spectra for the output pulses are as reproduced in Fig. 2(a). We can see that two distinct spectral features exist, one peaked at 1.63 μm and another centered at 1.33 μm. This result can be contrasted with the spectrum of the incident pulses, which, as shown in Fig. 2(a) by the dashed curve, has a central wavelength of 1.52 μm and a bandwidth of 32 nm. When a dichroic beam splitter is used, the spectral components at longer and shorter wavelengths could be spatially separated such that the individual temporal features for each component were recorded, as shown in Figs. 2(b) and 2(c). [Note that the dichroic beam splitter has a high reflectivity for the anti-Stokes signal and that the ringing on the reflectivity curve for the coating leads to the observed small amount of ripple in the spectral region beyond 1.4 μm in Fig. 2(c).] The intensity autocorrelation trace for the Stokes signal [see the inset in Fig. 2(b)] shows a soliton-like feature. [Note that the component referred to in this paper as the Stokes signal includes the residual spectral components at wavelengths near or longer than the incident laser wavelength; see Figs. 2(a) and 2(b).] The central peak is associated with an actual pulse duration of 75 fs, which is slightly shorter than that of the incident pulses. In contrast, the anti-Stokes signal has a duration of 300 fs, which is significantly longer than the incident and the corresponding Stokes signals.

To gain some insight as to how the spectral characteristics of the propagating pulses change along the fiber, we performed a cutback experiment. The monitored spectra for the pulses exiting from different lengths of fiber under approximately the same incident condition are shown in Fig. 3. Interestingly, the shortest fiber length [L_f = 30 cm, trace (a) in Fig. 3] already shows a relatively large amount of spectral extension. Nevertheless, a significant anti-Stokes signal does not occur until the fiber length reaches 0.6 m [trace (c) in Fig. 3]. This gives a clear indication of the region within the fiber where the four-wave mixing process is initiated. After the onset of four-wave mixing, we see an associated spectral shift of the Stokes and anti-Stokes signal toward longer and shorter wavelengths. [Compare trace (d) with trace (c) in Fig. 3.]

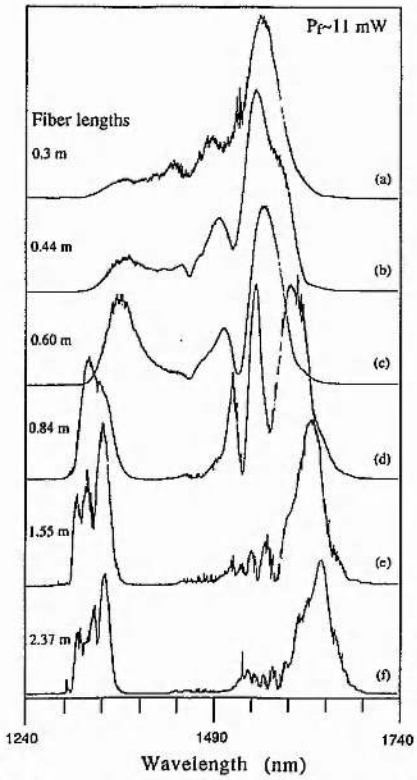

Fig. 3. Cutback measurement of the spectrum for the propagating pulses in six different fiber lengths where the incident conditions were maintained: $P_f \approx 11$ mW; $\Delta\tau_i = 80 \sim 90$ fs.

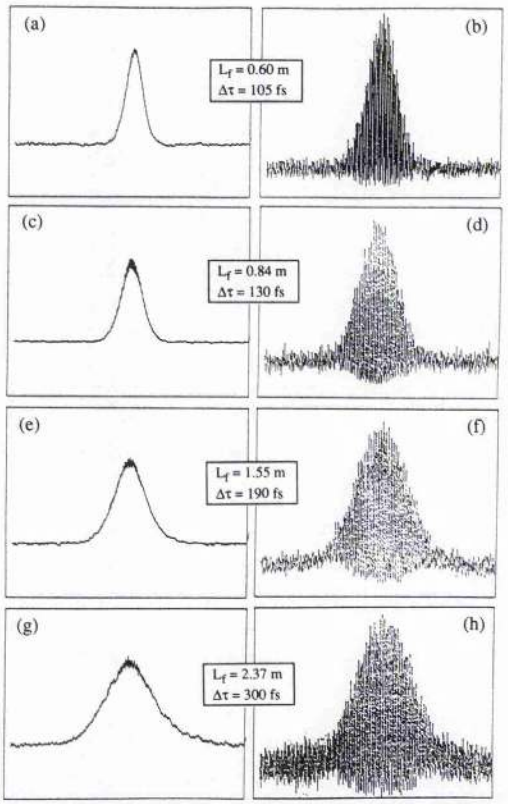

Fig. 4. Four pairs of intensity and interferometric autocorrelation traces for the anti-Stokes pulses [the corresponding spectra are the left part of the traces shown in Figs. 3(c)–3(f)].

However, as the pulses propagate further in the fiber the central wavelength of the anti-Stokes signal remains essentially unchanged, as indicated by traces (d)–(f) in Fig. 3. This result is different from the situation where the fiber length is fixed while the optical power of the incident pulses is varied.[3] As mentioned above, varying the optical power leads to the tuning of the anti-Stokes signal. The obvious modulation structure on the anti-Stokes spectra shown in the traces (e) and (f) reproduced in Fig. 3 indicates the involvement of SPM at these wavelengths. However, the spectral bandwidth of the anti-Stokes signal was not noticeably increased. For traces (c) and (d) in Fig. 3 we can see that, in contrast to the anti-Stokes counterpart, the change of Stokes signal along the fiber is rather complicated. This change may be due to the mixture of and interaction between the processes of four-wave mixing, SPM, and self-Raman effect.

The temporal features of the anti-Stokes signal exiting from different lengths of fiber were investigated by the use of a prism to separate it from the Stokes wave (see Fig. 1) and then by the use of an autocorrelator to measure intensity and interferometric autocorrelation traces. Associated with the spectra shown in Fig. 3(c)–3(f), the autocorrelation traces of the anti-Stokes wave are recorded as shown in Fig. 4. From Figs. 4(a), 4(c), 4(e), and 4(g), we see that the duration of the anti-Stokes pulses increases monotonically with the fiber length (or the propagation distance). Correspondingly, the interferometric traces [(b), (d), (f), and (h) in Fig. 4] indicate an increased frequency chirp in the recorded pulses.

For the spectral and temporal data given in Figs. 3 and 4, the bandwidth–duration products for the anti-Stokes pulses can be deduced to be 0.82, 1.02, 1.49, and 2.35 for the 0.6-, 0.84-, 1.55-, and 2.35-m fiber lengths, respectively. Such values indicate the degree of frequency chirp associated with the anti-Stokes pulses. The relatively large frequency chirp within the initial anti-Stokes signal $\Delta\nu\Delta\tau = 0.82$ could be transferred from the chirped pump wave during the early stage of the four-wave-mixing process, that is, as a result of cross-phase modulation.

It is believed that the SPM of the incident 1.52-μm signal is responsible for producing the particular wavelength at which the phase-matching condition for four-wave mixing is met. In other words, the shorter-wavelength part of the SPM-extended spectrum acts as a pump wave in the four-wave-mixing process. Thus, from an energy conservation point of view, only half of the incident signal can be converted to the actual pump wave for four-wave mixing. If we take the conversion efficiency of this pump to four-wave mixing to be somewhere between 50% and 100%, say 75%, then the percentage of the total incident energy that contributes to the anti-Stokes signal will be $1/2 \times (75\% \times 1/2) = 3/16$. Therefore, ignoring any loss inside the fiber, we can expect an energy ratio of the shorter wavelength (anti-Stokes) to the entire longer wavelength (Stokes) signals to be 3/16:13/16, that is, 1:4. This simply means that if the average power of the spectral component near 1.33 μm is 1 mW measured by a power meter located after the dispersive prism in Fig. 1, a similar measurement for the remaining spectral components [most having wavelengths $\geq$1.5 μm, for example, trace (f) in Fig. 3] would give an average power of 4 mW. In our experiment the measured maximum ratio was approximately 1:5. This discrepancy could have arisen because we assumed too high a conversion efficiency or because we ignored the drain of energy to the Raman signal.

For the spectral data shown in Figs. 3(c)–3(f) the measured energy ratios of the anti-Stokes to Stokes for the four fiber lengths are as shown in Fig. 5, where the energy conversion efficiency from 1.52 to 1.33 μm is given. Interestingly a maximum conversion efficiency of ~14% exists for the 0.84-m-long fiber. When the incident pulse duration was varied while the average power was kept constant (that is, as the peak pulse power was varied), the optical power of the anti-Stokes wave also changed. An example of this is shown in Fig. 6, from which we can see that for a fiber length of 1.55 m the average power of the

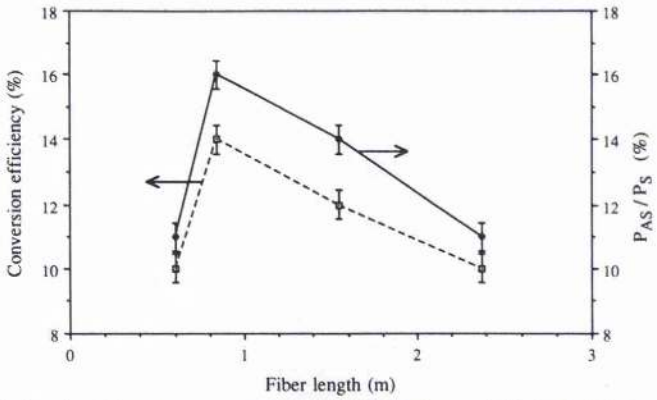

Fig. 5. Energy conversion efficiency from 1.52 to 1.33 μm (dashed curve) and the average power ratio of anti-Stokes to Stokes wave (solid curve) as a function of fiber length.

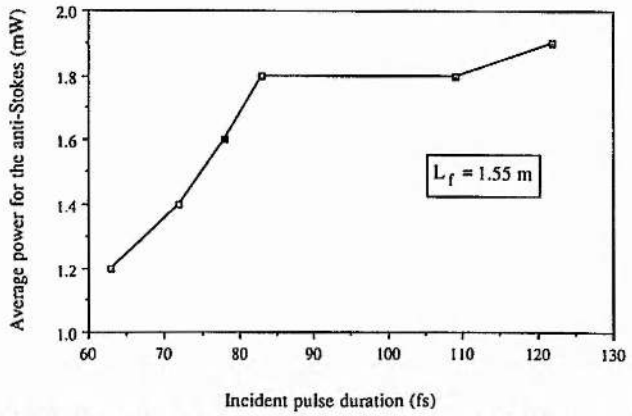

Fig. 6. Variation of the average power of the anti-Stokes signal at the exit of a 1.55-m-long fiber as a function of incident pulse durations (with $P_i = 13$ mW).

anti-Stokes wave increased as the incident pulses became broader. For the point that relates to $\Delta\tau_i = 122$ fs in Fig. 6, the recorded anti-Stokes power level reaches 1.9 mW. In this case because the incident power P_i is 18 mW and the exiting power P_f is 13 mW, we can deduce that the ratio of the anti-Stokes to Stokes signal is approximately 1:5, and the conversion efficiency from 1.52 to 1.33 μm is 16%. If we assume that the peak conversion observed for the 0.84-m-long fiber (Fig. 5) implies that such a fiber provides an interaction length that is close to the coherent length, then the tendency shown in Fig. 6 would indicate that, for the 1.55-m-long fiber to be close to a coherent length, the incident pulses should be broader. Hence an even higher conversion efficiency might be obtained if the system parameters were optimized. In general, for a chosen fiber length and a given coupling power, an optimum incident pulse peak power will exist. With this optimum pulse duration a maximum conversion efficiency from 1.52 to 1.33 μm can be achieved.

CONCLUSIONS

By pumping an Er-doped monomode optical fiber with sufficiently powerful femtosecond pulses at 1.52 μm such that a SPM-mediated four-wave-mixing process is initiated, we were able to produce femtosecond pulses near 1.33 μm. With the incident average power at a level of 10 mW, the average power of the anti-Stokes wave is typically 1 mW. The observed maximum upconversion efficiency (from 1.52 to 1.33 μm) is 14% for 80-fs incident pulses and 16% for 122-fs incident pulses. The 16% value is close to a predicted value of 20% based on a simple analysis.

Being distinct from their Stokes counterparts, the anti-Stokes pulses have durations that exceed those of the incident pulses. Typically for 80-fs incident pulses at 1.52 μm, the duration of anti-Stokes pulses (which are found to be frequency chirped) is ~100 fs at the location where they are generated. Because the anti-Stokes wave (centered at 1.33 μm) lies in the normal dispersion region of the fiber, these pulses broaden as they propagate.

ACKNOWLEDGMENTS

Funding for this research by the UK Science and Engineering Research Council is gratefully acknowledged. Z. Su also acknowledges postgraduate studentship support through a British Council Technical Cooperation Training Award.

REFERENCES

1. W. Sibbett, "Femtosecond laser sources for near-infrared spectroscopy," Inst. Phys. Conf. Ser. **126,** 1–8 (1991); R. L. Fork, C. V. Shank, C. Hirlimann, R. Yen, and W. J. Tomlinson, "Femtosecond white-light continuum pulses," Opt. Lett. **8,** 1–3 (1983); J. Squier and G. Mourou, "Tunable solid-state lasers create ultrashort pulses," Laser Focus World **28**(6), 51–58 (1992).
2. A. S. Gouveia-Neto, A. S. L. Gomes, and J. R. Taylor, "Femtosecond soliton Raman generation," IEEE J. Quantum Electron. **24,** 332–340 (1988); P. N. Kean, K. Smith, and W. Sibbett, "Spectral and temporal investigation of self-phase modulation and stimulated Raman scattering in a single-mode optical fiber," IEE Proc. (Pt. J) **134,** 163–170 (1987).
3. X. Zhu and W. Sibbett, "Propagation characteristics of femtosecond pulses in erbium-doped monomode optical fibers," IEEE J. Quantum Electron. **27,** 101–113 (1991).
4. X. Zhu and W. Sibbett, "Experimental study of the primary mode-locking parameters of a coupled-cavity KCl:Tl color-center laser," J. Opt. Soc. Am. B **7,** 2187–2191 (1990).

Coupled-cavity mode locking with passive semiconductor waveguides

R. S. Grant, Z. Su, G. T. Kennedy, and W. Sibbett

J. F. Allen Physics Research Laboratories, University of St. Andrews, St. Andrews KY16 9SS, Scotland, UK

J. S. Aitchison

Department of Electronics and Electrical Engineering, University of Glasgow, Glasgow G12 8QQ Scotland, UK

Received March 23, 1993

Coupled-cavity mode locking of a KCl:Tl color-center laser has been achieved with passive waveguides fabricated in the AlGaAs material system. The ultrafast refractive nonlinearity at the half-band gap is exploited by the laser to produce pulses as short as 230 fs at operating wavelengths of ~1520 nm.

Ultrafast all-optical switching has been demonstrated recently with AlGaAs-based semiconductor waveguide structures at photon energies corresponding to approximately half the band-gap energy.[1,2] At these wavelengths nonlinear phase shifts greater than 2π rad have been directly observed in straight guides[3] owing mainly to minimal competition from nonlinear absorption but also with the assistance of a localized enhancement in the nonlinear refractive index related to two-photon transitions (real or virtual, depending on wavelength).[4] Nonlinear index coefficients of $n_2 \approx +1 \times 10^{-13}$ cm^2 W^{-1} have been estimated for this material,[1-3] i.e., >100 times stronger than that observed for fused-silica-based optical fibers. This relatively high magnitude, together with their potential for inducing nonlinear phase shifts on the order of π rad, makes these semiconductor guides attractive replacements for optical fibers in coupled-cavity mode-locked lasers.[5]

Coupled-cavity color-center lasers are arguably the most versatile optical pulse source in the 1.55-μm spectral region. They combine broad-frequency tunability with high output-pulse energy. Furthermore they can be switched from femtosecond to picosecond operation by reverting to synchronous mode locking, and unlike synchronously pumped optical parametric oscillators they can operate continuous wave. Although passive mode locking with a semiconductor saturable absorber[6] is a simpler technique than coupled-cavity mode locking, it relies on a resonant nonlinearity. Hence it is relatively inefficient with the 5–6 W of pump power required to obtain output powers of a few tens of the milliwatts, and both pulse duration and output power are strongly wavelength dependent. In this Letter we describe the mode locking of a coupled-cavity KCl:Tl color-center laser in which a passive AlGaAs waveguide has been incorporated into the control cavity. Pulse durations of <250 fs are obtained at average output powers of 50–70 mW for <2 W of pump power.

The coupled-cavity laser was constructed in the conventional Fabry–Perot configuration as shown in Fig. 1, with mirrors M0 and M1 forming the master cavity and M1 and M2 the control cavity. The KCl:Tl crystal was pumped at average powers of up to 2 W by a mode-locked Nd:YAG laser, and the useful output of the color-center laser was provided by the insertion of a 50/50 beam splitter (BS) located in the control cavity. In previous experiments in which a semiconductor optical amplifier was used as a nonlinear element in our coupled-cavity lasers,[5,7] care had to be taken to minimize parasitic reflections from the facets. The antireflection coatings on the device were found to be inadequate, and a complex approach involving two optical isolators was used to obtain stable operation.[7] In the experiments described here we opted to fabricate the passive AlGaAs waveguides at an angle to the (cleaved) facets, so that light entered and exited the guide at Brewster's angle, thus rendering antireflection coatings unnecessary.

The waveguides were grown in AlGaAs onto a GaAs substrate with molecular beam epitaxy. The 1.5-μm-thick $Al_{0.18}Ga_{0.82}As$ guiding layer was sandwiched between buffer and upper cladding layers, both with 24% Al composition. Twelve parallel guiding ribs with widths varying from 3.0 to 5.5 μm were revealed in the 1.5-μm-thick upper cladding layer to a height of ~1.3 μm with reactive-ion etching. With an estimate for the modal index the Brewster angle was calculated to be 73.3°. The substrate (see inset of Fig. 1) had dimensions of length × width = 4.15 mm ×

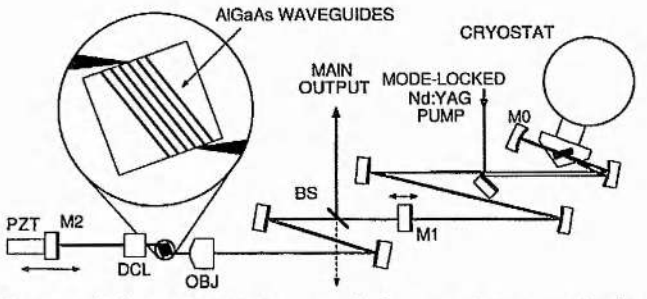

Fig. 1. Schematic of the coupled-cavity laser with the AlGaAs substrate shown within the inset. PZT, piezoelectric translator.

0146-9592/93/191600-03$6.00/0

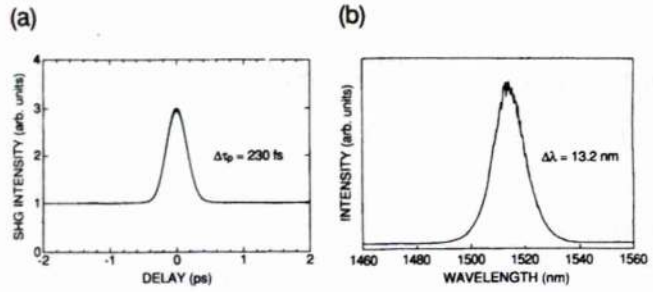

Fig. 2. (a) Intensity autocorrelation and (b) corresponding spectrum of the 230-fs pulses from the main output.

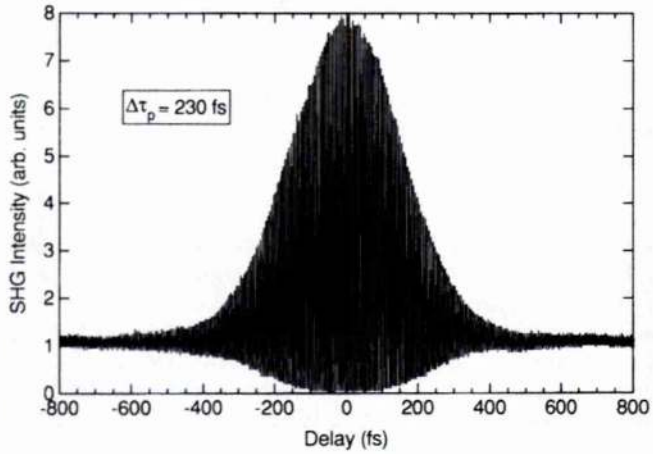

Fig. 3. Interferometric autocorrelation data for the 230-fs pulse.

5.35 mm, with 4.33-mm-long guides. This relatively large substrate presented at the Brewster angle necessitated the use of coupling lenses with working distances >2 mm, and hence light was coupled in with a 10× microscope objective (OBJ), with the exit beam collected with a diode collimating lens (DCL) with a numerical aperture of 0.276. This beam was focused onto mirror M2 and retroreflected.

The throughput of the guide was typically 15% for the initial pass, and the effective reflection coefficient for the combined waveguide and mirror M2 was estimated to be just <2%. (Typically we would have an equivalent reflection coefficient of ~50% when using an optical fiber in the control cavity.) The poor efficiency is primarily related to modal mismatches caused by Brewster angling of the substrate and by the use of long-working-distance lenses, although the linear loss of the guide also contributes. Fortunately the parasitic reflectivity of the device as seen by the master cavity (mirror M2 blocked) was a factor of ~500 smaller, so this did not prevent mode locking. The most stable mode-locking condition was observed when the transmission of the common mirror M1 was increased to 22%, which resulted in average output powers of ~50–70 mW in the main output (see Fig. 1).

As is normal with coupled-cavity lasers that rely on refractive nonlinearities the lengths of the master and control cavities were required to be matched to within a fraction of a wavelength. This was achieved by using stabilization electronics to control the position of mirror M2, which was mounted on a piezoelectric translator.[8] Normally the error signal would be derived by monitoring the average output power but the low level of feedback in the laser described here was insufficient to induce significant interferometric fluctuations of the power levels in either of the two output beams. However, successful long-term stabilization was achieved by monitoring the second harmonic of the main output power. In contrast the latter more complicated approach was not required in previous experiments where the semiconductor optical amplifier was used even though the feedback level was less. The active waveguide[7] differs in that it suffers from significant nonlinear attenuation, which in turn causes a large modulation of the output of the secondary output as the laser switches alternately from mode-locked to continuous operation with changes in the length of the control cavity.

Self-starting of the mode locking was not observed during these experiments, and the Nd:YAG pump laser had to be operated in the mode-locked regime for coupled-cavity mode locking to be initiated. This is not surprising because the nonlinearity in the waveguide has an ultrafast recovery time and is therefore relatively weak during the initial stages of pulse formation. Self-starting mode locking was observed with the active waveguide[7] because it relied on self-phase modulation primarily associated with the much stronger resonant nonlinearity related to carrier density changes.

With no bandwidth-limiting elements in the laser cavity, pulses as short as 230 fs (assuming a sech pulse shape) were obtained (see Figs. 2 and 3 for intensity and interferometric autocorrelation profiles respectively) with bandwidth–duration products of 0.39. The intensity autocorrelation and spectrum for the pulse returning from the control cavity measured at the subsidiary output (shown by the dashed line in Fig. 1) are reproduced in Fig. 4. The temporal (120%) and spectral (30%) broadening of the return pulses is consistent with the combined action of self-phase modulation and normal group-velocity dispersion in the semiconductor waveguide. From this spectral broadening we estimate that the peak nonlinear phase shift in the steady state was between $\pi/2$ and π rad. Temporal broadening arising from nonlinear absorption was expected to be minimal at this value of phase shift, especially given that the laser operated at wavelengths longer than the two-photon band edge (1504 nm). This was confirmed by the insignificant modulation (~2%) in the feed

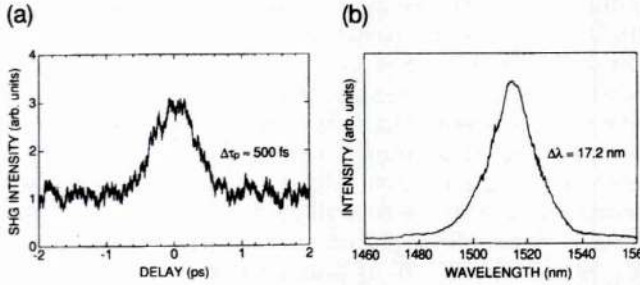

Fig. 4. (a) Intensity autocorrelation and (b) spectrum fo pulses from the subsidiary output taken under the sam conditions as the data for Figs. 2 and 3.

back power measured at the subsidiary output when switching from continuous to mode-locked operation.

The low intensity level of the control signal returning to the main cavity prevented the use of bandwidth-limiting and tuning elements. Unstable operation resulted when a thin (0.8-mm-thick) quartz plate was inserted into the cavity, probably because of insufficient nonlinear phase shift at the steady state. We anticipate that considerable improvements in the laser performance will be possible once the overall throughput is increased by use of alternative substrate geometries. For example, a reduction in the rib angle from 16.7° to 10° or even 7° (relative to the facet normal) may be possible without significantly compromising the parasitic reflectivity caused by external and internal reflection,[9] while allowing better coupling at the input facet. Furthermore by use of curved guides so that the guiding rib meets the exit facet at normal incidence the chip itself will become the retroreflector. The expected increase in efficiency will make shorter guides feasible, thus minimizing the effects of group velocity dispersion in the guide, and result in the generation of sub-200-fs pulses. Moreover by use of a nonlinear Michelson cavity configuration the laser could be made considerably more compact. Finally further gains in efficiency may be obtained by use of multiple-quantum-well waveguides, where a factor of 2 enhancement in the nonlinearity has been observed.[10]

Compared with optical fibers, passive AlGaAs waveguides have several advantages. The high nonlinearity allows compact arrangements and thus results in considerable passive stability and high immunity to thermal drift. Furthermore the guides are polarization preserving and require no index-matching fluid to avoid backreflections due to the angled ribs. The nonresonant nature of the waveguide nonlinearity suggests that, after the above improvements in waveguide design have been implemented, femtosecond operation should be possible over a large fraction of the gain bandwidth of the laser with only a single sample. This technique should also be suitable for mode-locking NaCl:OH^- lasers, erbium lasers (guided wave or bulk), and, with adjustment of the band-gap energy, Cr:forsterite lasers. Ultimately it may be possible to fabricate miniature integrated Michelson interferometers for use with InGaAsP semiconductor lasers.

In summary, we have successfully mode locked a color-center laser with passive semiconductor waveguides at wavelengths in the vicinity of the half-band gap, with pulse durations of <250 fs being recorded. The performance of the laser is limited mainly by the poor coupling efficiencies associated with this initial waveguide design. We expect that changes in this design, together with the use of a nonlinear Michelson cavity configuration, will permit shorter pulses and greater stability.

This work was supported by the Science and Engineering Research Council (SERC) through the Nonlinear Optical Waveguides Initiative. Z. Su and G. T. Kennedy gratefully acknowledge support through a British Council Technical Cooperation Training Programme Award and a SERC Cooperative Award in Science and Engineering with Bell Northern Research Europe Ltd., respectively.

References

1. J. S. Aitchison, A. H. Kean, C. N. Ironside, A. Villeneuve, and G. I. Stegeman, Electron. Lett. **27,** 1709 (1991).
2. K. Al-hemyari, J. S. Aitchison, C. N. Ironside, G. T. Kennedy, R. S. Grant, and W. Sibbett, Electron. Lett. **28,** 1090 (1992).
3. S. T. Ho, C. E. Soccolich, M. N. Islam, W. S. Hobson, A. F. J. Levi, and R. E. Slusher, Appl. Phys. Lett. **59,** 2558 (1991).
4. M. Sheik-Bahae, D. C. Hutchings, D. J. Hagan, and E. W. Van Stryland, IEEE J. Quantum Electron. **27,** 1296 (1991).
5. P. N. Kean, X. Zhu, D. W. Crust, R. S. Grant, N. Langford, and W. Sibbett, Opt. Lett. **14,** 39 (1989).
6. C. E. Soccolich, M. N. Islam, K. Möllmann, W. Gellermann, and K. R. German, Appl. Phys. Lett. **61,** 886 (1992).
7. R. S. Grant, P. N. Kean, D. Burns, and W. Sibbett, Opt. Lett. **16,** 384 (1991).
8. F. Mitschke and L. F. Mollenauer, IEEE J. Quantum Electron. **QE-22,** 2242 (1986).
9. D. Marcuse, J. Lightwave Technol. **7,** 336 (1989).
10. H. K. Tsang, R. S. Grant, R. V. Penty, I. H. White, J. B. D. Soole, E. Colas, H. P. LeBlanc, N. C. Andreadakis, M. S. Kim, and W. Sibbett, Electron. Lett. **27,** 1994 (1991).